Strömgren Photometry of Open Clusters

NGC 6134 and NGC 3680

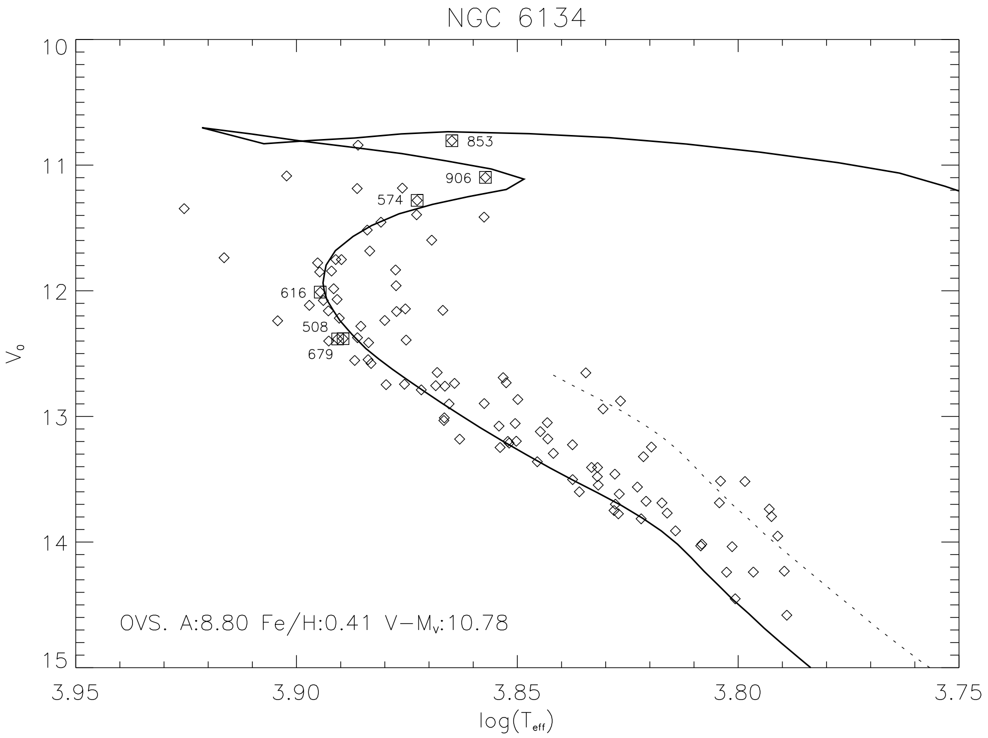

Master Thesis

Hans Bruntt

Institute of Physics and Astronomy
Aarhus University

January 1999

Preface

In the spring of 1996 I visited the European Southern Observatory (ESO) in Chile for three weeks. Originally, PhD student Michael Viskum from Aarhus University was supposed to make time resolved spectroscopy of two variable stars, FG Virginis and α Circini, and was given two weeks observing time at the Danish 1.54m telescope.

For some reason the observer that was supposed to have the telescope after Viskum changed his mind, and Viskum was given the extra observing time: In all he had 21 nights at the telescope.

At that time I was working on my bachelor thesis on solar models [11], until one day my advisor Søren Frandsen asked me if I wanted to go with Viskum to Chile. Frandsen had a very good idea about some objects that could be observed from Chile, that would yield very interesting results. The extra week of observing time given to Viskum was to be used for this project.

The target objects were the open clusters NGC 6134 and NGC 3680. Open clusters are excellent laboratories for testing stellar models as will be described in chapter 1.

One of the goals of this project is to improve the colour-magnitude diagrams of the two open clusters and to determine their ages and distances by using isochrone fitting. By using the Strömgren photometric system, I will also be able to derive the basic stellar parameters:

- The effective temperature, $T_{\rm eff}$
- The metal content of the atmosphere, $[Fe/H]$
- The interstellar reddening, $E(b-y)$

The two young clusters have ages around one billion years. The somewhat younger of the two, NGC 6134, has a turnoff in a very interesting region: It contains somewhat evolved stars of class A5 to F5 with masses round $2\mathrm{M}_\odot$. This is inside the instability strip where some main sequence stars show variability: The region of the δ Scuti variables. The theory of stellar pulsation is well understood today (*cf.* chapter 1), and is an important tool for probing the physics inside the stars.

A search for variable stars in NGC 6134 was performed in 1989 and 1991 by Kjeldsen and Frandsen [38] who discovered five δ Scuti stars in the instability strip. Two years later the same cluster was observed even more carefully from two sites (ESO and SAAO in South Africa) by Frandsen *et al.* [29] and another δ Scuti star was found.

To be able to construct detailed stellar models of the six known δ Scuti stars in NGC 6134 the following information is needed:

- Oscillation frequencies (photometry)
- Basic stellar parameters (photometry)
- Rotational velocities (spectroscopy)
- Cluster membership assignment (spectroscopy)

The oscillation frequencies have been measured by Frandsen *et al.* [29]. With the photometry presented in this thesis we now have the second of the four pieces needed to "solve the puzzle". The spectroscopic data is still missing, but will be achieved in spring 1999. The combination of the information obtained by using photometry and spectroscopy will put severe constraints on the oscillation models: We will then be able to probe the inside of these stars in detail.

Several hundred δ Scuti stars have been observed among field stars: An example is FG Virginis. I observed FG Vir and the rapidly oscillating Ap star α Circini over a period of 22 nights by using the SAT 50cm telescope mounted with a photometer with Strömgren filters. In this thesis I will also present the information derived from this data set.

* * *

I would like to thank a few people who have supported and advised me throughout the process that has led to this thesis. First of all thanks to Torben Arentoft for convincing me that astronomy is very exciting. Also thanks to Frank Grundahl for giving me the first introduction to the mysteries of CCD photometry of stellar clusters. Thanks to Michael Viskum with whom I survived 22 nights of observations at the European Southern Observatory, La Silla in May 1996. Also thanks to Hans Kjeldsen for fruitful discussions and for reading the first draft of this thesis. His comments have greatly improved the presentation of the results. I wish to thank Kim Lang with whom I spent two weeks at the Lick Observatory in California in the spring of 1998. Thanks to my advisor Søren Frandsen for helping me throughout this project. Also thanks to Poul Erik Nissen for giving invaluable advice concerning the subtleties of the Strömgren system. Also thanks to Jørgen Christensen-Dalsgaard for supplying the theoretical isochrones. I am also very grateful to a few people outside the "astronomical circles" - especially Malene Vestergård, Jens N. Nielsen, and Søren Dideriksen - for all kinds of support! And finally a special thanks to Karen Bruntt for carefully reading through this manuscript, thus improving my "broken English".

Hans Bruntt, - January 17th 1999.

Guide

A guide to the contents of the chapters and appendices of the thesis is presented below.

Introduction

- 1. Introduction to astrophysical concepts and tools applied in the thesis

Open Clusters: NGC 6134 and NGC 3680

- 2. Known properties - and presentation of the new Strömgren observations
- 3. Calibration and reduction of raw science data
- 4. Transformation to the Strömgren standard system
- 5. Presentation of the final results of the open clusters

The δ Scuti Star FG Vir and the roAp Star α Cir

- 6. Known properties of the variables and presentation of the new observations
- 7. Reduction of the raw light curves
- 8. Presentation of the results obtained for the variable stars

Conclusion and Outlook

- 9. Conclusive remarks - what should be done next?

In the appendices A-G I have collected various additional information

- A. Description of the Strömgren photometric system
- B. Properties of theoretical isochrones
- C. Complete log of observations
- D. An example of the output from the photometric reduction programme "MOMF"
- E. Final Strömgren indices of the open clusters
- F. Instructions on how to get the results of this thesis by anonymous `ftp`
- G. Summary in Danish (Oversigt over indholdet af specialet på dansk)

Table of Contents

Chapter 1

Observation of the Stars

The Sun of our solar system is located in one of the arms of a spiral galaxy - the Milky Way. It is located close to the galactic plane and about 8.5 kpc from the centre (*e.g.* Haud [33]). From this spot astronomers have studied the stars and nebulae in the night sky through many centuries. It is amazing to think of what we know about the Universe today. Within the last century technological advances and progress in theory have allowed astronomers to give a very detailed description of the objects around us. We now have detailed knowledge of the structure and evolution of the stars. We also have a good idea of how the Milky Way was formed and how it has evolved to the present state.

In the preface of this thesis I have given a short overview of the goal of this thesis: By using Strömgren photometry I will determine the essential astrophysical parameters for the two open clusters NGC 6134 and NGC 3680, *i.e.* their ages, distances, interstellar reddenings, and metallicities. I have also studied the two variable stars FG Vir and α Cir in the Strömgren filters, which will yield detailed information about the physics of these stars. In this introductory chapter I will give the background information needed to understand how this information can be achieved, *i.e.* by using photometry and asteroseismology.

The first two sections in this chapter is a short introduction to the structure and formation of the Milky Way galaxy to let the reader know something about the stellar system that the objects I have studied are part of.

1.1 The Structure of the Milky Way Galaxy

Studies of individual stars and stellar clusters show that at least four different populations exist (*e.g.* chapter 11 of Gilmore [31]): *The halo population* is a nearly spherical distribution of stars with very low metallicity (population II). This is the oldest component in the Milky Way. About one percent of the halo stars are found in globular clusters: They are gravitationally bound systems containing up to a million stars. These are the oldest objects in the Universe whose ages can be determined with a relatively low error. The oldest globular clusters have ages of 16 ± 3 Gyr[1] - which sets a lower limit to the age of the Universe, *e.g.* Vandenberg *et al.* [69]. The low scatter in age of the globular clusters gives a hint that the initial formation of stars in the Milky Way was quite rapid. There is essentially

[1] Gyr is the abbreviation of giga years, *i.e.* billion years.

no gas left in the halo and hence no star formation takes place. *The disk population* is a relatively flat distribution of stars and gas. The ages of disk stars (population I) have a much greater range. Actually, new groups of stars are still being formed from large gas clouds, while some groups exist that are nearly as old as the youngest globular clusters: These groups of stars are the open clusters. The objects I have studied are of this type and I will describe the properties of them in detail in section 1.5. There is evidence that a disk population of somewhat older stars exists - *the thick disk*. The spatial distribution and kinematic properties of the stars in the thick disk lie between the values of the halo and the thin disk population. The fourth population is found in the central part of the galaxy: *The bulge*. Here the density of stars is large and star formation and chemical evolution have been rapid relative to the disk populations.

1.2 The Formation of the Milky Way Galaxy

The Milky Way galaxy is thought to be the result of the collapse of a gigantic gas cloud around 16 billion years ago, *cf.* the age of globular clusters. So far few complete models of the formation of the Milky Way exist, *i.e.* ones which agree with all of the observational facts. Two classical models with this aim are regarded as at least containing the right ideas.

One model was proposed by Eggen *et al.* [25] who suggest an initial rapid contraction which involved star formation: The remains of this process are the metal poor halo stars and the halo globular clusters. The inner parts of the halo collapsed into a population of disk stars. The fact that the age of the oldest open clusters (disk objects) falls in a range just below the age of halo globular clusters (0-10 Gyr) speaks for a gradual transition of the halo and disk system.

The other classical theory was proposed by Searle and Zinn [61] who had evidence of a significant spread in the age of the halo globular clusters. According to this model star formation did not commence until the cloud had collapsed significantly and the disk started to form. The observation of old halo objects is then explained by the gravitational capture of nearby dwarf galaxies (like the Magellanic Clouds), which contain both stellar clusters and field stars. Evidence for such a capture has been reported by Ibata [34].

To be able to answer the questions about the formation of the Milky Way, we need accurate determinations of the ages, metallicities, and reddenings of the stellar clusters. These are the only objects available for reliable estimates of ages in our galaxy. It is essential that a whole range of ages are considered. Unfortunately only few old open clusters exist (about 20 with ages > 5 Gyr have been observed, Janes *et al.* [35]).

For a more detailed discussion of the structure and formation of the Milky Way the reader may consult the review article concerning the application of old open clusters by Friel [30] or the more specific study of age determination of open clusters by Janes *et al.* [35]. For a review of the difficulties involved in age determination of stellar clusters with emphasis on various sources of error (observationally and theoretically) turn to Vandenberg [69].

1.3 Tools for Studying the Stars

To be able to deduce the properties of individual stars that constitute the Milky Way one has to have detailed information about the physics of the stars. A widely used method is observing integrated light from the stars, *i.e.* photometry. When using this tool, one gets information about the conditions in the *atmosphere* of the stars.

For example by measuring the difference in flux in two different wavelength intervals using filters that select only part of the light, one can determine the colour of a star, which may be translated to the temperature in the atmosphere. Other basic parameters of stellar atmospheres can be derived by using different filters, *i.e.* by subtracting details of the star by using the information contained at different wavelengths. In this thesis I have derived essential information about stars in two stellar clusters using photometry with the Strömgren filters. An introduction to the Strömgren photometric system and its calibration is found in appendix A.

Using photometric filters does not yield the detailed information that can be obtained by using spectroscopy, where the flux at each wavelength within *e.g.* 0.1 Ångström can be studied. By comparing the spectrum of a star with theoretical models, it is for example possible to determine the temperature of the atmosphere and abundances of *individual* elements. The width of the spectral lines can also be used to determine the projected rotational velocity of the stars, *i.e.* $v \sin i$.

When observing the spectra of stars, only a few stars can be observed at the same time contrary to photometry where several hundred stars can be observed at once using a CCD detector.

In recent years a tool to probe the *inside* of the stars has become available. It turns out that some stars show variation in *e.g.* luminosity. This has been interpreted as the result of waves oscillating in the plasma of these stars. As the waves penetrate the star, their nature, *i.e.* observable properties like period, gives information about the internal physical properties of the star. The study and interpretation of variable stars is called asteroseismology: "Seismology of stars". I will return to this subject in section 1.6.

1.4 The Structure and Evolution of Stars

To be able to tell how the Milky Way was formed and how is has evolved one has to have information about stars created at different times. In other words what astronomers want is a precise determination of the ages and properties of different groups of stars. By looking at differences among stars at different ages, one can say something about the evolution of the Milky Way. For example young stars are formed from remains of matter that has existed in older - now "dead" - stars. During the life of a star the content of heavy elements rises in the core where nuclear fusion supplies the energy that is radiated from the surface. Consequently, stars that are formed from such processed material have a higher content of heavy elements or similarly "higher metallicity". The subtleties of this issue is discussed in Pagel [55].

When stars form, it is the result of a giant cloud of gas that contracts. The mass of such a cloud allows for many stars to be created - several thousands perhaps. These processes started soon after the Milky Way galaxy was starting to form. Indeed some of the oldest such clusters of stars created still exist. These are the globular clusters which may contain from a hundred thousand to a million individual stars! The creation of stars has been going on ever since the Milky Way was formed - at least 16 Gyr ago, *i.e.* the age of the oldest globular cluster (Vandenberg [69]). Another kind of stellar clusters is also found - the open clusters. The name is derived from the less dense nature of these clusters. Open clusters may contain less than a hundred and up to more than a thousand stars (Friel [30]).

We are not able to detect the evolution of any individual star - due to the extremely slow evolution of stars (several Gyr depending on mass). In a stellar cluster the age and the material that the stars are made of is almost the same. The small deviations in age are negligible compared to the age of the stars. The lifespan and detailed evolution of each star in the cluster then depend essentially only on its mass.

With a sample of stars of different masses one can determine differences in the evolution of these stars. A convenient way of showing the different properties of stars in such a cluster is the Hertzsprung-Russel (HR) diagram[2]. A sketch of the HR diagrams of the two clusters I have observed is shown in figure 1.1. The abscissa measures the temperature with higher temperatures to the left. The ordinate measures the luminosity of each star.

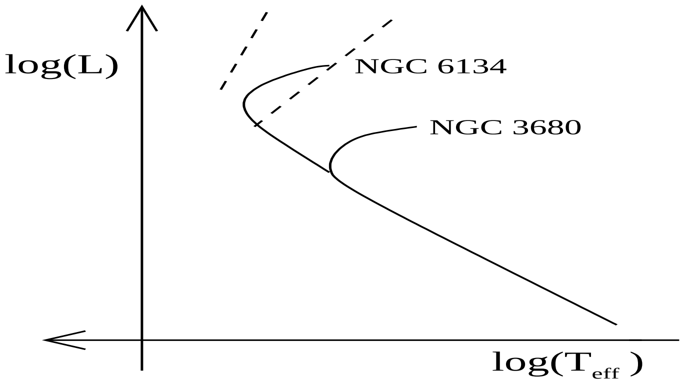

Figure 1.1: A sketch of how the stars are distributed in the Hertzsprung-Russel diagram of the two open clusters NGC 6134 and NGC 3680. As described in the text NGC 6134 is the younger of the two, - hence the turnoff stars have higher luminosity, temperature, and mass. Note that the main sequences of the two clusters are the same. This is not exactly true for the observed clusters because the chemical composition of the stars in the two clusters differ. The dashed lines indicate the Cepheid instability region, *cf.* figure 1.2 and section 1.6.3.

As can be seen, there is a distinct relationship between temperature and luminosity. Theoretical calculations of the structure of stars show that stars with higher mass have higher luminosity and temperature, Pols *et al.* [57]. This is true for the stars on the *main sequence* - lower right. These stars have lower mass compared to the turnoff stars and are currently in the core Hydrogen burning phase. Stars below a certain mass are situated on the main sequence. Stars that are more massive are found *above* the main sequence - this is called the *turnoff* region. These are evolved stars whose core is more of less depleted

[2]Figure 1.1 is a Hertzsprung-Russel diagram which shows a double logarithmic plot of the luminosity as a function of effective temperature. The HR diagram is analogous to the colour magnitude diagram (CMD) which is a plot of magnitude as a function of a colour index, *i.e.* the observed parameters. Note that $\log T_{\rm eff} \propto$ colour and $\log L \propto$ magnitude.

in Hydrogen. In this phase the core is contracting and the outer parts of the star are expanding - altogether giving a higher luminosity. These are the most massive stars in a cluster and are in the final part of their lives. When Hydrogen is completely exhausted in a star, it has evolved to become a red giant star. This is followed by a short phase of Helium core burning - lasting roughly 20% of the total lifespan of a star (section 31.2 of Kippenhahn and Weigert [36]). The Helium core burning stars are located above of the main sequence on the horizontal branch. After this relatively short phase these stars will undergo a rapid transition in which the outer envelope eventually is expelled - observable as a sphere of gas around the inner remaining (very faint) stellar core - a white dwarf (*e.g.* chapter 12 of Jørgen Christensen-Dalsgaard [19]).

The location of the turnoff stars in the observed colour-magnitude diagram (CMD, *cf.* footnote (2) on page 4) is determined by the *age* and *metallicity* of the cluster. In very young clusters the turnoff is populated by massive stars with high temperature and luminosity, whereas in old clusters the turnoff is located at lower values of these parameters. The reason is simply that stars with lower mass and hence lower luminosity use up their supply of Hydrogen "fuel" more slowly. Hence they are found on the main sequence for a longer time than the more massive stars.

Theoretically one can determine the shape of the main sequence and the location of the turnoff as a function of cluster age and metallicity. In the models one computes how stars with a range of different masses evolve from age 0 (with all stars on the Zero Age Main Sequence, ZAMS) to some later time. The resulting theoretical CMDs are known as *isochrones* (Greek for "same age"). By fitting isochrones to observed CMDs, it is hence possible to estimate the age of a cluster, *cf.* appendix B. In this way astronomers have shown that the globular clusters have ages around 16 Gyr (Vandenberg [69]) while open clusters have ages from 0.5 to 10 Gyr, *e.g.* Janes *et al.* [35].

Another application of CMDs and theoretical isochrones is the comparison of the detailed morphology of the turnoff. At a significant level this is not the same in different stellar models: Some show a sharp or a soft turnoff, some show different kinds of loops *etc.* This can be used to infer which model is correct but this requires precise photometry.

- As has been emphasized stellar clusters provide an excellent laboratory to test the stellar structure and evolution of stars. In this thesis I have used theoretical isochrones to determine the age and distance to the open clusters NGC 6134 and NGC 3680, *cf.* chapter 5.

For a more detailed description of the issues discussed here, consult the introductory notes by Christensen-Dalsgaard [19] or the more advanced textbook by Kippenhahn [36].

1.5 Fundamental Characteristics of Open Clusters

Open clusters are sparsely populated systems of a few tens or several hundreds of stars. The total mass of a typical open cluster lies in the range $10^2 - 10^3$ $M_\odot$ although newly formed clusters are thought to contain up to 10^4 $M_\odot$. As may be deduced from these numbers they are much less densely populated than the globular clusters with masses in the range $10^4 - 10^6$ $M_\odot$. This explains the name *open* cluster.

More than a thousand open clusters have been detected, *e.g.* Friel *et al.* [30]. They all consist of population I disk stars, *i.e.* stars made of processed stellar material. Of this large sample of clusters only few have been studied in detail: This includes a determination of interstellar reddening, metallicity, cluster age, and distance to the cluster. It is also important to determine which of the stars in the field are actually members of the cluster: This can be done using spectroscopy to determine the radial velocities of the stars in the field. Stars with similar radial velocities are interpreted as being members of the cluster. Another constraint is that the cluster stars must have the same amount of interstellar extinction as they are located in the same spatial direction and at the same distance. To allow for the clusters to be used as probes of disk formation, a large sample of clusters with precise parameters is needed. The ages range from 0-10 Gyr with the majority falling in the range 0-1 Gyr - known as the *young* open clusters, *e.g.* Friel *et al.* [30].

As mentioned earlier, only few *old* open clusters exist. Theoretical studies of the effect of an encounter of a cluster with a giant interstellar cloud show that this will be able to make the cluster dissolve completely, *e.g.* Terlevich [66]. Following the passage of the cloud, the stars of the cluster are no longer a gravitationally bound system, and the stars will merge with the field stars and will be unrecognizable as former cluster members.

This explains why most open clusters are so young. The description above also explains the spatial distribution of old open clusters: They are found at great distances from the galactic plane and at some distance from the galactic centre. More specifically, their orbits are not going through the areas where the concentration of interstellar gas is high. For some specific numbers of the spatial distribution Janes *et al.* [35] note that the characteristic distances from the plane follow decreasing exponential functions with scale heights of 55 and 375 pc for the young and old open clusters respectively. They also state that no old open clusters have been observed within 7 kpc from the galactic centre where the concentration of gas is larger.

Another characteristic of open clusters is the lack of low mass stars. Specifically one of the clusters I have observed - NGC 3680 - has no single members below 1.4 $M_\odot$ (Nordström *et al.* [53]). Realistic estimates of the distribution of the number of stars formed within a given mass range show that many low mass stars and few massive stars are formed. Theoretical simulations of the dynamical evolution of such a system show that indeed the low mass stars will be less tightly bound and finally disappear from the cluster, *e.g.* Marcos *et al.* [47].

For a detailed description of the properties of open clusters, consult the review article referred to above, *i.e.* Janes *et al.* [35].

1.6 Stellar Oscillations

A part of my work has been dedicated to the study of variable stars. In the open cluster NGC 6134 six such stars of δ Scuti type and a blue straggler have been observed, Frandsen *et al.* [29]. I have also examined the variability of two field stars that are known variables, *i.e.* FG Vir and α Cir. In this section I will give a short description of the known properties of - and the results from the interpretation of - the variability in the Sun and other stars. This is done as to give the reader an insight into the information that can be achieved.

1.6.1 Variability of the Sun

The most well-studied star is the Sun: In the early 1960'ies Leighton [44] reported the first observations of the now well-known five-minute oscillations of the Sun. In the last few years the SoHo-satellite has provided spatially resolved Doppler-images of the Solar disk - this is one of several projects that have yielded exciting results about the Sun.

In a star like the Sun the oscillations are excited in stochastic turbulent processes in the convective envelope. So far only acoustic modes - p-modes - have been observed. The oscillations are driven by perturbations in pressure, hence the name p-modes. The observations of these oscillations give information about the sound speed inside the Sun, which is directly related to physical parameters, *i.e.* the ratio of temperature to mean molecular weight. The amplitudes of the oscillations are very small - in Doppler shift about 15 cm/s - in luminosity of a few micro magnitudes (*i.e.* intensity changes of the order 10^{-6}). Despite these low amplitudes, observations with modern instruments have revealed several thousand different modes, Christensen-Dalsgaard [20].

By using the theory of stellar oscillations and the observations of thousands of modes it is possible to test current Solar models. Examples of recent results are: 1) The depth of the solar convection zone has been determined by Christensen-Dalsgaard *et al.* [18]. 2) The internal rotation of the Sun has been mapped in the outer parts of the envelope by Tomczyk [67].

1.6.2 Properties of Stellar Oscillation Modes

Each oscillation mode is characterized by its degree l and azimuthal order m. These values correspond to the spherical harmonics $Y_l^m(\theta, \phi)$. The spherical harmonics describe the variation of an oscillation on concentric spheres with the spherical coordinates (θ, ϕ). For example modes of high degree show a large variation (*i.e.* different parts moving in or out) across the stellar disk. For stars other than the Sun we are only able to measure modes with low l, *e.g.* $l \leq 3$. Modes of high l will cancel with contributions from other high l modes.

The radial dependency of a mode is described by the n value - the radial order. The three values (nlm) is assigned to each observed frequency along with its amplitude. An oscillation penetrating a star from the surface will reach a certain depth (decreasing with the l value) before reaching a turning point and the oscillation will travel towards the surface where it is reflected, etc. Each mode of oscillation gives information about the part of the star that the mode has travelled through. For example if two modes penetrate to different depths, the frequency difference contains information about the layer between the two turning points.

1.6.3 Variability among other Stars

Stars that show variability are found in many regions of the Hertzprung-Russel (HR) diagram. In figure 1.2 I have shown the location of the known variable stars.

Among the stars located in a certain strip in the HR diagram there are many stars that oscillate: Often referred to as "The instability strip". In the case of the very luminous

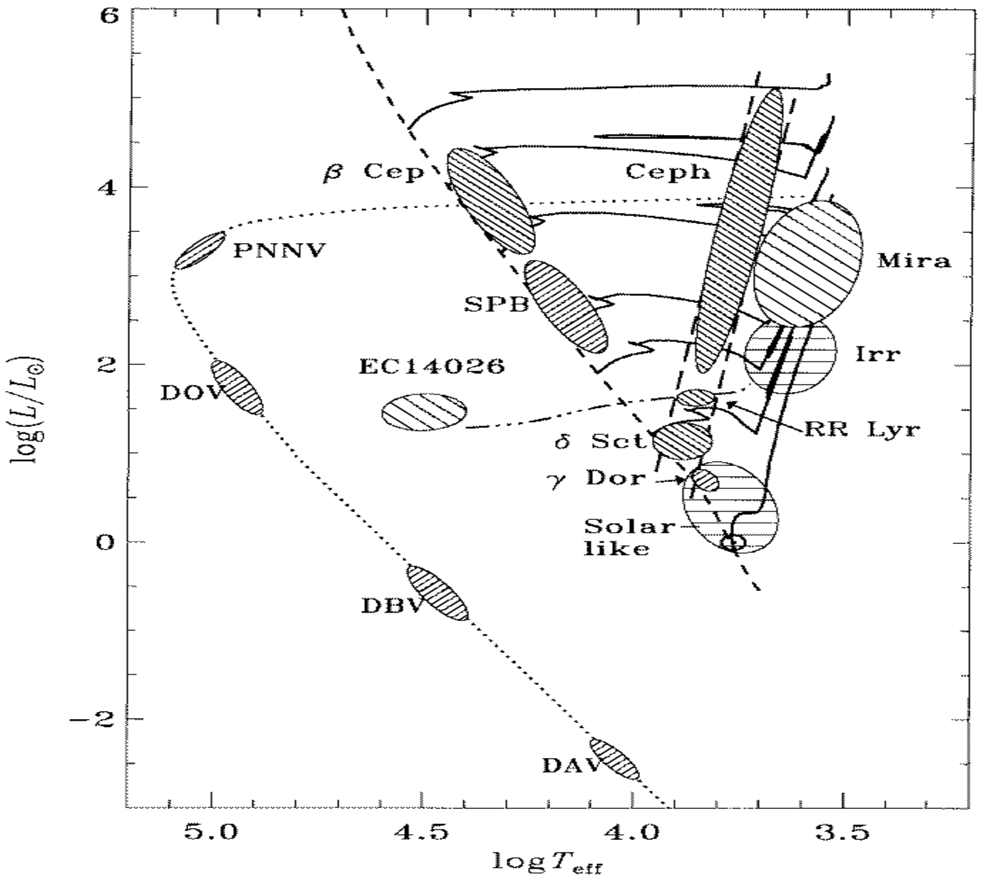

Figure 1.2: The location and names of known groups of variable stars. The δ Scuti stars (δ Sct) are found where the zero age main sequence (dashed line) and the Cepheid instability strip (Ceph) cross. The figure is adopted from Christensen-Dalsgaard [21].

giants in this strip, the amplitude of the variation is large and the periods are long. These are the so-called classical Cepheids. For the stars that are inside the instability strip but on or above the zero age main sequence (ZAMS) one also finds oscillating stars. They have much lower amplitudes and shorter periods: These are the δ-Scuti stars with masses around $2\mathrm{M}_{\odot}$.

It would be very interesting to learn more about the δ Scuti stars. They are main sequence stars with all degrees of development above the ZAMS. Hence in principle one should be able to study all stages of evolution from the ZAMS to the giant stage. These stars all have convective cores and it would be interesting to know more about the physics of convection as this is quite important for the detailed evolution and specifically the lifespan of stars with convective cores. One of the unanswered questions about convective stellar cores is how sharp the boundary between the convective core and the radiative envelope is. The age determination of stellar clusters relies on the fitting of isochrones to observed colour-magnitude diagrams. Some studies of clusters show that models with convective overshooting in the core are needed, *e.g.* Nordström *et al.* [53] and Demarque *et al.* [22].

The oscillations of stars in the instability strip are excited the κ-mechanism as shown by *e.g.* Cox [14]. Stellar models show that in some stars several modes of oscillation can be excited in the ionization zones by the κ-mechanism. Stars are thought to be in complete dynamical equilibrium in their core burning phases but local deviations are indeed possible. When a part of the star contracts due to an oscillation, the temperature and density of the gas will generally increase. The contraction leads to a lower opacity, according to Kramer's opacity, *i.e.* $\kappa \sim \rho T^{-7/2}$: This volume of the star will absorb less energy and hence gradually cool - the area will then expand. This leads to a damping of the oscillation. In the outer parts of the star where the gas is only partially ionized the gas will ionize further due to a contraction and the temperature does not rise significantly. This means that the opacity does not become lower and this volume of gas will absorb more radiation. As the volume expands, the energy "stored" as additional excitation will be released. Thus the ionization zone acts as a heat reservoir and the oscillation is excited.

The location of the ionization zones depends on the structure of the star. The most important ionization zone for stars in the instability strip is He^+ around 30.000 K. This explains the blue boundary of the instability strip: At the blue end of the strip the location of this He^+ ionization zone is very close to the surface where the density is very low and the heat capacity of the zone too small to allow for excitation of oscillation modes. The location of the red end of the instability strip is somewhat more complicated and I refer to more advanced texts, *e.g.* Baker & Gough [4].

In most cases only a few modes have been observed in δ Scuti stars. I have observed FG Vir which is the most well-studied δ Scuti star: 24 modes have been detected by Breger [9]. The detected modes are all of low degree ($l < 3$) as discussed in section 1.6.2.

Calculations of stellar models for main sequence stars inside the instability strip show that several modes of oscillation are to be expected. It is puzzling that only a small fraction of these modes is actually observed. This is a very annoying fact when trying to construct stellar models from observations of oscillation frequencies: Several different models fit the observations but which is the correct one? There have been theoretical suggestions as to explain why only some modes are excited, *e.g.* Dziembowski [23].

For an introduction to the theory of stellar pulsation including a description of the location of the instability strip, consult the lecture notes by Christensen-Dalsgaard [20].

1.6.4 Mode Identification

The detected amplitude of a mode depends on the excitation mechanism in the star - but also on *how* the amplitude is measured. For all stars (excluding the Sun) the stellar disk cannot be resolved. Hence when a star is observed one is measuring the mean value (be it luminosity, colour or Doppler shift) averaged over the stellar disk. For example when determining the amplitude of an oscillation by measuring the Doppler shift of spectral lines, one gets different contributions from the central part and near the edge of the stellar disk. The Doppler shift is a measure of the radial velocity of the oscillation, but as the central part of the disk is moving along the line of sight, the edges of the star are moving perpendicular to this, thus giving no contribution to the Doppler shift (*i.e.* $v_D \propto \cos(\theta)$). When measuring different modes, the measured amplitudes are consequently weighted towards the central part of the disk. When measuring the amplitude of luminosity variations, each part of the disk gives an equal contribution to the measured value.

The measured amplitudes when using Doppler shifts (A_D) and luminosity variations

(A_L) show different dependency of the l value of the mode. As a first approximation the amplitude ratio A_D/A_I will be the same for modes with the same value of l. By comparing the amplitude ratios it would thus in principle be possible to determine which modes have equal l value.

Above I have omitted the effect of limb darkening. This comes about as the light that is observed in fact comes from smaller geometrical depths of the atmosphere of a star when observing the edges of a stellar disk compared to the central part. In fact the intensity measured at the edges is an integral of a more extended part of the upper atmosphere that consists of cooler and less opaque gas. Limb darkening can only be observed directly in the Sun as this is the only star where one can resolve the stellar disk. For other stars one sees the effect of limb darkening indirectly. Because of the dependency of opacity of the stellar atmosphere on wavelength the effect of limb darkening is *larger* for intensity measurements at *longer* wavelengths.

- I have used Strömgren *uvby* measurements of FG Vir and α Cir to examine the wavelength dependency of the amplitude, and hence examine the amount of limb darkening (chapter 8).

Stellar oscillations can also be measured through the equivalent width of spectral lines (EQW $\propto$ area of a spectral line). Bedding *et al.* [7] have shown that the equivalent width of spectral lines depends on the distance to the centre of the stellar disk (like limb darkening in measured intensity). This is explained by the fact that spectral lines of different elements form over a varying extent (*i.e.*depth) in the atmosphere of a star. For example the Balmer (Hydrogen) lines show strong centre-to-variation whereas *e.g.* the FeI line shows essentially no such dependency. To be specific, when measuring the amplitude of a mode in the Balmer lines, the largest contribution to the amplitude comes from the central part of the stellar disk.

As suggested by Bedding *et al.* [7], mode identification can be performed by comparing the amplitude ratios measured by using *e.g.* simultaneous measurements of intensity and equivalent width amplitudes or measurements of the equivalent width of the Balmer lines and FeI.

- Michael Viskum has used the results of both spectroscopy and photometry to try to determine the modes of known oscillation frequencies of the δ-Scuti star FG Vir (Viskum [72]). These results were derived from data obtained from Chile in May 1996 where I participated. The spectroscopy was done with the Danish 1.54m telescope and the photometry was done with the Danish 50cm SAT (Strömgren Automatic Telescope). I reduced the photometric data from 22 nights of observations with SAT. As I contributed to this work, I will discuss the results thoroughly in chapter 8.

When trying to determine which modes one has observed, other problems are also present: How does the rotation of the star influence the modes? How do the modes evolve as the core converts Hydrogen to Helium? Theory predicts that the nature of a mode (p or g-mode) may change during the evolution of a star. When constructing stellar models of an observed star, it is important to take these facts into account. When comparing observations with stellar models, generally several models fit.

- One way to get ahead is to determine the basic stellar parameters of the observed stars: $T_{\text{eff}}, [Fe/H]$, age, and distance. This is exactly what the results of this thesis will yield in the case of the six known δ Scuti stars in the open cluster NGC 6134 (chapter 5 and 9), as was mentioned in the preface of this thesis.

For a specific and more thorough description of the issues discussed here, consult the introductory notes by Christensen-Dalsgaard [20] or the work by Bedding *et al.* [7].

Chapter 2

Observations of the Open Clusters NGC 6134 and NGC 3680

From April 29th to May 3rd 1996 I observed the two southern open clusters NGC 6134 and NGC 3680. I used the Danish 1.54m telescope with the Strömgren $uvby - \beta$ filters in the filter wheel of the DFOSC (Danish Faint Object Spectrograph and Camera). An introduction to the Strömgren photometric system is given in appendix A.

In this chapter I will first describe the known properties of these two objects before giving an account of the observations I have made.

2.1 Properties of NGC 6134 and NGC 3680

In this section I will give a short presentation of the open clusters I have observed. This includes known basic parameters of the clusters, finding charts, and a summary of earlier observations.

In table 2.1 I present the known basic parameters of NGC 6134 and NGC 3680. The data for NGC 6134 are taken from Kjeldsen *et al.* [38]. The metallicity of $[Fe/H] = 0.25$ is taken from Lyngå [45] while Claria *et al.* [13] have found $[Fe/H] = 0.05$ by using red giants in the cluster. The data for NGC 3680 are taken from Nordström *et al.* [53]. Estimated uncertainties (the standard deviation quoted in the published papers) on distance modulus $(V - M_V)$, age, turnoff mass, interstellar reddening $(E(b-y))$, and metallicity $([Fe/H])$ are about 0.2, 0.3, 0.1, 0.005, and 0.05 respectively for NGC 3680. For NGC 6134 the uncertainties for the same parameters are 0.2,0.2,-,0.04 and 0.1. Note that the turnoff mass has not been estimated by Kjeldsen *et al.* [38].

A few things should be noted: As can be seen from the table, both clusters are *young* open clusters. The distances are similar but the reddenings differ. The turnoff of NGC 6134 is inside the instability strip.

2.1.1 NGC 3680

In figure 2.1 I present a finding chart for the open cluster NGC 3680. This is also the applied reference frame, *i.e.* the star numbers of all measurements correspond to the star numbers of this frame. A few of the reference star numbers are indicated (corresponding to

Table 2.1: Basic parameters for the observed open clusters

NGC	α (2000.0)	δ (2000.0)	d (kpc)	V - M_V	Age/Gyr	M_{TO}	$E(b-y)$	$[Fe/H]$
6134	16^h24^m	$-49°09$	0.91	11.25	0.89	-	0.32	0.25/0.05
3680	11^h25^m	$-43°14$	1.26	10.50	1.45	1.9	0.034	0.11

the numbering of Nordström *et al.* [53]). The exact location (x, y) of each star is available along with the results of the Strömgren photometry of this thesis through anonymous `ftp` as described in appendix F.

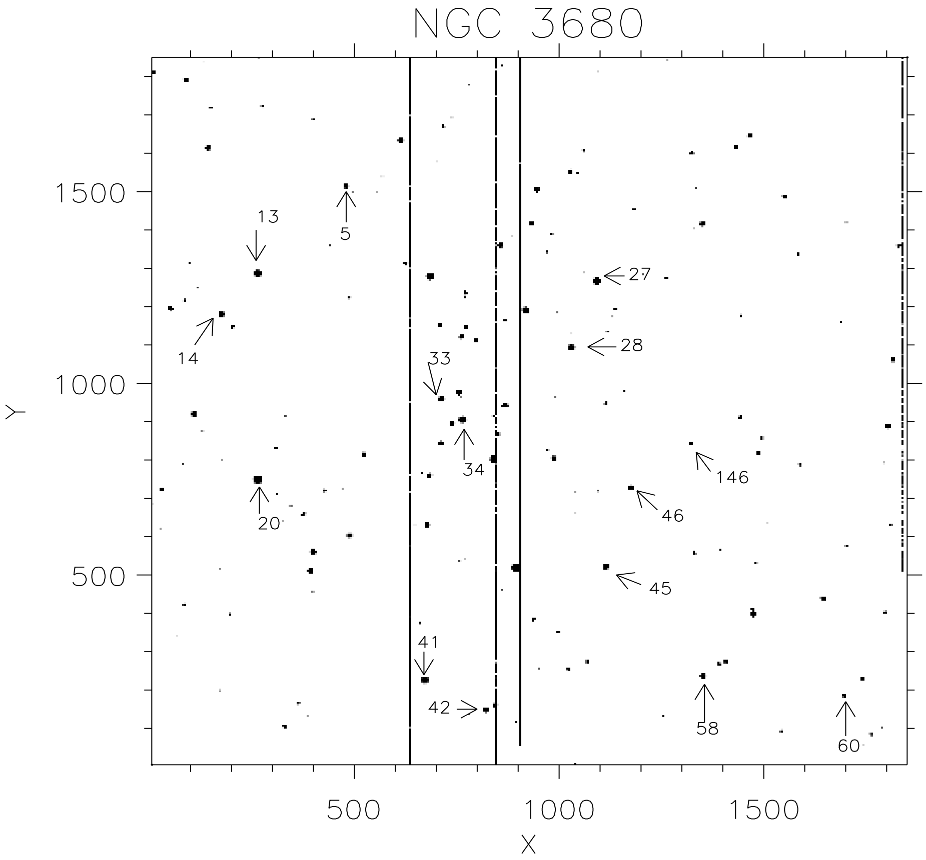

Figure 2.1: CCD reference frame "dfsc1856" of the central part of the open cluster NGC 3680. The numbers of a few stars have been indicated, which correspond to the numbering used by Nordström *et al.* [53]. Note the three bad columns on the CCD.

NGC 3680 has been observed many times before in very great detail. There are four important papers: These include the early work by Eggen [24] 1969 (UBV) and later by Nissen [49] 1988 ($uvby - \beta$). Their data are both photoelectric measurements of the brightest stars in the cluster. CCD photometry has been carried out by Twarog *et al.* [68] 1989 ($uvby$) and Nordström *et al.* [53] 1996 (by). The study by Nordström *et al.* also includes radial velocity measurements to test for membership and dynamical properties of the cluster. For a thorough comparison of the four sets of observations consult Nordström *et al.* [53].

The detailed radial velocity measurements by Nordström *et al.* of 109 stars gave the following result: About 60% of the observed stars are field stars. Of the remaining cluster members more than 50% are binaries. This information explained the earlier discovery of a "bimodal turnoff" by Nissen [49]: One plausible explanation given by Nissen at that time was that the observed stars were actually two slightly different stellar populations of different age and/or metallicity. With the radial velocity data Nordström *et al.* were able to distinguish which stars were cluster members in the observed colour-magnitude diagram. It turned out that *one* well defined isochrone could be fitted to the distribution of cluster stars. It should be mentioned that the theoretical isochrones that include overshooting in the convective core gave the better fit.

An interesting conclusion in the article by Nordström *et al.* is that the stars of the cluster with masses less than 1.5 $\mathrm{M}_\odot$ are all binaries. When a cluster is formed the majority of mass is found in stars of low or moderate mass (*e.g.* $\mathrm{M} < 2\ \mathrm{M}_\odot$). Consequently many light stars should be expected in *very* young clusters. N-body simulations of the dynamical evolution of a distribution of stars show that indeed light stars "evaporate" from the cluster as they are weakly bound to the cluster, *e.g.* Eggleton [27]. But this does not include the binary systems whose total mass is larger.

Another source of mass loss from a cluster is the gradual conversion of the most massive stars into white dwarfs or even neutron stars. In the last stages of stellar evolution of these stars a severe mass loss occurs due to the loss of the envelope. It is even dubious if the remnants of these dead stars are still gravitationally bound to the cluster. By assuming reasonable conditions, Nordström *et al.* find that the initial mass of the cluster was of the order 1200 $M_\odot$ ($\sim$ 2000 stars) and today 3% of this mass is left in the remaining cluster members (around 70 stars).

- To conclude I note that the results of this thesis will improve our knowledge of NGC 3680. This cluster has already been observed in the Strömgren filters, although previously the β indices have only been determined for eight turnoff stars. Most importantly, previously published results rely on a standard transformation based on the observations of the turnoff stars by Nissen [49], *i.e.* using a very limited range in $b - y$. As noted by Nordström *et al.* [53] the calibration of the fainter stars of the cluster may be erroneous. I use standard stars with a greater range in $b - y$ which will improve the calibration of these stars.

2.1.2 NGC 6134

In figure 2.2 I show the reference image for NGC 6134 with the star numbers of the variable stars indicated. The (x, y) positions of the stars and the Strömgren photmetry of this thesis are available through anonymous `ftp` as described in appendix F.

This cluster has not been observed as much as NGC 3680. The most recent observations were made using broadband UBV filters and were carried out by Kjeldsen and Frandsen in 1989 [37] and 1991 [38] who determined the interstellar reddening and estimated the distance and age of the cluster, *cf.* table 2.1. Their photometry was supplemented with the observations by Viskum [71] (1994). High speed photometry has been done by Frandsen

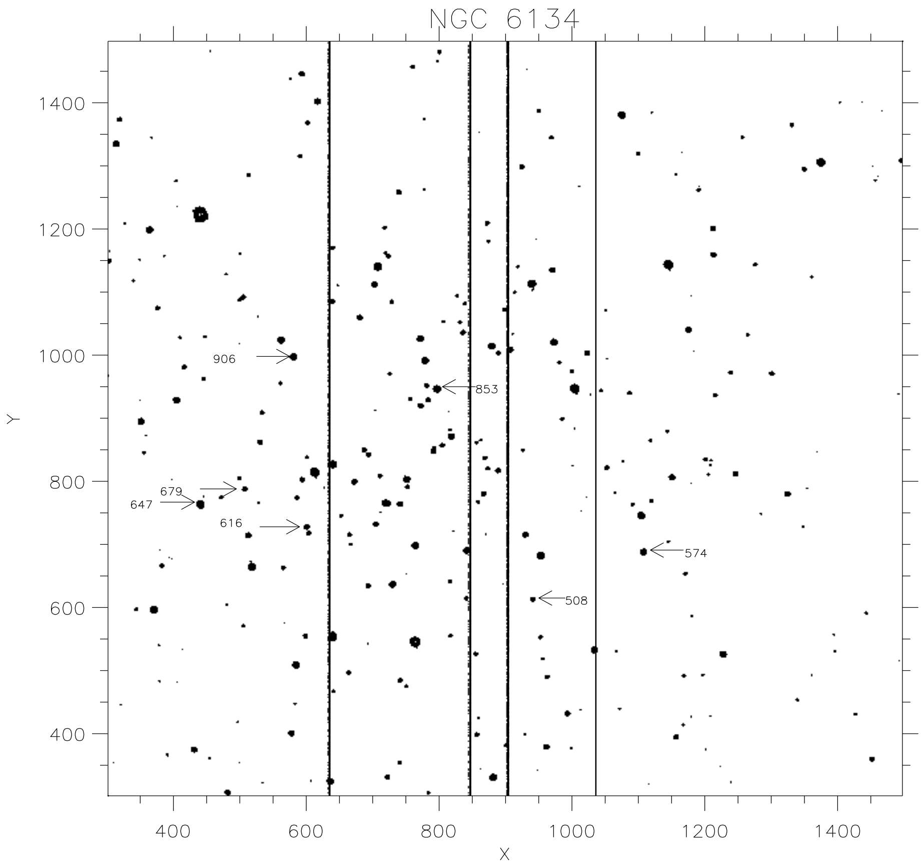

Figure 2.2: CCD reference frame "dfsc1448" of the central part of the open cluster NGC 6134. The star numbers of the known variable stars are indicated. Three of the bad columns on the CCD are also seen.

et al. [29] (1996) in order to detect variable stars. They found six variables of δ Scuti type and one blue straggler. According to the CMD found by Viskum [71] the δ Scuti stars are all among the most massive stars in the cluster, *i.e.* they are located in the turnoff region. This is also inside the instability strip that predicts the location of the observed δ Scuti stars.

The star numbers of the known variables are (508,574,616,*647*,679,853,906) which correspond to stars (397,348,159,*53*,87,161,9) in Frandsen *et al.* [29], *cf.* table 9.1 in this thesis. The star number printed in *italics* is the star number of blue straggler.

Claria *et al.* [13] have examined the red giants of NGC 6134 to infer the interstellar reddening and metallicity of the cluster. As noted earlier, their results do not agree with the metallicity found in the catalogue of open clusters by Lyngå [45], *cf.* table 2.1.

- With the Strömgren photometry presented in this thesis I will be able to determine essential properties of NGC 6134: The distance, age, interstellar reddening, and the metallicity of the cluster - hopefully with greater accuracy than what has been achieved earlier, as both the quantity (more stars) and quality (flat field correction, intermediate band filters) of the photometry is good.

2.2 The Danish 1.54m Telescope and the DFOSC

During the nights from April 29th to May 3rd 1996 I used the Danish 1.54m telescope at La Silla. All nights were "photometric" although some haze was visible in the morning on some nights. The seeing was in the range 1.2-1.8".

The telescope was mounted with a Loral/Lesser CCD (Charge Coupled Device) camera. A CCD is a two dimensional array of light sensitive pixels that detect incoming photons. The Loral/Lesser CCD has 2052 by 2052 such pixels. Each star covers 3-8 pixels when the seeing is good. A CCD has a very high quantum efficiency in a wide interval in wavelength - around 70% of all photons in Strömgren b and y are detected. Much of the light is lost before it enters the CCD camera, though - in the optics of the telescope and the DFOSC (Danish Faint Object Spectrograph and Camera). Around 10% of the light entering the telescope is detected.

Unfortunately, the Loral/Lesser CCD mounted on the Danish 1.54m telescope was not sensitive to the most energetic photons, *e.g.* in the wavelength range of the Strömgren u-filter. This means that the Strömgren photometry is not complete. The sensitivity of the pixels falls off rapidly when going from the centre to the edges of the CCD. According to the telescope manual, this is due to a failed UV-flood, which also explains the lack of sensitivity in u. For this reason only the central 1850x1850 pixels have been used for photometry. Another fault of the CCD was the eight bad columns: Vertical lines of pixels with unreliable signal which may be due to the amplification process when the CCD signal is read out (amplifier B in high gain was used).

The field of view covered a large area of the sky: 13.3' by 13.3' - which meant that a large part of both open clusters could be covered within one frame. I have included more details about the CCD in table 2.2.

Table 2.2: CCD statistics for Loral/Lesser CCD (W11-4)

Area Covered	2052 X 2052 pixels
Field of View	13.3' X 13.3' ($\simeq$0.39"/pixel)
Conversion factor	1.31 e^-/ADU (High gain)
Readout Noise	7.2 e^-
Bias Level	$\simeq$ 490 ADU
Dark Current	$\simeq$ 2.5 $^-$ / pixel / hour at -100°C
Bad Columns	734,735,946,947,1005,1006,1137,1840
Cooling	Nitrogen

2.3 Observations of the Open Clusters

I have done $vby-\beta$-photometry of about 160 stars around centre of the cluster NGC 3680. A log of observations is found in table 2.3. A more comprehensive list of observations including exposure times, airmass *etc.* is found in appendix C.

I have also done $vby-\beta$-photometry on NGC 6134. About 700 stars have been observed around the central part of the cluster. The basic parameters for the cluster - like interstellar reddening and metallicity - are quite uncertain. As mentioned earlier six δ Scuti stars and a blue straggler have been detected in the cluster by Frandsen *et al.* [29]. The goal that I hope to achieve with the Strömgren photometry is also to derive precise effective temperatures of these variable stars.

As hinted at in section 1.6.4, when knowing both the basic parameters of the cluster and the previously determined pulsation periods - it will be possible to construct detailed models of the stars. Of course it would also be necessary to know which stars are actually members of the cluster in order to use the parameters derived for the cluster. It also turns out that the rotational velocities of variable stars affect the pulsation periods in a subtle manner. My advisor Søren Frandsen has been granted observing time for doing spectroscopy of stars in NGC 6134 in spring 1999. The combination of all these pieces of information will allow for the ultimate test of stellar modelling of these stars. As all constraints from the observed properties of the stars must be met, it will be possible to investigate, *e.g.* the amount of convective overshooting in core.

Table 2.3: Log of observations of the open clusters NGC 6134 and NGC 3680 in the Strömgren filters. The two β filters are labelled Wide and Narrow.

Cluster	u	v	b	y	β(W)	β(N)	Total
NGC 6134	(1)	19	18	24	10	14	85
NGC 3680	0	11	17	9	7	8	52

As seen from table 2.3 I obtained 85 frames of NGC 6134. The exposures were deliberately taken with the stars positioned differently on the frames: The telescope was sometimes shifted a few arc seconds and/or the CCD camera was rotated 180 degrees. This was done in order to correct for an expected error in the flatfields due to scattered light problems. I will describe this procedure later in section 3.3. A complete log of observations is presented in appendix C.

Chapter 3

Photometric Reductions

In this chapter I will describe my laborious efforts of calibrating the CCD photometry obtained with the Danish 1.54m telescope. This includes fundamental calibrations of the CCD but also the photometric reductions of the open clusters and the Strömgren standard stars. A key issue of this thesis is my attempt to correct for large scale flat field errors, which will be described carefully in this chapter.

3.1 CCD Calibration

In order to calibrate the CCD photometry of the open clusters and obtain the Strömgren standard colours, I made five kinds of exposures. These are described briefly below. In the following I will then go through the steps taken by using the information derived from each different type of frame.

- A series of flat field exposures with increasing integration time to examine the linearity of the CCD .
- Bias frames to correct for the offset charge on the CCD.
- Flat fields: In order to correct for an expected variation in the sensitivity to light of each pixel on the CCD I took exposures of a homogeneous light source. At dusk and in the early morning I took exposures of the sky in areas with no stars. In the day time I also took some "domeflats" - using a quartz lamp to illuminate the inside of the dome. Exposures were taken of a clean white surface on the inside of the dome. This was done in all Strömgren filters.
- The target objects were the open clusters NGC 6134 and NGC 3680. I took exposures in five of six Strömgren filters: vby and β(W+N). I only took one 30 minute exposure in u to confirm that the CCD was not sensitive to light in this wavelength range.
- In order to convert the instrumental magnitudes to the Strömgren standard system I observed 19 Strömgren standard stars selected from the catalogue by Erik Heyn Olsen (EHO) [54].

In the next sections I will describe the CCD calibration: Linearity test, bias subtraction, and flat fielding. After these reductions I have used the software package "MOMF" to reduce the frames of the open clusters, which will also be described carefully. Following these "basic reductions", I will turn to the description of the flat field correction in section 3.3. For the reduction of the standard stars I wrote an IDL programme to do aperture photometry as the stars were defocused to different degrees. This is described in section 3.4. The extinction correction and standard transformation will be carried out in chapter 4 by using the results of the present chapter.

3.1.1 Linearity of the CCD

Ideally the signal that is read out from the CCD will depend linearly on the flux of photons. In other words, a short and a long exposure should give the same number of photons per second. At some level all CCDs suffer from nonlinearities, at least when the count level is close to the saturation limit of the CCD. According to the telescope manual the Loral/Lesser CCD should be linear within 1%, Storm [65].

The output of the CCD is measured in ADU (Analogue to Digital unit) which may be converted to the flux by multiplying with the gain factor for the CCD. I used the CCD in high gain and the conversion factor is 1.31 photons per ADU. The flux is obtained by dividing by the exposure time. The magnitude can then be calculated by using $m = -2.5 \log F + C$, where F is the flux and C is some constant.

To examine any non-linearities in the sensitivity of the CCD, I took flat field exposures (without any filter). The following series of measurements were made with "exposure times": 1,2,1,3,1,4,... *etc.* up to 33. The exposure times are measured as *the number of times the shutter has been opened*. This was done in order to be able to ignore any dead time in the shutter.

After subtracting the bias level of each flat field, I determined the average ADU level in a box of 200×700 pixels near the centre of the CCD: Between the two bad columns at $x = (735, 946)$. The mean value of all exposures with n openings of the shutter ($ADU(n)$) was then divided by n times the ADU level in an exposure with just one shutter opening ($ADU(1)$). Ideally this value, $L(n)$, should be equal to 1 for all n:

$$L(n) = \frac{ADU(n)}{n \times ADU(1)}. \tag{3.1}$$

$ADU(1)$ was determined from the short exposures ($n = 1$) taken just before each of the longer exposures, *i.e.* exposures with $n > 1$. The values of $L(n)$ have been plotted for $n = 1 - 33$ as a function of $ADU(n)$ in figure 3.1.

As can be seen from the figure, the spread in $L(n)$ is up to 5% at all values of $ADU(n)$. A mean value of about $<L> \simeq 1.00 \pm 0.02$ is found. It is not possible to determine any systematic trend from this data. The explanation of this result could be that the light source (quartz lamp) that was used is variable at the observed 5% level over a period of a few minutes. Two points seem to deviate strongly from the mean at ~ 21000 and ~ 52500 ADU. This is thus explained by a significant change in the flux from the quartz lamp.

The conclusion of the linearity test is that no non-linearity can be traced from the calibration data. A non-linearity below 2% could be present. In the following reductions I

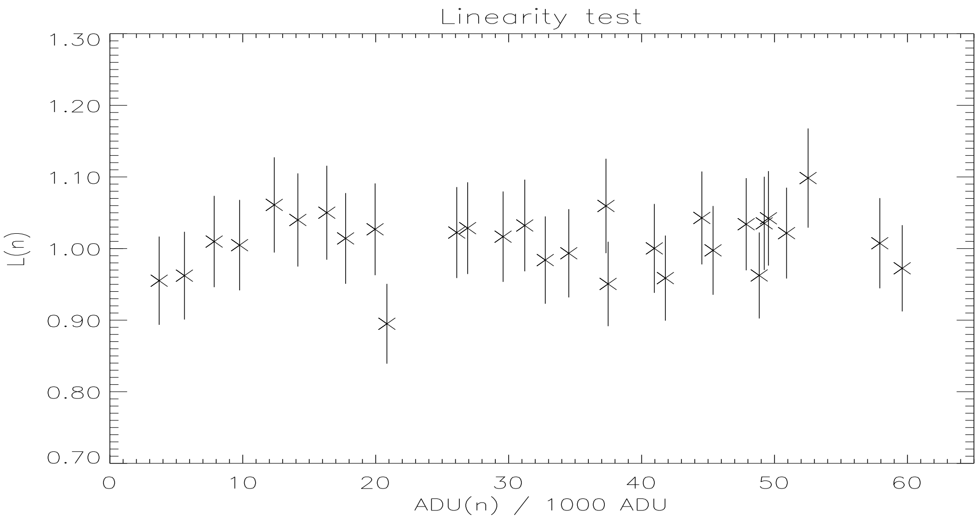

Figure 3.1: The result of the linearity test. It is not possible to detect any non-linearity below the 2% level from these data.

have rejected all measurements with a pixel level above 50000 ADU when doing photometry - for safety's sake. The saturation limit of the CCD is 65535 ADU.

3.1.2 Bias Frames

Some CCDs have an overscan region, *i.e.* an array of pixels where no light is detected. The mean of this region gives the mean bias level on each frame. This is not the case for the Loral/Lesser CCD that I used. Therefore I took several 0 second exposures to obtain the bias level.

Actually it was also necessary to take two kinds of bias frames. For the open clusters the whole CCD (2052 $\times$ 2052 pixels) was read out - but for the EHO standard stars only the central part of the CCD was read out, *i.e.* a "window" of 750 $\times$ 400 pixels. It turned out that the bias level was somewhat smaller when bias frames in this window were taken compared to the bias full frames. There was also a 5% gradient from left to right on the window frames not seen on the bias full frames. This effect probably comes about in the readout procedure (the amplification of the signal *etc.*). In figure 3.2 I have shown plots across a row in a window and a full bias frame. Note that the plotted rows are identical on the CCD.

It was expected that the slowly varying temperature of the instrument would affect the bias level. Consequently, several bias frames were taken during the nights in order to map this. The observed signal in each pixel (x, y) can thus be written as:

$$\mathrm{ADU}_{(x,y)}(\mathrm{obs}) = \mathrm{ADU}_{(x,y)}(0) + \mathrm{BIAS}_{(x,y)}(\mathrm{T}_{\mathrm{inst}}) \tag{3.2}$$

For the full frame bias images I found that the ADU level indeed varied with temperature but with the same slope and mean level on each night. The temperature T_{inst} is printed in the header of each output file and is labelled T_{AMB}. This is an "ambient"

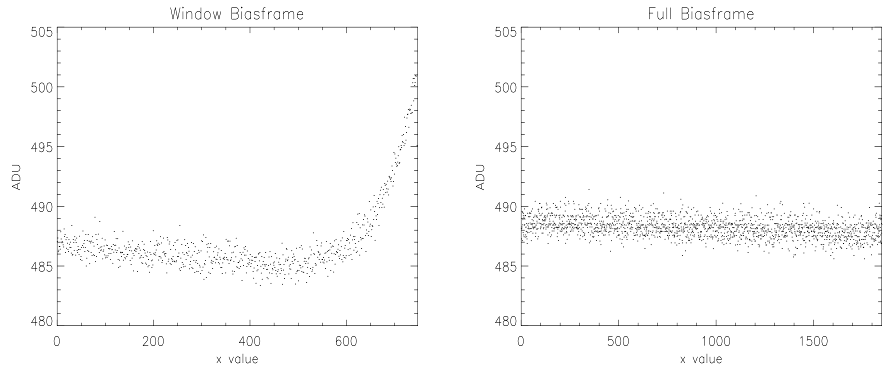

Figure 3.2: Row 925 in the window (left) and full frame bias (right) at $T_{\mathrm{AMB}} = 12.5$. These are the master bias frames made from the sorted median values of several bias frames.

measure, *i.e.* a smoothly increasing function of the temperature of the instrument (private communication: Anton Norup Sørensen, IJAF, Copenhagen).

The result is presented in figure 3.3. A linear relation between the bias level and T_{AMB} is assumed. This relation was found fitting the mean bias level of each frame as a function of temperature. The result of the linear fit is:

$$BIAS(T_{\mathrm{inst}}) = 476.9 + 0.9063 * T_{\mathrm{inst}} \tag{3.3}$$

The deviation from this relation is below 1 ADU. Changes in the bias level of this order are thus expected in the science frames. These differences will be subtracted in the reduction process, *i.e.* the background determination.

In order to correct for the pixel to pixel bias level differences I constructed a "master bias frame" using all bias frames after having corrected for the temperature dependency. The bias level of each pixel was found by taking the median from all bias frames. Values more than 3σ above the median were removed and the average of the remaining values was used in the "master" bias frame.

The same analysis was done for the window bias frames, but I found no temperature slope in the bias level. I have constructed a master bias frame like I did with the full bias frames. In figure 3.3 I have also shown the results for measured ADU levels of all window frames (lower right corner). Note that a significant spread in the ADU level is found - especially on the nights of May 2nd and 3rd. As discussed previously changes in the bias level are removed in the reduction process, *i.e.* when the background level is determined.

3.1.3 Flat Fields

It is expected that each pixel on the CCD (x, y) has different sensitivity to light. After correcting for the bias level of a flat field the observed number of ADU can be expressed as:

$$\mathrm{ADU}_{(x,y)}(\mathrm{obs}) = \mathrm{ADU}_{(x,y)}(0) * FF_{(x,y)}(\mathrm{filter}), \tag{3.4}$$

where FF describes the sensitivity of each pixel (x, y) for a given filter: $vby - \beta$.

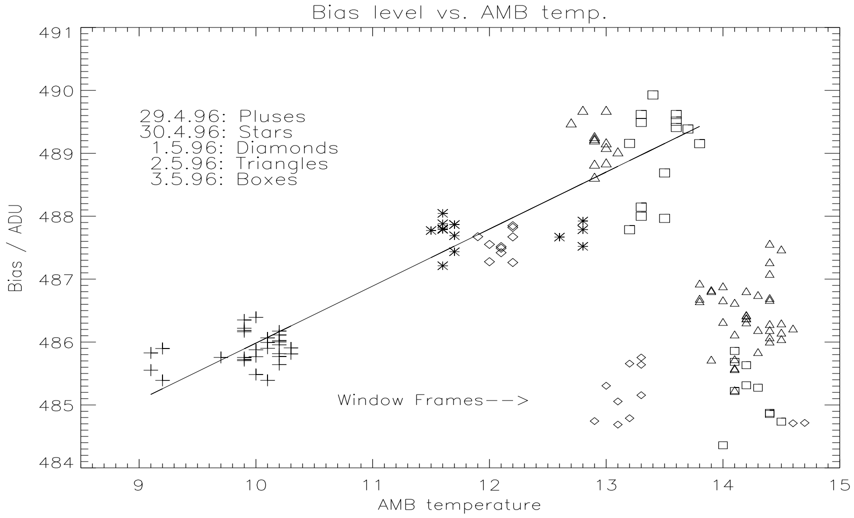

Figure 3.3: Bias level temperature dependency. On the abscissa is the AMB temperature and on the ordinate is the "3σ sorted" mean value of the central part of each bias frame. The points have been labelled according to the corresponding night of each observation. The window bias frames are the points to the lower right which show no significant dependency on temperature. The full frame bias images do show such dependency and a linear fit has been made to the points (equation 3.3).

To find the relative sensitivity of each pixel I took frames of evenly illuminated light sources: 1) Exposures of the sky at dusk or in the early morning (sky flats). 2) Exposures of the dome illuminated with a quartz lamp (dome flats). As for the bias frames I took flat fields with a full frame readout and a few using the 750×400 window. As might have been expected the window and full frame flat fields were very much alike, so I have used the full frame flats to correct both kind of frames.

On the other hand, I found out that the sky flats changed each night but that the dome flats were more "stable". For example one sky flat would show a gradient across the frame whereas in another exposure 5 minutes later (with the sky becoming brighter) there is no such gradient. In sky flats gradients can be explained by the variation of the brightness across the sky. With a field size of 13.3'x13.3' the gradient is estimated to be around 1% according to Andersen *et al.* [3]. If sky flats are used, errors of this size will be present. The described effect of a changing gradient within few minutes of observation cannot be explained by this. Instead of examining the unstable sky flats I have only used domeflats to determine the FF function for each filter. In each filter six-ten domeflats were obtained.

I found no significant change in the dome flat fields from night to night. This may be due to the fact that I did not take enough flat fields in order to detect such a variation or it may be because of the stability of the CCD sensitivity. I found the FF-function for each filter using the following procedure: For each flat field frame I found the mean value around the centre of the CCD (500 x 500 pixels, excluding bad columns) and normalized each frame with this value. Then I used all the normalized flat fields from all nights to find the "sorted average value" of each pixel, *i.e.* excluding measurements more than 3σ above the median value. In figure 3.4 I have presented two plots of the master flat field in the y filter. The plots show the normalized value along a column and a row at $x = 925$ and $y = 925$ respectively.

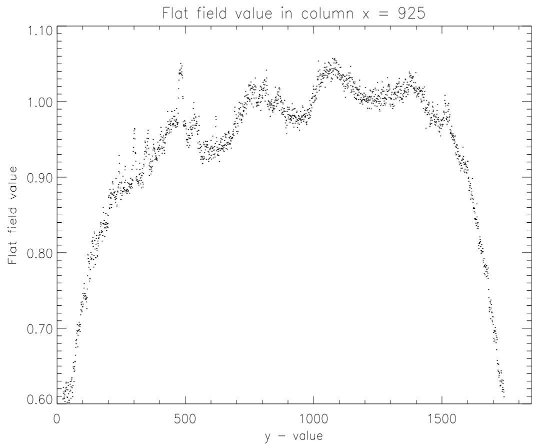

Figure 3.4: Values along the column $x = 925$ and row $y = 925$ of the master flat field in the y filer.

I should point out that the two β filters have the same central wavelength (*cf.* appendix A): As expected the flat fields are almost identical. The count level is much higher in $\beta(W)$ flats and I have used these to determine the master flat field for both β filters.

3.2 Photometry of Open Clusters

In this section I will describe the photometric reduction of the open clusters. This includes an introduction to the reduction software I have used (MOMF) and a description of how I have analysed and handled the output from the programmes.

3.2.1 The MOMF software package

Each frame was bias subtracted by using the bias master frame and the derived temperature dependency (equations 3.2 and 3.3). Then each frame was divided by the normalized flat field for the corresponding filter. To determine the instrument magnitudes, the MOMF reduction package by Kjeldsen and Frandsen [41] was used for the open clusters.

MOMF (Multi Object Multi Frame) is designed for the reduction of semi- and non-crowded fields. As opposed to other photometric software that use *either* aperture or PSF photometry (like DAOPHOT [63]), MOMF uses a *combination* of PSF-fitting and aperture photometry. Let me describe these two methods for determining the magnitude of a star.

With aperture photometry the magnitude is determined by placing an aperture around the centre of a star and counting the number of ADU in the aperture. The contribution from the background is determined by placing two concentric apertures with different radii centred on the star: By calculating the number of ADU between these two apertures the mean background level is determined.

PSF is the abbreviation of Point Spread Function. This function describes the structure of stars as seen on the CCD frame. A simple example is a two-dimensional Gaussian function. Real (observed) PSFs are more complex, however. Ideally stars are point sources, but the light is smeared as the light goes through the atmosphere of the Earth, and through the optics of the telescope and detectors. MOMF determines the PSF empirically from bright isolated stars on the CCD frame. The magnitude of each star on the frame is then determined by a simple scaling factor multiplied by the PSF which is centred on the target stars.

Generally PSF fitting gives the best result for faint stars whereas aperture photometry is a more secure method for bright stars. One problem with aperture photometry occurs if the field is crowded - in this case the light from neighbouring stars will inevitably be included in the magnitude determination. This problem is solved by using a PSF. On the other hand the PSF model is assumed to be the same for all stars everywhere on the CCD which is generally not the case.

As mentioned MOMF determines the magnitudes of stars by using an empirical PSF. The magnitude is then corrected by using aperture photometry. In this way - by choosing the right size of the aperture - the noise level will always be lower than if PSF or aperture photometry was used alone.

The basic steps in reducing each frame when using MOMF are these:

- The FIND routine detects the positions of the stars. If more than one frame is reduced at a time, a set of reference stars is chosen in order to detect any offset in position (due to errors in tracking, usually not more than a few pixels).

- MOMF selects suitable stars for the empirical PSF model, which can be either accepted/rejected interactively. I have rejected stars near the bad columns (<20 pixels) or near the edge of the CCD (<300 pixels). The PSF is purely empirical. It consists of two terms - a function describing the core, and a lookup table of residuals that are not removed by the core function. The fitted core function is of the form: $PSF = PSF_0 \exp(-r^2/S^2(r))$, where $S(r)$ is a function determined by the fit and r is the distance from the centre of the PSF.

- The sky background is determined as the median after three repeated 3σ clippings of the value of pixels between two concentric apertures centred on the position of each star. Note that close neighbouring stars will be included in this first background estimate, although the σ clipping will remove any high counts.

- By using the empirical PSF the stars are subtracted one at a time starting with the brightest star. Close neighbouring stars will always be fainter than the present star.

- When all stars have been removed, the sky value is redetermined, giving a more accurate result.

- As the PSF model is not perfect - due to *e.g.* the variation of the PSF across the field - MOMF now determines the correction to the PSF magnitude using aperture photometry of each star. MOMF determines the final magnitude using six different apertures with increasing radii. These radii are scaled according to the seeing (FWHM of the PSF stars). Typically radii of 3-10 pixels are used.

The output from MOMF is a list of star numbers, with corresponding coordinates and derived magnitudes using either of the six apertures. The frames of the open clusters NGC 6134 / 3680 each has about 700 / 150 stars. An example of the output file from MOMF is given in appendix D.

At the top of the output file are the six radii of the apertures. The magnitudes in each aperture is normalized according to the total flux in the PSF stars. When comparing frames, it is necessary to remove this zero point. The derived MOMF magnitude is expressed as

$$m = m_{\mathrm{PSF}} - 2.5\log(F), \tag{3.5}$$

where m_{PSF} is the zero point, and F is the measured number of ADUs.

As will be described in section 3.3, I have made exposures with different rotations and offsets in order to detect errors in the flat field. Consequently, the routines for locating the positions of the stars and extracting the magnitudes have to be run several times. In the log of observations of the two clusters (appendix C) I have written the set-numbers which correspond to frames with the same positions of the stars. For each set the finding routine was used (about 30 times each taking about one hour of computing time due to the large field). Once the FIND routine is finished the magnitudes are determined swiftly (taking around 5 minutes for each frame).

3.2.2 Choosing MOMF Aperture Size

In the following I will take a closer look at the derived MOMF magnitudes. The output files contain the determined magnitudes, when using six apertures with increasing radii (in y typically from 3-8 pixels). The radii of the six apertures of MOMF increase from ap1 to ap6. The sizes are scaled by the width of the PSF stars used in the reduction, and they depend on the seeing at the time of observation. Therefore the sizes of ap1-ap6 generally differs from one frame to another: But results when using different aperture radii are indeed comparable because of the scaling with the PSF stars on each frame. It should be noted that differences are expected using different aperture sizes, *e.g.* ap1 and ap6. For example the effect of neighbouring stars will be smaller when using a smaller aperture, but in this case the magnitude will be less reliable for faint stars. I have thus investigated the effect of applying different aperture sizes.

In figure 3.5 I show four plots of differences between the standard deviation of the y magnitude when using different MOMF aperture sizes (ap3 to ap6) as a function of magnitude. The standard deviation is calculated by using all the y frames of NGC 3680 after flat field correction and the removal of offsets between the frames.

As can be seen, the standard deviation when using apertures ap5 and ap6 are almost the same independent of magnitude, although there are differences for faint stars. This can also be seen when comparing apertures ap3 and ap4. But there are severe differences when comparing apertures ap3 and ap5 or ap4 and ap5: Most of the faint stars have larger deviations when using the larger aperture.

From this analysis I have chosen to use magnitudes with aperture ap4.

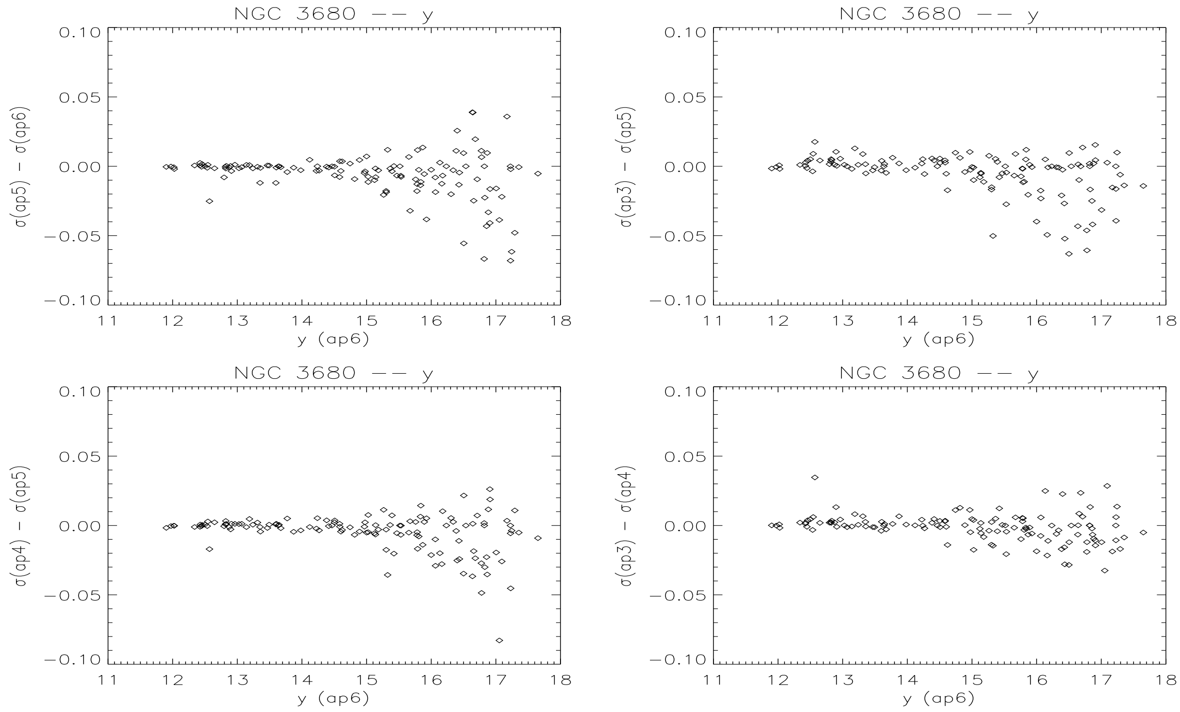

Figure 3.5: The four plots show differences between the standard deviation as a function of magnitude when using different aperture sizes, - *e.g.* ap6 is aperture 6.

3.2.3 Linking Measurements of Stars on Different Frames

On each frame with a different rotation angle of the camera or telescope offset the stars will have different positions of the CCD. To be able to combine the measurements of each star on all frames I have to make an identification (id) list for each frame. The id-list for each individual frame contains two numbers for all detected stars. The first number is the star number assigned by MOMF in a given frame and the other number refers to the star number in a reference frame. For NGC 6134 I have chosen the frame “dfsc1448” as the reference frame - a 70 seconds exposure in the y filter. For NGC 3680 the reference frame is “dfsc1856” - a 110 seconds exposure in the b filter. Actually the coordinates of the stars in these reference frames are found from the combination of several frames with the same telescope offset and rotation angle. For NGC 6134 only two frames have been used while 14 frames were used for NGC 3680 - in this way very faint stars are also detected.

For NGC 3680 I have inspected frames with large telescope offsets to determine the position of stars that lie outside the field of the reference frame. In this way the reference list was expanded with about 20 stars. The same task could have been done for NGC 6134, but I have not done this.

I have used the *Perl* script `xyfer3` to find the id lists (written by Søren Frandsen). The programme needs 3-8 input stars with (x, y) positions and corresponding star id numbers of the reference and input frame. The offset and rotation needed to fit these stars are then determined. When this is done the script determines which star id numbers correspond to each other for all observed stars. Stars that are more than 2 pixels off after the rotation and offset has been applied are rejected. The file names of the reference lists are found in the observation logs in appendix C.

To be able to compare the derived magnitudes of each star on different frames I have written a small IDL routine. This routine runs through a loop where the derived magnitudes from the MOMF result files are read into an array for each frame. The stars are then sorted into an array using the id lists. This array has entries (i, j, k) where i is the frame number, j is the star number in the reference frame, and k can take three values: 0 and 1 is for x- and y-position while $k = 2$ is the measured magnitude on frame i for star j. An example is NGC 6134 where the dimensions of the array for the y filter are (22,1602,3), - 22 frames, with (up to) 1602 stars, each with information about position on the CCD and the derived magnitude. If a star is not present in a frame or has been labelled "bad" by MOMF, the magnitude is set to 99.999.

In another array the airmass, exposure time, and night of observation of each frame i are stored. This information is read from the observation log which is also printed in appendix C for each open cluster.

As noted in the description of the MOMF software the magnitude in each aperture is normalized to the flux in the PSF stars. At the top of each MOMF output file a number indicates what the zero point of the magnitudes is, *cf.* equation 3.5. By subtracting this value (generally different from frame to frame) from the raw magnitudes, the magnitudes will be in the same system. This is done in another short IDL routine which also corrects for the different exposure times of the frames. The magnitudes are all converted to one second exposures: The number of ADU corresponding the (zero point corrected) MOMF magnitude is divided by the exposure time. The new magnitude is determined by using:

$$m_{ij} = -2.5 \log(ADU_{ij}/t_{\mathrm{exp},i}), \tag{3.6}$$

where $t_{\mathrm{exp},i}$ is the exposure time for frame i and ADU_{ij} is the count level determined by the MOMF magnitude in frame i for star j.

There are still offsets present in the magnitudes from frame to frame. This is due to the combination of these effects: 1) The exposures are taken over 5 nights at different airmasses and with (presumably) different extinction coefficients. 2) Errors in the flat field. 3) The presence of bad pixels or bad columns of the CCD. 4) Signal from cosmic rays that have hit the CCD during the exposure or readout. 5) The error introduced when trying to determine the magnitudes of stars with small spatial separations on the CCD. 6) Errors in the background determination. 7) Fluctuations are present due to photon noise statistics.

It may also be noted that cosmic rays and the some of the unreliable pixels in the bad columns are actually detected as stars. By ignoring stars that are not present in at least three different frames such spurious detections are rejected. Using this criterion, I find around 160 and 700 stars in the fields of NGC 3680 and NGC 6134 respectively.

3.3 Flat Field Correction

It has been known for a while that the Danish 1.54m telescope at La Silla suffers from problems with accurate flat fielding (better than 2%). The DFOSC mounted on the telescope is a focal reducer and such instruments have *sky concentration* problems: This problem is the result of multiple reflections of the flat field in the optics, *e.g.* Andersen *et al.* [3]. The image on the CCD will thus include ghost images of the flat field light source. Usually this is seen as an unusually high intensity in the central part of the CCD. Another problem is scattered light in the telescope and optics. Scattered light is the result of unwanted light not coming from the secondary mirror but which may enter the camera due to insufficient baffling.

To be specific the problem with scattered light and sky concentration occurs because the amount and pattern of scattered light is different in the flat fields and the exposures of target objects in the sky.

3.3.1 Flat Field Correction Software

Among others Michael I. Andersen *et al.* [3] have studied the described flat fielding problems. They have also proposed a method for correcting for this error. By taking exposures of a semi-crowded field of stars with different offsets of the telescope and rotations of the camera it is possible to make a map of how the magnitude of a star depends on the position on the CCD. If the flat fielding is not erroneous, no such dependency will be present.

To give an idea of how the flat field error arises take a look at figure 3.6. The plots show how the observed intensity of a star becomes dependent on the position on the CCD when applying a flat field with scattered light and sky concentration.

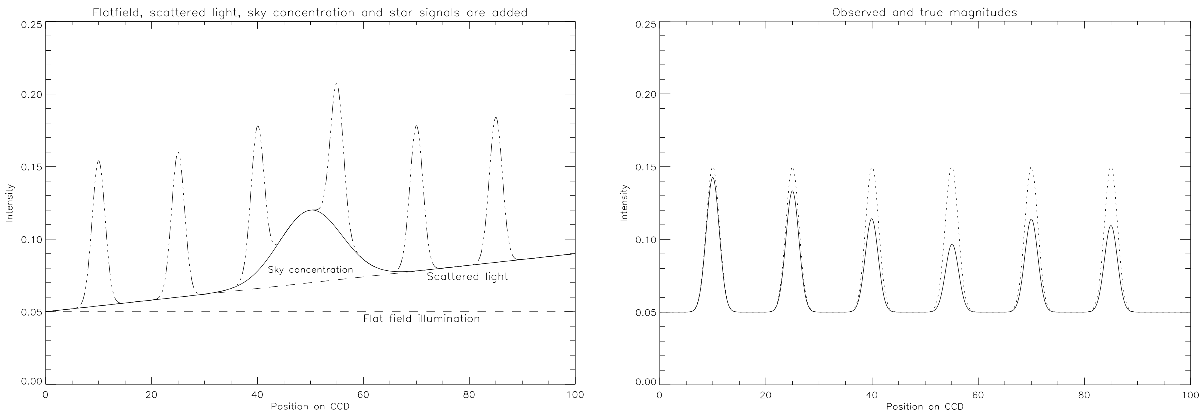

Figure 3.6: To the left contributions to observed intensity in a flat field along a row on the CCD are shown: Flat field source, scattered light, and sky concentration. On top of this combined intensity I have added a star observed at different positions. To the right I show the derived intensity of a star at different positions on the CCD using the flat field to the left (solid curve). Evidently the intensity depends on position. The dotted curve shows the true intensity that I wish to determine.

What is needed is an accurate determination of the sensitivity of each pixel on the CCD. This is also called the gain or the quantum efficiency. The gain is generally determined by the flat field exposures. The error in the flat field may be expressed as

$$Gain(x, y) = FF(x, y) * Err(x, y), \tag{3.7}$$

where $Gain(x, y)$ is the true gain value, $FF(x, y)$ is the flat field function determined by flat fields, and $Err(x, y)$ is the error in the gain calibration. When using the flat field to correct the flux from a star, the derived signal is

$$S(x,y) = I(x,y) * \frac{Gain(x,y)}{FF(x,y)} = I * Err(x,y), \tag{3.8}$$

where $S(x,y)$ is the derived signal and I is the true value - which is of course independent of position. By taking the difference of two measurements of the same star observed at different positions, it is possible to determine the error as a function of (x,y). If the same star is observed at positions (x_1,y_1) and (x_2,y_2), the difference in magnitude can be written as

$$\Delta S = S(x_2,y_2) - S(x_1,y_1) = I * (Err(x_2,y_2) - Err(x_1,y_1)). \tag{3.9}$$

Offsets between measurements are also present due to the fact that the frames are taken at different airmasses. But this offset can be assumed to be a constant for all stars on a given frame. These offsets are determined as part of the fitting routine.

Andersen *et al.* [3] have written software to correct for the flat field error. The software consists of two IDL routines. The main programme (`ff_err_fit`) is designed to determine the function which describes the Err-function for each value of (x,y). This requires that the observations are made with a range of offsets of the telescope and different rotations of the camera. The Err-function is a linear combination of orthogonal two-dimensional functions (2D). Andersen *et al.* have chosen low-order Chebychev polynomials. For high order polynomials (above 2) the polynomials are radial (functions of the length of the (x,y)-vector). The degrees of the 2D- and radial polynomials are given as input to the programme. The coefficients of each polynomial are then determined by the fitting procedure. The programme makes use of the SVDC routine (Singular Value Decomposition) described in *e.g.* Numerical Recipes in C [58]. For a more detailed description of how the programme works consult Andersen *et al.* [3]. In the next section I will give an example of the spatial dependency and the magnitude of the correction.

The output of the programme is the coefficients of the Chebychev polynomials and offsets between a reference frame (*i.e.* frame 0) and the other frames. Optionally the programme will save a file with the correction surface: `Cheb.fit` (this file is in *FITS* format). The correction frame has the same dimensions as the science frames (1850x1850 pixels). To correct for the flat field error the correction frame has to be multiplied by the flat field for the corresponding filter, or similarly the science frame has to be divided into it.

3.3.2 Application of the Flat Field Correction Software

The exposures of NGC 6134 were taken with different telescope offsets and CCD camera rotations which makes it possible to determine any large scale error in the flat fields. This is not the case for the frames taken of NGC 3680 nor the Strömgren standard stars. Thus I have determined the flat field correction by using *only* the frames of NGC 6134. This was done for each of the Strömgren filters. I thus stress that:

- The frames of NGC 3680 and the standard stars are corrected by applying the flat field correction found by using NGC 6134.

Table 3.1: Input arrays for `ff_correct`. Frame 7 is rotated 180° with respect to frame 1. The telescope offset is a little different for frame 8 and frame 1.

Frame N	Frame M	Magnitude Frame N	Magnitude Frame M	Position frame N x	y	Position frame M x	y
1	7	15.8307	15.8782	55.85	1673.37	1806.10	201.59
1	7	14.9220	14.9584	49.08	855.57	1815.78	1019.56
1	7	16.7570	16.8473	43.83	1676.88	1817.92	198.02
1	7	17.0200	17.0655	39.33	1305.84	1823.69	569.16
1	8	16.7748	16.8265	1562.02	991.580	1521.23	987.02
1	8	14.4680	14.5022	1523.90	255.870	1483.47	251.48
1	8	17.3067	17.2974	1513.31	1758.57	1472.20	1753.97
1	8	16.4222	16.4586	1516.05	474.330	1475.51	469.89

By using the observations of NGC 6134 and the software supplied by Andersen *et al.* [3] I am able to determine how the derived magnitudes depend on the position of the stars. As input to the programme I construct eight arrays: An array with the magnitudes of each star observed at different positions on the CCD. Another array of the same length contains the frame numbers that the observations come from for each star pair entry. The third and fourth array contain the positions (x, y) of each entry (*i.e.* observed star) on each frame. An excerpt from the arrays is presented in table 3.1.

In figure 3.7 I have shown a contour plot of the correction frame for the y filter: The correction is of the order 0-8% across the CCD. I found that the best result in all Strömgren filters was obtained by using Chebychev polynomials of 1st order (2D) and 4th order (radial polynomials).

Another IDL routine by Andersen *et al.* [3] applies the derived flat field correction: `ff_correct`. The input to this programme is the position (x, y), frame number, and magnitude of an array of stars. Using this programme is much less time consuming than if one had to apply the flat field correction to the science frames and then run MOMF on all the frames once again. In figure 3.8 I have shown examples of how the standard deviation of the magnitudes has improved after using the flat field correction: This is a histogram with a binning of the standard deviation (bin size: 2.5 mmag). The solid line shows the number of stars in each bin after the correction of the flat field and offsets between frames while the dashed line is the result when only the offsets are removed. I have shown the result for the y and β(W) filters.

The flat field correction of the β frames does not improve the standard deviation significantly. An improvement is seen for the brightest stars, *i.e.* stars with $\sigma < 0.015$ before the correction (dashed curve). This is also the case for the y filter, but the improvement is certainly greater.

3.3.3 Criteria for Stars Included in Flat Field Correction

The results of the previous section agree with the results by Andersen *et al.* [3]. They state that the expected correction across the field is less than 2% in y. If stars in with errors of this size (0.02 mag or more) are included in the fitting procedure the derived correction is not reliable. To be specific it is not possible to determine if a faint star measured with a

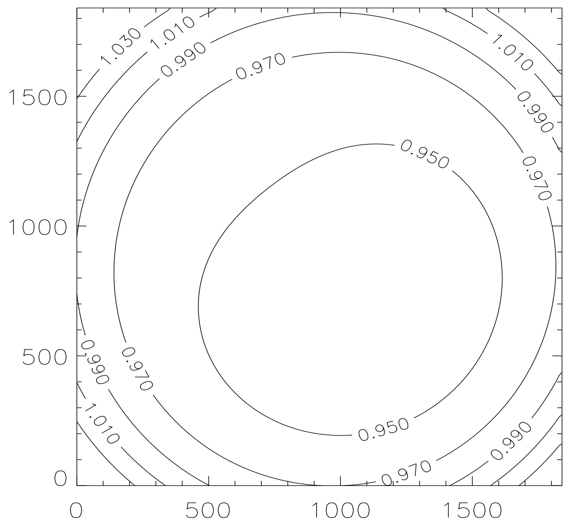

Figure 3.7: Contour plot of the correction frame that has been applied to the flat field for the y filter. Note that a errors of 2-8% are present when going from the centre to the edges of the CCD. The correction is somewhat smaller in the other Strömgren filters.

slightly higher magnitude in one frame compared to the reference frame is due to the flat field error or because of the noise due to photon counting statistics.

I have therefore given some criteria that the observation of each star must meet in order to be included in the fit.

- The star must be located in the central part of the CCD. The reason is that quantum efficiency is quite low close to the edge. I set the limit to 200 pixels: Consequently, stars in a 1450x1450 box centrally located on the CCD is used. This is a somewhat larger area than what is referred to as "the 1250x1250 box reliable for photometry of high precision" in the telescope manual, Storm [65].

- The minimum distance to one of the bad columns on the CCD: Stars within eight pixels from a bad column are removed.

- The minimum distance to the nearest star: This is set to five pixels. As the example of a MOMF output file in appendix D shows, the magnitude determination for stars with a close neighbour is uncertain at a level significantly above the flat field error.

- The expected standard deviation of measurements of each star is estimated using the total number of ADU found by MOMF, *i.e.* $\sigma = 1/\sqrt{\Sigma ADU}$. Stars with $\sigma > 0.015$ mag are excluded.

I have written an IDL routine that allows for each of these criteria to be switched on or off. The routine is used after the measurements of all stars have been read from the MOMF result files and sorted according to the reference frame, as described in section 3.2.3.

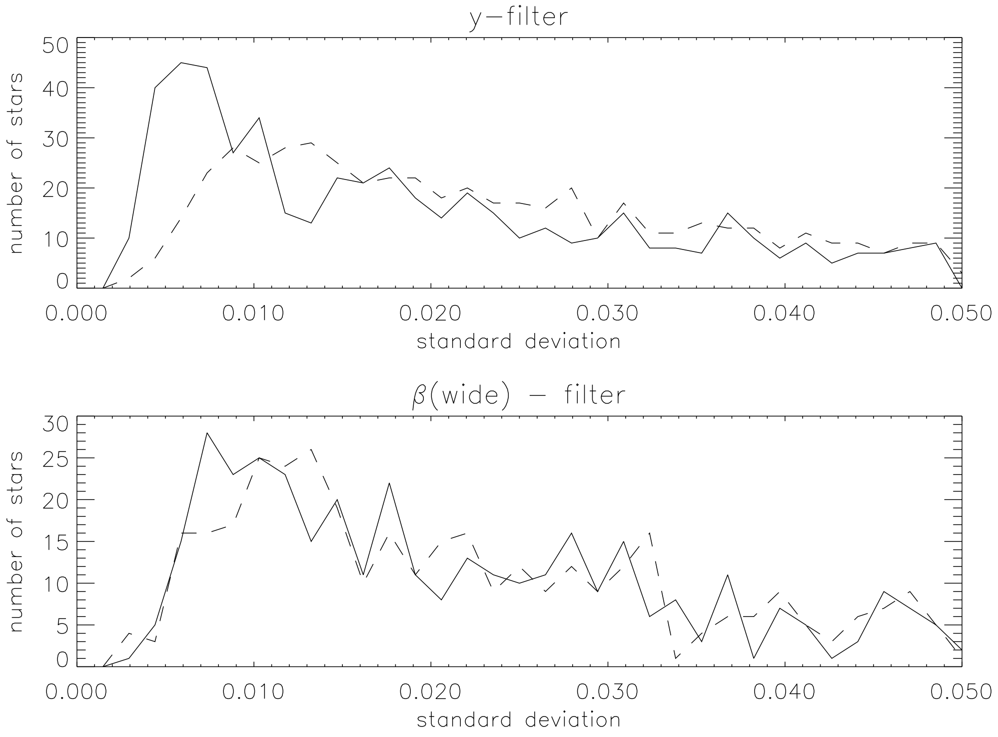

Figure 3.8: Histograms of the number of stars with standard deviation in a given range. The results are shown for two filters: y and β (W). The solid line is the histogram of the flat field corrected magnitudes whereas the dashed line is for the raw data (both corrected for offsets between frames).

Experiments with different criteria show that the flat field correction does give better results when only stars that fulfill these criteria are used in the fitting procedure. I found that the removal of stars not satisfying the last criteria (max expected noise level allowed) does not turn out to improve the results significantly. I also found that it is of course important not to use *too* strict criteria - there has to be *some* stars left in the frames in order to be able to determine the correction.

I note that after running the correction programme with the selected stars I remove star pairs that have large differences in magnitude after the correction is applied. The limit is set to 0.05 mag for all filters. Errors of this order may be due to erroneous background determination or the presence of cosmic ray events or a bad pixel near one of the stars. When this is done the fitting programme is run again. This gives an overall lower noise level.

3.4 Photometry of Strömgren Standard Stars

I observed 19 Strömgren standard stars from the extensive catalogue by Erik Heyn Olsen (EHO) [54]. This catalogue contains the Strömgren colours derived from photoelectric measurements. The EHO catalogue contains nearly all F and G stars brighter than $V = 8.5$. The stars I have selected were observed 3-5 times is each of the Strömgren filters (excluding u!).

Table 3.2: Strömgren colours and positions of the 19 observed standard stars taken from E.H.Olsen [54].

HD	V	$b-y$	m_1	c_1	δm_1	δc_1	n	β	n_β	$\alpha(2000.0)$	$\delta(2000.0)$
63066	9.102	.425	.162	.337	.085	.079	2	2.577	2	$07^h 46^m 55^s.9$	$-04^\circ 57' 14''.2$
64121	7.432	.547	.307	.384	.194	.141	5	2.553	2	$07^h 49^m 27^s.6$	$-54^\circ 48' 39''.3$
64942	8.389	.406	.196	.315	.029	.038	2	2.598	1	$07^h 55^m 58^s.9$	$-09^\circ 47' 48''.9$
66061	7.670	.619	.156	.411	.503	.234	4	2.625	3	$07^h 59^m 41^s.7$	$-48^\circ 16' 47''.3$
70830	8.944	.410	.160	.325	.068	.053	2	2.569	2	$08^h 23^m 54^s.4$	$-06^\circ 19' 08''.8$
81351	7.622	.234	.177	.736	-.003	.174	1	2.724	1	$09^h 23^m 07^s.2$	$-52^\circ 53' 08''.1$
83047	8.201	.194	.163	.887	.023	.203	1	2.743	1	$09^h 35^m 37^s.3$	$-08^\circ 35' 19''.3$
105513	9.264	.240	.136	.785	-.037	.240	2	2.714	1	$12^h 08^m 54^s.4$	$-55^\circ 43' 41''.6$
107956	8.064	.298	.168	.416	.006	.001	1	2.660	1	$12^h 24^m 21^s.8$	$-25^\circ 12' 38''.5$
109972	9.152	.371	.171	.368	.030	.051	4	2.641	1	$12^h 39^m 09^s.6$	$-34^\circ 16' 17''.6$
111721	7.983	.512	.166	.302	.247	.050	22	2.549	99	$12^h 51^m 26^s.1$	$-13^\circ 29' 11''.7$
122956	7.240	.662	.177	.500	.550	.364	6	2.538	5	$14^h 05^m 13^s.3$	$-14^\circ 51' 23''.0$
128279	8.039	.467	.55	.262	.260	.020	16	2.545	99	$14^h 36^m 48^s.1$	$-29^\circ 06' 28''.9$
132475	8.560	.396	.77	.289	.139	.001	15	2.578	99	$14^h 59^m 51^s.7$	$-22^\circ 00' 20''.1$
133913	7.785	.303	.109	.523	.066	.116	4	2.658	4	$15^h 07^m 25^s.7$	$-15^\circ 24' 58''.8$
134409	8.225	.367	.149	.492	.050	.170	4	2.626	3	$15^h 09^m 56^s.1$	$-06^\circ 43' 02''.3$
155458	8.164	.501	.46	.956	.340	.704	3	2.743	3	$17^h 11^m 48^s.4$	$-03^\circ 20' 53''.2$
160959	8.570	.216	.166	.640	.013	.013	1	2.718	1	$17^h 44^m 45^s.2$	$-39^\circ 50' 52''.3$
161770	9.693	.480	.50	.299	.290	.053	1	2.568	3	$17^h 47^m 46^s.5$	$-09^\circ 36' 08''.0$

In table 3.2 I present a table of the 19 standard stars that I have used. Typical standard errors on the indices go from 4 mmag in $b-y$ to 12 mmag in the β index. The stars were selected with a wide range in $b-y$ in order to be able to determine the dependency of the standard transformation on temperature. As can be seen from the table these stars are relatively bright: V magnitudes range from 7.240 to 9.102 which may be compared to the turnoff stars of NGC 3680 and NGC 6134 that have $V \sim 12$. With such a large telescope as the Danish 1.54m the bright standard stars will saturate the CCD whose limit is 65535 ADU very fast - 4-6 seconds for the brightest star in the y filter. There are two problems to be considered:

The duty cycle is extremely low for such a low exposure time as most of the time will be used for the CCD to be read out (75 seconds for a full frame). For very short exposure times one will expect errors in the actual exposure time, as the precision of the shutter closing time could affect the result ($\sim$10ms according to the telescope manual [65]). The solution to these problems is to defocus the telescope: In this way the photons from a star are distributed over a large area of pixels, and it is possible to take much longer exposures.

I have considered using the MOMF package for the reduction of the standard stars. This could have been done if I had rebinned the window frames. The position of the stars and the degree of defocusing are different for each frame. This means that I will have to run MOMF on each frame individually ($\sim$ 400 frames). Thus I have decided to write a reduction programme myself that will reduce all frames at once.

After bias subtraction by using the master window bias frame (section 3.1.2) and flat fielding (section 3.1.3), I apply the flat field correction found, using the results of section 3.3.2. This is done by using the correction surfaces found in each of the Strömgren filters. I only use the part of the surface corresponding to the (750×400) window that was read out from the CCD. The correction is applied multiplying the correction surface with the (bias subtracted and flat fielded) science frames of the appropriate filter.

The IDL programme then determines the magnitude of each star using ten different apertures with increasing radius. The apertures are chosen so the area using aperture $n+1$ is equal to the area using aperture n times 1.1. The aperture radii range is 24 to 103 pixels.

The centre of the apertures is determined by finding the *centre of light* of the stars on each frame. A box of 30x30 pixels is placed around the approximate centre of each star (found by visual inspection) and the centre of light is computed using the well known expression for the centre of mass:

$$\mathbf{R} = \sum_{x,y}(ADU_{(x,y)} * \mathbf{r}) / \sum_{(x,y)} ADU_{(x,y)}, \tag{3.10}$$

where $\mathbf{r}$ is the position vector (x, y) of each pixel and $ADU_{(x,y)}$ is the corresponding pixel value.

I determine the background level by finding the median and standard deviation of pixels between two concentric apertures with a radii of 75 and 85 pixels. Pixels with values of more than three times the standard deviation (3σ) from the median value are excluded and a new median value is found. This procedure is done twice to find the background level as the average value of the remaining pixels.

I found that the radii of the background apertures should be chosen with care. This is illustrated in figure 3.9. There I show two curves of growth for an observation of HD 109972 in the y filter using different background aperture sizes.

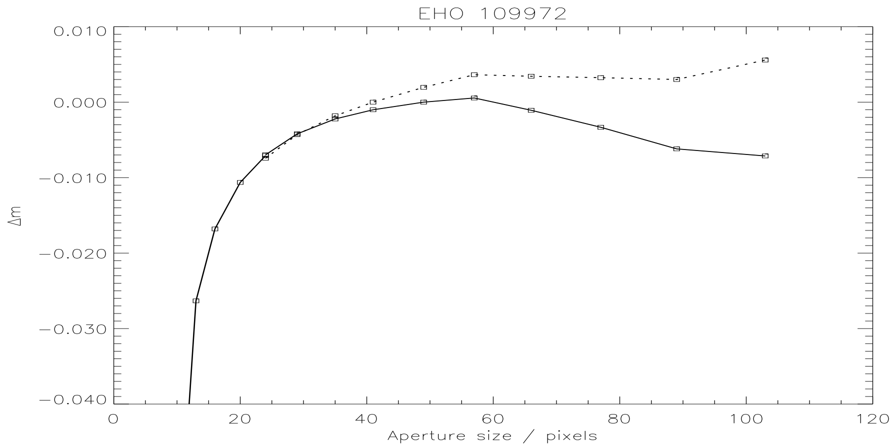

Figure 3.9: Curves of growth using aperture photometry with increasing aperture radii. For the solid curve the background level was estimated by using two concentric apertures of radii 45 and 65. The dashed curve is the curve of growth when using background aperture radii of 75 and 85. Notice that the derived magnitude of the star becomes lower (brighter) as Δm increases.

The solid line shows the result using background aperture radii of 45 and 65, whereas the dashed line is for background aperture radii of 75 and 85. When using the smaller background aperture radii light from the star is included, hence the background level is estimated to be too high. This explains that the solid line goes down after reaching a maximum at an aperture radius of 57. At a radius of 80 the dashed curve is very nearly flat. Using the implications of this and other similar plots for other stars, I have decided to use background aperture radii of 75 and 85 for all frames.

As the degree of defocusing is different from frame to frame, some kind of procedure is necessary to choose the "right" aperture size for each frame. The idea is to get as much light as possible without using an aperture that is too large, which will give higher noise because of the uncertainty in the determination of the background level.

It is also important not to include any light from neighbouring stars and to be careful about including signal from bad columns. Thus stars whose centre of light is less than 30 pixels from a bad column are excluded. If an aperture includes pixels of a bad column, I use the magnitude derived from the largest aperture that does not overlap with a bad column. This was done as I found that the curve of growth makes a jump when the apertures overlap with a bad column. I tried "removing" bad columns by giving each pixel in a bad column the 3σ sorted mean value of the horizontally neighbouring 6 pixels on each side of the column, but this "smearing process" did not improve the result.

To give an idea of the "size" of the stars of the CCD frame I have shown surface and contour plots of an observed standard star with different degrees of defocusing in figure 3.10.

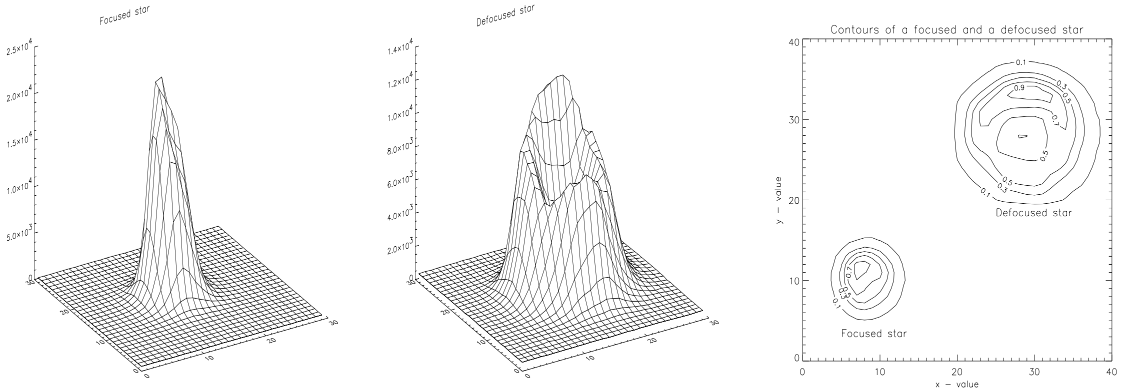

Figure 3.10: Surface and contour plots of two observations of HD 109972. The focused star is a $\beta(N)$ exposure and the defocused one is a y exposure. In the surface plots (left) the value on the z axis is the number of ADU. In the contour plot (right) each star is normalized by the highest ADU value.

Using apertures from 24 to 103 pixels I find the relative gain in magnitudes from aperture a to $a+1$ expressed as: $\delta m_{a+1} = (m_a - m_{a+1})/m_a$. For each frame I construct the *relative* gain curve: δm_{a+1}, for $a = 1 - 9$. The relative gain curve determines the slope of the curve of growth for each aperture size.

As expected the curves of growth flatten when going to large enough apertures. The value where the curve becomes flat depends on the degree of defocusing. I found that the most reasonable solution was to select the aperture where the gain-curve has flattened out to a certain level. I use the *smallest* aperture where the relative gain curve fulfills the criterion: $\delta m_{a+1} < 2.5 \times 10^{-4}$. As examples of the curves of growth I have presented a few in figure 3.11 where I have indicated which aperture is chosen by using the criterion expressed above.

As the aperture size grows, the derived magnitude of the star gets smaller (more bright) until some point when the signal from the star is below the background signal. The reason for the continuous growth of HD 64942 in figure 3.11 is a faint neighbouring star about 85 pixels from the standard star. In the case of HD 66061 and HD 81351 some of the curves have zero slope at large aperture sizes. The reason is (as explained above) that I have

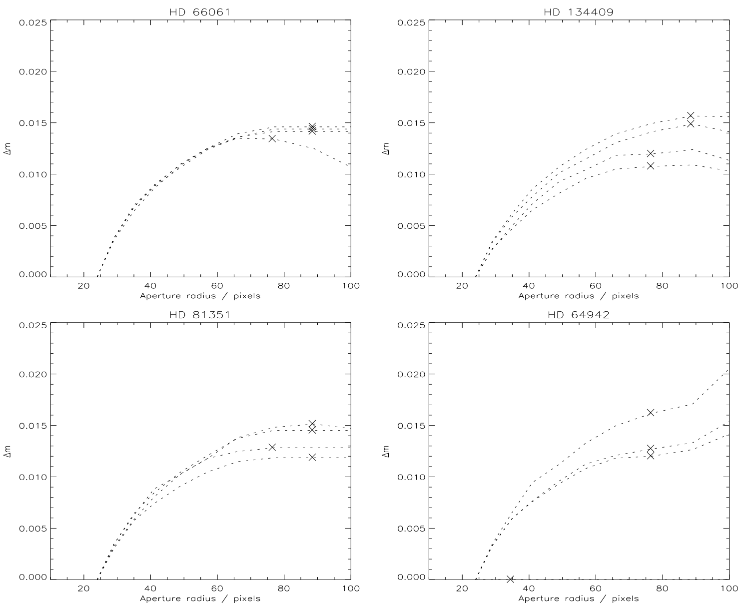

Figure 3.11: Curves of growth for observations of four standard stars. The size of the aperture is on the abscissa and the magnitude is on the ordinate - subtracted by the magnitude of the smallest aperture radius (23 pixels). The applied aperture size for each observation is indicated by an $\times$ symbol.

ignored all magnitude determinations that overlap with a bad column. The magnitude of all apertures overlapping with a bad column is given the value in the largest aperture *not* overlapping with a bad column. The result is that the magnitude is overestimated by perhaps 2-3 mmag in the worst case.

In chapter 4 I will use the magnitudes of the standard stars to derive the transformation of observed magnitudes to standard magnitudes.

3.5 Comparison with MOMF Magnitudes

Below I present the results of a test of how the magnitudes determined by the MOMF software and my own IDL aperture reduction programme described above compare. It is of utmost importance that the magnitudes are the same when using either method.

I have used the aperture programme on four frames of NGC 3680: Two in each of the b and y filters (110 and 50 second exposures). I selected six stars present in all frames. They are of different magnitudes and are all found in the central part of the CCD at least 40 pixels from their nearest neighbour or a bad column.

I used small aperture sizes as the stars of NGC 3680 are well focused: I used ten aperture radii in the range 5-40 pixels. The aperture size was chosen by using the same procedure as for the standard stars, - thus choosing the aperture where the curve of growth is nearly flat.

I have compared the derived magnitudes with the values found by MOMF in figure 3.12 below. As can be seen in the plots, the magnitudes agree very well in both b and y for the brightest stars. The error bars in the plot to the right are estimated from the number of detected photons for each star. The reason for the large differences for the faint stars is mainly due to the uncertainty in the determination of the sky background.

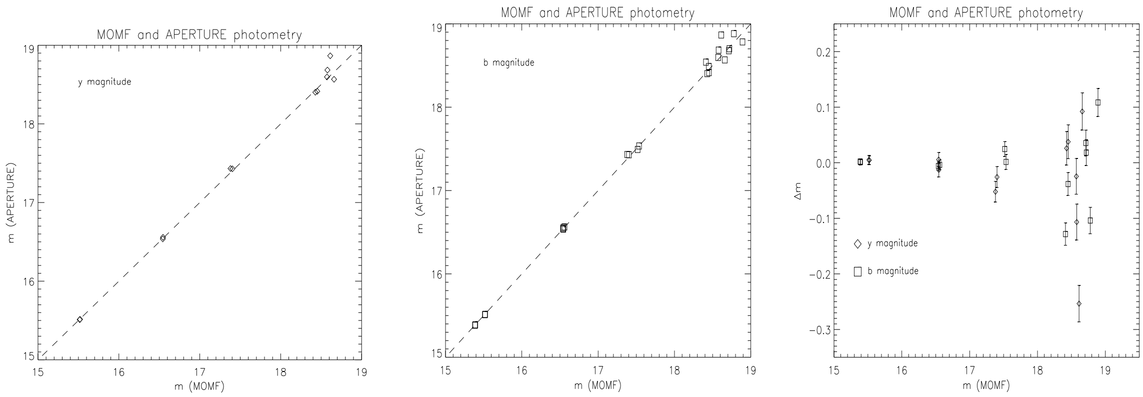

Figure 3.12: The plots to the left and in the middle show the relation between magnitudes determined by MOMF and my IDL aperture programme in the y and b filters respectively. The plot to the right shows the differences between the MOMF and the "aperture" magnitudes.

The standard stars that I have reduced with aperture photometry are *very* bright. Their V magnitudes are $\simeq 4$ smaller than the turnoff stars in the clusters. Thus I have a very high count level for all standard stars.

The results presented above show that the aperture and MOMF magnitudes agree in this case.

3.6 Summary of Chapter 3

In this chapter I have described the various steps I have taken to calibrate the CCD photometry of the open clusters and the Strömgren standard stars. The results I have arrived at are:

- I am not able to determine any non-linearity of the CCD below 2%
- I have reduced the open clusters by using MOMF
- I have corrected the flat fields by using the software by Andersen *et al.* [3] leading to an improvement of the photometric precision
- I have reduced the Strömgren standard stars by using aperture photometry. I have written a programme which takes the different degrees of defocusing of the stars into account
- For high count levels the magnitudes from MOMF and the aperture photometry agree

With the photometric reductions being done I will now turn to the conversion of the instrumental magnitudes to the Strömgren standard system by using the results obtained in this chapter.

Chapter 4

Conversion to the Strömgren Standard System

In this chapter I will use the results derived in the previous chapter to determine the Strömgren standard indicies for the stars in the open clusters NGC 3680 and NGC 6134. To do this I go through two steps of calibration:

- By using observations made at different airmasses, I will determine the correction of the instrumental magnitudes for atmospheric extinction.
- In order to convert the instrumental magnitudes to the Strömgren standard indices I use the observed standard stars.

Each step will be described in the sections of this chapter. I will also compare my results for the open clusters with previously published values for the Strömgren indices.

4.1 Extinction Correction

To determine how the magnitude of a star varies during the night because of the extinction in the atmosphere of the Earth, it is necessary to take exposures at different positions in the sky. On photometric nights the extinction depends only on the path length of the light through the atmosphere. This is expressed as:

$$m_{\text{obs}} = m_0 + k * \text{airmass}(Z) \simeq m_0 + k * \sec(Z), \tag{4.1}$$

where m_{obs} is the observed magnitude, m_0 is the true magnitude of the star, k is the extinction coefficient and $\sec(Z)$ measures the path length depending on the zenith distance, Z. For example at the zenith, $Z = 0$ and the airmass is 1. When using the sec function one neglects the curvature of the Earth and its atmosphere. At airmass 2.00 the error is about 0.5%. Although the effect is negligible compared to other sources of error, I have corrected the airmasses for this effect by using the formulas in chapter 9 of Birney [8].

The amount of extinction is determined by the constant k which depends on wavelength. The atmosphere is less transparent at short wavelengths, *e.g.* $k_v > k_y$. As the Strömgren

β filters have the same central wavelength, it is expected that the extinction is the same in these filters.

On non-photometric nights cirrus clouds cause significant additional extinction. This makes it difficult to determine the true magnitude of a star, as the measured magnitude is then dependent on time - not only on the zenith distance. Even on photometric nights the measured extinction coefficient may differ from night to night due to the changing transparency of the atmosphere.

In the next subsections I will describe how I have derived the extinction coefficients by using both the open clusters and the Strömgren standard stars. In section 4.1.3 the results are compared.

4.1.1 Extinction Coefficients: Open Clusters

In order to determine how the extinction coefficients vary with time and zenith distance I have used two samples of stars, *i.e.* stars in the open clusters NGC 6134 and NGC 3680. The open clusters were observed on April 29th to May 3rd 1996. The criteria for the stars that are included are that they must be bright and isolated. By using reasonable conditions 30-50 stars that are present on all frames are selected in each filter. I have written an IDL routine that selects the stars and determines the average magnitude of the selected stars in each exposure.

The result for all filters is shown in figure 4.1 below. The plots show the mean magnitude of the selected stars for exposures at a range of airmasses on different nights. For each night the zero point is defined as the magnitude obtained at the lowest airmass. To determine the extinction coefficients, I have made a linear fit to the points. The slope determines the extinction coefficient. The result for each filter is shown in table 4.1.

To estimate the error in the determination of the extinction coefficients, I have tried to remove a random frame on each night. This gives severe differences on nights where only three or four frames were taken: Typically the changes are of the order 0.02 and 0.01 on nights 1 and 2. On the other hand night 3 is not so sensitive to this: Changes below 0.01 are found. These results can be explained by the few number of observations that fall in a narrow range in airmass. Only minor changes in transparency of the atmosphere are needed to explain the observed error.

4.1.2 Extinction Coefficients: Standard Stars

On the nights from May 1st to May 4th I observed 19 Strömgren standard stars. Each night four-five standard stars were observed. On May 1st and May 2nd I also observed the open clusters. It would thus be interesting to compare the extinction coefficients when using either set of data.

The extinction coefficients that need to be found are k_v, k_b, k_y, and k_β as expressed in equation 4.1. I set up this equation for each Strömgren index:

$$(STR)_{\text{EHO}} = k_A * (STR)_C + k_B, \tag{4.2}$$

where $(STR)_{\text{EHO}}$ is the standard Strömgren index found in the EHO catalogue [54]: $b-y$, $v-b$, or $\beta = \beta(N) - \beta(W)$. Note that $v-b = m_1 + (b-y)$. In equation 4.2 k_A and k_B are

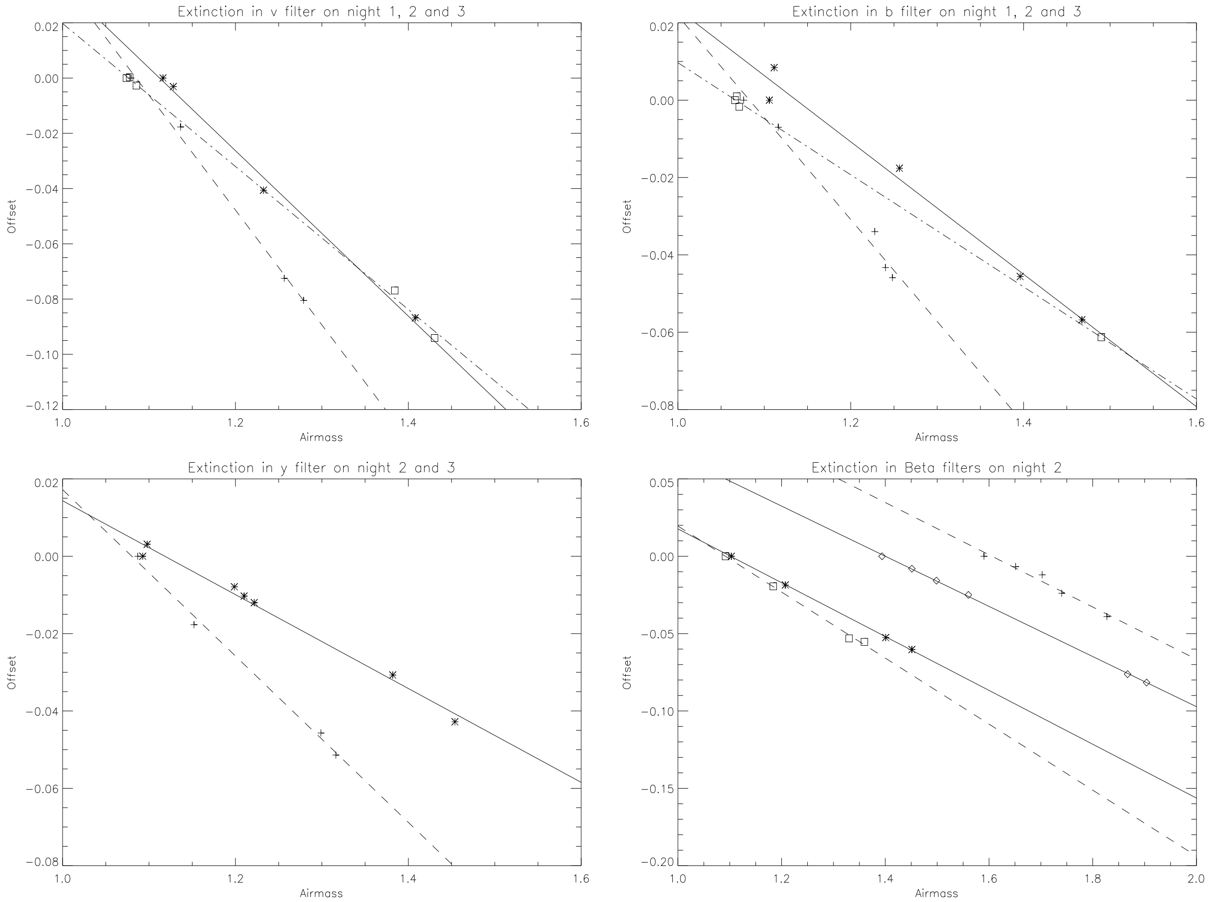

Figure 4.1: Determination of extinction by using several isolated bright stars in the field of NGC 6134. The plots show the magnitude offset at a given airmass compared to the measurement at the lowest airmass on each night. The slopes of the fitted lines determine the extinction coefficients, which is quoted in table 4.1. The symbols in vby correspond to: Night 3: $*$, night 2: $+$, night 1: Box. The results for the β filters on night 2 are plotted, NGC 6134: Box (N), * (W), NGC 3680: + (W), diamond (N).

the standard transformation coefficients and $(STR)_C$ is the instrumental Strömgren index corrected for extinction:

$$(STR)_C = STR_2 - k_2 * \text{Airmass} - (STR_1 - k_1 * \text{Airmass}), \tag{4.3}$$

where STR_1 and STR_2 are the observed values for two filters. Similarly k_1 and k_2 are the extinction coefficients of the corresponding filters that I wish to determine. The equation that I want to solve is equation 4.2 with the substitution of equation 4.3 for $(STR)_C$.

I have used the IDL function SVDC also used to find the flat field correction described in section 3.3. SVDC is a mathematical method used to solve linear equations with more equations than unknown coefficients, which is exactly the case for the present problem, *cf.* Press *et al.* [58]. I have written an IDL routine that sets up the equations above, which are then given as input to the SVDC routine.

For example I use the $b-y$ index to find the extinction coefficients of $k_1 = k_y$ and $k_2 = k_b$ by using $STR_1 = y$ and $STR_2 = b$. For each of the four nights a different set of extinction coefficients are determined whereas the standard transformation coefficients (k_A, k_B) are assumed to be the same for all nights. Thus the number of unknown coefficients are: Four extinction coefficients for b and y and two standard transformation coefficients, *i.e.* the problem has ten unknowns.

As each star is observed at a range of different airmasses for each filter, several equations like 4.2 are set up. Typically each star is observed five times in b and y thus giving 25 equations. Only three of the standard stars were observed on more than one night.

The residuals of the fitting procedure for the Strömgren indices are shown in figure 4.2. The extinction coefficients that I have derived are presented in the next section in table 4.1, where I compare the results, when using either the open clusters or the standard stars. These are the extinction coefficients corresponding to equation 4.1.

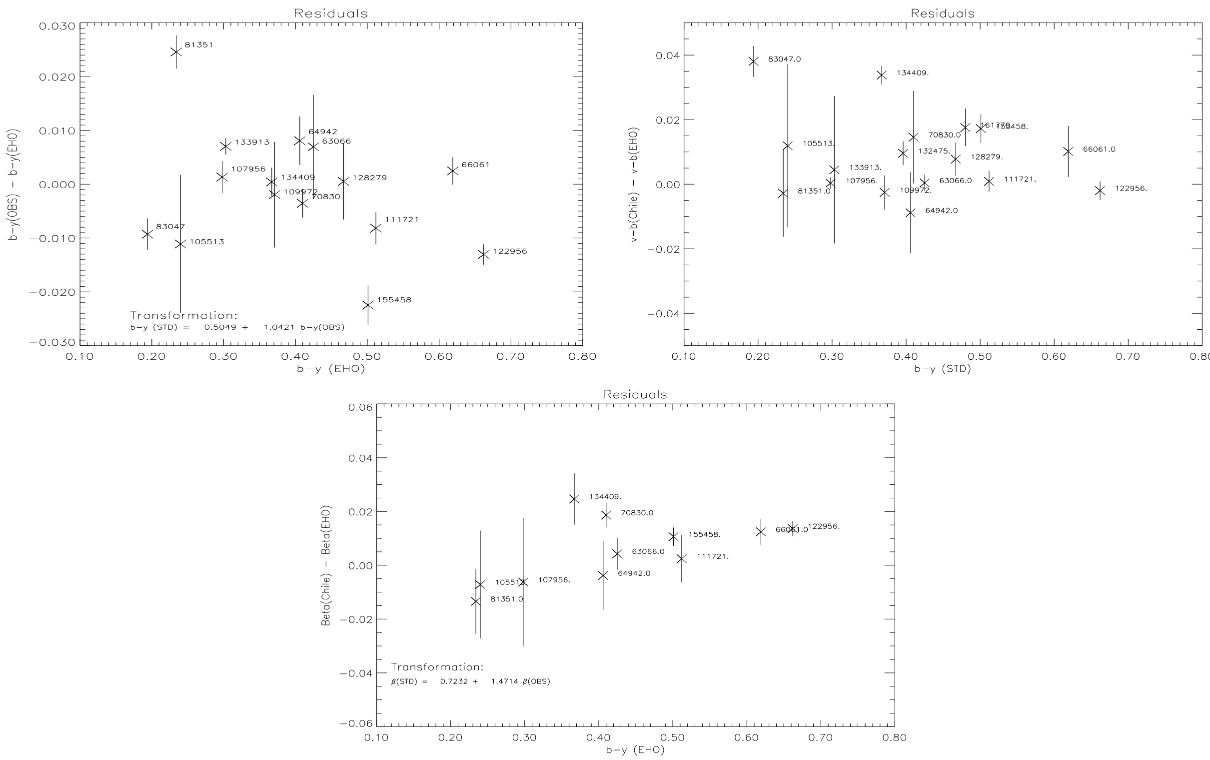

Figure 4.2: Determination of extinction coefficients when using the observed Strömgren standard stars. The plots show the residuals after a simultaneous fit of the extinction coefficients and transformation coefficients to the standard Strömgren values of the EHO catalogue. Top left: $b-y$, top right: $v-b$, bottom: β.

To test the reliability of the derived coefficients, I remove one star from each night. It turns out that the extinction coefficients are "stable" within 0.01 on all nights, excluding May 1st (night 2). This will be discussed more extensively in the next section.

The extinction coefficient for the b filter is determined when using both $b-y$ and $v-b$. The derived coefficients agree within 0.01, excluding again May 1st (night 2). This may be due to the fact that only four standard stars were observed on this night or due to unstable weather conditions. I have used the mean value of k_b obtained from these two fits.

It can be seen that on nights 2-4 the derived extinction coefficients for the vby filters are similar when using the standard stars, while on night 5 the extinction coefficients are all somewhat higher. This is most likely due to a change in the transparency of the atmosphere.

I have only fitted one β extinction coefficient as the β filters have the same central wavelength. I found that the coefficients for each night were not well-determined. When removing one star from the fit, the extinction coefficient for that night changed up to ± 0.03! I have then made a fit where the extinction coefficient is assumed to be the same on all nights, thus limiting the number of unknown coefficients. The derived extinction coefficient changes little when one or two stars are removed from the fit. I regard this solution as being the most reasonable.

Note that the transformations of the instrumental magnitudes to the standard system of the $b-y$ and β indices have also been found. The transformation is printed on the residual plots in figure 4.2. Note that this is the transformation obtained when solving for the extinction coefficients and the transformation at the same time. The coefficients of the transformations deviate from what I find in section 4.2 (*cf.* figures 4.4 and 4.6). There I have determined the standard transformation of the Strömgren indices *after* the removal of the atmospheric extinction by using the extinction coefficients determined here.

4.1.3 Evaluation of Extinction Coefficients

The result of the extinction determination is shown in table 4.1: This includes the results when using NGC 6134, NGC 3680, and the standard stars.

For NGC 3680 only a few exposures were obtained. There was only a significant spread (ΔAirmass > 0.3) in airmass for the β filters on night 2. The observations of the standard stars were made over a period of four nights. As seen from the table, both the open clusters and the standard stars were observed on two of the nights, *i.e.* nights 2 and 3.

Table 4.1: Extinction coefficients in the Strömgren filters when using photometry of open clusters and standard stars. "-" means that the data did not allow for a determination of the extinction coefficient. "*" indicates an unreliable estimate, *i.e.* a standard error of typically ± 0.02. "!" is explained in the text.

Night	Data	k_v	k_b	k_y	$k_{\beta(W)}$	$k_{\beta(N)}$	k_{b-y}	k_{v-b}
(1) April 30th	NGC 6134	0.252	-	0.138	-	-	-	-
(2) May 1st	NGC 6134	*0.42	*0.267	*0.218	0.186	*0.210	0.049	*0.20
(3) May 2nd	NGC 6134	0.29	0.166	0.121	-	-	0.045	0.124
(2) May 1st	NGC 3680	-	-	*0.09	0.177	0.160	-	-
(2) May 1st	Std. stars	0.280	*0.17	*0.11	!0.140	!0.140	*0.06	*0.11
(3) May 2nd	Std. stars	0.286	0.168	0.118	!	!	0.050	0.118
(4) May 3rd	Std. stars	0.294	0.169	0.112	!	!	0.057	0.125
(5) May 4th	Std. stars	0.320	0.193	0.131	!	!	0.062	0.127

A few notes for the entries in table 4.1: a) The night numbers indicated (1-5) correspond to the numbers in the log files of appendix C. b) Values labelled * are unreliable: Either due to a small range of airmass (< 0.3) or a significant change (> 0.02) in the derived extinction coefficient when one or two points are removed from the fit. c) The standard star measurements from all nights were used to determine a mean extinction coefficient for the β filters (indicated by the "!" symbol). d) It was not possible to determine the extinction in all filters on all nights (the symbol "-" is used). This was due to the fact that the exposures were taken over a short period of time and hence there was no spread in airmass, *i.e.* $\Delta(\text{Airmass}) < 0.2$.

At a first glance the results are well explained by what was pointed out earlier: The extinction on a given night is larger in filters with shorter central wavelengths.

It is noteworthy that night 3 is the only night where the extinction coefficients when using NGC 6134 and the standard stars seem to agree! I have interpreted this as night 3 being a true photometric night with the extinction coefficients being constant over the night. On night 2 this is *not* the case (compare the result using NGC 6134 and the standard stars).

The extinction coefficients on night 2-4 of the standard stars agree with the values found in the "ESO User's Manual" [60]. The values found there are the mean extinction coefficients of many photometric nights. The values quoted there are:

- $k_y = 0.11, k_b = 0.17, k_v = 0.27$.

As can be seen the colour extinction coefficients of these values are $k_{b-y} = 0.06$ and $k_{v-b} = 0.10$. These values are in reasonable agreement with my results, although the standard stars are in better agreement in this case. Still the value I find for k_{v-b} is somewhat higher.

The extinction coefficient of the two β filters was difficult to determine when using only the open clusters as there was little spread in airmass of these observations. The exception is the NGC 3680 exposures of $\beta(N)$ on night 2. The somewhat higher value of the extinction in $\beta(W)$, *i.e.* $\Delta k_\beta \simeq 0.02$ on this night gives an idea of the uncertainty in the determination of the extinction coefficient. These exposures are taken at almost the same time and with the same range in airmass! Within the uncertainty, say 0.02mag, the k_β found when using NGC 3680, $k_\beta = 0.17 \pm 0.02$, does not agree with the value found using the standard stars, *i.e.* $k_\beta = 0.14 \pm 0.01$. The even higher value that is found when using the data for NGC 6134, *i.e.* $k_\beta = 0.19 \pm 0.02$, indicate that the weather conditions on night 2 were indeed unstable.

The derived value of k_β using the standard stars does not change significantly if some of the standard stars are removed from the fit. I have thus used this value for k_β. This value is in better agreement with the standard extinction coefficient for La Silla (ESO User's Manual 1993, [60]) which is:

- $k_\beta = 0.15$

4.1.4 Extinction Correction of Open Clusters

As stated above I have found that the extinction coefficients of the standard stars on night 3 are the most reliable. The determination is insensitive to which stars are included in the fit, and the results agree with the standard extinction coefficients for La Silla. The procedure described in the following is used for both clusters in all Strömgren filters.

For the open clusters I have thus used the extinction coefficients found when using the standard stars on night 3. The extinction is subtracted by using equation 4.1. For the measurements of on night 3 I then determine the median value and standard deviation (σ) of the magnitude of each star: Measurements that lie more than 3σ from the median value are excluded and the average of the remaining measurements are used to find the mean magnitude.

The magnitude offsets between frames on all nights (including night 3) are then determined by using the extinction corrected magnitudes from night 3, which are found as described above. Stars with low standard deviation ($\sigma < 0.01$ mag) and at least three measurements are used to determine the offset of each frame. This last criterion is relaxed to only two measurements in the β filters for NGC 3680 (as only two exposures were made in these filters on night 3). After removing the offsets I determine the final magnitude, standard deviation, and total number of measurements which are stored in a file.

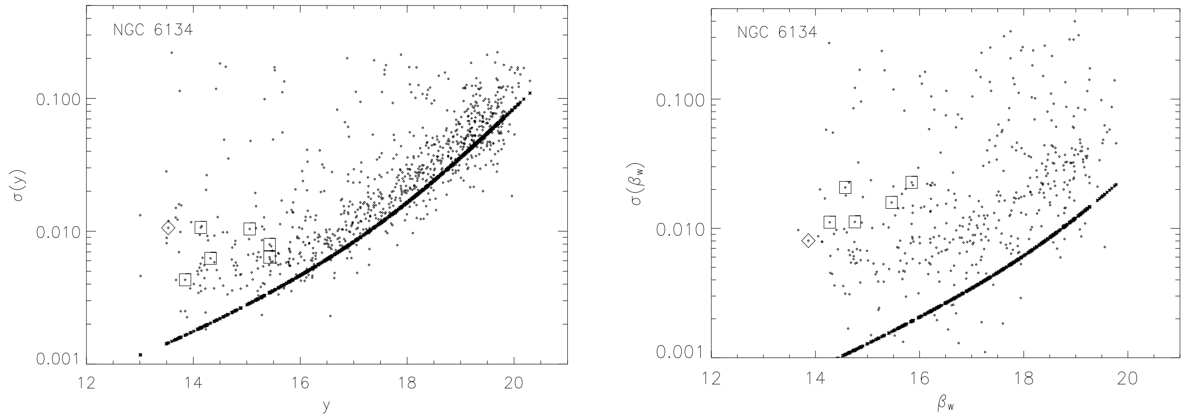

Figure 4.3: Logarithmic plots of the standard deviation as a function of magnitude in the y and $\beta(W)$ filters for stars in NGC 6134. The boxes indicate the positions of the δ Scuti stars and the diamond is the blue straggler. The curved solid lines are the theoretical predictions.

For each star in the clusters I now have the instrumental magnitude and standard deviation. The magnitudes now need to be transformed to the standard system by using the observed standard Strömgren stars. This procedure is described in section 4.2

In figure 4.3 I have shown how the standard deviation depends on magnitude in y and $\beta(W)$ filters for stars in NGC 6134. As expected faint stars have higher standard deviation than bright stars.

For each star I have calculated the expected photometric noise by using theoretical predictions. I consider three sources of noise namely scintillation, photon counting statistics, and errors in the PSF / background determination. I have applied the equations (3) and (38) given in Kjeldsen *et al.* [40]. The result is plotted with large symbols in figure 4.3. As can be seen other sources of error are present for the $\beta(W)$ filter, *e.g.* errors not removed by the flat field correction.

4.2 Transformation to the Standard System

I have used the observed Strömgren standard stars to obtain the transformations needed to go from the instrumental system to the standard system. Before I am able to to this I have corrected the instrumental magnitudes for the large scale flat field error as described in section 3.3. Then the atmospheric extinction has then been subtracted as described in the section above. After these corrections I have determined the mean magnitude of each star in the Strömgren filters. The measured magnitudes of a star that deviate more than 3σ from the median value are rejected. The Strömgren indices are by found using the definitions in appendix A.

I will now go through the calibration of each of the Strömgren indices and compare my results with previously published data.

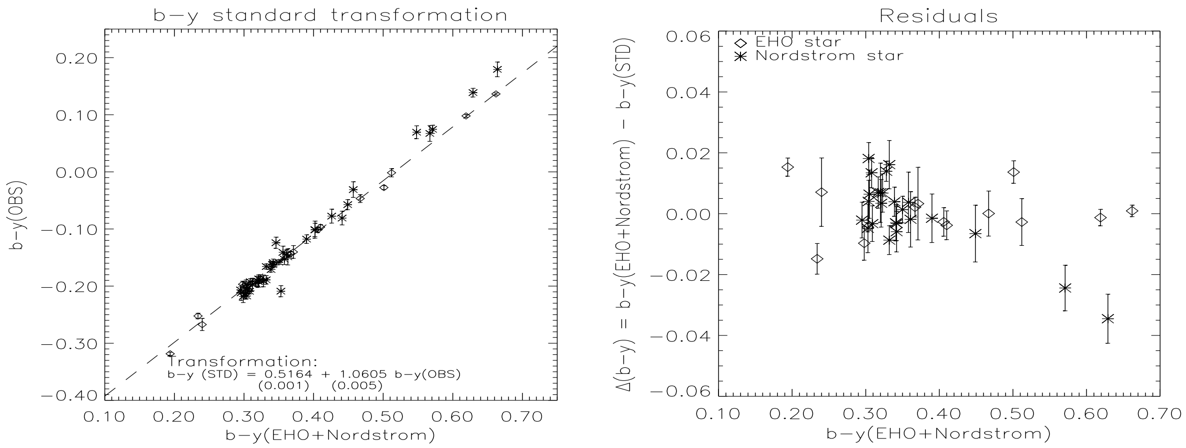

Figure 4.4: To the left I show the relation between observed $b - y$ and the standard $b - y$ value of the EHO catalogue (diamonds). The linear transformation is plotted and printed on this plot. To the right I show the residuals after applying the standard transformation. Note that a few the NGC 3680 stars are also plotted (*).

4.2.1 The $b - y$ index

In figure 4.4 I show the relation between the observed $b-y$ and the standard values found in the catalogue by Erik Heyn Olsen [54], *cf.* table 3.2. In the plot the instrumental and standard indices of some of the observed "secondary standard" stars in NGC 3680 are also shown, *i.e.* stars with low standard deviation ($\sigma < 0.015$).

Evidently, the observed and standard magnitudes correlate in the range 0.2< $b-y$ <0.7. I have made a linear fit to obtain the standard transformation by using the IDL routine `linfit`, which also takes the standard deviation of the observed magnitudes as input. In this way stars whose index is not well determined observationally are given low weight. The standard transformation is shown in the plot to the left: The numbers in parenthesis are the standard deviations of the coefficients. The residuals when using the transformation are shown to the right as a function of colour ($b-y$). No evident colour term is seen. Note that the error bars in this plot do not include the error in the transformation coefficients.

I have compared the transformed $b-y$ colour to the results of Nordström *et al.* [53] and Twarog *et al.* [68]. The result is shown in the figure 4.5. In these plots I have shown the range in $b-y$ of the stars used for the standard transformation: Nordström *et al.* [53] and Twarog *et al.* [68] have used only the brightest stars in NGC 3680, *i.e.* stars around the turnoff region which were measured by Nissen [49]. In the dashed part of the calibration range of figure 4.5 only two stars are present. As can be seen I have used a somewhat broader range in $b-y$ compared to Nordström *et al.* [53] and Twarog *et al.* [68]. This

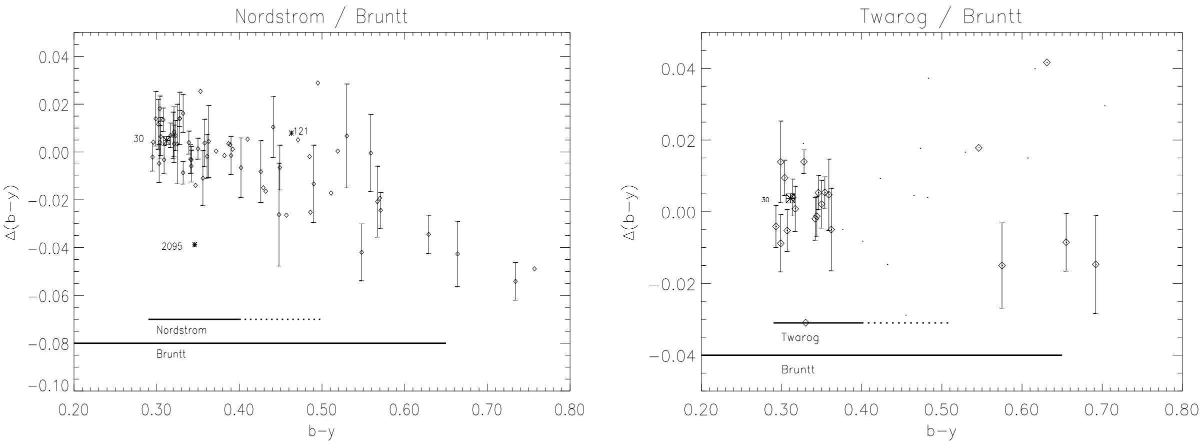

Figure 4.5: Comparison of $b-y$ index of stars in NGC 3680. I show the differences between my results and what was obtained by Nordström *et al.* [53] (left) and Twarog *et al.* [68] (right). I have shown the approximate range of the stars used for the standard transformation. Error bars are shown for stars with $\sigma < 0.02$. Stars 30, 121, (double stars) and 2095 are indicated.

easily explains the systematicly increasing difference in $b-y$ when going to redder stars. Consequently, I assert that my calibration of $b-y$ for stars with $b-y > 0.4$ is more reliable than Nordström *et al.* [53] and Twarog *et al.* [68].

4.2.2 The β index

The instrumental β index also correlates well with the standard β index, as can be seen in figure 4.6. The standard deviation is quite high for some of the stars. This is explained by the presence of a bad column near the star on some exposures (this was discussed in section 3.4).

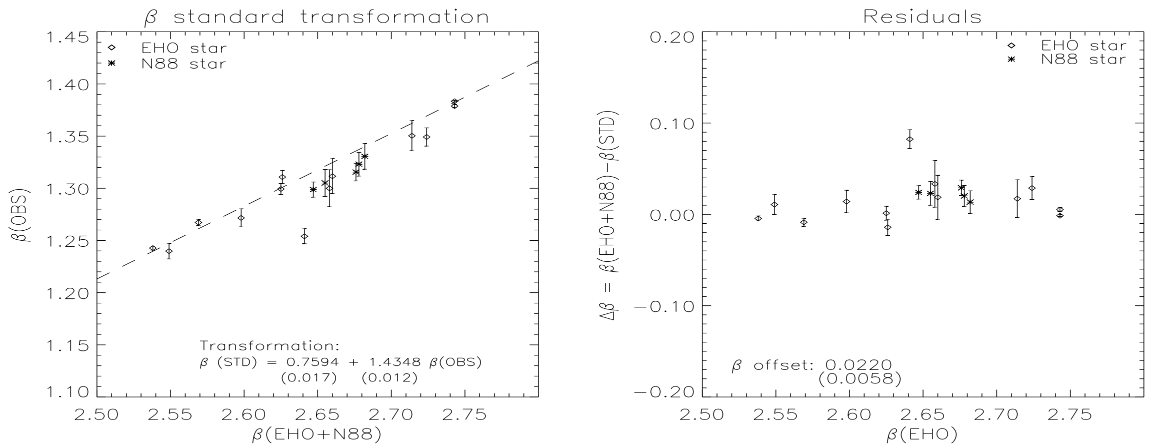

Figure 4.6: To the left I show the relation between the observed β and the standard β index. The linear transformation is plotted and quoted. To the right I show the residuals when using this transformation. Also plotted are five stars which Nissen [49] also observed. A significant offset is present between the β values of Nissen [49] and the present results.

Stars that deviate more than $\Delta_{lim} = 0.05$ magnitudes from the standard β index after the transformation are excluded, and a new linear fit is calculated (13 standard stars fulfill this criterion). I note that for some of the standard stars the β index of the EHO catalogue is determined from only 1 observation (*cf.* table 3.2). This may explain why some stars fall outside Δ_{lim}.

I have determined a linear standard transformation which is printed in the plot to the left in figure 4.6. As seen from the residuals, the observations do now allow for the determination of an additional second order term.

More importantly, there is a significant offset present compared to the results of NGC 3680 by Nissen [49]. I have corrected for the offset, $\Delta\beta = 0.022$. The standard transformation I have obtained is made from only 13 standard stars observed over a period of four nights. Nissen [49] has observed ~ 30 standard stars *each* night. I have thus decided that his standard transformation is more reliable.

It is important to note that the Strömgren standard stars I have used are F and G type stars. The stars near the turnoff region of NGC 6134 are A type stars, hence the standard transformation I have determined may cause errors for the β index of the brightest stars in this cluster.

4.2.3 The V magnitude

In figure 4.7 I have shown the relation between instrumental V and standard V magnitude including both the standard stars and the some of the secondary standards in NGC 3680 as observed by Nordström *et al.* [53].

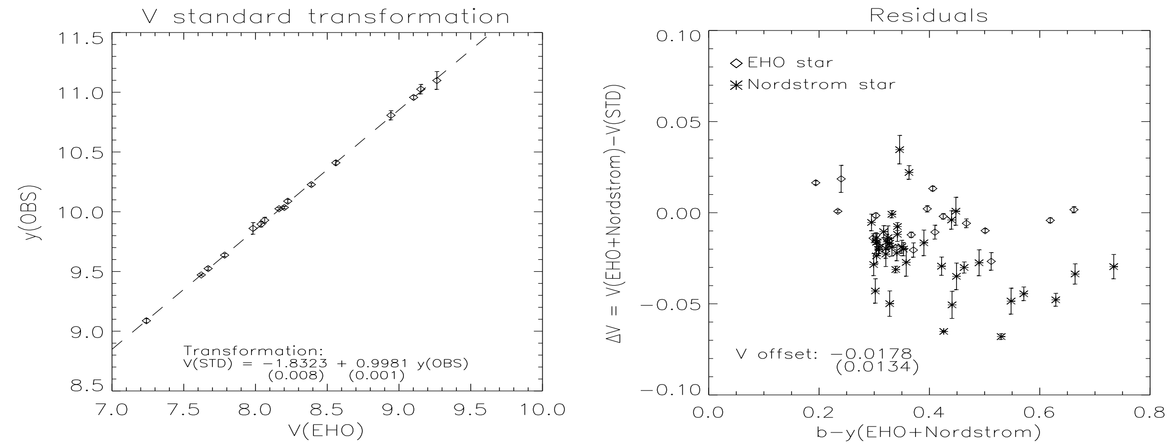

Figure 4.7: To the left I show the relation between instrumental y and standard V magnitudes. The linear transformation is also plotted and printed. To the right I show the residuals when using this transformation. Also plotted are the differences in V for stars from NGC 3680 observed by Nordström *et al.* [53].

An offset of $\Delta V = -0.018$ between the values of Nordström *et al.* [53] and the present results is seen. The V magnitude is a measure of the *absolute flux* from a star, and is more difficult to determine accurately than the Strömgren indices which measure *differences in flux*. A small error in the extinction coefficient for y may explain the result.

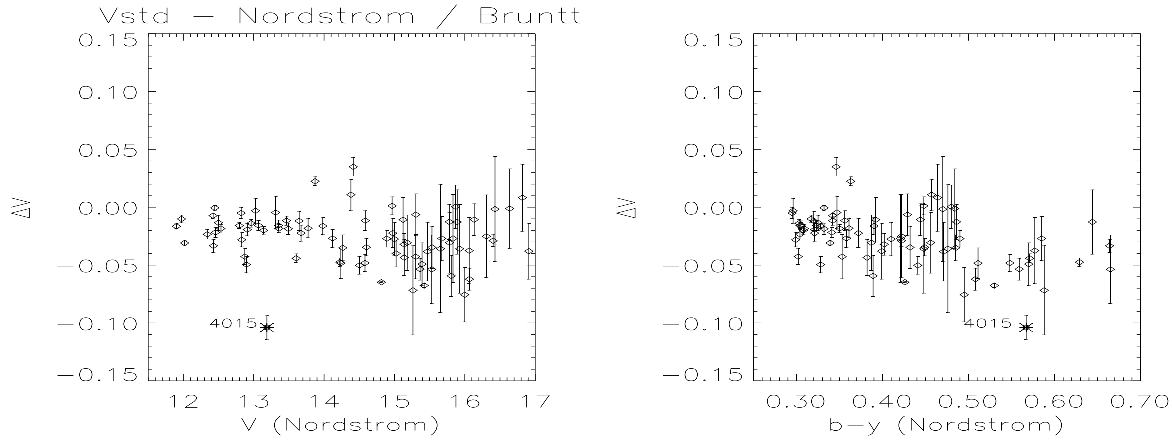

Figure 4.8: Comparison of V magnitudes of stars in NGC 3680. I show the results of Nordström *et al.* [53] and my results. Apparently the V magnitude of the relatively bright star 4015 disagrees with the result of Nordström *et al.* [53].

To investigate this difference more explicitly I have compared the V magnitudes determined by me and Nordström *et al.* [53]. The deviation as a function of V and $b-y$ in shown in figure 4.8. Note that only stars with small standard deviations are plotted ($\sigma < 0.03$). Obviously, cool (low $b-y$) and hence faint stars deviate the most. As mentioned earlier Nordström *et al.* [53] have calibrated their stars to the turnoff stars observed by Nissen [49] . Hence the dataset by Nordström *et al.* is calibrated by using standard stars with only a limited range in $b-y$ (0.25-0.5). This may explain the dependency on $b-y$ of the observed deviation between Nordström *et al.* [53] and my results.

4.2.4 The m_1 index

In figure 4.9 I present the result for the m_1 transformation by using the standard stars. The correlation between observed m_1 and standard m_1 is not so strong. This can also be seen more qualitatively on the relatively high standard deviation of the transformation coefficients. This is also evident from the residuals in the plot to the right of figure 4.9. The standard deviation of the standard m_1 index is around 0.02 mag.

On the plots I have also shown the measurements of stars in NGC 3680 by Nissen [49]. These secondary standard stars agree well with the primary standard stars. This indicates that the standard transformation is correct for stars near the turnoff of NGC 3680 which are F type stars with $b-y \simeq 0.3$. The F type stars in NGC 6134 have $b-y \simeq 0.5$ because of the high interstellar reddening of this cluster. Apparently there is a systematic trend in the right plot of figure 4.9, *i.e.* a colour dependency of the deviation may be present. Although this is somewhat speculative, as there are only few standard stars in the calibration, the m_1 index of the F stars of NGC 6134 may be overestimated by $\Delta m_1 \simeq 0.02$ mag. This is important for the determination of the metallicity which is calibrated for the F type stars. I will discuss this further in section 4.5 and 5.3, where I determine the metallicity.

- The final Strömgren indices for the open clusters are found in appendix E and are available through anonymous `ftp` as described in appendix F.

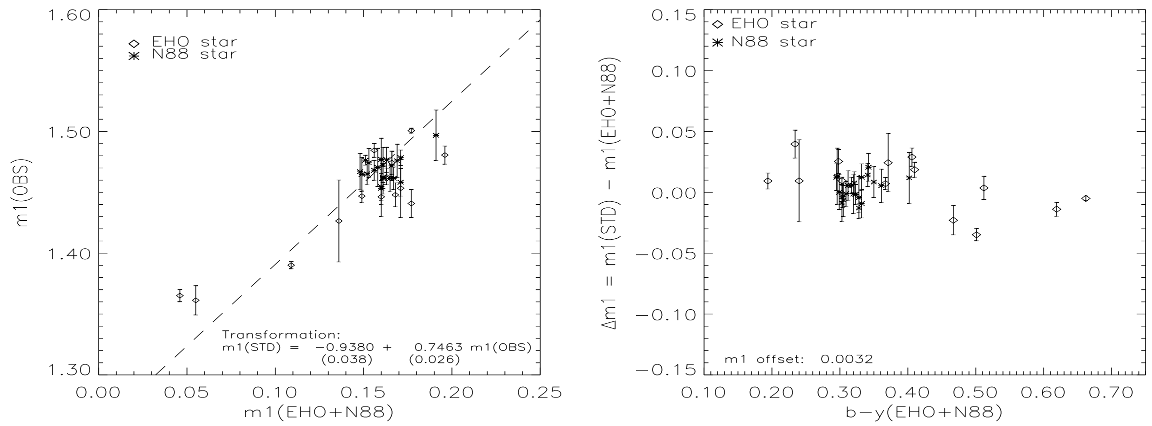

Figure 4.9: Standard transformation of the m_1 index (left) and the residuals after the fit (right).

4.3 The Balmer Discontinuity Index

I am not able to determine the Balmer discontinuity index, c_0, as the CCD was not sensitive to light in the u filter. In this section I will describe how I have estimated the c_0 index of the stars that may be cluster members of NGC 6134. I have not done this for NGC 3680, as the c_0 index has been measured for the stars near the turnoff by Nissen [49] and Twarog *et al.* [68].

A star is regarded as a probable cluster member if its interstellar reddening, $E(b-y)$, is close to the median value, $<E(b-y)>$, of the stars in the field. Thus I define probable cluster members as stars satisfying: $|E(b-y) - <E(b-y)>| < 0.06$. This limit corresponds to $3 \times \sigma(E(b-y))$. I will determine $E(b-y)$ of all stars in section 5.2.

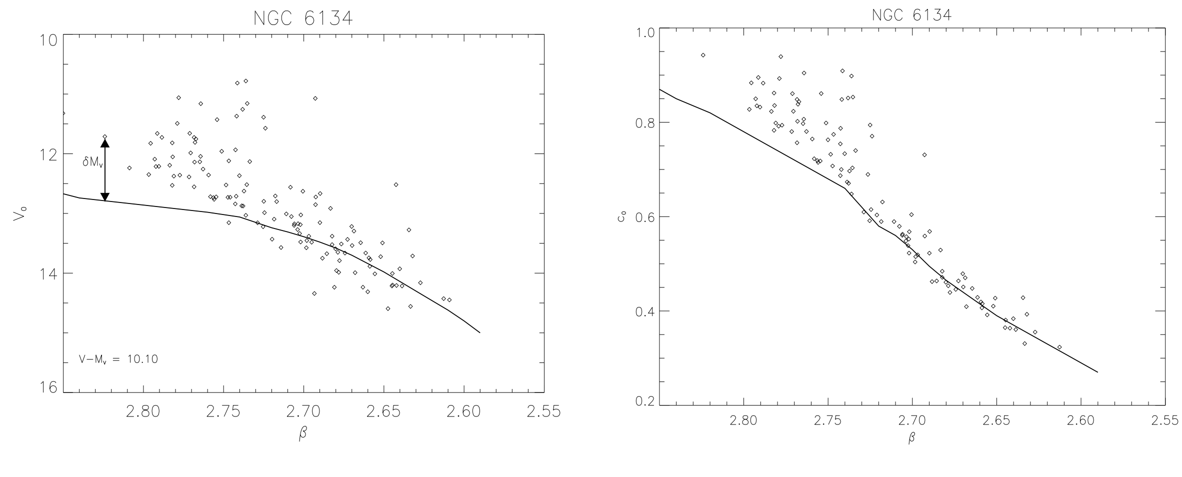

Figure 4.10: Left: V_0 as a function of β for the observed stars in NGC 6134 that are "probable cluster members". The solid line is the standard relation of Crawford [15], [17]. Note that this relation has been shifted $V - M_V = 10.1$, as to make the relation fit the lower main sequence of stars. Right: The offset δM_V (indicated on the left plot for one star) has been translated to the c_0 index by using equation 4.4.

In appendix A I have described the Strömgren photometric system, including the Balmer discontinuity index, c_0. In this appendix I have described the application of this index: c_0 depends on temperature, but it also measures to what extent a star has evolved above the ZAMS.

Stars in a stellar cluster that are of relatively low mass have only evolved little because of their long evolution time scale. Consequently, their c_0 index is close to the value for a ZAMS star of the same temperature. At the other end of the mass range we find the stars around the turnoff. These stars are highly evolved and thus have a high c_0 index compared to ZAMS stars of the same temperature.

The evolution above the ZAMS of a star in a cluster can be measured by the c_0 index or through the quantity $\delta M_V = M_V(ZAMS) - M_V$, where $M_V(ZAMS)$ is the absolute V magnitude of a ZAMS star, and M_V is the observed absolute V magnitude. $M_V(ZAMS)$ is the value at the same temperature as the observed star, measured by *e.g.* the β index.

Crawford has calibrated $M_V(ZAMS), \beta$, and c_0 for bright stars near the Sun. The calibration for F type stars ($2.59 < \beta < 2.72$) is found in Crawford [15], while the calibration for A type stars ($2.72 < \beta < 2.88$) is available in Crawford [17], *cf.* table A.1 of appendix A. In figure 4.10 I show the observed V magnitudes as a function of β for NGC 6134. Only stars that agree with the $E(b-y)$ criterion defined above are plotted.

The relation between δM_V and c_0 has been determined by Nissen [49] for F stars:

$$\delta M_V = f * \delta c_0 = (9 + 50(2.72 - \beta)) * \delta c_0, \tag{4.4}$$

where $\delta c_0 = c_0 - c_{0,\mathrm{ZAMS}}(\beta)$. Crawford [17] has made a similar calibration for A stars, and finds a value of $f = 9$ which is in agreement with equation 4.4 at $\beta = 2.72$.

By using these calibrations I have determined the c_0 index for the stars in NGC 6134 which fulfill the criterion (for interstellar reddening) described above. A presentation of the method used and the resulting c_0 indices is presented in figure 4.10. I note that unresolved double stars will of course have unreliable c_0 indices. The numerical values of the c_0 indices can be found in appendix E.

4.4 Johnson UBV Magnitudes of NGC 6134

Viskum [71] has made broad band Johnson-UBV measurements of NGC 6134. I have compared the Strömgren $b-y$ and Johnson $B-V$ colours which are both measures of the temperature (the response function of these bands are show in figure A.1, appendix A).

I have 106 stars in common with the observations by Viskum [73]. In figure 4.11 I have shown the relation between the two temperature sensitive indices. Only stars with $\sigma(b-y) < 0.02$ are plotted (~ 60 stars).

As can be seen there is a significant spread the relation between $b-y$ and $B-V$. From the plots in figure 4.11 I have estimated $\sigma(B-V) \simeq 0.02$. When using the calibration $(B-V)_0 = -2.4\log(T_{\mathrm{eff}}) + 9.562$ of Kjeldsen [39], the observed $\sigma(B-V)$ corresponds to an error in T_{eff} of 5%. This is significantly above the uncertainty when using only the photometric precision of $b-y$ which corresponds to 2.5% in T_{eff} (to obtain this result I have used the results of the photometric precision of section 4.4 for the brightest stars and equation 5.1).

In figure 4.12 I present the difference in V magnitude determined by Viskum [71] and the present work. The differences are plotted as a function of both V and $b-y$. As was the case for the comparison of V magnitudes with Nordström *et al.* [53] in figure 4.8 there is a small offset error, *i.e.* $\Delta V = -0.033$. Note that this is computed ignoring 3σ outliers. No significant dependency of colour is seen in the plot of the residuals to the right in figure 4.12, indicating that the standard transformation is essentially correct.

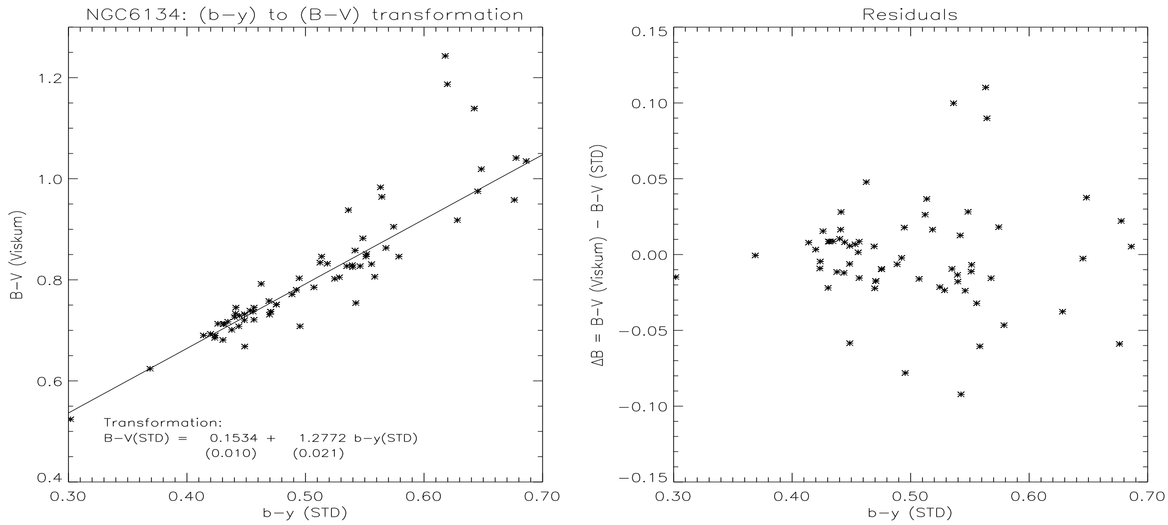

Figure 4.11: The relation between my result for Strömgren $b-y$ and Johnson $B-V$ measured by Viskum [71]. I have determined a linear relation written in the plot (left). In the plot to the right I show the residuals using this transformation.

4.5 Photometric Precision / Accuracy

It is of great interest to know the photometric precision the Strömgren indices. In figures 4.13 and 4.14 below I show the standard deviation of the derived Strömgren indices as a function of the derived V magnitudes for NGC 6134 and NGC 3680. The β and m_1 index have somewhat higher standard deviation than the $b-y$ colour. The reason for the standard deviation being relatively high for the β index is because of the low counts in the narrow β filter. The m_1 index is calculated from the combination of four magnitudes (equation A.8), from which the photometric errors are added.

In table 4.2 I have quoted the approximate standard deviation of Strömgren indices for the stars around the turnoff of each cluster, *i.e.* F type stars for NGC 3680 and A type stars for NGC 6134. I have also quoted the result for F type stars in NGC 6134, *i.e.* stars with $V \simeq 15$. The F type stars are important as the metallicity of cluster can be determined from these stars by using the m_1 and the β index.

For the turnoff stars the precision is comparable to the precision of the photoelectric measurements by *e.g.* Erik Heyn Olsen [54]. It will certainly be interesting to use the Strömgren indices to determine the basic parameters of the open clusters, which I will do in the next chapter.

It is important to keep in mind that in addition to the photometric precision found here, systematic errors may also be present. Now I am turning to the *accuracy* as opposed to *precision* of the photometry.

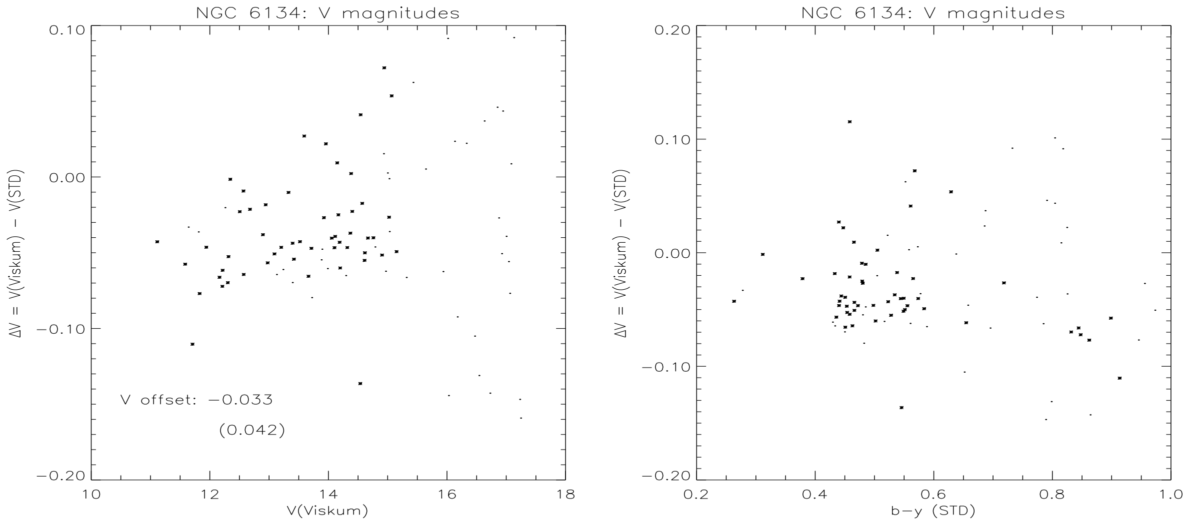

Figure 4.12: Difference in V magnitudes of stars in NGC 6134: I show the results of Viskum [71] and the results presented in this thesis. The plot to the left shows the difference ΔV as a function of V while the plot to the right shows the ΔV as a function of standard $b-y$. Large points have $\sigma(V) < 0.005$ while small points have $\sigma(V) < 0.01$.

Systematic errors may come from erroneous extinction coefficients or errors because too few standard stars are used to find the standard transformation. An example is the V magnitudes that I have found for NGC 3680 and NGC 6134. Compared to previous measurements I find offsets of $\Delta V = -0.018$ mag and $\Delta V = -0.033$ mag for these clusters, *cf.* sections 4.2.3 and 4.4. A systematic offset of $\Delta\beta = 0.022$ mag was found for the β index when comparing my results for NGC 3680 with what was determined by Nissen [49] in section 4.2.2.

My results for the $b-y$ and m_1 indices for NGC 3680 agree well with Nordström *et al.* [53] and Nissen [49]. Special caution should be exerted with the m_1 index, though, as significant residuals were seen in the standard transformation (figure 4.9). It is reassuring that the m_1 index agree with what was obtained by Nissen [49] for NGC 3680. For NGC 6134 a systematic offset of 0.02 mag may be present as discussed in section 4.2.4. This corresponds to the metallicity being extimated to be too high by 0.3 dex, *cf.* equation A.10 of appendix A.

Table 4.2: Approximate standard deviations of the Strömgren indices for stars near the turnoff (TO) of NGC 6134 and NGC 3680. For NGC 6134 I have also quoted the standard devitation for type F stars, *i.e.* stars with $V \simeq 15$.

Cluster	V	$b-y$	m_1	β
NGC 6134, TO	0.004	0.007	0.009	0.010
NGC 6134, F	0.010	0.020	0.020	0.020
NGC 3680, TO	0.004	0.007	0.008	0.016

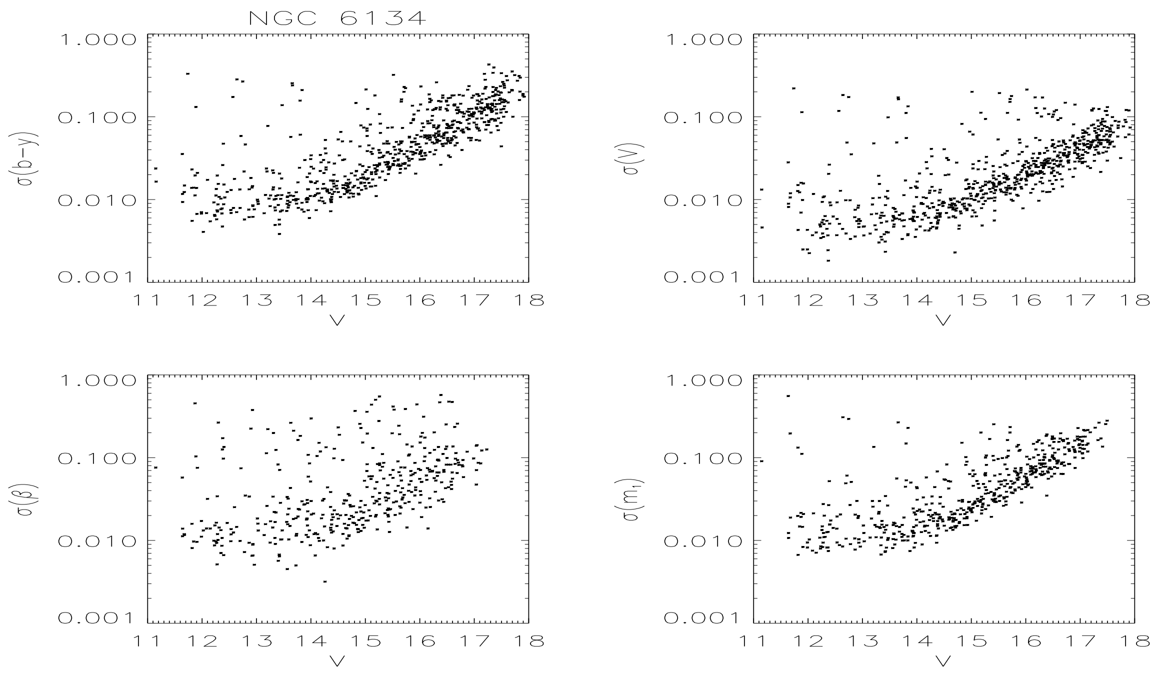

Figure 4.13: Standard deviation of the Strömgren indices for the observed stars in NGC 6134 as a function of V magnitude. The complete list of Strömgren indices and standard errors is found in appendix E.

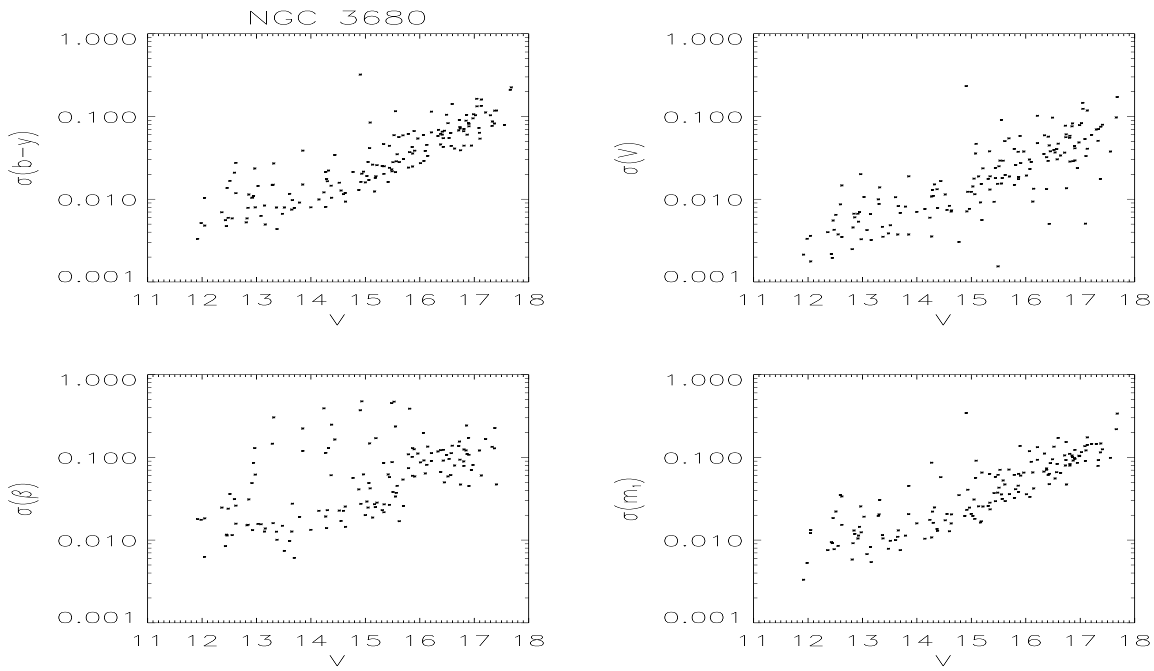

Figure 4.14: Standard deviation of the Strömgren indices for the observed stars in NGC 3680 as a function of V magnitude. The complete list of observed Strömgren indices and standard errors is found in appendix E.

4.6 Summary of Chapter 4

Summary of the most important results and conclusions of this chapter:

- I have used both the open clusters and the standard stars to determine the extinction coeffients. It was difficult to determine the extinction coeffients as there was little spread in airmass, *i.e.* errors of ± 0.01 may be present in the extinction coefficients

- I have used the observed Strömgren standard stars to determine the transformation of the instrumental magnitudes to the Strömgren indices

- The Strömgren indices for NGC 3680 agree with previous results by Nordström *et al.* [53], Twarog *et al.* [68], and Nissen [49], although small offsets (~ 0.02 mag) are seen in β and V. I have corrected for this offset in the β index. The m_1 index may have an offset error of $\Delta m_1 \simeq 0.02$ for stars in NGC 6134!

- I have calibrated the $b-y$ colour with a wider range in $b-y$ of the standard stars, than what has been done previously by *e.g.* Nordström *et al.* [53] and Twarog *et al.* [68] for stars in NGC 3680. I assert that my calibration is more reliable for the faint stars in this cluster, *i.e.* stars with $b-y > 0.4$

- There is a small offset in the V magnitude for NGC 6134 when compared to what was obtained by Viskum [71]. The temperature sensitive indices $b-y$ and $B-V$ (Viskum) are well correlated

Chapter 5

Observational Results: NGC 6134 and NGC 3680

In this chapter I will present the astrophysical results of the open clusters NGC 6134 and NGC 3680. I will derive the following properties of the clusters:

- Interstellar reddening, $E(b-y)$
- Metallicity, $[Fe/H]$
- Distance, d
- Age, A

NGC 6134 is the cluster for which I have obtained the most extensive amount of data, while the results of NGC 3680 have been used as a secondary reference in the standard transformation (*cf.* chapter 4). The results presented here are perhaps most interesting for the primary target NGC 6134, as previously published work does not have such an extended sample of stars, *i.e.* Kjeldsen *et al.* [38] and Viskum [71]. As NGC 3680 is considered a well-calibrated cluster, the astrophysical parameters derived in the present work are expected to agree with previously published results, *e.g.* Nordström *et al.* [53].

5.1 Colour-Magnitude Diagram

In figure 5.1 below I present the observed colour-magnitude diagrams (CMD) for the open clusters NGC 6134 and NGC 3680. In each diagram ~700 (NGC 6134) and ~ 160 (NGC 3680) stars are plotted. I have indicated the seven known variable stars of NGC 6134 and the 14 single stars that are cluster members of NGC 3680 as determined by the spectroscopy of Nordström *et al.* [53]. I have corrected the V magnitude and the $b-y$ colour for interstellar reddening. Hence, the CMDs appear as if there was no interstellar extinction. Larger versions of the CMDs are found in appendix E.

The CMDs cannot be compared directly, though, as they are not located at the same distance and the clusters are made from gas with quite different contents of heavy elements. Still, it is evident that the turnoff stars of NGC 3680 are found at somewhat higher values

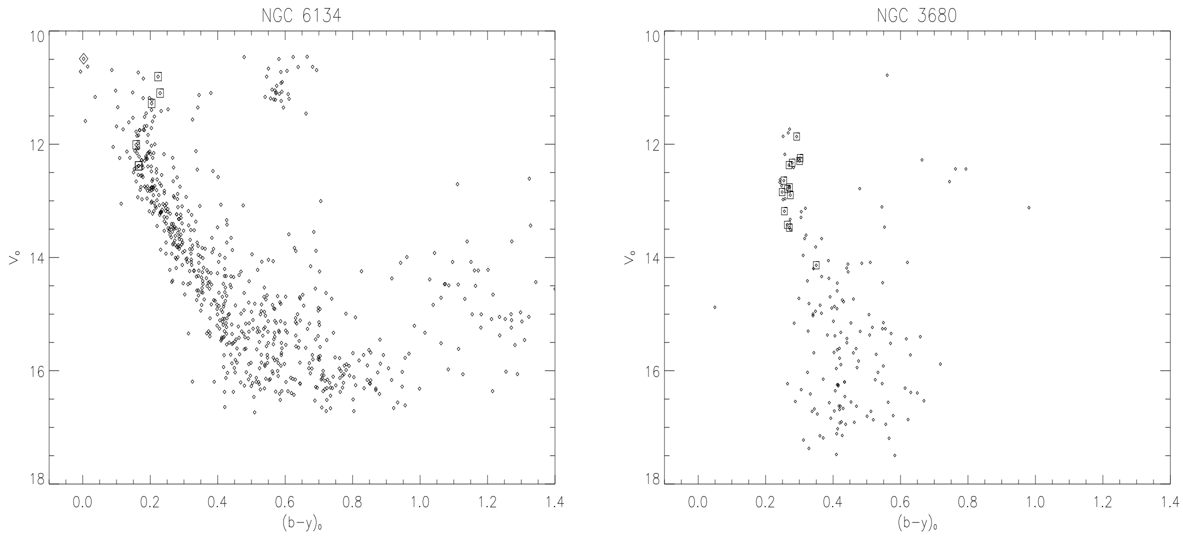

Figure 5.1: The CMD of NGC 6134 (left). Known variable stars are indicated, - squares are δ Scuti stars and the diamond is the blue straggler. In the CMD of NGC 3680 (right) I have indicated the stars that are single cluster members according to Nordström *et al.* [53].

of $(b-y)_0$ than for NGC 6134, hence they are cooler and of lower mass. The immediate conclusion is that NGC 3680 is some what older than NGC 6134.

Frandsen *et al.* [29] have detected seven variable stars in NGC 6134 of which six are of δ Scuti type. According to figure 1.2 the δ Scuti stars are found where the Cepheid instability strip and the zero age main sequence cross. The position and width of the instability strip have been investigated observationally by Rodriguez *et al.* [59]. In figure 5.2 I show the turnoff region of the CMD of NGC 6134. Also plotted are the red and blue borders of the observationally determined instability region according to Rodriguez *et al.* It is reassuring that the six δ Scuti stars are indeed lying in this region.

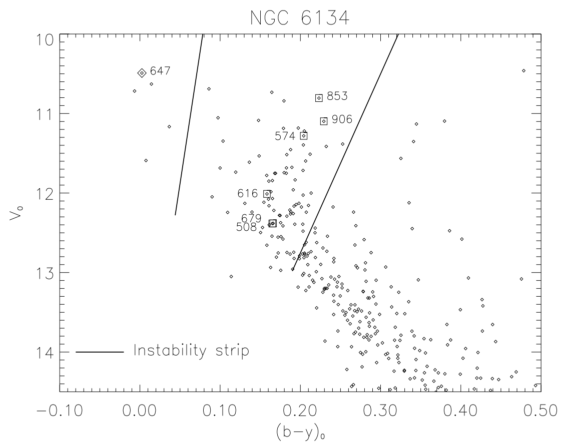

Figure 5.2: The turnoff region of the CMD of NGC 6134. The known δ Scuti stars are plotted with squares. The solid lines indicate the instability strip as determined observationally by Rodriguez *et al.* [59].

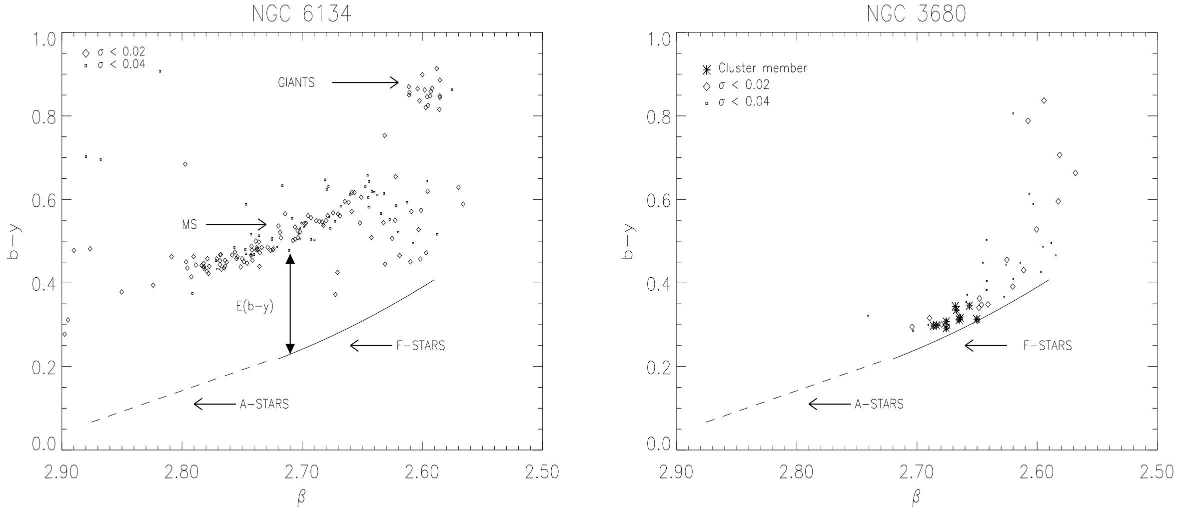

Figure 5.3: The plots show the $b-y$ colour of the observed stars as a function of measured β index for both clusters. Stars with low standard deviation are plotted with larger points. I have also plotted the relation of Crawford [15],[17], for stars near the Sun, *i.e.* stars with essentially no interstellar reddening: The solid line is the calibration for F type stars while the dashed line is for A type stars. In the plot of NGC 6134 I have indicated the position of the main sequence (MS) stars and the giant stars. In the plot of NGC 3680 the symbol * is used for the confirmed cluster members (according to Nordström *et al.* [53]).

5.2 Interstellar Reddening of the Clusters

In the following I will determine the interstellar reddening of individual stars of both clusters. I will use this to find out which stars in the CMD are probable cluster members. Having this information is important as I will fit isochrones to these stars.

The interstellar reddening $E(b-y)$ can be found using the β and $b-y$ values of the main sequence stars in the open clusters. To the first order $E(b-y)$ can be found using only these two quantities. In figure 5.3 I show how they depend on each other. In this figure I have also shown the relation for stars near the Sun, *i.e.* where the interstellar reddening is negligible. This is taken from the calibrations of Crawford for F stars ($2.59 < \beta < 2.72$) [15] and A stars ($2.72 < \beta < 2.88$) [17].

Unlike the β index the $b-y$ colour depends on the amount of interstellar reddening. This fact may be used to determine the interstellar reddening. As seen in figure 5.3 the stars of NGC 6134 have very high $b-y$ values compared to the unreddened stars (solid/dashed line). On the other hand the interstellar reddening is very small for NGC 3680.

The precise value of the interstellar reddening $E(b-y)$ is found by using the calibrations of Crawford [15],[17] with a small correction which was noted by Nissen [49]. Specifically, I use equations A.2-4 of appendix A to calculate the unreddened $b-y$ value for each star, *i.e.* $(b-y)_0$, which can be derived from the β, c_0 and m_0 indices. I note that as a first approximation I have neglected the small term including the c_0 index: As I have not measured the Strömgren u magnitudes, I cannot determine this index.

The m_0 value is the reddening corrected m_1 index (equation A.9), which requires knowledge of $E(b-y)$! Consequently, I have to determine $E(b-y)$ iteratively. For NGC 6134 I use the previously determined $E(B-V)$ of Kjeldsen *et al.* [38] as a first guess, *i.e.*

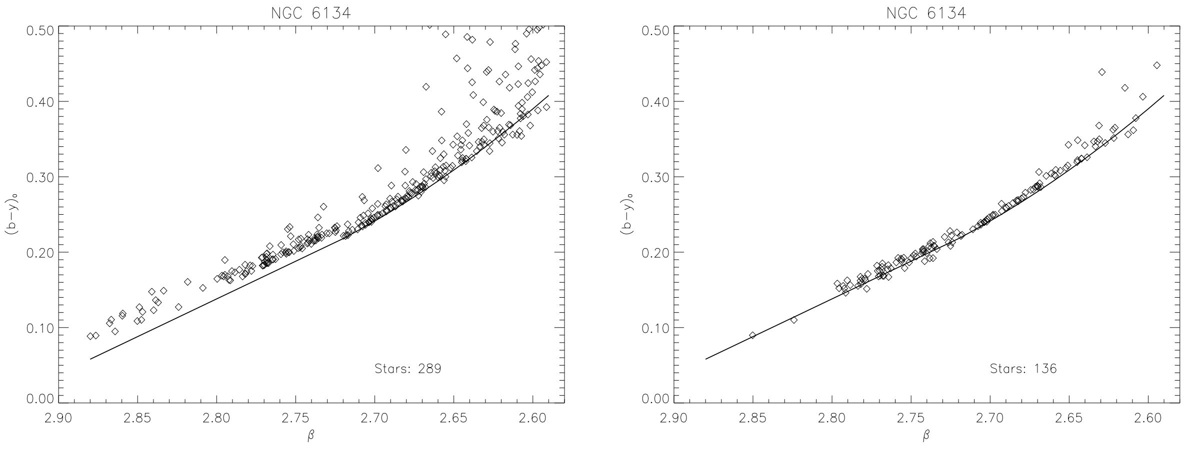

Figure 5.4: The plots show the reddening corrected b_y as a function of β for stars in NGC 6134. The standard relations of Crawford are also plotted (solid line). The plot to the left shows the result neglecting the term including the Balmer discontinuity index c_0, while in the plot to the right I have included this in the calculations.

$E(b-y) = 0.322$, *cf.* table 2.1. Using this value I am able to determine $(b-y)_0$ and thus also the reddening by subtracting this value from the observed $b-y$.

I then compare the derived value of $E(b-y)$ with the initial guess. If the difference is larger than $\delta_{lim} = 0.002$, I recalculate $E(b-y)$ using the new value.

In this way I iteratively derive the mean $<E(b-y)>$ value of all the stars. Ideally the stars should be distributed around the relation of Crawford. The result after four iterations is shown in the plot to the left of figure 5.4. There is a significant offset from the standard relation for stars with high a β index, *i.e.* the A stars. This is explained by the neglect of the term including the Balmer discontinuity index in equations A.3-4. In these equations the term δc_0 measures the c_0 index compared to the value of the ZAMS. As the turnoff stars of NGC 6134 are evolved type A stars, their values of c_0 will certainly deviate from the ZAMS value!

Having obtained this result I found a way to determine the c_0 without having measured the u magnitudes. This is described in section 4.3. After inclusion of the term in c_0 I found the relation plotted to the right in figure 5.4.

For NGC 3680 I used $E(b-y)$ published by Nissen [49] as the initial guess, *i.e.* $E(b-y) = 0.034$, *cf.* table 2.1. In this case I used the c_0 indices published by Nissen [49]. According to the spectroscopy of Nordström *et al.* [53] only 14 stars in my sample are confirmed single cluster members! As described in Nordström *et al.* [53] many of the field stars have values of $E(b-y)$ and $[Fe/H]$ that are similar to the cluster stars. I included a few stars that were not examined spectroscopically by Nordström, but the final $E(b-y)$ was not changed significantly by this, *i.e.* within the standard deviation of the derived value. The $E(b-y)$ value of all stars is presented in appendix E.

I have shown the results of the reddening determination of all stars as histogram plots to the left in figure 5.5 (NGC 6134) and 5.6 (NGC 3680). For both clusters it is evident that quite a few stars in the field have $E(b-y)$ more than *e.g.* 3σ from the mean value. The cluster stars are assumed to have the same distance and hence also the same interstellar reddening. As a first approximation stars whose $E(b-y)$ fall outside the 3σ limit are not

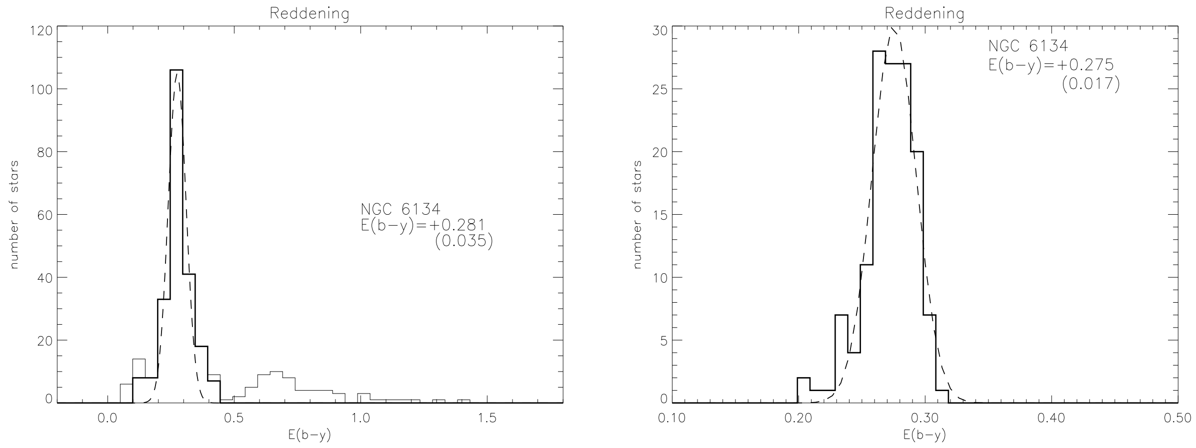

Figure 5.5: Histogram of the derived values of interstellar reddening for NGC 6134 (left) of all stars, ignoring the c_0 term. The second plot includes only stars for which c_0 has been determined. Notice that the ranges on the abscissa and ordinate are different. I have fitted a Gaussian to the histograms.

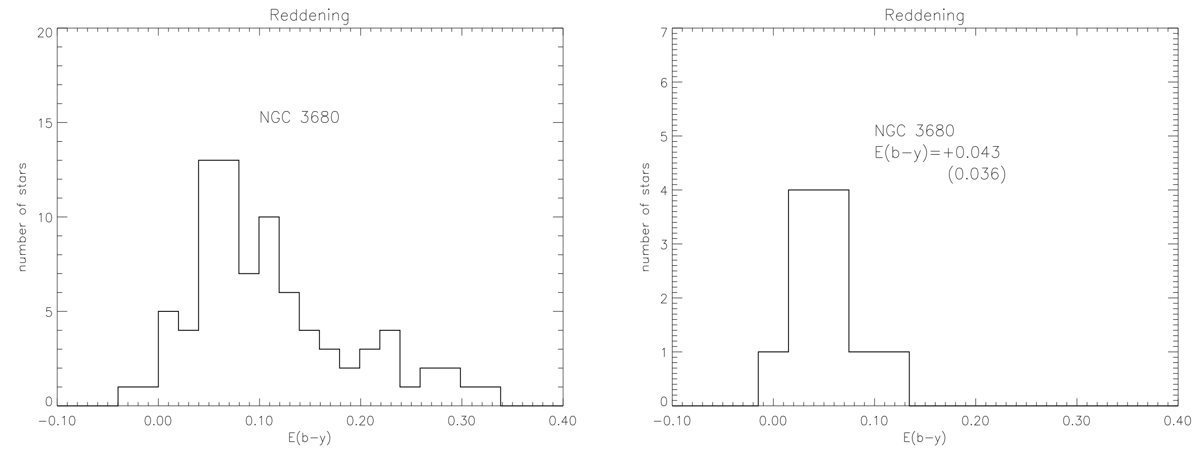

Figure 5.6: Interstellar reddening for stars in NGC 3680. All stars with measured $E(b-y)$ are shown to the left. Stars that are confirmed cluster members are plotted to the right (11 stars). The mean value and standard deviation of these stars are printed.

members of the cluster. In the plots to the right of figures 5.5 and 5.6 I show the result when including only "probable" cluster members.

The result when using the probable cluster members is shown in table 5.1. For NGC 6134 I have quoted the value obtained by fitting a Gaussian distribution to 140 stars in the histogram to the right in figure 5.5. I also quote the standard deviation of the mean value for these stars ($\sigma_E = \sigma/\sqrt{N}$). For NGC 3680 I have quoted the mean value and standard deviation (of the mean value) of the 11 stars that are single cluster members according to Nordström *et al.* [53] for which I have determined $E(b-y)$.

In table 2.1 I have quoted previously published values for the interstellar reddening of the open clusters which may be compared with the results in table 5.1. For NGC 3680 Nissen [49] also used Strömgren photometry and found $E(b-y) = 0.034 \pm 0.005$ which is in agreement with my results.

Table 5.1: Mean interstellar reddening of "probable cluster members" in NGC 6134 and NGC 3680

Cluster	$E(b-y)$	σ_E
NGC 6134	0.275	0.002
NGC 3680	0.043	0.011

For NGC 6134 Kjeldsen *et al.* [38] have found $E(b-y) = 0.32 \pm 0.04$. Claria *et al.* [13] find $E(b-y) = 0.25 \pm 0.02$ from their study of 24 red giants in the field of NGC 6134. Both of these studies use Johnson UBV photometry. My result also seems to agree with the previous results for NGC 6134.

I note that a systematic error in the β index of ± 0.01 will shift $E(b-y)$ by ± 0.02, while an offset in the $b-y$ colour of the same size shifts $E(b-y)$ by ± 0.01. Offsets of this size may be present because of the uncertainty of the extinction coefficients, *cf.* section 4.1.

5.3 Metallicity of the Clusters

The Strömgren m_1 index is correlated with the metallicity, $[Fe/H]$, for F type stars, *i.e.* stars with $2.59 < \beta < 2.72$. The relation has been calibrated by Nissen [50] and I have quoted the result in equation A.10. For stars of earlier type, *i.e.* A stars, there is apparently no simple correlation between metallicity and m_1. Crawford [17] speculates that the m_1 index may depend on the rotational velocity for A stars.

In figure 5.7 I have plotted the (reddening corrected) m_0 index as a function of the β index for NGC 6134 and NGC 3680. Also plotted is the Hyades standard relation according to Crawford [15], [17]. Note that only stars with a "well-determined" m_0 index are plotted, *i.e.* $\sigma(m_0) < 0.05$. For NGC 3680 I have plotted the known cluster members with a "*" symbol.

As can be seen from the plot to the left of figure 5.7 the F stars of NGC 6134 define a narrow sequence with m_0 values larger than the Hyades cluster. According to the calibration by Nissen [49] (equation A.10) this means that NGC 6134 has a higher metallicity that the Hyades, *i.e.* $[Fe/H] > 0.12$ (Cayrel *et al.* [12]). On the other hand the plot to the right of figure 5.7 shows that the cluster members of NGC 3680 have almost the same or perhaps a somewhat lower metallicity than the Hyades.

I have calculated the metallicity for all F type stars in both clusters by using equation A.10. In the plots to the left of figure 5.8 and 5.9 I show histograms of the result for all F type stars in NGC 6134 and NGC 3680 respectively. In the plot to the right of figure 5.8 I have plotted the result for stars in NGC 6134 that fall within 3σ of the mean interstellar reddening, $E(b-y)$, *i.e.* the probable cluster members (52 stars). In the plot to the right of figure 5.9 I show the result for 12 single cluster members, *i.e.* when using the membership assignment by Nordström *et al.* [53]. Apparently two stars lie significantly above and below the mean value of ten of the stars.

In table 5.2 below I give the final result for the mean metallicity of cluster members of the two clusters when excluding 3σ outliers. Also quoted is the standard deviation of the mean value $(\sigma/\sqrt{N})$. The metallicities found here are used as input to the isochrone fit

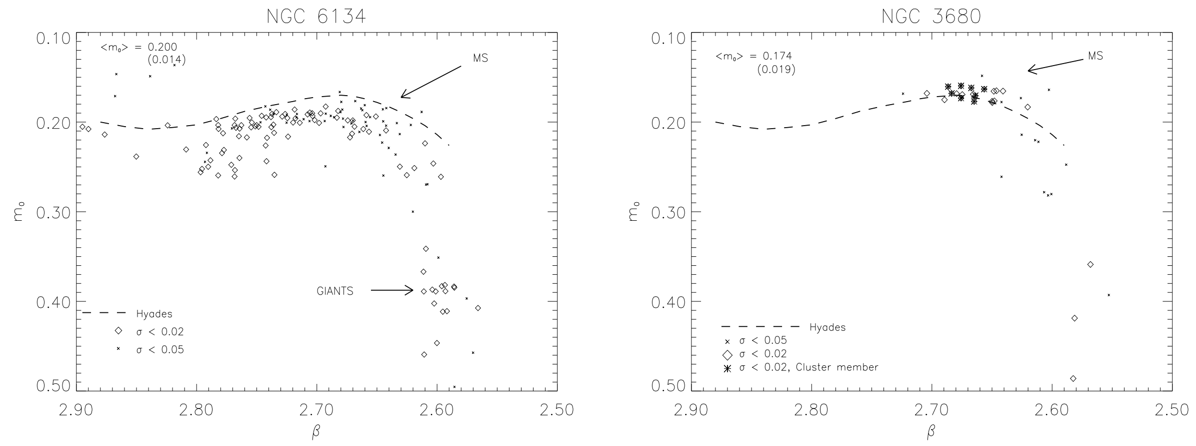

Figure 5.7: The relation between m_0 and β for stars in NGC 6134 (left) and NGC 3680 (right). Also plotted is the standard Hyades relation taken from Crawford [15], [17].

which is described in section 5.4.

The result for NGC 3680 agree reasonably well with the result of Nissen [49] who found $[Fe/H] = 0.11 \pm 0.05$ for nine single cluster members as identified by Nordström *et al.* [53] . My result for NGC 6134 is somewhat higher than what is quoted in Lyngå [45], $[Fe/H] = 0.25$. The source of this result is not quoted in Lyngå ! The metallicity found by Claria *et al.* [13] is $[Fe/H] = 0.05 \pm 0.10$. They have analysed 24 red giants in the field of NGC 6134 by using various methods, *i.e.* UBV, DDO, and Washington photometry, which yield quite different results in the range $-0.16 < [Fe/H] < 0.08$.

Table 5.2: Mean metallicity of "probable cluster members" in NGC 6134 (52 stars) and NGC 3680 (10 stars). The metallicity of NGC 6134 may be erroneously high (hence the *).

Cluster	$[Fe/H]$	$\sigma_{Fe/H}$
NGC 6134	*0.41	0.02
NGC 3680	0.03	0.02

As discussed in section 4.2.4 (and 4.5) the m_1 index of NGC 3680 agree with what has been measured previously by Nissen [49] . On the other hand a systematic offset in m_1 of the order 0.02 mag may be present for NGC 6134 (overestimated), because the m_1 standard transformation is not reliable for the F stars of this cluster. An offset of this size corresponds to a change in $[Fe/H]$ of -0.3 dex! Therefore the metallicity of NGC 6134 should be not regarded as being well determined. This shows the limits of the Strömgren photometry, when the indices are not well calibrated. It would thus be very interesting to determine the metallicity of NGC 6134 by doing spectroscopy.

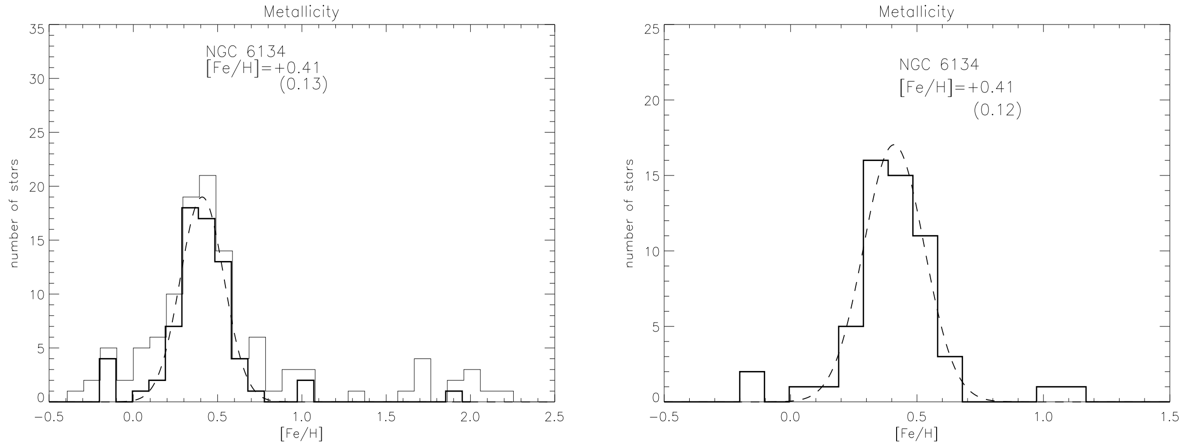

Figure 5.8: Metallicity for stars in the field of NGC 6134. In the left plot the result is shown for all stars. To the right I have plotted the result for stars that are probable cluster members, *i.e.* stars with interstellar reddening within 3σ of the mean value, *cf.* table 5.1. Note that the scales on the plots are different. In each figure I have fitted a Gaussian to the distribution (dashed curve).

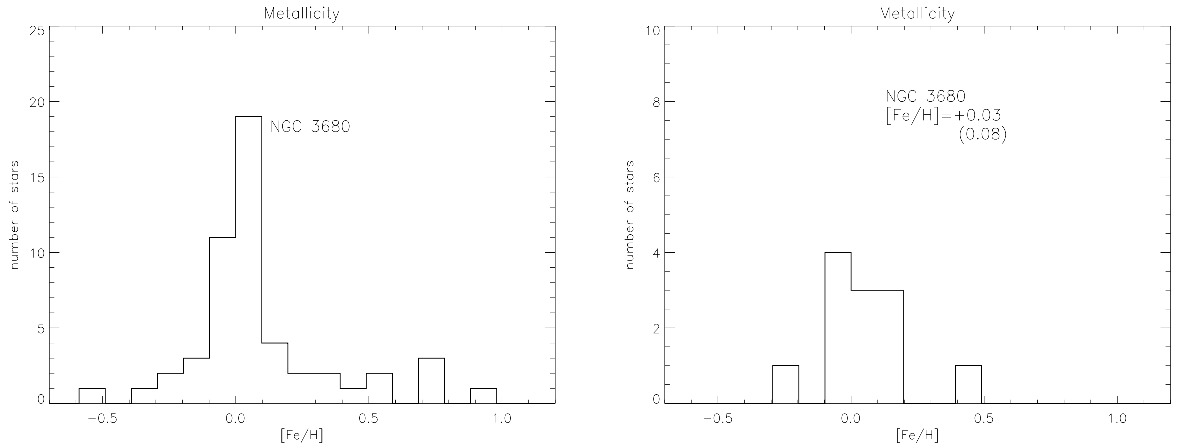

Figure 5.9: Metallicity for stars in 3680. To the left $[Fe/H]$ is plotted for all stars in the field. In the right plot only stars that are cluster members according to Nordström *et al.* [53] are included.

5.4 Cluster Ages and Distances

In order to determine the distances and ages of the observed clusters, I have fitted isochrones to the observed colour-magnitude diagrams. This method is described qualitatively in section 1.4.

I have used the software package by Pols *et al.* [57] to calculate theoretical isochrones. In appendix B I have described these isochrones, and examined the general dependency on age and metallicity. I have used two different models, one using standard stellar structure and evolution models and one that includes overshoot in the convective cores.

The programme requires essentially three input parameters: The age and metallicity, and which of the two models is desired. The programme then calculates the evolution of a grid of stars with increasing masses with the specified metallicity and the desired theoretical model from age zero to the age given as input. The output of the evolution programme is a list of effective temperatures, T_{eff} and luminosities, L for the grid of stellar masses.

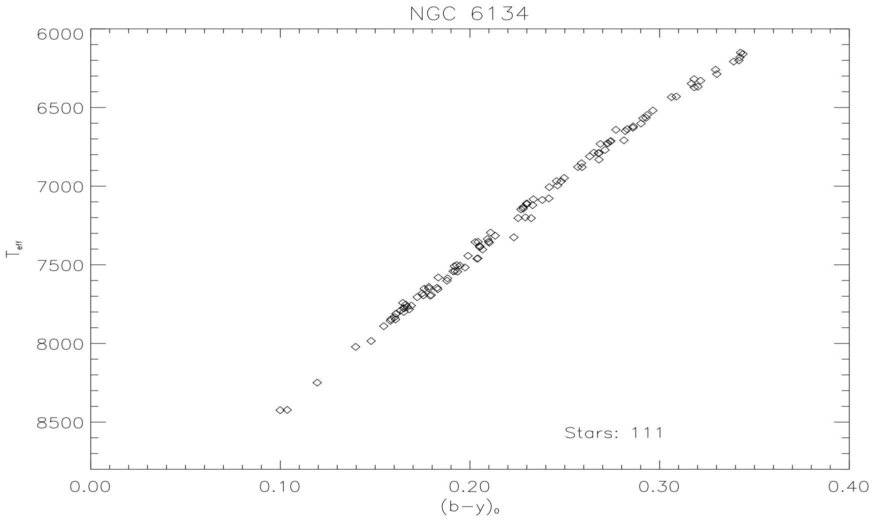

Figure 5.10: The derived effective temperatures, T_{eff}, when using the calibration of Alonso *et al.* [2]. The effective temperature is shown as a function of $(b-y)_0$ for stars in NGC 6134 that are probable cluster members.

There are several problems that must be considered when fitting theoretical isochrones. The first problem is the transformation of the theoretical values, *i.e.* T_{eff} and L to the observed values, *e.g.* $b-y$ and V. The software package by Pols *et al.* [57] uses synthetic stellar spectra of Kurucz [43] to determine the Johnson $B-V$ colour and the absolute V magnitude: M_V. I have used the well-calibrated results of Alonso *et al.* to obtain T_{eff} from the Strömgren indices I have derived. Equation (9) of Alonso *et al.* [2] reads:

$$\begin{aligned}\theta_{\text{eff}} = \;& 0.537 + 0.854(b-y) + 0.196(b-y)^2 \\ & - 0.198(b-y)c_0 - 0.026(b-y)[Fe/H] - 0.014[Fe/H] - 0.009[Fe/H]^2,\end{aligned} \tag{5.1}$$

where the Strömgren indices are corrected for interstellar reddening, and $T_{\text{eff}} = 5040\text{K} \;/\; \theta_{\text{eff}}$. This calibration is valid for main sequence stars in the range $4000K < T_{\text{eff}} < 7200K$

and $-3.0 < [Fe/H] < 0.5$. The term including c_0 accounts for the effect of stellar evolution, which is important for stars in the turnoff region of the clusters.

As mentioned previously my observations of NGC 6134 do not allow a direct calculation of the c_0 index, but I have determined it "indirectly" in section 4.3. On the other hand c_0 has been determined for the turnoff stars of NGC 3680 by Nissen [49], and I have used these results to obtain T_{eff}. The standard deviation of T_{eff} is 200-300K for the turnoff stars. In the isochrone fit I have excluded stars with $\sigma(T_{\text{eff}}) > 400K$.

The derived effective temperatures of the stars in NGC 6134 for which I have inferred the c_0 index are plotted in figure 5.10, *i.e.* stars that are probable cluster members. Note that a few stars fall outside the calibration interval of Alonso *et al.* [2]. Most importantly, the six known δ Scuti are among these. As can be seen T_{eff} is still growing "smoothly" with $(b-y)_0$ at these high temperatures. This indicates that the determined values of T_{eff} for the turnoff stars in NGC 6134 are not "far off", *i.e.* the terms in equation 5.1 do not change very strongly when going outside the calibration limits. In the paper by Alonso *et al.* [2] they have also plotted a few hot stars that fall outside the calibration limit, and their effective temperatures also follow the smooth increase with $(b-y)_0$. Still, systematic errors may be present for these stars.

The unknowns when fitting the theoretical isochrones are the age, metallicity, interstellar reddening, and the distance modulus. I have used the interstellar reddening and metallicity determined in section 5.2 and 5.3, *cf.* table 5.1 and 5.2. Thus only two parameters are allowed to vary: Cluster age and distance.

5.4.1 Isochrone Fit of NGC 6134

I have used the interstellar reddening $E(b-y) = 0.275$ to correct $b-y$ and V. Note that the interstellar reddening of V is $A_V = 4.3\,E(b-y)$, according to equation 5.14 of Nissen [51]. I have calculated isochrones with a range of ages with fixed metallicity $[Fe/H] = 0.41$. This corresponds to $Z = 0.04$ which is somewhat outside the "safety limit" of the isochrones by Pols *et al.* [57]. I have fitted the isochrones by shifting them vertically in the CMD, and in this way determined the distance modulus $(V - M_V)$.

In figure 5.11 I present the result of the best fit of age and cluster distance for NGC 6134 when using both isochrones of standard and overshooting models. In the plots I have indicated error bars above the isochrone, which correspond to the standard errors of a typical star in the turnoff region, *i.e.* $\sigma(T_{\text{eff}}) = 200K$ and $\sigma(V) \simeq 0.007$. The values I have obtained for age ($\log A$) and distance modulus are indicated in the plot and in table 5.3.

It seems that the isochrone with standard stellar models (right) fails to account for all the stars above the turnoff. The isochrone with overshoot models (left) has a more extended hook after the turnoff, and accounts for the stars that are actually seen there.

The mass of the stellar model at the reddest point of the hook is indicated on the plots: 2.55 $M_\odot$ for overshoot models (close to star 906) and 2.46 $M_\odot$ for the standard models (close to star 574). Note that the isochrones are similar on the lower main sequence. This is because the effect of overshooting has little impact on the detailed evolution of relatively light stars: On each plot I have indicated the position of the stellar model with a mass around $1.5 M_\odot$.

In the plot to the left of figure 5.11 I have plotted the lower end of the isochrone when

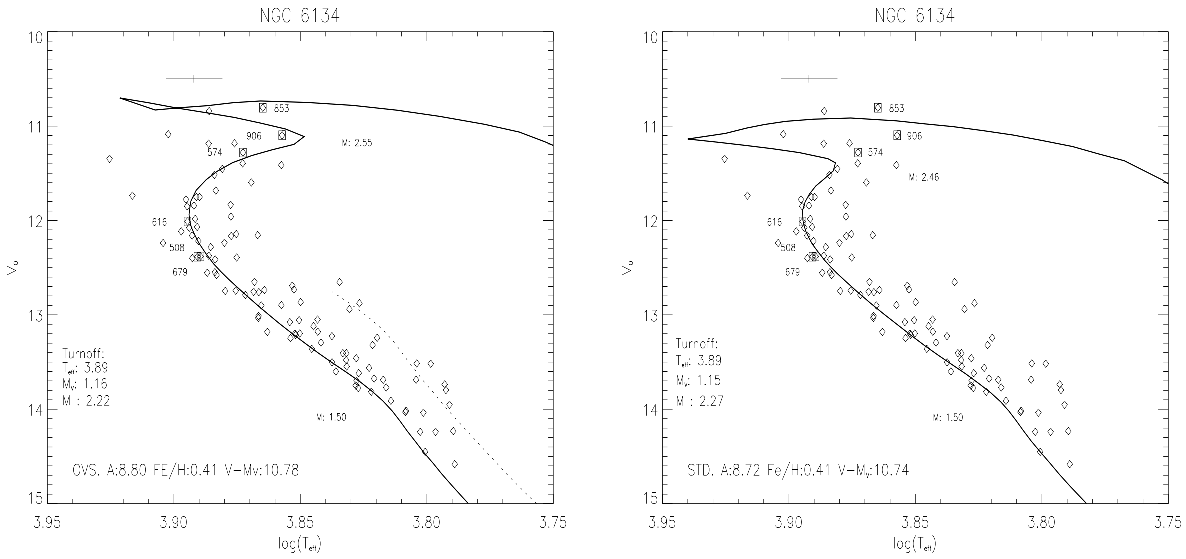

Figure 5.11: The isochrones that give the best fit to the stars of NGC 6134. To the left I have used an isochrone including overshoot while the plot to the right is a standard model. The applied age ($\log A$), metallicity ([Fe/H]), and distance modulus are indicated in the plots, as well as the parameters of the isochrone at the turnoff.

it is shifted 0.75mag in M_V (dashed line). This indicates the approximate sequence of binary stars in NGC 6134. Close binaries will be observed as being one star. If they are of equal mass, and hence equal V and $T_{\rm eff}$, the binaries will appear in the CMD at $T_{\rm eff}$ and $V_B = V - 0.75$. This is obtained from the definition of magnitudes. A single star with flux F has $V = -2.5 \log F + c$ and the combined light of two such stars has $V_B = -2.5 \log(2F) + c = -2.5 \log(F) - 0.75 + c$. Also shown in the plots are the characteristics of the stellar model at the turnoff, *i.e.* effective temperature, absolute magnitude, and mass. In table 5.3 I show the results of the isochrone fit.

The results can be compared to the previously published values, which I have shown in table 2.1. In the following I refer to my results when using the overshoot models. The values I have derived for the age and distance of NGC 6134 are somewhat different from the values published by Kjeldsen *et al.* [38]. I find a distance modulus close to 0.5 magnitudes smaller than reported by Kjeldsen *et al.*: $V - M_V = 11.25 \pm 0.20$. I will try to account for this "large" difference:

As noted earlier my determination of the interstellar reddening is 0.05 smaller than what was found by Kjeldsen *et al.* This gives a difference in the (reddening corrected) V_0 of $\Delta V_0 = 4.3 \times 0.05$mag $\simeq 0.22$ mag. When using my value of $E(b-y)$ the V_0 magnitudes that are 0.22 mag larger.

Kjeldsen *et al.* determined the age and distance but they used older isochrones with different input physics ("standard models" with different opacity tables). It is not clear from the paper by Kjeldsen *et al.* [38] what metallicity they have used, but it is probably isochrones with solar metallicity ($Z \simeq 0.02$). I have used isochrones with $[Fe/H] = 0.41$ ($Z \simeq 0.04$). According to figure B.3 of appendix B higher metallicity will shift the isochrones toward lower absolute magnitudes. This is in accord with the result of Perrin *et al.* [56] who find that

$$\Delta M_V = -15\Delta Z + 3\Delta Y. \tag{5.2}$$

Assuming $\Delta Y = 0$ and inserting the difference $\Delta Z = 0.02$ yields $\Delta M_V = -0.30$. Thus the lower end of my isochrone lie approximately $\Delta M_V = 0.22 - 0.30 = -0.08$, *i.e.* below the isochrone applied by Kjeldsen *et al.*

I have reexamined the isochrone fitting of the observed CMD in Kjeldsen *et al.* [38] (their figure A12). The explanation for the apparently discrepant distance moduli is that the determination by Kjeldsen *et al.* may be uncertain by as much as 0.5 mag, as the lower main sequence of their sample of stars is not very well-defined.

It is important to note that Kjeldsen *et al.* only had ~ 60 stars in their sample compared to ~ 700 in my sample, - of which I have labelled ~ 150 as being probable cluster members. In other words I have a much more well-defined sequence of stars to make the isochrone fit to.

It is difficult to locate the position of the turnoff from the data by Kjeldsen *et al.* [38]. The fact that I have used isochrones with a high metallicity leads to a significantly lower age compared to Kjeldsen *et al.* , as can be seen in figure B.3 in appendix B. This explains that the age found by Kjeldsen *et al.* ($A = 890 \pm 150$ Myr) is somewhat higher than what I find.

To be able to determine the distance and age of NGC 6134 more accurately we need to know which of the stars are cluster members. It would also be helpful to know the metallicity with greater accuracy. I have used isochrones with very high metallicity, but as noted in section 4.2.4 and 5.3 the value I have found is maybe too high. This will of course affect the distance and age determination. The membership assignment and the determination of metallicity can be done by doing spectroscopy.

5.4.2 Isochrone Fit of NGC 3680

For NGC 3680 I have observed only 14 stars that are confirmed single stars and cluster members according to Nordström *et al.* [53]. I have performed a fit to these stars by using the Pols *et al.* [57] isochrones with the distance modulus and age as free parameters. I have applied the values of $E(b-y)$ and $[Fe/H]$ determined in section 5.2 and 5.3. The result of the best isochrone fits is shown in figure 5.12.

Note that only 11 stars are plotted as I do not have the c_0 index for all 14 stars. Hence, I am not able to determine the effective temperatures for three of these stars (*cf.* equation 5.1).

As was the case with NGC 6134 the isochrone that uses overshoot models agrees better with the distribution of stars near the turnoff. I stress that in this case I only have a very limited sample of stars. I also note that the results agree with Nordström *et al.* [53] who found $V - M_V = 10.5 \pm 0.3$ and $A = 1430 \pm 100$Myr, *cf.* table 2.1. This is perhaps not too surprising as the V magnitudes and Strömgren $b - y$ agree well with Nordström *et al.* [53] , *cf.* figures 4.5 and 4.7. It is an important fact that we have used different $T_{\rm eff}$ calibrations and isochrones: Thus it is reassuring that (recent) theoretical calculations of different authors give the same overall result.

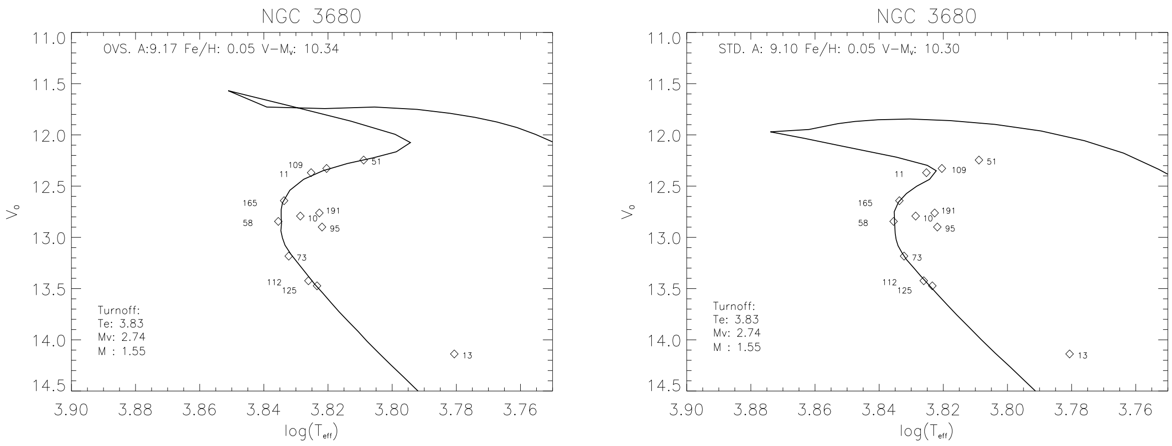

Figure 5.12: The overshoot (left) and standard isochrones (right) that give the best fit to NGC 3680.

I have estimated the standard errors of the fitting parameters by changing the parameters a little as to determine how much this changes the isochrone. When doing this I am also bearing in mind the uncertainty of the observations indicated with error bars in figure 5.11. The standard deviation of the age is $\sigma(A) \simeq 10 - 15\%$ (or 100-200Myr for the two clusters). The standard deviation of the distance modulus is $\sigma(V - M_V) \simeq 0.2$ which corresponds to $\sigma(d) \simeq$ 60pc for the two clusters. As noted previously I have used the metallicity $[Fe/H] = 0.41$ for NGC 6134, which may be too high (*cf.* section 5.3). This will change both the distance (smaller) and the age determination (older), *cf.* figure B.3 in appendix B.

Table 5.3: Results of the isochrone fit to the observations of NGC 6134 and NGC 3680 using either overshoot (OVS) of standard (STD) models.

Cluster:	NGC 6134		NGC 3680	
Isochrone:	OVS	STD	OVS	STD
Age (Myr)	630	525	1480	1260
$V - M_V$	10.78	10.74	10.34	10.30
d (kpc)	1.43	1.41	1.17	1.15

5.5 Stellar Mass of the Variables in NGC 6134

I have estimated the mass of the six known δ Scuti stars in NGC 6134. This is done by using the overshoot isochrone, that I have fitted to the cluster in section 5.4.1. In figure 5.13 I show a part of this isochrone around the turnoff region. Also shown is the location of the δ Scuti stars with their id numbers indicated.

The isochrone consists of several points in the V and $T_{\rm eff}$ plane[1]. The points correspond to stars with different stellar mass, which is indicated in figure 5.13. Note that beyond the

[1] The output of the isochrone programme is the absolute magnitude, M_V - but the isochrone has been shifted as to fit the V magnitudes of the stars on the lower main sequence. Hence I use the V magnitude.

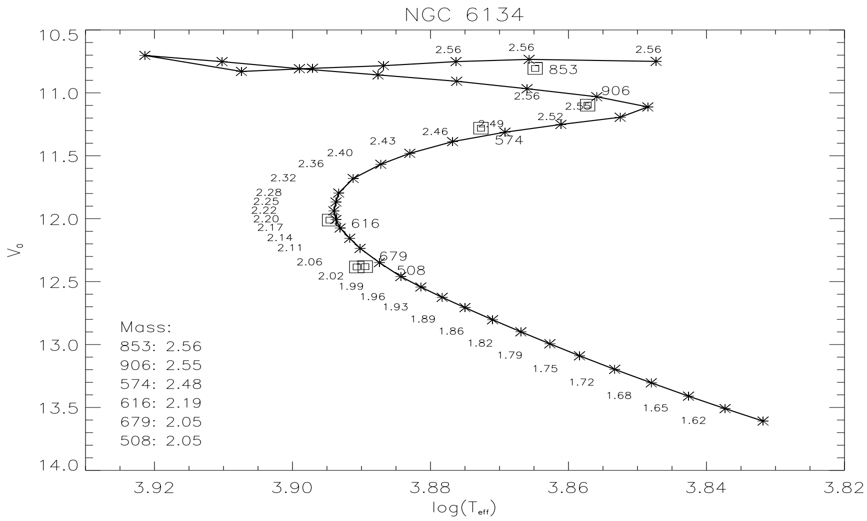

Figure 5.13: The region around the turnoff for the isochrone including overshoot that gave the best fit to NGC 6134 (*cf.* figure 5.11). The stellar mass is indicated along the isochrone. Also plotted are the six known δ Scuti stars with their id number.

turnoff loop the mass of the stars of the isochrone increase very slowly, which is due to the fast evolution in the final part of the Hydrogen core/shell burning.

I have estimated the masses of the δ Scuti stars by interpolating the mass of the stars on the isochrone with the same value of V. I used the IDL routine `spline_c` for this task. The result is quoted in figure 5.13 and in table 9.1, where the mass is in units of solar masses, $M_\odot$.

I note that in chapter 9 I will summarize the results presented in this chapter and give useful ideas for additional projects on these open clusters. There I will also cite the astrophysical quantities I have determined for the variable stars in NGC 6134, which may be interesting for future investigations.

Chapter 6

Observations with SAT: FG Vir and α Cir

During the nights from April 28th to May 18th 1996 I used the Strömgren Automatic Telescope (SAT) to obtain the light curves of FG Virginis and α Circini measured through the Strömgren filters: $uvby-\beta$. In this chapter I will describe the SAT instrument. Then I will summarize the known properties of the target stars, which is followed by a description of the observations that I have made. In the chapter 7 I will describe the reductions and in chapter 8 I will interpret the results that I have obtained.

6.1 The Strömgren Automatic Telescope

The Strömgren Automatic Telescope (SAT) is a 50cm telescope mounted with a six-channel photometer. The photometer has two modes of observation: Either $uvby$ or β filters are used. In $uvby$ mode a reflection grating sends the light through the four Strömgren filters and then through photomultiplicators where the signal is amplified and recorded. In β mode a mirror is inserted which directs the photons to a beam splitter: This transmits 80% of the light through the narrow (N) β-filter and 20% through the wide (W) β-filter. The two modes of observation are consequently: Either $uvby$ at once or β $(N+W)$ at once.

The observations can be programmed using a PC, hence the name "Automatic Telescope". The programme for controlling the telescope needs a list of each observation with the possibility of making a loop of observations.

The SAT was used to find the changes in magnitude with time (light curve) for two known variable stars. The target stars were the δ Scuti star FG Vir and the roAp star α Cir.

6.2 Properties of FG Vir and α Cir

FG Vir (HD 106384) is the most well-studied of the known δ Scuti variables. The periods and amplitudes of 24 modes have been determined photometrically by Breger [9]. The strongest mode has a period of 1.9 hours ($f = 147\mu$Hz) with an amplitude of 31 mmag (in Strömgren v filter). It has a visual magnitude of $V = 6.5$. Some of the most recent results are found in Viskum *et al.* [73] who have used spectroscopy and the photometry presented in this thesis to perform a mode identification of the strongest modes in FG Vir. The importance of and techniques for identifying modes is described in section 1.6.4.

α Cir (HD 128898) is a roAp star: A rapidly oscillating star of spectral type A - peculiar. The Ap stars have high abundances of certain heavy elements. It is thought that the reason for this is diffusion processes related to the strong magnetic fields ($\sim$ few kG) seen in these stars, *e.g.* Baldry [5]. α Cir is the most well-studied of the few observed $\sim$ 30 variable stars of its kind. Five modes have been determined photometrically by Kurtz [42] from 130 hours of observation. The strongest mode has a period of 6.8 minutes ($f = 2442\mu$Hz) with an amplitude of 2.55 mmag (in Strömgren v filter), *i.e.* a factor $\sim$ 12 lower than the strongest mode of FG Vir. The visual magnitude of α Cir is $V = 3.2$.

6.3 Observations with SAT

To be able to detect variability in the target stars FG Vir and α Cir, two nearby comparison stars were selected: By determining the difference in magnitude between the variable and the comparison star the variation intrinsic to the variable star is measured. For FG Vir the comparison star HD 105912 was observed - a well-studied star that shows no variability at a very low level (Breger [9]). For α Cir I used HD 129422 as the comparison star. In table 6.1 I present the basic observational data for the target stars.

Table 6.1: Basic parameters for SAT targets. The quoted frequency and corresponding period (in hours or minutes) are for the mode with the largest amplitude. The values are from Breger [9] and Kurtz [42]

Star	α (2000.0)	δ (2000.0)	f / μHz	P	V	$b-y$
FG Vir	$12^h14^m15^s.45$	$-05°42'59''.5$	147.12	1.89h	6.58	0.159
HD 105912	$12^h11^m21^s.80$	$-03°46'44''.3$	-	-	6.95	0.279
α Cir	$14^h42^m30^s.41$	$-64°58'30''.5$	2442.0	6.83m	3.19	0.136
HD 129422	$14^h45^m17^s.41$	$-62°52'32''.0$	-	-	5.36	0.185

To be able to detect an oscillation, two or more observations must be made during the period of the oscillation. This poses an optimization of how to observe: Each observation must have enough counts to allow for a reliable determination of the magnitude (longer exposures). At the same time observations should be taken at several points during each oscillation period to allow for a determination of the period (shorter exposures).

At least two measurements must be made during an oscillation to be able to determine the period. The maximum value of the frequency corresponding to the shortest period that can be determined from a set of observations is called the Nykvist frequency. This is expressed as:

$$\nu_N = 1/P_N = 2/\Delta t, \tag{6.1}$$

where P_N is the Nykvist period and Δt is the time between two measurements. In the next section I will estimate the Nykvist frequencies for the observations.

6.4 The Observational Programme

For the first part of the night FG Vir was observed with the following input to the SAT-programme: HD 105912, FG Vir, HD 105912, FG Vir, background, FG Vir. Each entry in this list is actually four observations: Two exposures in *uvby* were done and then two with β (N+W). The exception is the background exposure where only one exposure was made with each mode of observation (*uvby* or β). The exposure times were 95 seconds for HD 105912, 60 seconds for FG Vir, and 20 seconds for the background determination.

The duty cycle for FG Vir in each filter is about 28%. The duty cycle is computed as the exposure time used on FG Vir in the observation loop in a given filter divided by the duration of the complete loop. I have added 5 seconds each time the telescope is moved to a different target (6 times). The result is: Exposure time in each loop for *uvby* or β(N+W) for FG Vir: 360sec (6 minutes). Total time elapsed in a loop: 1270sec (21.2 minutes).

A similar sequence was used for α Cir and the comparison star HD 129422. As the target star is much brighter in this case the integration times were 20 seconds for both α Cir, HD 129422, and background. This gave a duty cycle of about 26%.

An estimate of the "Nykvist limit" is determined by computation of the average time between two measurements of the target star. The result is $\nu_N \simeq 2100\mu$Hz or $P_N \simeq 8$ minutes for FG Vir. For α Cir the result is $\nu_N \simeq 3000\mu$Hz or $P_N \simeq 5.5$ minutes. This is quite close to the period of the main oscillation at 6.8 minutes - but the sampling should do.

On some nights the weather was not photometric and only β was observed: As the central wavelength is the same for both filters, the β index is less sensitive to atmospheric instabilities. FG Vir was not observed on the nights of April 29th and 30th because the Moon was too close to the star. A log of the observations is presented in table 6.2 below.

Table 6.2: Log of observations of FG Vir and α Cir with 50cm SAT. The first observation of α Cir on April 27th corresponds to HJD 2450201.766

FG Vir				α Cir			
Date	Filter	Obs. time Hours	No. of pts.	Date	Filter	Obs. time Hours	No. of pts.
Apr 27	$uvby-\beta$	0	0	Apr 27	$uvby-\beta$	4.1	88
Apr 28	$uvby-\beta$	7.1	62	Apr 28	$uvby-\beta$	1.2	20
Apr 29	–	0	0	Apr 29	$uvby-\beta$	11.0	221
Apr 30	–	0	0	Apr 30	$uvby-\beta$	11.0	233
May 1	$uvby-\beta$	6.9	69	May 1	$uvby-\beta$	4.1	92
May 2	$uvby-\beta$	6.8	46	May 2	$uvby-\beta$	4.1	88
May 3	$uvby-\beta$	7.2	48	May 3	$uvby-\beta$	4.1	83
May 4	$uvby-\beta$	6.4	42	May 4	$uvby-\beta$	4.1	85
May 5	β	7.0	83	May 5	β	3.2	111
May 6	β	5.2	51	May 6	β	3.4	87
May 7	–	0	0	May 7	–	0	0
May 8	$uvby-\beta$	6.9	46	May 8	$uvby-\beta$	1.4	32
May 9	$uvby-\beta$	3.2	22	May 9	–	0	0
May 10	$uvby-\beta$	7.3	48	May 10	$uvby-\beta$	3.3	71
May 11	$uvby-\beta$	7.4	49	May 11	$uvby-\beta$	3.2	71
May 12	–	0	0	May 12	–	0	0
May 13	$uvby-\beta$	7.2	45	May 13	β	1.4	31
May 14	$uvby-\beta$	6.4	42	May 14	$uvby-\beta$	3.1	66
May 15	β	4.2	51	May 15	–	0	0
May 17	$uvby-\beta$	6.4	43	May 17	$uvby-\beta$	3.4	62
May 18	$uvby-\beta$	3.1	21	May 18	$uvby-\beta$	1.8	32

6.5 Photometric Precision

To give an idea of how small a variation of the signal one can detect, I need to calculate the expected noise level of each observation. This is important for both the target stars and the comparison stars. The main contributions to the noise level are scintillation in the atmosphere and photon shot noise. In addition to these sources of error, variations in the sensitivity of the instrument will also be added to the noise level. In the following I will estimate the contribution from the two main error sources.

The relative noise due to variation of the atmosphere (scintillation) can be calculated by using this expression

$$\sigma_{\text{scint}} \simeq 0.09 D^{-2/3} \chi^{3/2} e^{-h/8km} \Delta t^{-1/2}, \tag{6.2}$$

taken from Young [74]. Here D is the telescope diameter in centimetres, χ is the airmass (a mean airmass of 1.4 is used in the following), h is the height above sea level of the observatory in kilometres, and Δt is the exposure time in seconds.

The relative noise level because of (Poisson) photon noise is simply

$$\sigma_{\text{photon}} = 1/\sqrt{N}, \tag{6.3}$$

where N is the number of counted photons. This can be approximated by the following expression:

$$\sigma_{\text{photon}} \simeq 0.011 D^{-1} \Delta\lambda^{-1/2} \Delta t^{-1/2} 10^{0.2V}, \tag{6.4}$$

taken from Kjeldsen [40]. Here D is the telescope diameter in centimetres, $\Delta\lambda$ is the effective width of the filter (filter + optics + telescope), and Δt is the exposure time, and V is the visual magnitude.

In table 6.3 I have shown the relevant numbers and expected noise levels for the observed stars. I have used the values $\Delta\lambda \simeq 30, 23, 15, 3$nm for the filters $u, y, \beta(W), \beta(N)$, taken from Nissen [51]. Note the relatively high noise for the faint comparison star of α Cir. The noise level could be brought down by taking longer exposures, but as I wanted to detect variations with a period of 6.8 minutes in α Cir, I had to make this trade off between low noise level for the comparison star and a high sampling rate of α Cir.

Table 6.3: Expected noise level (in mmag) of target stars and comparison stars. I have cited values for the u and y filter and the β index.

Star	V	σ_u	σ_y	σ_β	σ (scint)
FG Vir	6.58	3.5	4.0	12.1	0.50
HD 105912	6.95	3.3	3.8	11.4	0.39
α Cir	3.19	1.3	1.4	4.4	0.86
HD 129422	5.36	3.4	3.9	12.0	0.86

Chapter 7

Reduction of SAT data

The Strömgren Automatic Telescope was used to find the changes in magnitude with time for two known variable stars. The target stars were the δ Scuti star FG Vir and the roAp star α Cir. A description of the observational techniques I have used is found in chapter 6. In this chapter I will describe how I have reduced the raw light curves, and how I have used the measurements of the comparison stars to find the variation *intrinsic* to the variable stars.

7.1 Reduction Procedure

The raw observation files for each night consist of information about each measurement: The name of the target object, Julian Date of the observation, integration time, airmass, which filter was applied, and the number of counts measured.

The raw observation files were reduced by using a Fortran software package originally written by Erik Heyn Olsen. A thorough manual by Vaz [70] is available.

The main programme `tprp` extracts the magnitudes from the raw observation files. The counts measured are corrected for extinction by using standard Strömgren coefficients and the instrumental magnitude is determined by applying the integration time of the observation. The instrument magnitudes are converted to standard magnitudes by using coefficients appropriate for the spectral type of the target stars.

The latitude and longitude of the observatory must be entered in the input file for the reduction programme. This (along with the observing time and date) is used to compute the heliocentric Julian date (HJD).

Measurements made within a certain time limit, set in the input file, are treated as one observation (with a lower photon noise level). For FG Vir the main oscillation period is around 1.9 hours. Consequently, I have "binned" measurements made within 1.7 minutes. The integration time was 60 seconds for FG Vir, thus two consecutive measurements are binned. For the rapidly oscillating star α Cir measurements made within 0.7 minutes are binned. The integration time for α Cir was 20 seconds, so that two consecutive measurements are binned. The binning factor for the measurements of FG Vir and α Cir is nearly always two.

The final output of the programme is a list of all observations with the time of observation (HJD) and the measured magnitudes. The HJD in the files corresponds to the time when the integration of the first measurement started - remember the binning factor of two. Thus I have added 60 and 20 seconds to the HJD so that the corrected HJD now corresponds to the mean HJD of the two measurements.

As has been described in chapter 6, the observations also included observations of a comparison star for each target star. This was done in order to be able to remove any variation in magnitude due to changes in the transparency of the atmosphere. The standard stars were observed twice for every three measurements of the target stars. In the reductions I have used two different techniques for removing the variation of the comparison star, which I will describe in the following.

7.1.1 Light Curve of α Cir

The raw light curve of α Cir shows variation that is not intrinsic to the star, which is seen in figure 7.1 below. The plots show the light curves of α Cir and the comparison star in the y filter and in the β index for one night of observations ($\simeq$ 11 hours on two different nights). As can be seen from the figure the comparison star and α Cir are fainter in the beginning of the night in the y filter. The light curve of the β index (on a different night) also shows the same "smooth" variation for α Cir and the comparison star during the night.

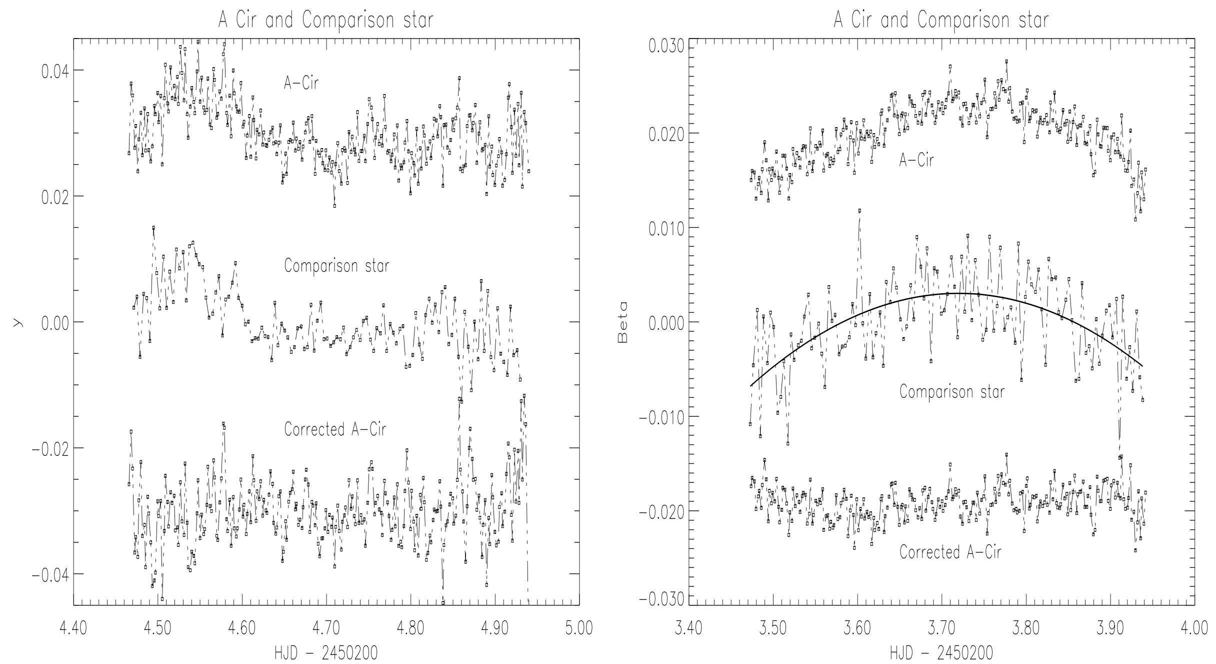

Figure 7.1: Light curve of α Cir (top) and the comparison star (middle) in the Strömgren y filter (left) and the β index (right). The light curves at the bottom are the light curves of α Cir after the subtraction of the comparison star. The abscissa measures the heliocentric Julian date and the ordinate shows the measured magnitude.

There is a significant variation in the light curve of the comparison star. This is due to photon noise. The comparison star is quite faint ($V = 5.4$) but it is observed with the same exposure time as α Cir. In table 6.3 I have estimated the expected noise level for the observed stars: The noise level of the comparison star is expected to be around three times higher than for α Cir. The relative noise of the comparison star is around 3 mmag in the *uvby* filters which is comparable to the expected amplitude of the main mode for α Cir as found by Kurtz [42]: 2.55 mmag in Strömgren v. Hence, care should be taken when subtracting the comparison star.

I have subtracted the light curve of the comparison star by using the IDL function `spline` to infer the magnitude of the comparison star at the time of each observation of α Cir. I note that I have also tried to remove the variation seen in the comparison star by using low order polynomials, but the overall result was the same as obtained by using the `spline` function. This `spline` method was applied in the *uvby* filters.

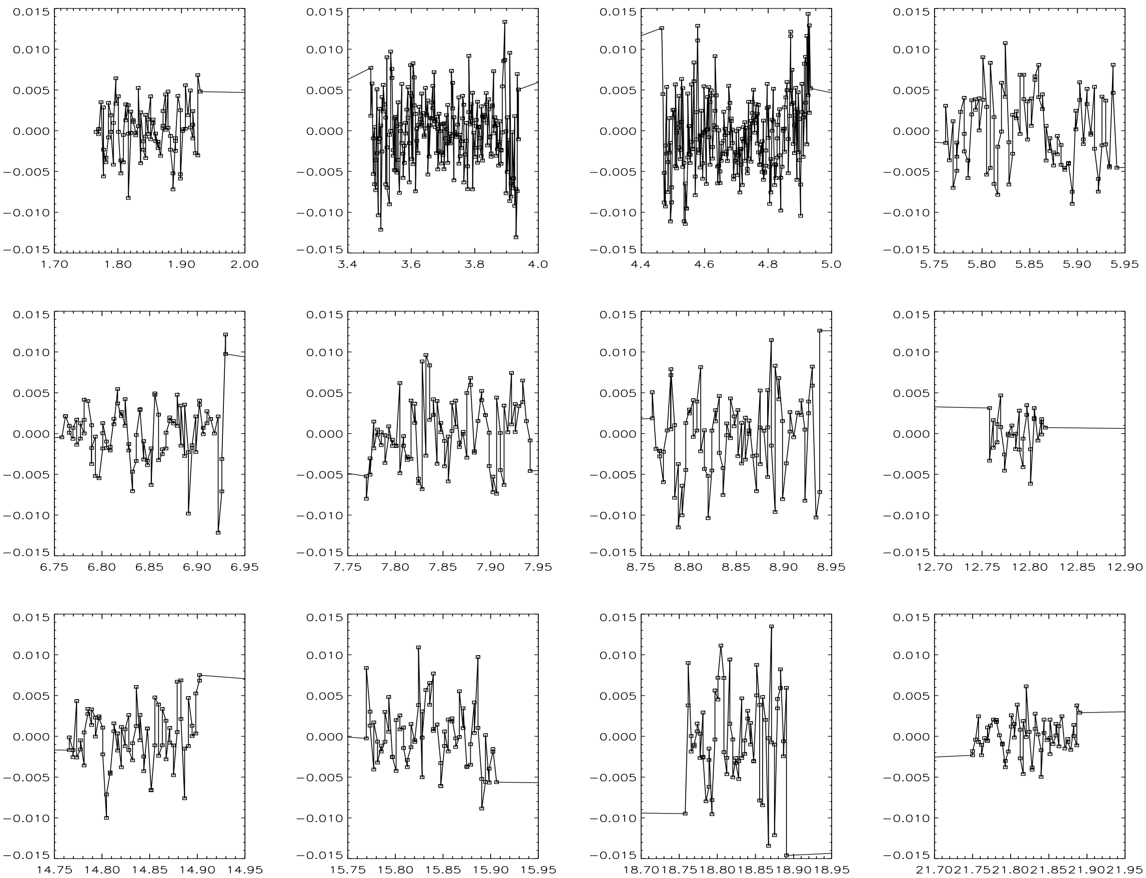

Figure 7.2: Light curve of α Cir in the Strömgren y filter. The abscissa is HJD - 2450200.

In the β index the variation of the standard star is larger than for α Cir, as can be seen in the plot to the right in figure 7.2. This agrees with what was expected from the calculations of the photon noise level, *cf.* table 6.2. For the light curve of the β index I used second order polynomials to remove the slow variation of the signal during the nights. An example is the 2nd order polynomial fitted to the β light curve of the comparison star in figure 7.1. It appears that the amplitude of the variation of the β index for α Cir must be found at a level below 1 mmag!

After subtraction of the comparison star the mean level of the light curve of each night was shifted to zero. The resulting light curve of α Cir is shown in figure 7.1 for one night. In figure 7.2 I show the final result for all nights in the y filter.

7.1.2 Light Curve of FG Vir

For the reduction of FG Vir I have fitted a low order polynomial (1st or 2nd order) to the light curve of the comparison star on each night. This polynomial was subtracted from the light curve of FG Vir. For each night the light curve was then shifted as to give a mean magnitude of zero. This was done for observations in all the Strömgren filters.

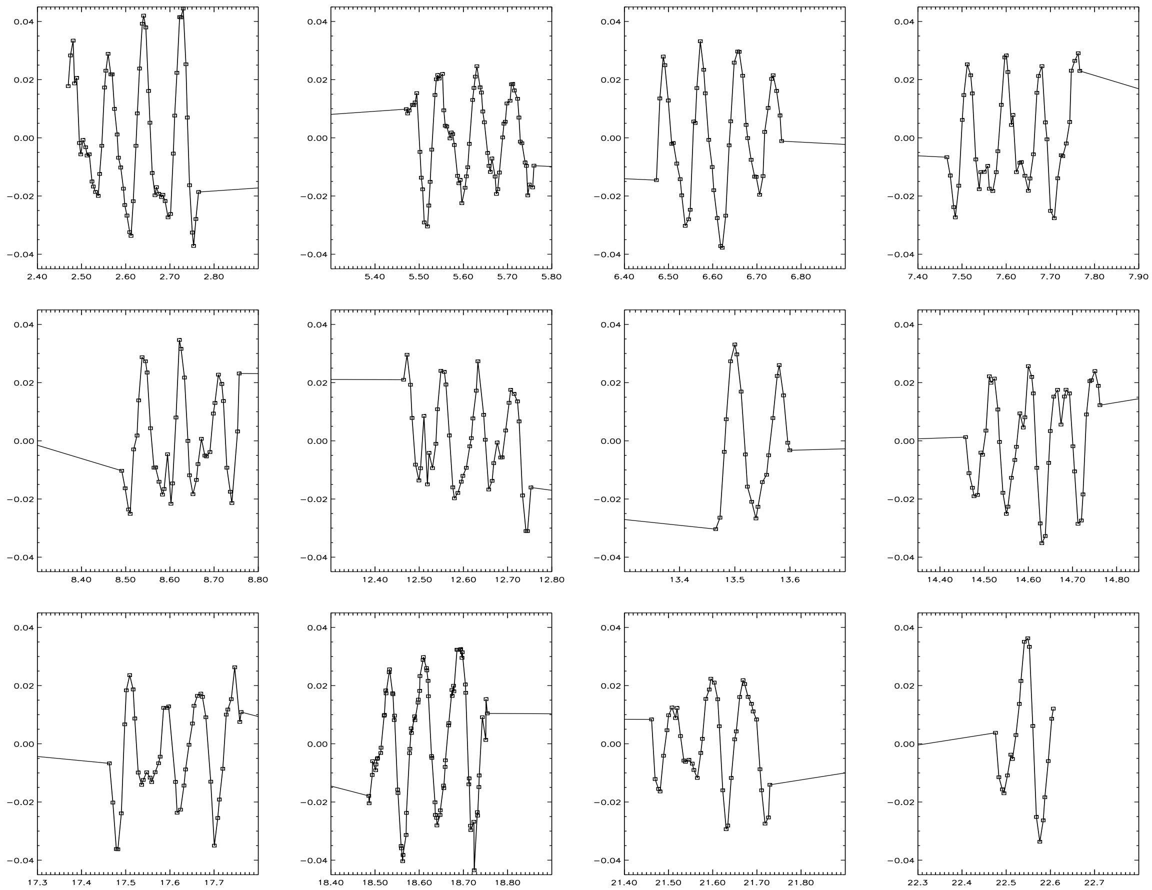

Figure 7.3: The light curve of FG Vir in the y filter on twelve of the fifteen nights that the star was observed. On the remaining three nights only few observations were made due to bad weather conditions. The abscissa shows HJD - 2450200.

The resulting light curve of FG Vir in the y filter can be seen in figure 7.3 for 12 of the 15 nights that FG Vir was observed. The main oscillation period of 1.9 hours with an amplitude of $A_y \sim 25$ mmag is clearly seen.

7.2 Time String Analysis

A description of the theory of Fourier analysis in relation to astronomy can be found in *e.g.* Frandsen *et al.* [28] or in the introductory chapters of the lecture notes by Christensen-Dalsgaard [20]. In the following I assume that the reader is familiar with this subject.

The light curves in the Strömgren filters show the variation in magnitude as a function of *time*. By calculating the Fourier transform, one determines the amplitude spectrum of the light curve. The amplitude spectrum shows the distribution of amplitude with *frequency*. To say it loosely: If a periodic signal is present in the light curve, a peak will show up at the corresponding frequency in the amplitude spectrum.

I have used the software package `period98` by Michael Sperl [62] to analyze the light curves of FG Vir and α Cir. This programme needs a file with two columns as input: One with the time of observation and the other with the measured magnitudes. The programme also needs to know in which frequency interval the Fourier analysis is to be carried out. For FG Vir the previously determined frequencies are in the range 100-400μHz or 9-35 cycles per day (cyc/day). For α Cir the range is 2300-2600μHz or 200-225 cyc/day.

I have used the previously published frequencies by Kurtz [42] and Baldry *et al.* [6] for α Cir and by Breger [9] for FG Vir as input to `period98`. The frequencies are very accurate because they are determined from a huge set of data. On the other hand, little is known about the *amplitudes* in the Strömgren filters. I have used `period98` to determine the amplitudes at each fixed input frequency.

Below I present some figures that show the results of the time string analysis. To get an idea of the quality of the data, I show the spectral window of *ubvy* measurements for FG Vir and α Cir at the top of figure 7.4. The spectral window shows how a single frequency will appear in the amplitude spectrum. This calculation was performed by `period98`. The spectra have been shifted to the principal frequencies of FG Vir and α Cir.

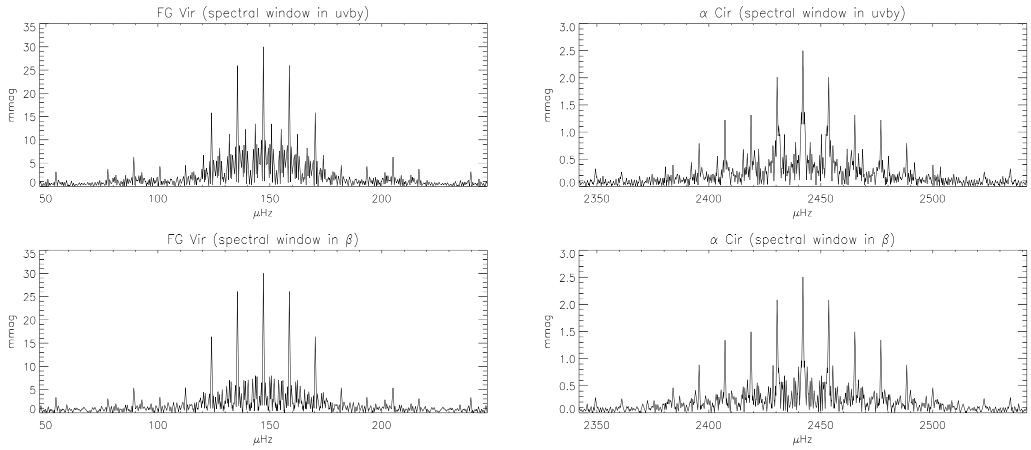

Figure 7.4: The spectral window of the observations of FG Vir (left) and α Cir (right) in $uvby$ and β.

Both spectral windows show significant alias frequencies. These are spaced with equal intervals of $f_a = 1/$ day $\simeq 11.57$ μHz. This corresponds to the nightly gap in time between each set of measurements. There are also significant amplitude at the aliases at 2 and 3 $\times f_a$, as *uvby* was not observed on some nights due to bad weather conditions. I have also shown the spectral window for the β observations, *i.e.* the two lower plots of figure 7.4. As expected the spectral window is somewhat better for both stars as β was observed on (nearly) all nights.

7.2.1 Amplitude Determination of Modes in α Cir

I used the light curve analysis programme `period98` by Sperl [62] to derive the amplitude of the most dominant mode of α Cir. In figure 7.5 I present the amplitude spectra for the α Cir light curves. Note how the amplitude falls off when going from Strömgren v to y. This may be compared to the corresponding result to FG Vir, *cf.* figure 7.7. Apparently the decrease in amplitude is stronger for α Cir.

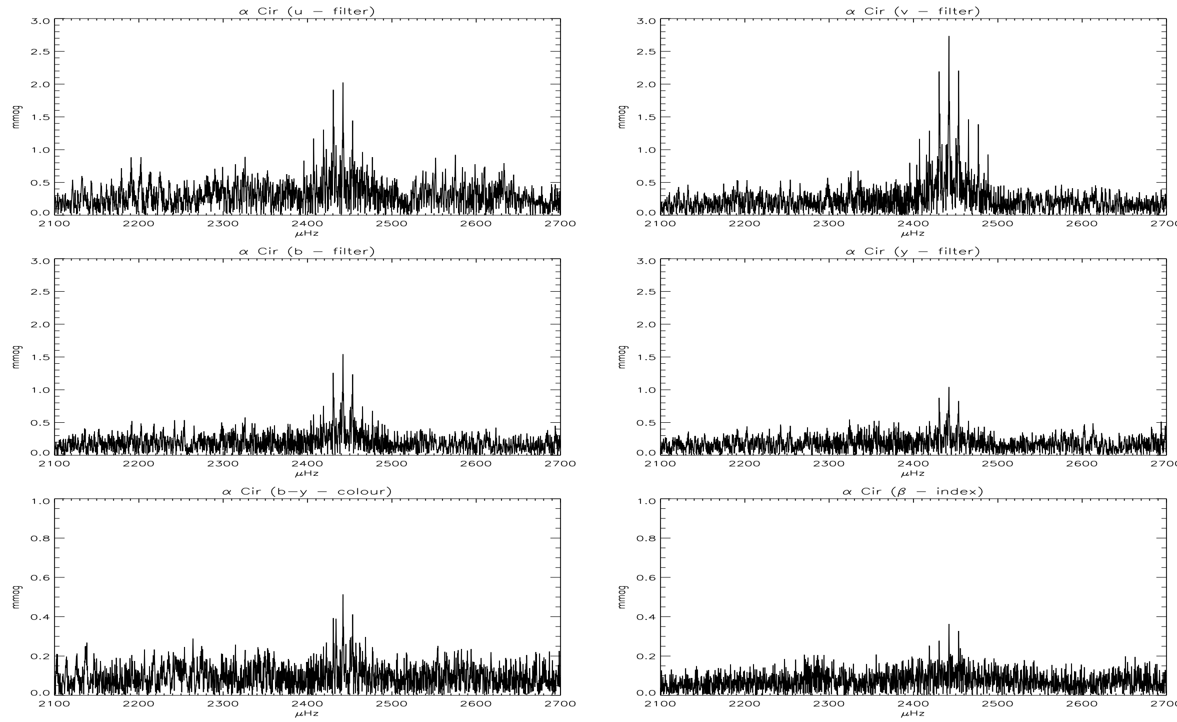

Figure 7.5: Amplitude spectra of α Cir in $uvby$, $b-y$, and β around the primary frequency at 2442 μHz. Note how the amplitude falls off when going from v to y.

The amplitude in both $b-y$ and β are much lower that the individual Strömgren filters (note the different scale on the ordinate). Both $b-y$ and β are measures of the effective temperature in the atmosphere, *cf.* appendix A. According to the definition of effective temperature $F \propto T_{eff}^4$, *i.e.* a small variation in T_{eff} yields a relatively large variation in flux, which explains the observed amplitude difference in the light curves and thus also the amplitude spectra of *e.g.* $b-y$ and y.

In figure 7.6 I show the amplitude spectrum in the v filter in greater detail (left). Only one mode stands out very clearly at 2442 μHz. The complex spectral window explains the many side bands seen in figure 7.6 (and 7.5). In the plot to the right of figure 7.6 I have removed the principal mode: No other peaks are visible above the noise level.

Table 7.1: Measured amplitudes in the Strömgren filters of the principal mode of α Cir. The results of Kurtz [42] and my results (Bruntt) are quoted.

Kurtz			Bruntt									
Frequency		v	u		v		b		y		β	
μHz	c / day	mmag	mmag	S/N	mmag	S/N	mmag	S/N	mmag	S/N	mmag	S/N
2442.03	211.0	2.55	2.26	12.9	2.60	10.7	1.42	9.2	0.95	4.0	0.10	2.1

I have used the frequencies determined by Kurtz [42] to find the amplitude of an additional six modes: The amplitudes of these modes are below $\sim 2\sigma$! Thus, I am not able to determine the amplitudes with reliable certainty for these weak modes.

In table 7.1 I have quoted the amplitude measured by Kurtz *et al.* [42] in the Strömgren v filter along with the values I have obtained for the Strömgren filters. The agreement in the v filter is satisfying, given the estimated S/N level of $\simeq 11$, *i.e.* $A_v \simeq 2.60 \pm 0.24$.

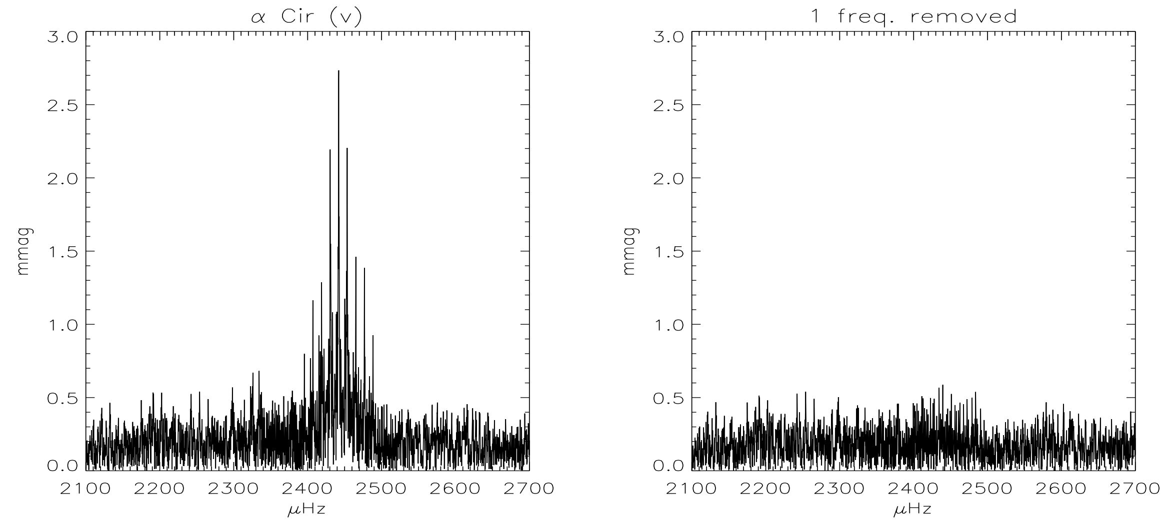

Figure 7.6: Amplitude spectrum of α Cir in Strömgren v is shown to the left. To the right I show the amplitude spectrum after removal of the primary mode. No significant signal is seen above the noise level.

7.2.2 Amplitude Determination of Modes in FG Vir

The amplitude spectra in the Strömgren filters and in the $b - y$ and β index of FG Vir are shown in figure 7.7. All spectra show significant amplitude at the principal frequency of 147.2μHz. The f_a aliases are clearly seen. Note that the amplitude is decreasing with increasing wavelength - I will interpret this in this chapter 8. The behaviour is similar to what was seen for α Cir, although the decrease in amplitude from *e.g.* v to y is not so strong.

In figure 7.8 I show the result when I have subtracted the primary frequencies. To be specific sine waves with the amplitude, frequency, and phase derived by the programme are subtracted from the observed light curve, and the Fourier analysis is redone with this "cleaned" light curve.

In table 7.2 I have shown the derived amplitudes in the Strömgren filters. I have included only the frequencies where the signal to noise ratio (S/N) is above 3 in the u

filter. The eight strongest modes fulfill this criterion.

Also printed in table 7.2 are the amplitudes measured by Breger [9] in the Strömgren v filter. The S/N ratio of the amplitudes of Breger are $\simeq 200$ for the principal mode and $\simeq 30$ for the weaker modes, *i.e.* the amplitudes are significantly more accurate than my results. Using the quoted S/N levels of Breger and those quoted in table 7.3, I find that my results for the amplitudes in v agree with the results published by Breger within the standard deviation.

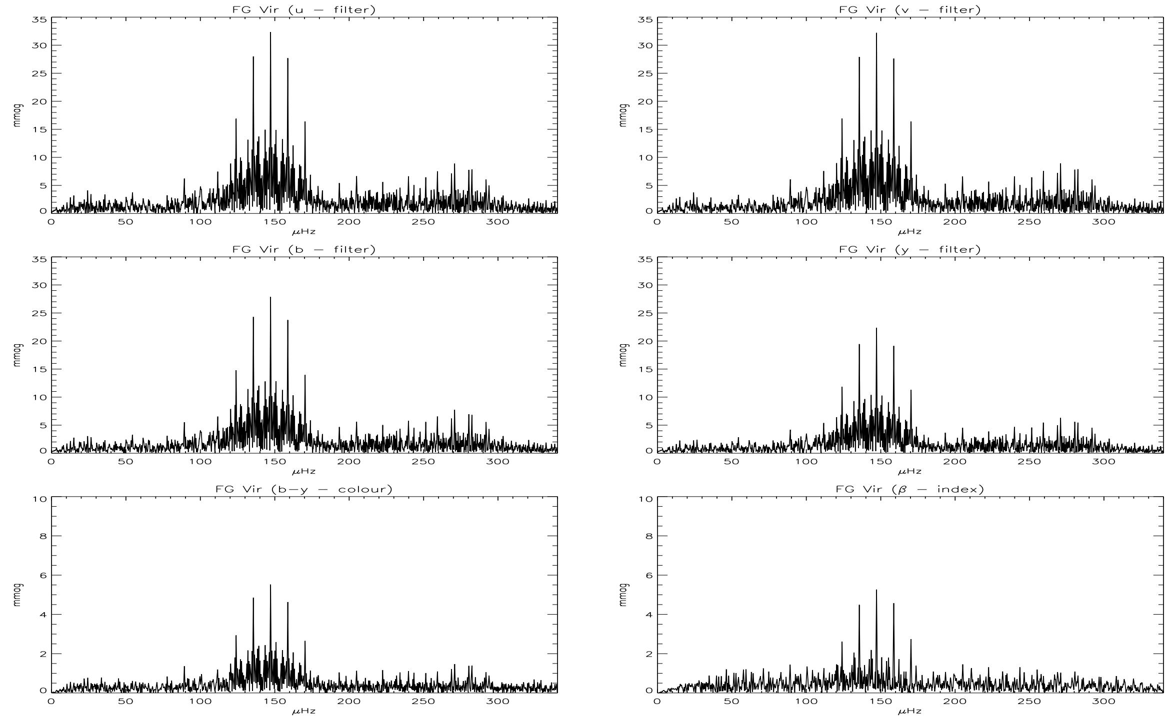

Figure 7.7: Amplitude spectra in the Strömgren filters and the $b-y$ and β index of FG Vir. A decrease in amplitude of the principal mode at 147μHz is seen when going from u to y.

Table 7.2: Derived amplitudes in the Strömgren filters of the eight strongest modes of FG Vir (Bruntt). Frequencies are taken from Breger [9]. Also quoted are the measured v amplitudes of Breger.

	Breger			**Bruntt**									
	Frequency		v	u		v		b		y		β	
ID	μHz	c / day	mmag	mmag	S/N	mmag	S/N	mmag	S/N	mmag	S/N	mmag	S/N
f_1	147.179	12.72	31.2	31.90	64	31.78	64	27.50	55	22.04	55	5.20	17
f_2	280.417	24.23	6.4	6.24	12	6.27	13	4.59	9.2	4.80	12	0.72	2.4
f_3	270.872	23.40	5.7	7.70	15	7.74	15	5.44	11	5.60	14	1.36	4.5
f_4	243.653	21.05	5.06	4.04	8.1	4.04	8.1	3.12	6.2	2.94	7.4	1.11	3.7
f_5	229.954	19.89	5.0	3.61	7.2	3.56	7.2	3.55	7.1	2.79	7.0	0.49	1.6
f_6	140.672	12.15	4.7	6.31	13	6.31	13	5.85	12	4.57	11	0.97	3.2
f_7	111.762	9.66	5.0	5.27	11	5.34	11	6.74	13	3.88	9.7	1.04	3.5
f_8	106.471	9.20	4.3	3.67	7.3	3.91	7.8	3.10	6.2	2.72	6.8	0.78	2.6

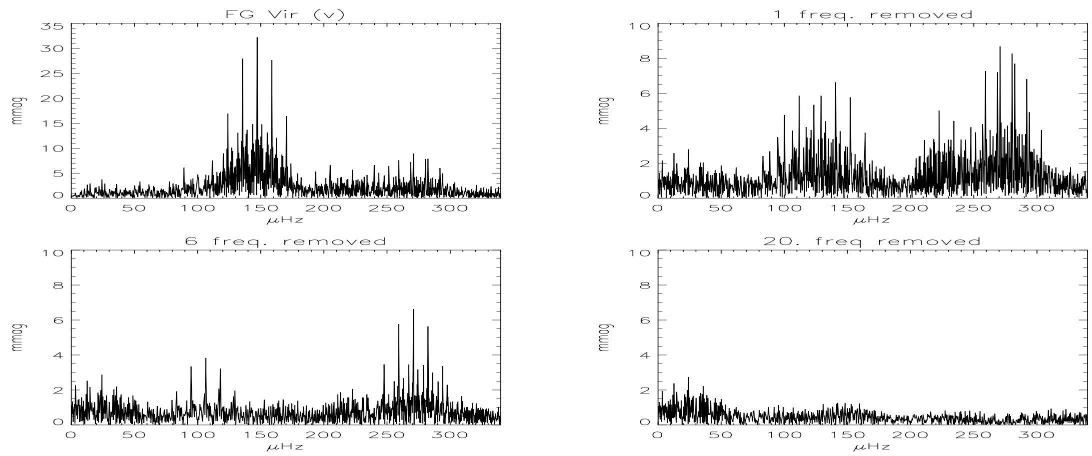

Figure 7.8: The amplitude spectra of FG Vir in Strömgren v - with the principal mode, six modes, and 20 modes removed.

7.2.3 Analysis of the Results from `period98`

In this section I will explain how I have estimated the standard error of the derived amplitudes, *i.e.* to be able to estimate the S/N ratios given in the tables 7.1 and 7.2. I tested the accuracy of the results from `period98` by using a few synthetic time strings. I constructed a light curve that was the sum of ten sine waves with different amplitudes, frequencies, and phases:

$$S(t) = \sum_{i=1}^{10} A_i \sin(2\pi\nu_i t + \phi_i) + V(t), \tag{7.1}$$

where A_i is the amplitude of the each sine wave, ν_i is the frequency, ϕ_i is the phase, and $V(t)$ is the light curve of the observed variable star. Note that the sampling rate (number of data points per time) of S and V is the same. The synthetic light curve is added to the observed light curve of α Cir in the u filter to be able to estimate the noise level of the observations.

I used a range of amplitudes, phases, and frequencies - but "within range" of the derived results of α Cir. For example, the primary mode in the u filter of α Cir has $A = 2.2$ mmag, $\nu = 211$ cyc/day. For the synthetic light curve I used sine waves with amplitudes in the range 1-3 mmag and frequencies in the range 150-230 cyc/day.

I found the amplitudes of the light curve by using `period98`. I then determined the difference between these amplitudes and the *true* amplitudes (A_i) of the sine waves in $S(t)$. The same was done for the phases. In both cases I gave the true frequencies as inputs to `period98`. This is analogous to what I have done for α Cir and FG Vir: In these cases by using the accurately determined frequencies by Breger [9] and Kurtz [42].

To estimate how well the frequencies are determined I let the frequencies be a free parameter. This gives an idea of the uncertainty of the frequency found by `period98` when using the SAT data. The results are shown in figure 7.9.

Note that the frequencies are in cycles per day: Multiply by 11.574 to get the frequency in μHz, *e.g.* the main frequency of α Cir is 210.99 cyc/day or 2442 μHz.

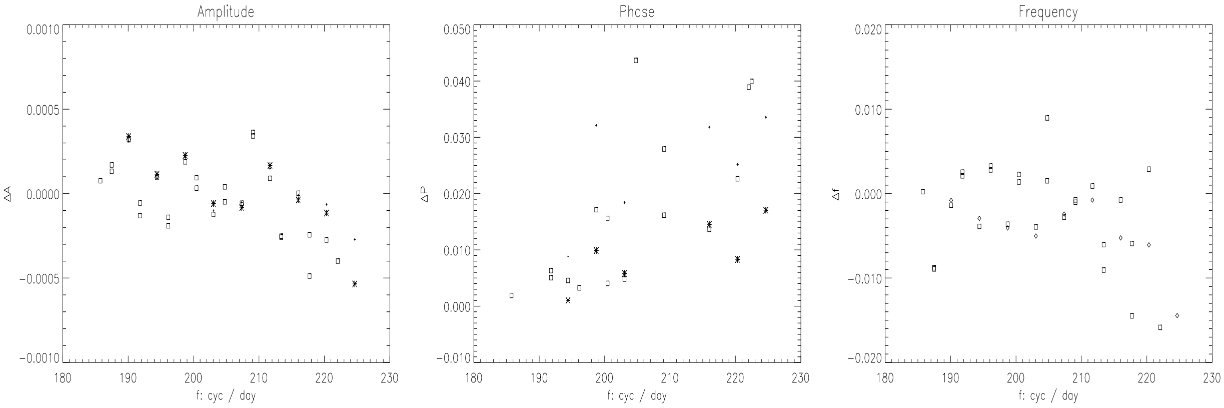

Figure 7.9: The difference between the amplitude (left), phase (middle), and frequency (right) of the true value and what is found by `period98` by using the simulated data. Note that in the first two cases the frequency is fixed at the *true* value. Symbols: +, box and * are the results for input sine waves with amplitudes of 1, 2, and 3 mmag respectively.

From the results in figure 7.9 I estimate the standard error in the derived amplitudes and phases to be of the order 0.2mmag and $0.04 \simeq 15°$ respectively (fixed frequency). The error when trying to determine the frequency is around 0.04 cyc/day ($\simeq 0.5\mu$Hz). The reason for the high deviation at frequencies above 220 cyc/day is that this is relatively close to the Nyquist frequency, estimated to be 260 cyc/day for the α Cir observations, *cf.* section 6.4.

The error in the amplitude of the observed variable stars can also be estimated by measuring the mean level in the amplitude spectrum when the known frequencies are removed. I have computed this in a 10 cyc/day box around the primary frequencies of α Cir and FG Vir. For α Cir this gives results that agree with the error of the amplitude determination of the synthetic light curve which was described above.

In table 7.3 I have given results of the estimation of the noise level of the amplitudes. The results have been used to determine the signal to noise ratio of the amplitudes in tables 7.1 and 7.2.

Table 7.3: Estimated noise level around the primary frequency of FG Vir and α Cir in $uvby$, $b-y$ and β index. Values are in mmag.

Star	u	v	b	y	$b-y$	β
FG Vir	0.5	0.5	0.5	0.4	0.2	0.3
α Cir	0.2	0.2	0.2	0.2	0.1	0.2

According to Kjeldsen [40] the noise in the amplitude spectrum can be calculated as $\sigma_{ampl} = \sigma_{lc} * \sqrt{\pi/N}$, where σ_{lc} is the standard deviation of each measurement (light curve), and N is the number of measurements. From the calculations quoted in table 6.3 I found $\sigma_{lc}(\alpha \text{ Cir}) \simeq 1.4$ mmag and $\sigma_{lc}(\text{FG Vir}) \simeq 4$ mmag (y filter), thus $\sigma_{ampl}(\alpha \text{ Cir}) \simeq 0.1$ and $\sigma_{ampl}(\text{FG Vir}) \simeq 0.3$. I have here used $N = 700$ and $N = 600$ for α Cir and FG Vir respectively. The estimated standard deviation of the amplitude using this approach is somewhat lower than the values quoted in table 7.3. This indicates that other noise sources are present in addition to the photometric noise. Among possible sources are the errors introduced in the reduction, especially the subtraction of the comparison stars.

Chapter 8

SAT Results for FG Vir and α Cir

In the preceding chapter I analysed the light curves in the Strömgren filters of the variable stars FG Vir and α Cir . Using Fourier techniques, I have obtained the amplitudes of the principal mode(s) in each of the Strömgren filters, *cf.* tables 7.1 and 7.2. In this chapter I will give an account of how these amplitudes may be interpreted to infer valuable information about these stars.

8.1 Mode Identification of Oscillations in FG Vir

The amplitudes in the Strömgren filters of FG Vir derived in this thesis have been used by Michael Viskum to identify which modes are detected when using a new technique that applies both spectroscopic and photometric data. I have described how this can be done in the introduction, *i.e.* section 1.6.4. More specific information on this technique can be found in Bedding *et al.* [7].

Viskum has presented the results of this work in his PhD thesis [72] and in the following paper, to which I have contributed with the Strömgren data:

- Viskum, M., Kjeldsen, H., Bedding, T. R., Dall, T. H., Baldry, I. K., Bruntt, H., Frandsen, S., Astron. Astrophys. **335**, 549-560 (1998). *Oscillation Mode Identification and Models for the δ Scuti Star FG Virginis.*

Viskum has used measurements of the amplitude of the variation in the Hydrogen Balmer lines, metallic lines, and the amplitude in the Strömgren filters presented here. The results are collected in figure 8.1 below which is adopted from Viskum *et al.* [73].

The abscissa shows the ratio of the amplitude in the variation of the equivalent width of the Hα line to the amplitude of the Strömgren *uvby* filters (the average value of the amplitude in all filters). The ordinate shows the ratio of the amplitude in Hα to the amplitude in FeI. The eight modes with the highest amplitudes are plotted in the diagram with the frequency of each mode (in μHz) indicated. Note that the amplitude in equivalent width is measured in ppm (10^{-6}) whereas the amplitude in the Strömgren filters is in mmag (10^{-3}).

The amplitude ratios separate the frequencies into three groups. The group of three frequencies with the lowest amplitude ratios (lower left) are interpreted as $l = 0$ (radial)

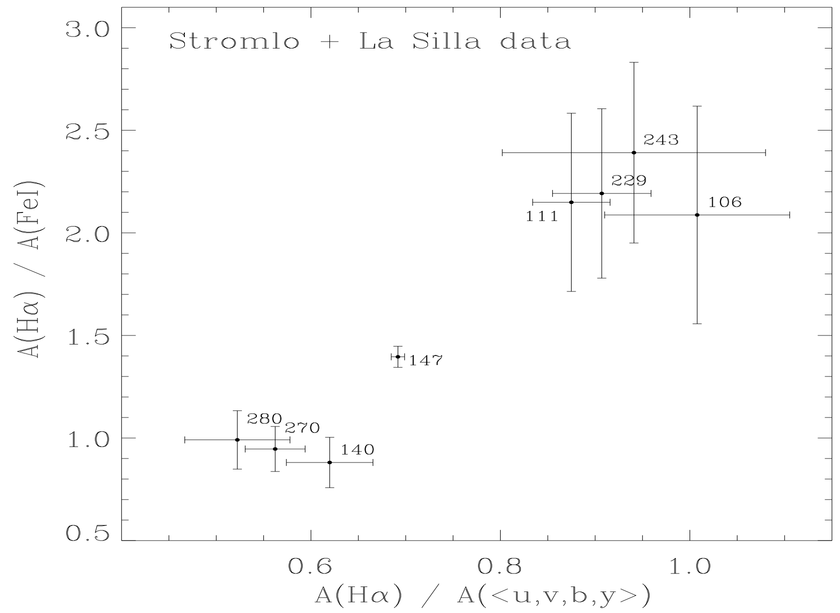

Figure 8.1: Amplitude ratios Hα / FeI and Hα / *uvby* of eight modes in FG Vir. The frequency in μHz of each mode is indicated. The figure is taken from Viskum *et al.* [73].

modes, while the main mode at 147.2μHz has $l = 1$ (dipole), and the four modes with the higher amplitude ratios have $l = 2$ or higher. The interpretation of the diagram is based on the work by Bedding *et al.* [7] and is also described in chapter 3.1 of Viskum [72]. The result is supported by the recent analysis of Breger *et al.* [10] who have used a different technique.

I note that the detailed study by Viskum *et al.* [73] shows that the f_2 mode at 280.4μHz is probably an $l = 1$ mode. Viskum has used the ratio of the frequency of the two confirmed radial ($l = 0$) modes to construct a homologously scaled stellar model of mass 2.2 $M_\odot$ with Solar metallicity to estimate the physical parameters of FG Vir. By doing this Viskum is able to derive the mean density of the star. When using the determination of $T_{eff} = 7500 \pm 100K$ by Mantegazza [46] and a reasonable mass-luminosity relationship, - the radius, and mass of FG Vir can be derived.

The result is quoted in table 8.1, which is taken from Viskum *et al.* [73].

Table 8.1: Derived astrophysical parameters when using asteroseismic data for FG Vir. This table is taken from Viskum *et al.* [73].

$\rho/\rho_\odot$	0.1645 ± 0.0005
R / $R_\odot$	2.227 ± 0.012
$L/L_\odot$	14.1 ± 0.9
$M/M_\odot$	1.82 ± 0.03
$\log g$	4.002 ± 0.003
Distance (pc)	84 ± 3

I note that the distance and the value of $\log g$ agree very well with HIPPARCOS parallax measurements and a determination of $\log g$ by using spectroscopy, Mantegazza [46].

As stressed by Viskum the standard deviations on the parameters in table 8.1 are very low compared to the values obtained if only the HIPPARCOS distance and T_{eff} were known: The standard deviation of $\log g$ and M is an order of magnitude lower! The explanation for this improvement is the accurately determined mean density, ρ. This result truly shows the power of asteroseismology when a reliable mode identification has been made.

To be able to interpret the information contained in all of the eight identified modes, a more refined evolutionary model of FG Vir is needed. A more accurate determination of T_{eff} and Z is also important to be able to do this. If some of the modes are g modes (or mixed p/g modes), interesting information could be inferred about the conditions near the convective core of FG Vir. Actually, Viskum *et al.* suspect that the high frequency radial mode, *i.e.* $f_3 = 270.9\mu$Hz, could be a g mode. This mode will contain information about the conditions near the convective core of FG Vir.

8.2 Node in the Principal Oscillation mode of α Cir

The variability of the roAp star α Cir has been studied by various methods. The most recent work has been published by Kurtz *et al.* [42], Medupe *et al.* [48] (both use photometry), and Baldry *et al.* [6] (spectroscopy). In the following I will compare the results I have obtained on α Cir with what has already been achieved.

I have measured how the amplitude of the principal mode at 2442 μHz of α Cir varies with the central wavelength of the Strömgren filters. This has been done earlier by Medupe *et al.* [48] in five broadband filters (UBVRI). In figure 8.2 I show the results of this thesis (squares) and Medupe *et al.* [48] (diamonds). In the figure is also shown the theoretical prediction when using a model atmosphere taken from Medupe *et al.* [48], *i.e.* the solid line labelled “numerical”.

Both sets of observation agree that the decrease with increasing wavelength is stronger than predicted by theory. As Medupe *et al.* [48] and Baldry *et al.* [6] both discuss, the observed decrease of the amplitudes with wavelength has two main contributions. One is the effect of limb darkening. When the amplitude of an oscillation is measured, the result is an average value over a certain range of depth in the atmosphere of the star. This range is different when using filters with different central wavelength because the opacity of the atmosphere changes with wavelength. In other words the amount of limb darkening depends on wavelength.

This explains the dependency of amplitude with wavelength of the theoretical curve. The observations show a stronger dependency than the theoretical prediction. A plausible explanation for this was proposed by Medupe *et al.* [48]: The observations show that the *temperature amplitude of the oscillation* becomes smaller when going to greater depth in the atmosphere of α Cir.

This conclusion is in accord with the results of Baldry *et al.* [6] when using spectroscopy. They measured the Doppler shift of the Hα line with respect to atmospheric (telluric) spectral lines of O_2. This was done by measuring the shift at different depths of the Hα

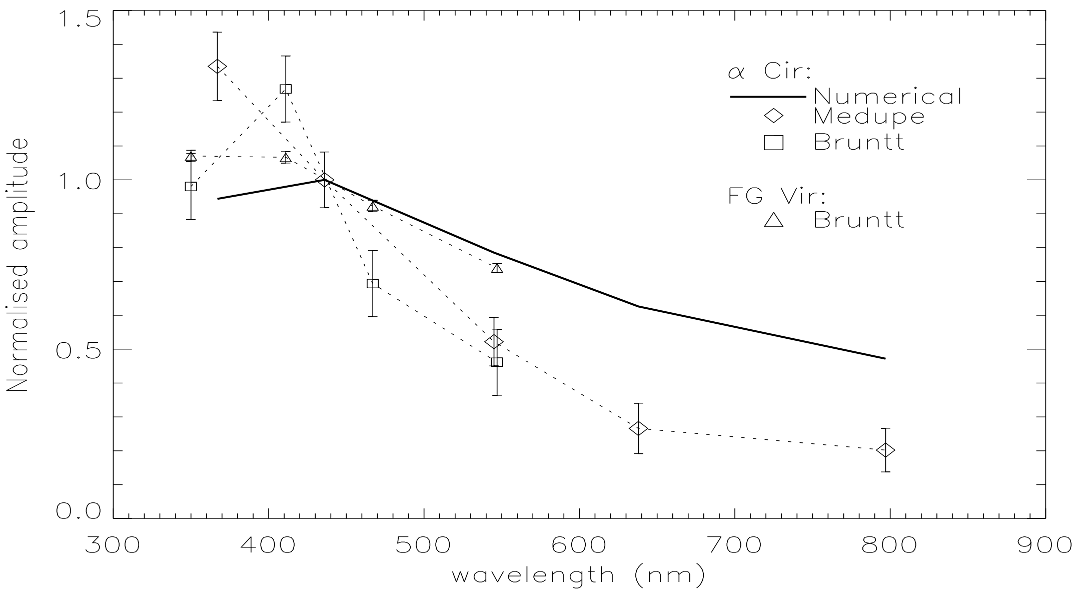

Figure 8.2: The graph shows the observed and theoretically predicted amplitude dependency on wavelength. All amplitudes have been normalized to the amplitude at 436nm (Johnson B filter). The solid line shows the theoretical calculation by Medupe *et al.* [48]. The symbols are the observed amplitude ratios by Medupe *et al.* [48] (diamonds) and myself (boxes). Note that both sets of observation show a stronger decrease with increasing wavelength than predicted by theory. Also plotted are the amplitudes of FG Vir (triangles).

line. The formation depth in the atmosphere of a spectral line increase from the core to the wings of the line (as described in *e.g.* chapter 13 of Gray [32]). This method is thus analogous to the intensity measurements: The change in amplitude with depth is measured.

In this way Baldry *et al.* [6] has shown that the amplitude does indeed decrease when going from the wings to the core of the Hα line, *i.e.* from higher to deeper layers in the atmosphere. In fact their results show that at some depth there is no Doppler shift at all and at even deeper layers the Doppler shift rises again.

This is interpreted by Baldry *et al.* [6] as evidence for a node in the principal oscillation mode. Theory predicts that the observed modes in roAp stars are of high order (n), *i.e.* there are many nodes in the radial part of the oscillation. This agrees with the fact that a node is present at relatively high layers in the star (section 3.4 of Baldry *et al.* [6]).

To conclude, the study by Medupe *et al.* [48] is supported by my observations. These results and the work of Baldry *et al.* [6] both speak for the interpretation that a node is present in the atmosphere of α Cir. This is a remarkable result and shows the applicability of asteroseismology very clearly: By applying this tool, we are able to probe the physics inside the stars.

It would be exciting to use the technique of mode identification by Bedding *et al.* [7] which was applied on FG Vir by Viskum *et al.* [73] on α Cir as well. Baldry *et al.* [6] and Kurtz *et al.* [42] have observed at least four frequencies of very low amplitude in addition to the known principal mode. Being able to do a mode identification of the detected modes in α Cir requires very accurate high resolution spectroscopy. This would yield very detailed information about the physics of this roAp star.

Finally, I note that I have also plotted the observed amplitudes of the principal mode in the Strömgren filters for FG Vir in figure 8.2 (triangles). As seen from the figure the amplitudes of FG Vir decrease with wavelength as predicted by the theoretical model. I stress that the theoretical atmospheric model which was used to model α Cir is quite different from a δ Scuti star, *e.g.* the chemical composition is very different for the peculiar A stars. Contrary to roAp stars that all oscillate in high overtones (high n), δ Scuti stars oscillate in low overtones ($n < 6$), *i.e.* there are few nodes in the radial part of the oscillation. This is in agreement with the observations, *i.e.* there is evidently no node present close to the surface of FG Vir, as seen in α Cir.

Chapter 9

Conclusion

In this chapter I will summarize the results obtained in this thesis and discuss future observations of the objects that I have studied.

For the open clusters NGC 6134 and NGC 3680 I have made a careful and thorough reduction of the raw data (chapter 3 and 4). One of the goals of my work was to improve the flat fielding. Large scale errors were mapped by taking exposures of NGC 6134 with different shifts of the telescope and with different rotator positions of the CCD camera. Using this technique I have determined how the magnitude of a star depends on its position on the CCD, thus removing an important error source. This correction greatly improved the result for the brightest stars in the field of both NGC 6134 and NGC 3680, especially in the y filter, *cf.* figure 3.8.

I have used the Strömgren indices to determine the interstellar reddening and metallicity for the open clusters which is presented in chapter 5. I have used theoretical isochrones to determine the distance and age of the clusters. In both cases I find that the isochrones which include overshoot are in better agreement with the observations. Below I will discuss the results for each cluster.

NGC 3680 has been studied in great detail by Nordström *et al.* [53]. My results agree with what has previously been obtained. Still, the photometry of $\simeq 160$ stars presented in this thesis is of great value. I note that Nordström *et al.* have used only the turnoff stars to calibrate their photometry. In this thesis I use a wider range in $b-y$ of the standard stars, thus providing a better calibration for the fainter stars of the cluster. In addition to this, I have also produced V and $b-y$ magnitudes for a range of stars not observed previously. I have also determined the Strömgren β and m_1 indices to infer the metallicity, $[Fe/H]$ and interstellar reddening, $E(b-y)$ for most of the observed stars, thus supplementing the early observations of Nissen [49]. The results for NGC 3680 are:

- Interstellar reddening, $E(b-y) = 0.043 \pm 0.011$
- Metallicity, $Fe/H = 0.030 \pm 0.024$
- Cluster distance, $d = 1.17 \pm 0.05$ kpc
- Cluster age, $A = 1.48 \pm 0.20$ Gyr

The Strömgren photometry presented in this thesis for $\simeq 700$ stars in the field of NGC 6134 is of excellent quality - and has greatly improved our knowledge of this cluster. Prior to the work presented here UBV photometry was available for only a limited sample of stars ($\simeq 150$) by Kjeldsen *et al.* [38] and Viskum [71].

For NGC 6134 I have determined the interstellar reddening with greater accuracy than what has previously been achieved. I have found a very high metallicity, but the result may be overestimated by 0.1-0.3 dex as the calibration of the m_1 index is not reliable for the highly reddened F type stars in NGC 6134, *cf.* section 4.2.4 and 5.3. If this is the case the distance (age) is over- (under-) estimated.

In the introduction to this thesis I discussed the goal of my work: The primary goal was the determination of basic stellar parameters of the open cluster NGC 6134. This has been achieved:

- Interstellar reddening, $E(b-y) = 0.275 \pm 0.002$
- Metallicity, $Fe/H = 0.41 \pm 0.02$
- Cluster distance, $d = 1.43 \pm 0.06$ kpc
- Cluster age, $A = 0.63 \pm 0.12$ Gyr

The results of the Strömgren photometry presented here will be of great value when it comes to the specific study of the known variable stars of the cluster, *cf.* Frandsen *et al.* [29]. Below I have presented the astrophysical quantities I have determined for these stars:

Table 9.1: Properties of the seven known variable stars in NGC 6134. Star number 647 is a blue straggler (B.S.).

ID_B	ID_V	Type	V	$b-y$	c_0	m_1	β	$E(b-y)$	$M/M_\odot$	T_{eff}	$L/L_\odot$
508	397	δ Scuti	13.566	0.440	0.794	0.149	2.777	0.258	2.05	7774	19.0
574	348	δ Scuti	12.463	0.479	0.851	0.112	2.738	0.264	2.48	7459	52.4
616	159	δ Scuti	13.193	0.433	0.823	0.125	2.771	0.251	2.19	7845	26.8
647	53	B.S.	11.673	0.277	-	0.209	2.898	-	-	-	-
679	87	δ Scuti	13.564	0.441	0.765	0.138	2.759	0.255	2.05	7752	19.1
853	161	δ Scuti	11.988	0.498	0.898	0.120	2.736	0.277	2.56	7325	81.4
906	9	δ Scuti	12.280	0.504	0.731	0.167	2.693	0.241	2.55	7198	62.2

Note that the c_0 index has been derived by interpolation, *cf.* section 4.3. The approximate masses of the stars rely on the isochrone fitting, *cf.* section 5.5. The temperature has been calculated by using the calibration of Alonso *et al.* [2], *cf.* equation 5.1. I note that the T_{eff} of these stars is outside the interval of the calibration and systematic errors may be present. The luminosity has been calculated by using

$$M_{bol} = -2.5 \log(L/L_\odot) + 4.75, \tag{9.1}$$

with

$$M_{bol} = V + BC - 5 \log d + 5 - A_V, \tag{9.2}$$

where BC is the bolometric correction and A_V is the interstellar absorption in V. I have used $BC = -0.06$ taken from Allen [1] and $A_V = 4.3\,E(b-y)$. For the distance modulus I have used the value found in chapter 5 when using the isochrone which includes overshooting, *i.e.* $(V - M_V)_{OVS} = 10.78$, *cf.* table 5.3.

Before we can expect progress in interpreting the information that is contained in the known oscillation frequencies of the variable stars in the cluster (Frandsen *et al.* [29]), we still need spectroscopic data for a range of stars in the cluster. This must be done in order to determine the projected rotational velocities, $v \sin i$, but also to determine if the variable stars are members of the cluster. As can be seen from the interstellar reddening of the δ Scuti stars in table 9.1, they all fall within 3σ of the mean value of the stars in the field, and are probably all members. Hopefully, in the near future we can apply the tools of asteroseismology on the δ Scuti stars in NGC 6134.

The Strömgren photometry presented in this thesis is available through anonymous `ftp` as described in appendix F.

I have measured the amplitudes of the variation in the Strömgren filters of the δ Scuti star FG Vir and the roAp star α Cir. The results for FG Vir have been used by Viskum *et al.* [73] to identify the modes of the eight strongest modes, *cf.* chapter 8. Their work has shown very clearly how valuable information can be derived when using the tools of asteroseismology. My 22 nights of observations of FG Vir have also been included in an extensive dataset which will be published by Breger *et al.* [10] in 1999.

My results on the roAp star α Cir are in agreement with the results of Baldry *et al.* [6] and Medupe *et al.* [48], *cf.* chapter 8. I have measured the amplitude of the principal mode in the Strömgren filters. There is a strong decrease in amplitude with increasing wavelength. This is evidence for a node in the principal oscillation mode, - relatively close to the surface! This star is among the most well-studied stars of its kind, and the dataset of Kurtz *et al.* [42] is still growing! Thus new information on this and other rapidly rotating peculiar A stars will be achieved in the future.

References

References

[1] Allen, C. W., *Astrophysical Quantities*, University of London, the Athlone Press (1976).

[2] Alonso, A. *et al.*, Astron. Astrophys. **313**, 873-890, *The empirical scale of temperatures of the low main sequence (F0V-K5V)* (1996).

[3] Andersen, M. I., Freyhammer, L., Storm, J., ESO, La Silla, *Gain Calibration of Array Detectors by Shifted and Rotated Exposures* (1995). May also be found in *Calibrating and Understanding HST and ESO instruments* by the same authors in: ESO Conference and Workshop Proceedings No 53, p87, Editor: Bienvenuti, P.

[4] Baker, N. H., Gough, D. O., Astrophys. J., **234**, 232-244, *Pulsations of model RR Lyrae stars.*

[5] Baldry, I., Bedding, T. R., Viskum, M., Kjeldsen, H., Frandsen, S., MNRAS **295**, 33-42, *Spectroscopy of the roAp star α Cir - I. Velocities of Hα and metal lines* (1998).

[6] Baldry, I., Viskum, M., Bedding, T. R., Kjeldsen, H., Frandsen, S., MNRAS, in press (1999). *Spectroscopy of the roAp star α Cir - II. The bisector and equivalent-width of the Hα line.*

[7] Bedding, T., Kjeldsen, H., Reetz, J., Barbuy, B., MNRAS, **280**, 1155f (1996).

[8] Birney, D. S., Cambridge University Press, *Observational Astronomy* (1991).

[9] Breger, M. et. al, Astron. Astrophys., **297**, 473f (1995).

[10] Breger, M. et. al, Astron. Astrophys., to be published in 1999.

[11] Bruntt, H., Bachelor Thesis, *Brintprofilen i Solen ud fra helioseismisk inversion af lydhastigheden*, IfA, 1996.

[12] Cayrel, R. *et. al.*, Astron. Astrophys., **146**, 249f.

[13] Claria, J. J., Mermilliod, J. C., Astron. Astrophys. Suppl., **95**, 429f (1992).

[14] Cox, J. P., *Theory of stellar pulsation*, Princeton Univ. Press, 1980,

[15] Crawford, D. L., Astron. J., **80**, 955f (Calibration of $F-G$ stars) (1975).

[16] Crawford, D. L., Mandwewala, N., PASP, **88**, 917f (1976).

[17] Crawford, D. L., Astron. J., **84**, 1858f (Calibration of A stars) (1979).

[18] Christensen-Dalsgaard, J. et al. Astronphys. J, **378**, 413-437 (1991). *The depth of the solar convection zone.*

[19] Christensen-Dalsgaard, J., *Lecture notes on Stellar Structure and Evolution*, IfA (1995).

[20] Christensen-Dalsgaard, J., IFA, Aarhus University *Lecture Notes on Stellar Oscillations* (1997).

[21] Christensen-Dalsgaard, J., *Workshop on Science with a Small Telescope*, MONS Workshop, editors Kjeldsen, H. and Bedding, T., IfA (1998).

[22] Demarque, P. et al., Astrophys. J., **426**, 165f (1994).

[23] Dziembowski, W., Acta Astron. **40**, 19f (1990).

[24] Eggen, O. J., Astrophys. J, **155**, 439f (1969).

[25] Eggen, O. J., Lynden-Bell, D., Sandage, A. R., Astrophys. Jour., **136**, 748f.

[26] Eggleton, P., MNRAS **163**, 179f (1973).

[27] Eggleton, P., found in: Hut, P., Makino, J. (editors) *Dynamical Evolution of Star Clusters*. IAU Symp. 174. Kluwer, Dordrecht, p. 213.

[28] Frandsen, S., Jones, A., Kjeldsen, H., Viskum, M., Hjort, J., Andersen, N. H., Thomsen, B., Astron. Astrophys., **301**, 123f (1995).

[29] Frandsen, S., Balona, L.A., Viskum, M., Koen, C., and Kjeldsen, H., Astron. Astrophys. **308**, 132-140, *Multisite CCD photometry of δ Scuti stars in the open cluster NGC 6134 (the first STACC campaign)* (1996).

[30] Friel, E. D., Annu. Rev. Astron. Astrophys, **33**, 381-414, *The Old Open Clusters of the Milky Way* (1995).

[31] Gilmore, G, *et al.*, *The Milky Way as a Galaxy*, 19^{th} SAAS-FEE (1989).

[32] Gray, D. F., *The observation and analysis of stellar photospheres*, Cambridge Univ. Press (1992).

[33] Haud, U. *et al.*, IAU Symp. 106, *The Milky Way Galaxy*, p85f (table 2) (1985).

[34] Ibata, R. *et al.*, Nature **370**, 194f (1994).

[35] Janes, K. A., Phelps, R. L., Astron. J., **108**, 1773-1785, *The Galactic System of Old Star Clusters: The Development of the Galactic Disk* (1994).

[36] Kippenhahn, R., Weigert, A., Springer-Verlag, *Stellar Structure and Evolution* (1994).

[37] Kjeldsen, H., Frandsen, Astron. Astrophys., **215**, 287-304 (1989).

[38] Kjeldsen, H., Frandsen, S., Astron. Astrophys. Suppl. Ser. **87**, 119-152, *Stellar photometric stability. II. Ages and distances for 13 open clusters with time series observations* (1991).

[39] Kjeldsen, H., Ph. D. thesis, *High Precision Photometry*, Aarhus Universitet (1992).

[40] Kjeldsen, H., Frandsen, S., PASP, **104**, 413-434, *High-precision time resolved CCD photometry* (1992).

[41] Kjeldsen, H., Frandsen, S., IFA, Aarhus University, *Manual: Description of MOMF Software*, (1997).

[42] Kurtz, D. M., Sullivan, D. J., Martinez, P., Tripe, P., MNRAS, **270**, 674f (1994).

[43] Kurucz, R. L., Proc. IAU Symp. 149, *The stellar population of galaxies*, p225 (1992).

[44] Leighton, R. et. al., Astrophys. J., **135**, 474f (1962).

[45] Lyngå, Catalogue of Open clusters, Lund Observatory (1987).

[46] Mantegazza, L., Poretti, E., Bossi, M. Astron. Astrophys. **287**, 95f (1994).

[47] Marcos, R. de La Fuente, Astron. Astroph. **301**, 407f (1995).

[48] Medupe, R., Kurtz, D. M., MNRAS, **299**, 371-378, *Determining temperature amplitude as a function of depth in the atmospheres of rapidly oscillating Ap stars* (1998).

[49] Nissen, P. E., Astron. Astrophys., **199**, 146-160, *The Fourth-Parameter problem in* $uvby - \beta$ *Photometry of Open Clusters* (1988).

[50] Nissen, P. E., Astron. Astrophys. **97**, 145f (1981).

[51] Nissen, P. E., IFA, Aarhus University, *Det Strömgrenske* $uvby - \beta$ *system og dets kalibrering for F0-G2 stars* (in Danish), (1994).

[52] Nordström, B., Andersen, J., Andersen, M. I., Astron. Astrophys. Suppl. Ser., **118**, 407-420 (1996). *Critical Tests of Stellar Evolution in Open Clusters: I. New Photometry and Radial Velocities for NGC 3680.*

[53] Nordström, B., Andersen, J., Andersen, M. I., Astron. Astrophys., **322**, 460-476, *Critical Tests of Stellar Evolution in Open Clusters: II. Membership, Duplicity, and Stellar and Dynamical Evolution in NGC 3680* (1997).

[54] Olsen, E. Heyn, Perry, C. L., Astron. Astrophys. **104**, 429f, and references herein (1994). Private communication: Updated values of the observed standard stars.

[55] Pagel, B. E. J., Lectures to IAC Winter School, *Chemical Evidence on Galaxy Formation and Evolution* (1993).

[56] Perrin, *et al.*, Astron. Astrophys. **54**, 779f (1977).

[57] Pols, O., Schröder, K. P., Hurley, J. R., Tout, C. A, Eggleton, P. P., MNRAS **298**, 525-536, *Stellar evolution models for* $Z = 0.0001 - 0.03$ (1998).

[58] Press, W. H., *et al.*, Numerical Recipes in C: The Art of Scientific Computing, Cambridge University Press

[59] Rodriguez, E., Lopéz de Coca, P., Rolland, A., *et al.*, Astron. Astrophys. Suppl., **106**, 21f (1996).

[60] Schwartz, H. E., Melnick, L., *The ESO User's Manual*, (1993).

[61] Searle, L, Zinn, R., Astro. Phys. Jour., **225**, 689f. (1978)

[62] Sperl, M., *Period 98 manual* (1998).

[63] Stetson, P. B., PASP, **99**, 191f (1987).

[64] Strömgren, B., Ann. Rev. Astron. Astrophys., **4**, 433f (1966).

[65] Storm, J., Reipurth, B., Augusteijn, T., Telescope Manual (ver. 0.4), *Observing at the Danish 1.54m Telescope. A User's Manual for the TCS and DFOSC*, ESO (1996).

[66] Terlevich, E., MNRAS **224**, 193f (1987).

[67] Tomczyk, S, et. al., Proc. Conference: *Windows on the Sun's interior*, Bull. Astron. Soc. India, **24**,245-250 (1996).

[68] Twarog, B. J. A., Twarog, B. A., Shodhan, S., Astron. J., **98**, 1634f, *CCD uvby photometry of the bimodal main-sequence cluster NGC 3680* (1989).

[69] VandenBerg, D. A., Bolte, M., Stetson, P. B., Annu. Rev. Aston. Astrophys. **34**, 461-510, *The Age of the Galactic Globular Cluster System* (1996).

[70] Vaz, L. P. R., *The reduction package for SAT* (1993).

[71] Viskum, M., Master Thesis: *Relativ CCD fotometri og frekvensanalyse af* δ *Scuti variable*, IfA, Aarhus Universitet (1994).

[72] Viskum, M., Ph. D. thesis: *Properties of Delta Scuti Stars*, IfA, Aarhus Universitet (1997).

[73] Viskum, M., Kjeldsen, H., Bedding, T. R., Dall, T. H., Baldry, I. K, Bruntt, H., Frandsen, S., Astron. Astrophys. **335**, 549-560 (1998).

[74] Young, T. A., Astron. Jour. **72**, 747f (1967).

Appendices

- A. The Strömgren Photometric System
- B. Isochrones
- C. Log of Observations: NGC 6134 and NGC 3680
- D. MOMF Output File
- E. Photometric Results for NGC 6134 and NGC 3680
- F. Anonymous `ftp`
- G. Summary in Danish (Dansk Resumé)

Appendix A

The Strömgren Photometric System

The late Danish astronomer Bengt Strömgren (1908-87) developed an intermediate/narrow band photometric system in the 1950'ies and 1960'ies which now bears his name. His work was made in collaboration with D. L. Crawford. A detailed description of the system is found in Strömgren [64]. In the following I will give an introduction to the system as this is the tool I make use of in the thesis. The review below is based on the introductory notes by Poul-Erik Nissen [51].

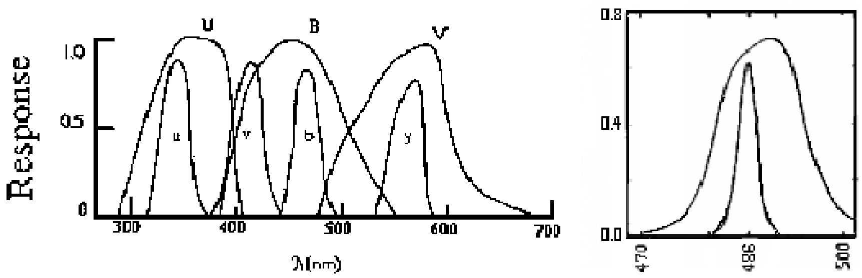

Figure A.1: The response function of the six Strömgren filters. To the left I have compared the intermediate band Strömgren *uvby* filters with the broad band Johnson UBV filters. To the right are the response functions of the two β filters. The figures have been adopted from Birney [8].

There are six filters in the Strömgren system: *uvby* and two β filters: A narrow (N) and a wide (W) one. The response functions of these filters are shown on figure A.1 above. In the figure I have also shown the location of the most widely used photometric filters: The broad band Johnson UBV filters. The reason for the terms *intermediate* band and *broad* band is clearly seen.

It should be noted that the full application of the Strömgren system is limited to a narrow range of spectral types: This range is defined as stars of spectral types from $F0$ to $G2$. This range is alternatively defined by the range $2.72 > \beta > 2.59$ or similarly $T_{\rm eff}$ in the range 7100-5800K. The Strömgren system has also been calibrated for type A stars although the metallicities of these hotter stars cannot be determined.

By measuring the flux in the wide and narrow filters around the H_β line at 486nm, one can determine the β-index. This is defined as the difference in magnitude between the two filters:

$$\beta = m_N - m_W. \tag{A.1}$$

The depth of the H_β line and hence the flux from this part of the spectrum depends sensitively on the effective temperature of the atmosphere. Larger absorption yields a higher β-index which again means a hotter atmosphere. As the central wavelength is the same for both filters, the index is independent of interstellar extinction.

To obtain a "useful" β-index one needs very precise photometry with errors below 1%, *i.e.* 0.01 magnitude. Since the filters are extremely narrow, long integration times and/or a large telescope is needed.

Another measure of temperature is the $(b-y)$ index. The difference in magnitude between the b and y filters is a measure of the slope of the continuum between 470 and 550nm. Unlike the β-index the $(b-y)$ index is shifted towards higher values by interstellar extinction, $E(b-y)$, which is also called reddening or colour excess. This fact can then be used to determine the amount of stellar extinction. Crawford [15] has determined the following relationship which shows some dependency on metallicity (δm_0) and the evolution above the ZAMS of the observed star (δc_0):

$$(b-y)_0 = 0.218 + 1.11\Delta\beta + 2.7\Delta\beta^2 - 0.05\delta c_0 - (0.1 + 3.6\Delta\beta)\delta m_0, \tag{A.2}$$

valid in the range $2.72 > \beta > 2.59$. The constant term in equation A.2 has been changed from 0.222 to 0.218. According to Nissen [49] this gives a better fit. In the equation above $\Delta\beta = 2.72 - \beta$ and $(b-y)_0$ is the value of $(b-y)$ corrected for interstellar extinction. The remaining symbols will be described shortly.

Crawford has also made a calibration for A type stars [17]. The result depends on the value of δm_0:

$$(b-y)_0 = 2.942 - 1.00\beta - 0.1\delta c_0 - 0.25\delta m_0 \text{ if } \delta m_0 < 0.00 \tag{A.3}$$

$$(b-y)_0 = 2.942 - 1.00\beta - 0.1\delta c_0 \text{ if } \delta m_0 > 0.00. \tag{A.4}$$

Having determined $(b-y)_0$ by using one of the equations (A.2-4), the interstellar reddening can be calculated by using

$$E(b-y) = (b-y) - (b-y)_0. \tag{A.5}$$

The Strömgren indices have been calibrated with $T_{\rm eff}$ by various authors. The most extensive work in this field is published in Alonso *et al.* [2], although limited to $T_{\rm eff} < 7200K$. In equation 5.1 I have shown their calibration of $T_{\rm eff}$.

The u and v bands are located at wavelengths below and above the Balmer discontinuity at $\lambda_B = 365$nm. In stellar atmospheres of stars of type F (and A) the most important source of absorption is H^-. The reason for the decrease in flux at wavelengths shorter than λ_B is explained by the fact that photons possessing the energy corresponding to this wavelength (or more) can excite electrons of Hydrogen in the $n = 2$ level. This additional amount of absorption leads to a decrease in flux.

The Balmer discontinuity index is defined as:

$$c_1 = (u - v) - (v - b). \tag{A.6}$$

The Balmer jump and hence c_1 is indirectly related to the pressure of electrons in the atmosphere which depends on the magnitude of gravity: In a giant star the gravity at the surface is relatively smaller compared to a main sequence star of equal mass. In other words: The surface gravity decreases as the star evolves above the ZAMS.

Consequently, the amount of absorption due to H^- in the atmosphere of an evolved star is smaller leading to a larger Balmer jump. More specifically, one can determine to what extent a star has evolved above the ZAMS due to the lower gravity in the atmosphere. If a significant amount of interstellar extinction is present, the c_1 index is shifted. The extinction corrected index is

$$c_0 = c_1 - 0.20 \times E(b - y), \tag{A.7}$$

according to Crawford and Mandwewala [16].

The δc_0-term in equation A.2 above, is defined as $\delta c_0 = c_0(\text{ZAMS}) - c_0$, where $c_0(\text{ZAMS})$ is the value for ZAMS stars which depends on β: In table A.1 I present this dependency.

Thus c_0 can be used to determine to what extent a star has evolved above the ZAMS, measured as $\delta M_V = M_V(ZAMS) - M_V$. It is also possible to determine the c_0 index if one knows δM_V. This is indeed possible for observations of a stellar cluster. If one assumes that the less massive stars of the cluster are still on the ZAMS, then the standard ZAMS relation of Crawford [15], [17] can be fitted to these stars, *i.e.* by shifting M_V to fit the observed V (the distance modulus). Having done this, one can measure how much the more massive stars have evolved above the standard ZAMS relation. I will describe this thoroughly in section 4.3 where I have used this technique to determine c_0 for the stars of the open cluster NGC 6134.

The amount of absorption due to heavy elements is measured through the magnitude in the v filter. In stars with high metallicity the absorption lines will be deeper and hence the v magnitude larger, *i.e.* a lower flux is observed. The definition of the colour that is essentially only dependent on metallicity is given by:

$$m_1 = (v - b) - (b - y). \tag{A.8}$$

Like the c_1-index m_1 is sensitive to interstellar absorption. The extinction corrected index is given by

$$m_0 = m_1 + 0.30 \times E(b - y), \tag{A.9}$$

according to the calibration of Crawford and Mandwewala [16].

Analogous to the δc_0-parameter, a δm_0 is defined as: $\delta m_0 = m_0(\text{Hyades}) - m_0$, where $m_0(\text{Hyades})$ is the value for the well-calibrated open cluster Hyades. This parameter depends on temperature measured through the β-index, as can be seen in table A.1. The calibration of the dependency of δm_0 on metallicity has been done by Nissen (1981) [50]:

$$[Fe/H] = 0.12 - \delta m_0 \times (10.5 + 50(\beta - 2.626)). \tag{A.10}$$

Table A.1: Relations among $uvby - \beta$ for F (left) and A (right) stars according to Crawford [15], [17]

$Fstars$				$Astars$			
β	m_0(Hyades)	c_0(ZAMS)	M_V(ZAMS)	β	m_0(Hyades)	c_0(ZAMS)	M_V(ZAMS)
2.72	0.177	0.580	3.14	2.88	0.200	0.930	2.30
2.71	0.174	0.560	3.21	2.86	0.205	0.890	2.50
2.70	0.172	0.530	3.29	2.84	0.208	0.850	2.64
2.69	0.171	0.495	3.38	2.82	0.206	0.820	2.70
2.68	0.170	0.465	3.48	2.80	0.203	0.780	2.76
2.67	0.171	0.440	3.60	2.78	0.196	0.740	2.82
2.66	0.174	0.415	3.74	2.76	0.188	0.700	2.88
2.65	0.178	0.390	3.88	2.74	0.182	0.660	2.96
2.64	0.183	0.370	4.04				
2.63	0.189	0.350	4.20				
2.62	0.196	0.330	4.36				
2.61	0.204	0.310	4.52				
2.60	0.214	0.290	4.70				
2.59	0.226	0.270	4.90				

This result which is valid for F0-G2 stars (β from 2.72 to 2.59) with [Fe/H] in the range -0.7 to 0.3. If a value of $\delta m_0 = 0.00$ is found, this corresponds to a metallicity of $[Fe/H] = 0.12$, - the value found for the Hyades.

Results obtained by using spectroscopy agree remarkably well with results from photometry. Note that the constant term in equation A.10 has been changed from 0.16 to 0.12 according to more recent results from a spectroscopic determination of the metal content of the Hyades by Cayrel [12].

In chapter 5 I will make extensive use of the calibrations cited above.

Appendix B

Isochrones

As described in section 1.4 it is very interesting to compare the observed colour-magnitude diagram (CMD) of a cluster of stars with theoretical calculations of the evolution of a sample of stars with different masses (isochrones). As discussed, one can determine the distance and age of a cluster if the metallicity and interstellar reddening is known. This is indeed the case for the two open clusters I have observed. In the following I will give a brief introduction to the theoretical models.

I have used some recent model calculations by Onno Pols *et al.* I will not go into detail about the input physics of the models which is described thoroughly in Pols *et al.* [57]. Basically, the evolution code is based on early work by Eggleton (1973) [26]. The original input physics of the code has been improved since then: A new equation of state, inclusion of pressure ionization and Coulomb interactions, and more recent opacity tables and reaction rates are used in the present models.

The Fortran programme supplied by Pols *et al.* takes the age and metallicity as input parameters. The output is an array of the luminosity and the effective temperature for range of stars with increasing mass. Typically 200 stars with masses from $0.5 - 25M_{\odot}$ are used. The output values can be either the result when using "standard" or "overshoot" models, which include overshoot in the cores of stars more massive than $M \simeq 1.2M_{\odot}$. The amount of overshoot is measured through the value of mixing length parameter, $\alpha = l_m/H_p$, that measure the length (l_m) that a convective element moves - relative to the local pressure scale height, H_p - before it loses its identity. This value is set to $\alpha = 2.0$. Using this value in the code produces a model consistent with observations of the radius of the Sun.

Below I have shown some calculated isochrones that use either "standard" and "overshoot" models. The result with an age of 1 Gyr and metallicity $[Fe/H] = 0.10$ is shown is figure B.1.

Pols *et al.* [57] has used the isochrones to fit the observations of six open clusters of different age and metallicity. The result of their analysis shows that models that include overshoot are needed to explain the width of the loop after the turnoff. As seen in figure B.1 the isochrone using overshoot models have a more extended loop in $T_{\rm eff}$. It can also be seen that the position (M_V,$T_{\rm eff}$) of the turnoff is quite different for the two models. Based on the results of Pols *et al.* [57], I have used isochrones calculated with overshoot models in the following.

In figure B.2 I show three isochrones of increasing ages (0.8, 1.0, and 1.2 Gyr) but with equal metallicity: $[Fe/H] = 0.10$. They show the trend explained in section 1.4, *i.e.* the stars located near the turnoff are of lower luminosity and temperature (and mass) as the age increases.

To show the dependency of the isochrones on metallicity, I have shown the results in figure B.3 for isochrones of equal age but with different metallicity.

I note that the range in metallicity for which the code by Pols *et al.* [57] is valid is $0.0001 < Z < 0.03$. This corresponds to $-2.3 < [Fe/H] < 0.22$ when using the expression $Z = 0.76/(3.0+37.425*10^{-[Fe/H]})$ in section 6 of Pols *et al.* [57] . Thus the high metallicity isochrones in figure B.3 are based on extrapolation and is erroneous to some level.

I intend to use the isochrones calculated by using the evolution code of Pols *et al.* [57] to determine the age of the open clusters NGC 6136 and NGC 3680, *cf.* section 5.4.

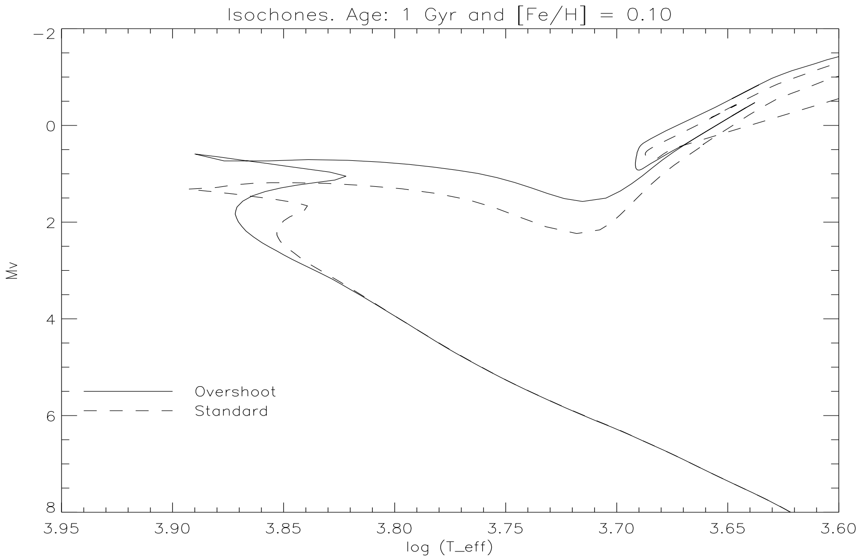

Figure B.1: Two isochrones when using different stellar models. Both isochrones are of age 1 Gyr and has metallicity $[Fe/H] = 0.10$.

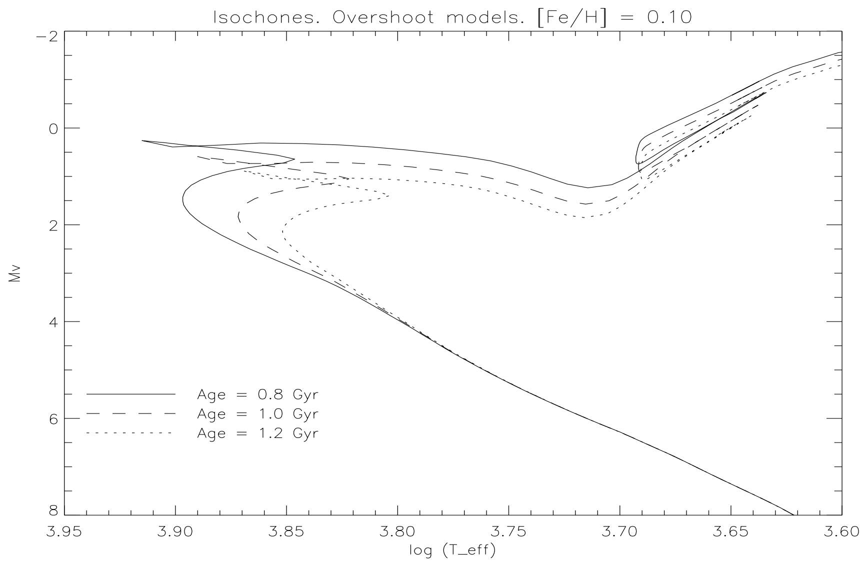

Figure B.2: Examples of isochrones when using overshoot models with the same metallicity but with different ages as indicated in the graph.

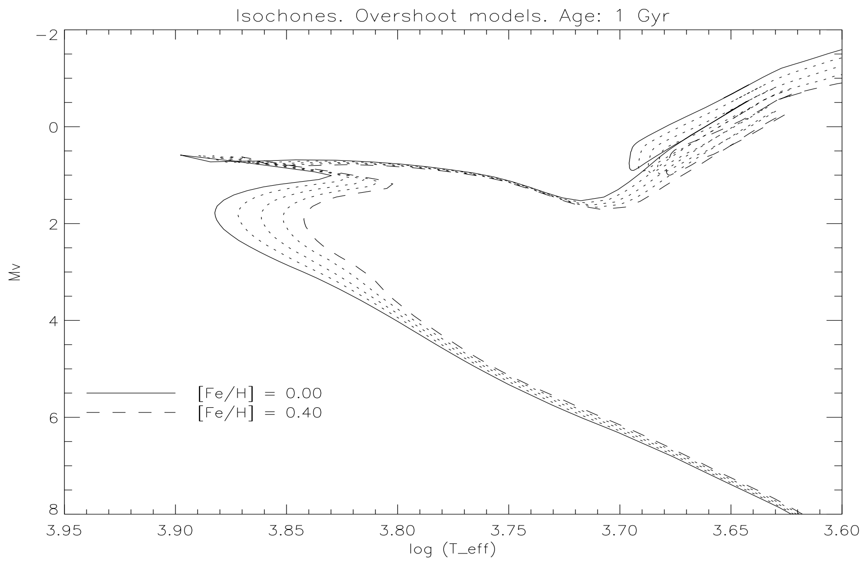

Figure B.3: Five isochrones when using overshoot models with the same the age with a range of metallicities: 0.0, 0.1,...0.4.

Appendix C

Log of Observations Made at La Silla, May 1996

This appendix contains the detailed log tables of the observations of the open clusters NGC 6134 and NGC 3680 made at La Silla. In each of the two tables C.1 and C.2 the following abbreviations apply: "Image" is the name of the raw image in fits format. "MOMF-file" is the name of the result file from the MOMF reduction. "Set" is the number referring to the different groups of frames. The positions of the stars in each group are different as the telescope has been shifted and/or the camera may have been rotated 180 degrees. "Trans" is the file that gives the relationship between the star numbers in the reference frame and stars in a given frame. "Filter" describes which filter was used with each image: 1,2,3,4,5 refers to the Strömgren-filters $vby\beta(W)$ and $beta(N)$. "Night" is the night number: 0 is April 29th, 1 is April 30th, 2 is May 1st, 3 is May 2nd, 4 is May 3rd - all in the year 1996. "Exp" is the exposure time. "ZD" is the zenith distance. "On/Off" describes which frames have been excluded for some reason - these frames are "off", *i.e.* value = 0.

Table C.1: Log of all observations of NGC 6134. The reference frame is printed in **bold**.

Image	MOMF-file	Set	Trans	Night	Filter	Exp	ZD	On/Off
dfsc1443	3219438.562	2	t1443	0	3	50	20.6	1
dfsc1444	3219438.732	2	t1444	0	3	60	23.6	1
dfsc1445	3219438.873	3	t1445	0	3	50	24.9	1
dfsc1446	3219439.150	3	t1446	0	3	50	25.6	1
dfsc1447	3219439.453	4	t1447	0	3	50	26.1	0
dfsc1448	3219439.620	1	t1448	0	3	70	26.7	0
dfsc1449	3219439.851	1	t1449	0	2	100	27.6	0
dfsc1450	3219440.187	5	t1450	0	2	70	28.4	1
dfsc1654	3219443.713	24	t1654	1	5	500	28.7	0
dfsc1655	3219443.840	24	t1655	1	5	500	30.7	0
dfsc1656	3219443.975	25	t1656	1	5	400	32.7	1
dfsc1657	3219444.112	25	t1657	1	4	400	34.3	1
dfsc1658	3219444.251	24	t1658	1	4	400	36.3	1
dfsc1639	3219443.067	6	t1639	1	2	70	20.3	1
dfsc1640	3219443.180	7	t1640	1	2	60	20.6	1
dfsc1641	3219443.282	21	t1641	1	2	60	21.0	1
dfsc1642	3219443.384	22	t1642	1	1	300	21.4	1
dfsc1643	3219443.487	23	t1643	1	1	300	21.9	1
dfsc1644	3219443.598	23	t1644	1	1	300	22.9	1
dfsc1659	3219444.389	24	t1659	1	3	50	38.7	1
dfsc1660	3219444.496	24	t1660	1	3	70	39.7	1
dfsc1661	3219444.615	24	t1661	1	3	150	40.7	1
dfsc1662	3219444.725	25	t1662	1	3	150	42.0	1
dfsc1663	3219444.839	25	t1663	1	1	400	43.8	1
dfsc1664	3219444.948	24	t1664	1	1	400	45.7	1
dfsc1665	3219445.056	24	t1665	1	2	60	47.9	1
dfsc1901	3219423.825	20	t1901	2	4	400	25.0	1
dfsc1906	3219424.105	15	t1906	2	4	300	34.1	1
dfsc1916	3219424.458	13	t1916	2	4	400	44.5	1
dfsc1917	3219424.577	13	t1917	2	4	400	46.5	1
dfsc1900	3219423.709	20	t1900	2	5	400	23.7	1
dfsc1905	3219423.987	15	t1905	2	5	500	32.4	1
dfsc1914	3219424.224	13	t1914	2	5	400	41.3	1
dfsc1915	3219424.340	13	t1915	2	5	400	42.7	1
dfsc1897	3216463.718	20	t1897	2	2	60	21.7	1
dfsc1898	3216554.132	20	t1898	2	1	400	22.1	1
dfsc1899	3219937.643	20	t1899	2	3	150	23.1	1
dfsc1902	3216385.266	15	t1902	2	2	60	26.4	1
dfsc1903	3216554.312	16	t1903	2	1	400	28.4	1
dfsc1904	3216557.291	16	t1903	2	3	100	29.8	1
dfsc1907	3216385.417	15	t1907	2	2	50	35.5	1
dfsc1908	3216385.551	13	t1908	2	2	50	36.3	1
dfsc1909	3216385.743	13	t1909	2	2	50	36.8	1
dfsc1910	3216453.064	13	t1910	2	1	300	37.3	1
dfsc1911	3216453.182	14	t1911	2	1	300	38.6	1
dfsc1912	3216400.940	14	t1912	2	3	150	39.7	1
dfsc1913	3216401.095	14	t1913	2	3	100	40.6	1
dfsc2229	3219779.576	27	t2229	3	4	400	30.8	1
dfsc2237	3219780.786	31	t2237	3	4	400	39.8	1
dfsc2238	3219780.968	31	t2238	3	4	200	41.4	1
dfsc2250	3219782.439	28	t2250	3	4	200	50.5	0
dfsc2228	3219779.448	27	t2228	3	5	500	28.9	0
dfsc2236	3219780.666	31	t2236	3	5	500	38.1	0
dfsc2239	3219781.150	31	t2239	3	5	280	42.5	1
dfsc2249	3219782.285	28	t2249	3	5	280	48.9	0
dfsc2222	3219778.361	26	t2222	3	3	150	23.8	1
dfsc2223	3219778.540	26	t2223	3	3	130	24.4	1
dfsc2224	3219778.738	26	t2224	3	2	60	25.3	1
dfsc2225	3219778.918	27	t2225	3	2	70	25.9	1
dfsc2226	3219779.100	27	t2226	3	1	400	26.4	1
dfsc2227	3219779.270	27	t2227	3	1	300	27.6	1
dfsc2231	3219779.755	29	t2231	3	3	100	33.5	1
dfsc2232	3219779.938	30	t2232	3	3	100	34.3	1
dfsc2233	3219780.118	31	t2233	3	3	100	35.1	1
dfsc2234	3219780.298	31	t2234	3	1	350	35.8	1
dfsc2235	3219780.480	31	t2235	3	2	60	37.3	1
dfsc2240	3219781.275	28	t2240	3	3	70	43.7	1
dfsc2241	3219781.442	28	t2241	3	2	40	44.3	1
dfsc2242	3219781.611	28	t2242	3	1	185	44.8	1
dfsc2246	3219781.782	28	t2246	3	3	70	46.6	1
dfsc2247	3219781.946	28	t2247	3	2	40	47.1	1
dfsc2248	3219782.120	28	t2248	3	1	185	47.6	0
dfsc2618	3218802.310	17	t2618	4	5	100	29.0	1
dfsc2619	3218802.439	17	t2619	4	5	600	29.8	0
dfsc2620	3218802.547	17	t2620	4	5	500	31.6	0
dfsc2608	3218800.955	17	t2608	4	3	150	22.2	1
dfsc2609	3218801.100	17	t2609	4	3	100	22.6	1
dfsc2610	3218801.227	17	t2610	4	3	70	23.1	1
dfsc2611	3218801.360	17	t2611	4	2	50	23.4	1
dfsc2612	3218801.477	17	t2612	4	2	60	23.8	1
dfsc2613	3218801.576	17	t2613	4	1	200	24.1	1
dfsc2614	3218801.739	17	t2614	4	1	200	24.9	1
dfsc2615	3218801.869	17	t2615	4	1	200	25.5	1
dfsc2616	3218802.003	17	t2616	4	1	400	26.2	1
dfsc2617	3218802.144	17	t2617	4	1	400	27.4	1

Table C.2: Log of all observations of NGC 3680. The reference frame is printed in **bold**.

Image	MOMF-file	Set	Trans	Night	Filter	Exp	ZD	On/Off
dfsc1429	3225639.905	50	w1429	0	1	300	99.9	0
dfsc1430	3225639.954	50	w1430	0	1	300	99.9	0
dfsc1431	3225639.980	51	w1431	0	1	300	99.9	0
dfsc1432	3225640.018	52	w1432	0	1	300	99.9	0
dfsc1433	3225640.053	52	w1433	0	2	100	99.9	0
dfsc1434	3225640.087	52	w1434	0	2	60	99.9	0
dfsc1435	3225640.114	53	w1435	0	2	50	99.9	0
dfsc1436	3225640.168	54	w1436	0	2	50	99.9	0
dfsc1437	3225640.235	54	w1437	0	3	50	40.2	0
dfsc1438	3225640.285	54	w1438	0	3	40	42.3	0
dfsc1600	3226157.165	59	w1600	1	2	50	26.7	1
dfsc1601	3225877.502	55	w1601	1	2	100	27.4	1
dfsc1602	3225878.221	55	w1602	1	2	60	28.3	1
dfsc1603	3225878.713	56	w1603	1	2	50	30.6	1
dfsc1604	3225879.169	57	w1604	1	2	50	32.7	1
dfsc1605	3225879.613	58	w1605	1	2	50	34.2	1
dfsc1847	3225891.498	60	w1847	2	3	50	27.8	1
dfsc1848	3225892.060	60	w1848	2	3	50	28.5	1
dfsc1849	3225892.707	60	w1849	2	3	50	28.9	1
dfsc1850	3226731.206	60	w1850	2	1	300	29.7	1
dfsc1851	3226731.561	60	w1851	2	1	300	31.1	1
dfsc1852	3226732.007	60	w1852	2	1	300	32.2	1
dfsc1853	3226151.185	60	w1853	2	2	60	33.7	1
dfsc1854	3226151.465	60	w1854	2	2	130	34.8	1
dfsc1855	3226151.794	60	w1855	2	2	130	35.4	1
dfsc1856	3226152.294	61	w1856	2	2	110	36.5	1
dfsc1857	3226152.721	61	w1857	2	2	110	37.1	1
dfsc1862	3225893.158	61	w1862	2	3	50	39.4	1
dfsc1863	3225893.478	61	w1863	2	3	50	39.8	1
dfsc1864	3226153.056	61	w1864	2	1	350	40.5	1
dfsc1865	3226153.327	61	w1865	2	1	350	41.9	1
dfsc1866	3226153.612	61	w1866	2	5	450	44.2	1
dfsc1867	3226153.941	61	w1867	2	5	400	46.5	1
dfsc1868	3226154.339	61	w1868	2	5	280	48.2	1
dfsc1869	3226154.774	61	w1869	2	5	100	50.2	1
dfsc1870	3226155.184	61	w1870	2	4	380	51.1	1
dfsc1871	3226155.523	61	w1871	2	4	250	52.8	1
dfsc1872	3226155.798	61	w1872	2	4	100	54.1	1
dfsc1873	3226156.058	61	w1873	2	4	240	55.0	1
dfsc1874	3226156.327	60	w1874	2	4	100	56.9	1
dfsc1875	3226156.594	60	w1875	2	5	100	57.7	1
dfsc1876	3226156.900	60	w1876	2	5	400	58.4	1
dfsc2207	3226742.384	62	w2207	3	1	350	56.1	1
dfsc2208	3226742.478	62	w2208	3	1	380	57.6	1
dfsc2209	3226742.567	62	w2209	3	2	110	59.4	1
dfsc2210	3226742.661	62	w2210	3	2	110	60.3	1
dfsc2211	3226742.754	62	w2211	3	3	45	61.0	1
dfsc2212	3226742.849	62	w2212	3	3	45	61.4	1
dfsc2213	3226750.299	62	w2213	3	5	400	62.2	1
dfsc2214	3226750.619	62	w2214	3	5	120	63.7	1
dfsc2215	3226742.923	62	w2215	3	4	240	64.5	1
dfsc2216	3226750.905	62	w2216	3	4	100	66.1	1

Appendix D

MOMF Output File

In this appendix I give an example of the output file from MOMF. The description of the MOMF photometric reduction programme is found in section 3.2. I present the output for 65 stars in the reference frame "dfsc1856" of NGC 3680: The ID, (x, y)-position, and the result of six apertures with radii (2.83, 4.25, 5.66, 7.08, 8.85, 10.61) pixels. A magnitude of 99.9999 means that some problem occurred in the determination of the magnitude, *e.g.* the star is too close to the edge of the CCD, a close neighbouring star, or a bad PSF fit because of a bad pixel/column *etc.* In the last row I have included the distance to the nearest star. Four close star pairs have been printed in **bold**, *i.e.* 61/62, 85/88, 102/104, 121/122. As can be seen the result is quite unreliable when comparing the magnitudes obtained with different apertures, especially for the faint stars 121/122.

Table D.1: Output from MOMF for 65 stars in the reference frame of NGC 3680.

ID	x	y	A1	A2	A3	A4	A5	A6	d_{min}
60	326.22	639.19	7.03248	7.02074	7.03826	7.05492	7.04783	7.04715	44.4780
61	370.31	652.78	6.77378	6.82625	6.96745	7.14399	7.10190	7.13335	**6.82401**
62	376.71	656.66	4.82785	4.83864	4.84550	4.84268	4.84624	4.85546	**6.82401**
63	1039.90	660.91	7.44185	7.18887	6.75355	6.65139	6.46536	6.33566	51.1735
64	107.21	662.46	10.07446	10.45884	10.92835	10.31099	9.06503	8.68748	97.2840
65	344.06	680.09	6.28779	6.30632	6.29576	6.30741	6.34774	6.40491	27.1152
66	312.89	708.64	6.34135	6.37683	6.37103	6.36555	6.35999	6.36172	42.2181
67	1041.76	712.41	7.09516	7.11119	7.13403	6.69075	6.44155	6.28234	51.1735
68	433.32	716.07	10.21891	10.57143	10.58572	10.02755	99.99990	99.99990	6.19457
69	1094.37	716.97	6.12955	6.12784	6.12592	6.13097	6.13331	6.16009	52.5424
70	426.99	719.06	4.55918	4.56603	4.56427	4.56454	4.56398	4.56508	6.19457
71	29.92	721.54	2.92539	2.99187	3.01196	3.02188	3.02554	3.02305	44.1755
72	470.13	726.01	6.52834	6.52429	6.51134	6.51083	6.53180	6.52838	37.0678
73	1175.79	727.61	3.36759	3.36597	3.36318	3.36137	3.36121	3.36135	50.7475
74	267.01	743.45	2.88177	2.80268	2.67553	2.39799	2.21983	2.10274	2.51204
75	262.90	751.50	3.15202	3.13930	2.88114	2.62499	2.16393	2.07785	2.63142
76	1294.89	758.07	10.68813	12.61640	99.99990	99.99990	99.99990	99.99990	88.3314
77	684.56	758.12	3.54434	3.51910	3.50951	3.50539	3.50272	3.49994	19.7622
78	1005.89	761.83	7.63981	7.62054	7.58927	7.52540	7.45090	7.44188	44.5956
79	665.82	764.59	5.67109	5.65812	5.64839	5.63102	5.63379	5.63033	19.7622
80	1157.61	775.31	7.49249	7.45452	7.40993	7.38412	7.38174	7.40420	50.7475
81	1388.44	778.83	99.99990	12.81243	99.99990	99.99990	99.99990	99.99990	90.3800
82	1589.31	786.89	5.52426	5.59406	5.62066	5.63094	5.62245	5.63768	106.096
83	80.78	787.53	6.21394	6.24718	6.26226	6.30325	6.30325	6.30173	83.1734
84	1796.55	791.71	6.24959	6.32884	6.36008	6.40453	6.43486	6.48196	94.3774
85	839.29	797.93	2.07823	2.05931	2.04156	2.14751	2.13693	2.10000	**7.32675**
86	176.60	800.11	6.85580	6.91664	6.98214	7.00958	7.04742	7.09445	88.3154
87	988.32	803.01	2.97588	2.95454	2.93836	2.93154	2.92869	2.92704	26.9815
88	839.39	805.27	2.63104	2.60301	2.53219	2.41475	2.35555	2.22625	**7.32675**
89	523.57	813.17	3.42210	3.40026	3.39232	3.39139	3.39160	3.39103	48.7576
90	1487.48	817.09	3.74849	3.78903	3.80799	3.81395	3.81528	3.81386	40.2798
91	1116.51	819.25	13.77762	99.99990	99.99990	11.14029	10.15579	11.01886	59.9435
92	971.33	824.06	5.26064	5.23600	5.21762	5.21700	5.20858	5.18932	26.9815
93	308.52	828.23	5.54451	5.54229	5.54445	5.54038	5.53814	5.54644	87.4074
94	1322.82	841.37	3.47415	3.48644	3.49507	3.49851	3.50148	3.50254	88.3314
95	711.02	842.58	3.14151	3.11526	3.09559	3.08958	3.08786	3.08849	58.2934
96	1496.45	856.42	5.15187	5.18992	5.21509	5.23362	5.23574	5.23341	40.2798
97	500.69	857.08	99.99990	99.99990	99.99990	99.99990	99.99990	99.99990	48.7576
98	128.73	874.57	6.36668	6.38349	6.40590	6.40744	6.39627	6.40258	39.6619
99	1805.05	885.75	3.07475	3.19248	3.24202	3.25933	3.26961	3.27124	94.3774
100	738.77	893.98	3.22842	3.18847	3.16790	3.16190	3.16316	3.16311	24.4866
101	183.53	901.13	6.89443	6.89935	6.90726	6.90543	6.89088	6.81221	30.1258
102	768.76	902.11	2.81337	2.84703	2.96449	2.66264	2.55964	2.60141	**1.39614**
103	761.21	903.78	3.18103	3.41984	3.38817	2.90238	2.79011	2.89502	2.46474
104	767.09	905.98	99.99990	99.99990	99.99990	4.43814	4.33638	4.34025	**1.39614**
105	766.36	907.46	3.55586	3.64276	3.78831	3.07672	2.85266	2.85753	1.65030
106	1444.59	910.42	4.62929	4.64533	4.66845	4.67289	4.67423	4.66948	74.8058
107	329.94	913.05	6.51901	6.52280	6.51939	6.53515	6.54130	6.53212	87.4074
108	840.08	914.19	5.87316	5.84502	4.63707	4.92490	99.99990	99.99990	32.6803
109	107.79	919.20	2.35068	2.38457	2.40064	2.40530	2.40485	2.40479	47.7266
110	1548.08	932.28	6.69183	6.74717	6.78036	6.79768	6.83084	6.84982	91.6291
111	1148.24	937.66	7.26866	7.23234	7.22803	7.24908	7.17684	7.17817	33.3124
112	870.41	940.57	3.68275	3.65083	3.62043	3.60112	3.56136	3.51062	9.70483
113	1115.43	945.10	5.07055	5.05025	5.03576	5.03185	5.03167	5.03514	33.3124
114	712.33	958.16	1.97771	1.94398	1.92544	1.91963	1.91781	1.91727	46.2475
115	990.07	963.99	6.79705	6.75078	6.74901	6.73155	6.70313	6.70897	121.816
116	755.64	975.48	2.86477	2.82423	2.80776	2.80494	2.80450	2.80321	46.2475
117	1161.83	979.29	99.99990	99.99990	12.00934	10.52771	10.24771	10.71277	42.7131
118	1164.07	1036.06	6.85266	6.83667	6.81658	6.76880	6.75574	6.72921	41.1509
119	1817.27	1059.24	3.71401	3.82287	3.88421	3.90741	3.91574	3.92049	43.7737
120	1154.37	1076.20	7.41152	7.37588	7.41223	7.44886	7.42521	7.34817	39.3809
121	1109.34	1078.50	10.34012	10.86426	11.26827	99.99990	10.48773	9.81426	**4.88060**
122	1112.66	1082.83	11.12738	11.51564	11.47407	99.99990	13.65320	11.67303	**4.88060**
123	1031.32	1092.76	2.02965	1.99647	1.96033	1.94567	1.93450	1.92603	36.0501
124	799.44	1110.37	3.76220	3.72448	3.70153	3.69665	3.69436	3.69407	38.1925

Appendix E

Photometric Results for NGC 6134 and NGC 3680

In the following I present the final standard Strömgren indices which are determined as described in chapter 4. I have also included the Balmer discontinuity index, c_0 for stars in NGC 6134, which was found in section 4.3. The result of the determination of the interstellar reddening, $E(b-y)$, which was obtained in section 5.2, is also given in the tables for each star. This is also the case for the metallicity, Fe/H, which was found in section 5.3

The results for NGC 6134 and NGC 3680 are presented in table D.1 and D.2, respectively. Before each table I have inserted the colour-magnitude diagram of the clusters. The tables are available through anonymous `ftp` as described in appendix F.

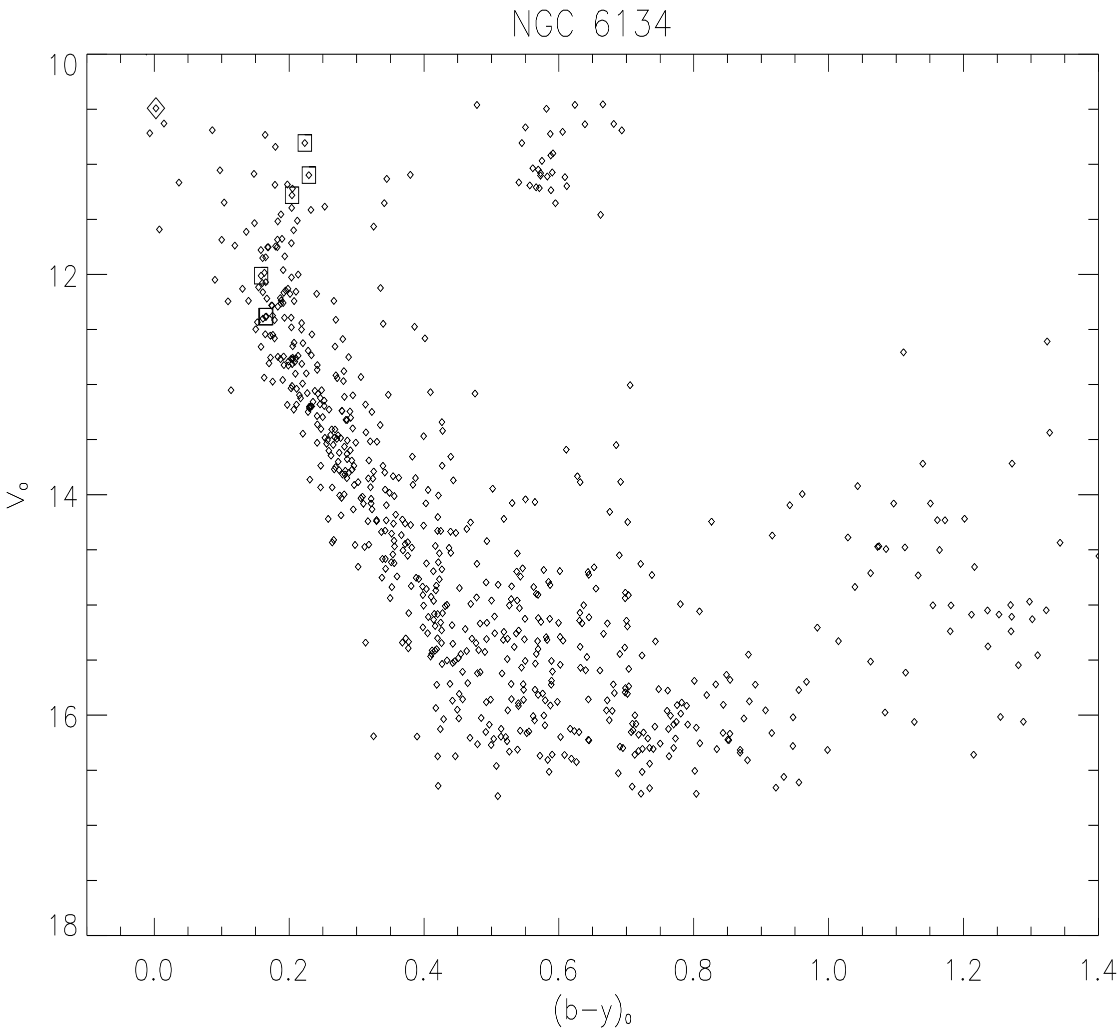

Figure E.1: Colour-magnitude diagram of NGC 6134. The known variable stars - according to Frandsen *et al.* [29] - are indicated. The squares are δ Scuti stars and the diamond is the blue straggler.

Table E.1: Photometric results for NGC 6134. ID_B is the star number I have used. ID_V is the star number in Viskum [71] and Frandsen *et al.* [29]. $ID_V = 0$ means that the star was not observed by Viskum. The star numbers of the seven known variable stars are printed in **bold**. I present Strömgren indices and standard errors for 701 stars in the field of NGC 6134. The results presented here as well as previously published data are available through anonymous `ftp`, *cf.* appendix F.

ID_B	ID_V	V	σ_V	$b-y$	σ_{by}	m_1	σ_{m_1}	β	σ_β	c_0	$E(b-y)$	σ_E	Fe/H	σ_{FeH}
4	0	15.876	0.020	0.689	0.038	0.235	0.058	2.595	0.063	-9.990	0.241	0.097	-9.90	-9.90
7	0	16.475	0.021	0.856	0.048	0.066	0.059	2.664	0.127	-9.990	-9.990	-9.990	-9.99	-9.99
9	0	16.558	0.017	1.511	0.033	-9.990	-9.990	-9.990	-9.990	-9.990	-9.990	-9.990	-9.99	-9.99
11	0	17.260	0.029	0.984	0.080	-9.990	-9.990	-9.990	-9.990	-9.990	-9.990	-9.990	-9.99	-9.99
12	0	15.569	0.035	1.304	0.050	0.400	0.099	2.627	0.030	-9.990	0.769	0.088	-9.90	-9.90
13	0	14.689	0.009	0.561	0.017	0.102	0.021	2.695	0.015	-9.990	0.310	0.025	0.43	0.30
14	0	16.142	0.029	0.813	0.123	0.087	0.147	-9.990	-9.990	-9.990	-9.990	-9.990	-9.99	-9.99
21	0	16.906	0.045	0.864	0.095	-9.990	-9.990	-9.990	-9.990	-9.990	-9.990	-9.990	-9.99	-9.99
23	0	16.751	0.043	0.907	0.144	-9.990	-9.990	-9.990	-9.990	-9.990	-9.990	-9.990	-9.99	-9.99
29	0	12.314	0.006	0.620	0.011	-9.990	-9.990	2.596	0.014	-9.990	-9.990	-9.990	-9.99	-9.99
31	0	15.113	0.016	0.596	0.020	0.119	0.032	2.618	0.437	-9.990	0.240	0.542	0.05	0.36
34	0	14.361	0.004	0.521	0.010	0.118	0.011	2.690	0.025	0.523	0.262	0.030	0.47	0.16
36	0	13.593	0.006	0.544	0.009	0.203	0.009	2.632	0.010	-9.990	0.180	0.016	0.87	0.10
38	0	17.191	0.050	0.837	0.086	-9.990	-9.990	-9.990	-9.990	-9.990	-9.990	-9.990	-9.99	-9.99
42	0	16.186	0.029	1.456	0.037	-9.990	-9.990	-9.990	-9.990	-9.990	-9.990	-9.990	-9.99	-9.99
45	0	15.210	0.015	0.553	0.023	0.133	0.027	2.748	0.051	-9.990	0.336	0.057	-9.99	-9.99
50	0	15.412	0.022	1.436	0.074	0.492	0.253	-9.990	-9.990	-9.990	-9.990	-9.990	-9.99	-9.99
55	0	17.489	0.053	0.999	0.122	-9.990	-9.990	-9.990	-9.990	-9.990	-9.990	-9.990	-9.99	-9.99
58	0	17.377	0.022	0.665	0.090	-9.990	-9.990	-9.990	-9.990	-9.990	-9.990	-9.990	-9.99	-9.99
60	0	13.615	0.007	0.428	0.009	0.132	0.010	2.779	0.015	0.792	-9.990	-9.990	-9.99	-9.99
70	0	16.641	0.096	0.998	0.141	-9.990	-9.990	2.753	0.235	-9.990	0.777	0.279	-9.99	-9.99
72	0	16.774	0.034	0.915	0.040	-9.990	-9.990	-9.990	-9.990	-9.990	-9.990	-9.990	-9.99	-9.99
73	0	16.441	0.012	0.812	0.059	0.080	0.092	2.924	0.071	-9.990	-9.990	-9.990	-9.99	-9.99
76	0	17.061	0.047	0.873	0.072	-9.990	-9.990	-9.990	-9.990	-9.990	-9.990	-9.990	-9.99	-9.99
79	0	13.305	0.003	0.610	0.013	-9.990	-9.990	2.637	0.034	-9.990	-9.990	-9.990	-9.99	-9.99
82	0	16.438	0.031	0.680	0.091	0.353	0.140	-9.990	-9.990	-9.990	-9.990	-9.990	-9.99	-9.99
83	0	14.263	0.020	0.751	0.041	-9.990	-9.990	-9.990	-9.990	-9.990	-9.990	-9.990	-9.99	-9.99
84	0	17.309	0.056	0.699	0.121	-9.990	-9.990	-9.990	-9.990	-9.990	-9.990	-9.990	-9.99	-9.99
87	0	13.790	0.017	1.599	0.024	0.582	0.045	2.643	0.024	-9.990	1.016	0.072	-9.90	-9.90
90	0	14.836	0.009	0.715	0.022	0.104	0.031	2.662	0.015	-9.990	0.407	0.030	0.76	0.38
91	0	17.068	0.053	1.057	0.142	-9.990	-9.990	-9.990	-9.990	-9.990	-9.990	-9.990	-9.99	-9.99
92	0	12.867	0.008	0.375	0.013	0.152	0.020	2.791	0.034	0.895	0.212	0.038	-9.99	-9.99
93	0	16.510	0.013	1.290	0.052	-9.990	-9.990	-9.990	-9.990	-9.990	-9.990	-9.990	-9.99	-9.99
95	0	14.549	0.032	0.610	0.066	0.227	0.083	-9.990	-9.990	-9.990	-9.990	-9.990	-9.99	-9.99
98	0	16.493	0.030	0.824	0.073	0.114	0.107	2.795	0.136	-9.990	0.634	0.157	-9.99	-9.99
100	0	17.542	0.066	0.987	0.250	-9.990	-9.990	-9.990	-9.990	-9.990	-9.990	-9.990	-9.99	-9.99
101	0	16.717	0.040	0.702	0.086	0.552	0.110	2.593	0.082	-9.990	0.100	0.184	-9.90	-9.90
103	0	16.862	0.057	1.129	0.074	-9.990	-9.990	-9.990	-9.990	-9.990	-9.990	-9.990	-9.99	-9.99
104	0	17.697	0.078	0.998	0.208	-9.990	-9.990	-9.990	-9.990	-9.990	-9.990	-9.990	-9.99	-9.99
106	0	16.891	0.048	0.740	0.071	0.337	0.126	-9.990	-9.990	-9.990	-9.990	-9.990	-9.99	-9.99
111	0	17.440	0.043	1.025	0.069	-9.990	-9.990	-9.990	-9.990	-9.990	-9.990	-9.990	-9.99	-9.99
113	0	12.534	0.009	0.870	0.013	0.284	0.019	2.611	0.014	-9.990	0.401	0.026	-9.90	-9.90
116	0	17.336	0.071	0.982	0.138	-9.990	-9.990	-9.990	-9.990	-9.990	-9.990	-9.990	-9.99	-9.99
119	0	15.135	0.009	0.617	0.017	0.146	0.030	2.640	0.034	0.384	0.276	0.046	0.63	0.34
121	0	15.802	0.014	0.631	0.026	0.132	0.041	2.647	0.029	-9.990	0.303	0.046	0.61	0.48
127	0	14.502	0.041	0.559	0.053	0.097	0.055	2.413	0.232	-9.990	-9.990	-9.990	-9.99	-9.99
128	0	15.164	0.014	0.624	0.026	0.095	0.029	2.680	0.028	-9.990	0.349	0.042	0.50	0.39
129	0	11.677	0.012	0.857	0.015	0.377	0.019	2.611	0.012	-9.990	0.348	0.025	-9.90	-9.90
131	0	13.358	0.007	0.476	0.010	0.103	0.017	2.926	0.022	-9.990	-9.990	-9.990	-9.99	-9.99
132	0	15.222	0.012	0.825	0.025	0.134	0.048	2.600	0.084	-9.990	0.413	0.114	0.52	0.48
135	0	16.600	0.025	0.738	0.088	0.268	0.126	2.617	0.056	-9.990	0.303	0.131	-9.90	-9.90
137	0	15.044	0.015	0.506	0.124	-9.990	-9.990	-9.990	-9.990	-9.990	-9.990	-9.990	-9.99	-9.99
138	0	16.345	0.126	0.874	0.155	-9.990	-9.990	2.664	0.030	-9.990	-9.990	-9.990	-9.99	-9.99
146	0	17.743	0.032	1.208	0.318	-9.990	-9.990	-9.990	-9.990	-9.990	-9.990	-9.990	-9.99	-9.99
147	0	16.387	0.029	1.258	0.153	-9.990	-9.990	-9.990	-9.990	-9.990	-9.990	-9.990	-9.99	-9.99
148	0	16.325	0.025	0.975	0.053	0.060	0.094	2.681	0.094	-9.990	0.687	0.124	-9.90	-9.90
153	0	17.551	0.071	0.847	0.238	-9.990	-9.990	-9.990	-9.990	-9.990	-9.990	-9.990	-9.99	-9.99
157	0	16.029	0.020	0.728	0.039	0.135	0.051	2.628	0.051	-9.990	0.362	0.077	-9.90	-9.90
160	0	14.870	0.009	0.593	0.012	0.125	0.018	2.661	0.014	0.429	0.289	0.021	0.58	0.23
163	0	16.500	0.024	0.857	0.082	0.107	0.130	2.755	0.099	-9.990	0.627	0.133	-9.99	-9.99
164	0	17.394	0.052	1.048	0.185	-9.990	-9.990	-9.990	-9.990	-9.990	-9.990	-9.990	-9.99	-9.99
167	0	17.895	0.061	0.997	0.181	-9.990	-9.990	-9.990	-9.990	-9.990	-9.990	-9.990	-9.99	-9.99
168	0	14.627	0.010	0.495	0.019	0.187	0.022	2.608	0.030	-9.990	0.112	0.044	0.25	0.21
171	0	14.239	0.013	0.513	0.021	0.108	0.023	2.736	0.032	0.648	0.294	0.040	-9.99	-9.99
177	0	14.220	0.004	0.486	0.010	0.114	0.012	2.721	0.020	0.604	-9.990	-9.990	-9.99	-9.99
179	0	16.709	0.036	0.718	0.072	0.180	0.080	2.624	0.087	-9.990	0.330	0.137	-9.90	-9.90
180	0	15.835	0.011	0.577	0.038	0.292	0.066	2.528	0.069	-9.990	-9.990	-9.990	-9.99	-9.99
183	0	16.443	0.028	0.941	0.063	0.077	0.076	2.841	0.067	-9.990	-9.990	-9.990	-9.99	-9.99

Continued on the next page...

NGC 6134 photometry, continued from the previous page

ID_B	ID_V	V	σ_V	$b-y$	σ_{by}	m_1	σ_{m1}	β	σ_β	c_0	$E(b-y)$	σ_E	Fe/H	σ_{FeH}
185	0	13.343	0.004	0.436	0.005	0.133	0.007	2.765	0.017	0.797	0.245	0.020	-9.99	-9.99
186	0	16.951	0.042	0.840	0.109	0.159	0.168	-9.990	-9.990	-9.990	-9.990	-9.990	-9.99	-9.99
189	0	15.260	0.015	1.426	0.027	0.400	0.065	2.595	0.027	-9.990	0.797	0.071	-9.90	-9.90
193	0	16.291	0.018	0.681	0.040	0.062	0.061	3.014	0.079	-9.990	-9.990	-9.990	-9.99	-9.99
194	0	17.498	0.030	1.144	0.044	-9.990	-9.990	-9.990	-9.990	-9.990	-9.990	-9.990	-9.99	-9.99
197	0	17.840	0.086	1.197	0.201	-9.990	-9.990	-9.990	-9.990	-9.990	-9.990	-9.990	-9.99	-9.99
198	0	14.305	0.008	0.492	0.013	0.208	0.017	2.645	0.044	-9.990	0.150	0.055	0.94	0.25
199	0	17.688	0.058	1.076	0.211	-9.990	-9.990	-9.990	-9.990	-9.990	-9.990	-9.990	-9.99	-9.99
200	0	15.275	0.028	1.901	0.083	0.320	0.106	2.655	0.070	-9.990	1.412	0.186	-9.90	-9.90
202	0	16.019	0.044	1.314	0.057	0.279	0.103	2.218	0.180	-9.990	-9.990	-9.990	-9.99	-9.99
203	0	16.788	0.030	0.732	0.070	0.184	0.084	2.549	0.078	-9.990	-9.990	-9.990	-9.99	-9.99
206	0	15.444	0.013	0.647	0.025	0.084	0.032	2.681	0.024	-9.990	0.375	0.037	0.46	0.42
208	0	15.858	0.011	0.701	0.031	-9.990	-9.990	3.074	0.136	-9.990	-9.990	-9.990	-9.99	-9.99
209	0	17.048	0.035	0.947	0.124	-9.990	-9.990	-9.990	-9.990	-9.990	-9.990	-9.990	-9.99	-9.99
210	0	16.046	0.028	1.797	0.083	-9.990	-9.990	2.660	0.199	-9.990	-9.990	-9.990	-9.99	-9.99
214	0	14.984	0.012	0.563	0.016	0.099	0.023	2.768	0.053	-9.990	0.373	0.056	-9.99	-9.99
217	0	14.898	0.017	1.547	0.026	0.525	0.102	2.614	0.025	-9.990	0.895	0.083	-9.90	-9.90
218	0	13.026	0.004	0.440	0.009	0.177	0.012	2.782	0.016	0.862	0.257	0.021	-9.99	-9.99
219	0	17.184	0.043	0.988	0.121	0.201	0.203	-9.990	-9.990	-9.990	-9.990	-9.990	-9.99	-9.99
220	0	16.524	0.027	0.643	0.050	0.187	0.096	2.650	0.082	-9.990	0.300	0.118	-9.90	-9.90
222	0	15.337	0.013	0.950	0.034	0.058	0.052	2.736	0.087	-9.990	0.704	0.094	-9.99	-9.99
223	0	17.607	0.065	0.901	0.276	-9.990	-9.990	-9.990	-9.990	-9.990	-9.990	-9.990	-9.99	-9.99
224	0	14.685	0.010	0.532	0.014	0.115	0.019	2.702	0.036	0.523	0.288	0.043	0.53	0.27
226	0	16.351	0.028	0.758	0.067	0.487	0.085	2.557	0.066	-9.990	-9.990	-9.990	-9.99	-9.99
229	0	15.913	0.014	1.408	0.055	0.398	0.075	2.585	0.066	-9.990	-9.990	-9.990	-9.99	-9.99
230	0	16.001	0.029	0.862	0.043	0.055	0.064	2.766	0.029	-9.990	0.654	0.055	-9.99	-9.99
231	0	12.534	0.006	0.616	0.007	0.128	0.009	2.657	0.012	-9.990	0.303	0.016	0.64	0.12
232	0	16.012	0.017	0.805	0.036	0.053	0.052	2.908	0.071	-9.990	-9.990	-9.990	-9.99	-9.99
234	0	16.336	0.020	0.848	0.075	0.019	0.102	2.795	0.095	-9.990	0.678	0.124	-9.99	-9.99
235	0	16.777	0.029	0.936	0.112	-9.990	-9.990	2.759	0.081	-9.990	0.726	0.144	-9.99	-9.99
236	0	12.151	0.004	0.850	0.005	0.306	0.007	2.611	0.014	-9.990	0.373	0.022	-9.90	-9.90
237	0	13.768	0.006	0.554	0.008	0.109	0.010	2.708	0.024	-9.990	-9.990	-9.990	-9.99	-9.99
238	0	17.331	0.037	0.831	0.144	-9.990	-9.990	-9.990	-9.990	-9.990	-9.990	-9.990	-9.99	-9.99
239	0	17.243	0.052	1.049	0.131	-9.990	-9.990	-9.990	-9.990	-9.990	-9.990	-9.990	-9.99	-9.99
240	0	16.946	0.032	1.023	0.055	0.047	0.180	-9.990	-9.990	-9.990	-9.990	-9.990	-9.99	-9.99
243	0	17.398	0.053	0.778	0.187	-9.990	-9.990	-9.990	-9.990	-9.990	-9.990	-9.990	-9.99	-9.99
245	0	17.380	0.048	0.796	0.093	0.338	0.171	-9.990	-9.990	-9.990	-9.990	-9.990	-9.99	-9.99
247	0	16.472	0.021	0.877	0.064	0.085	0.073	2.704	0.043	-9.990	0.625	0.082	-9.90	-9.90
248	0	17.138	0.047	0.799	0.096	-9.990	-9.990	2.902	0.122	-9.990	-9.990	-9.990	-9.99	-9.99
251	0	17.544	0.046	0.883	0.150	-9.990	-9.990	-9.990	-9.990	-9.990	-9.990	-9.990	-9.99	-9.99
252	0	16.152	0.027	1.573	0.083	-9.990	-9.990	2.675	0.014	-9.990	-9.990	-9.990	-9.99	-9.99
255	0	17.199	0.045	1.530	0.219	-9.990	-9.990	-9.990	-9.990	-9.990	-9.990	-9.990	-9.99	-9.99
258	0	14.650	0.009	0.674	0.016	0.050	0.021	2.916	0.030	-9.990	-9.990	-9.990	-9.99	-9.99
259	0	16.401	0.039	0.736	0.058	0.146	0.069	2.607	0.050	-9.990	0.338	0.093	-9.90	-9.90
260	0	16.427	0.025	0.793	0.044	0.029	0.073	2.786	0.111	-9.990	0.617	0.121	-9.99	-9.99
261	0	16.802	0.042	0.754	0.100	0.121	0.121	2.552	0.058	-9.990	-9.990	-9.990	-9.99	-9.99
262	0	16.185	0.021	1.429	0.084	0.288	0.126	2.599	0.114	-9.990	0.862	0.227	-9.90	-9.90
266	0	13.396	0.006	0.462	0.011	0.132	0.015	2.756	0.083	-9.990	0.261	0.084	-9.99	-9.99
267	0	15.730	0.014	0.965	0.028	0.051	0.052	2.690	0.028	-9.990	0.694	0.044	-9.90	-9.90
269	0	15.263	0.012	0.585	0.018	0.121	0.024	2.622	0.037	-9.990	0.234	0.051	0.07	0.25
271	0	17.320	0.044	0.985	0.114	-9.990	-9.990	-9.990	-9.990	-9.990	-9.990	-9.990	-9.99	-9.99
273	0	17.556	0.061	0.695	0.159	-9.990	-9.990	-9.990	-9.990	-9.990	-9.990	-9.990	-9.99	-9.99
276	0	17.306	0.045	0.892	0.093	-9.990	-9.990	-9.990	-9.990	-9.990	-9.990	-9.990	-9.99	-9.99
278	0	16.121	0.019	0.973	0.058	0.040	0.077	2.834	0.061	-9.990	0.824	0.087	-9.99	-9.99
279	0	12.866	0.004	0.458	0.006	0.165	0.008	2.771	0.009	0.861	0.264	0.015	-9.99	-9.99
280	0	17.186	0.043	0.853	0.086	-9.990	-9.990	-9.990	-9.990	-9.990	-9.990	-9.990	-9.99	-9.99
282	0	15.460	0.014	0.674	0.036	0.015	0.041	2.913	0.024	-9.990	-9.990	-9.990	-9.99	-9.99
286	0	13.017	0.005	0.468	0.010	0.114	0.015	2.768	0.018	0.838	0.283	0.023	-9.99	-9.99
287	0	14.602	0.009	0.703	0.014	0.056	0.018	2.880	0.028	-9.990	0.614	0.033	-9.99	-9.99
291	0	16.998	0.052	0.844	0.085	0.095	0.131	-9.990	-9.990	-9.990	-9.990	-9.990	-9.99	-9.99
292	0	15.893	0.049	1.337	0.107	0.404	0.124	-9.990	-9.990	-9.990	-9.990	-9.990	-9.99	-9.99
293	0	16.070	0.024	0.973	0.075	-9.990	-9.990	3.386	0.312	-9.990	-9.990	-9.990	-9.99	-9.99
294	0	17.917	0.074	0.784	0.175	-9.990	-9.990	-9.990	-9.990	-9.990	-9.990	-9.990	-9.99	-9.99
295	0	16.349	0.026	0.909	0.062	0.052	0.100	2.710	0.066	-9.990	0.670	0.099	-9.90	-9.90
296	0	13.445	0.005	0.463	0.010	0.148	0.015	2.809	0.010	-9.990	0.310	0.018	-9.99	-9.99
297	0	13.888	0.014	1.386	0.030	0.343	0.050	2.642	0.027	-9.990	0.900	0.064	-9.90	-9.90
298	0	17.555	0.049	0.721	0.134	-9.990	-9.990	-9.990	-9.990	-9.990	-9.990	-9.990	-9.99	-9.99
299	0	17.118	0.064	0.692	0.129	0.394	0.143	2.562	0.085	-9.990	-9.990	-9.990	-9.99	-9.99
300	0	15.091	0.011	0.659	0.081	-9.990	-9.990	-9.990	-9.990	-9.990	-9.990	-9.990	-9.99	-9.99
301	0	13.915	0.006	0.508	0.010	0.113	0.013	2.718	0.012	0.631	0.285	0.016	0.45	0.20
303	0	15.551	0.013	1.191	0.035	0.201	0.052	2.680	0.040	-9.990	0.856	0.071	-9.90	-9.90
304	0	12.780	0.003	0.482	0.006	0.134	0.009	2.724	0.007	0.771	0.247	0.014	-9.99	-9.99
307	0	17.287	0.040	1.017	0.130	-9.990	-9.990	-9.990	-9.990	-9.990	-9.990	-9.990	-9.99	-9.99
309	0	15.178	0.013	0.557	0.024	0.121	0.031	2.642	0.042	-9.990	0.233	0.057	0.22	0.35
312	0	15.430	0.007	0.977	0.047	0.074	0.061	2.698	0.037	-9.990	0.713	0.066	-9.90	-9.90
314	0	13.874	0.006	0.503	0.007	0.120	0.007	2.690	0.027	0.569	0.245	0.031	0.41	0.11
316	0	16.693	0.035	0.720	0.074	0.089	0.088	2.941	0.093	-9.990	-9.990	-9.990	-9.99	-9.99
317	0	17.307	0.056	0.789	0.142	-9.990	-9.990	-9.990	-9.990	-9.990	-9.990	-9.990	-9.99	-9.99
318	0	16.182	0.015	0.709	0.057	-9.990	-9.990	2.941	0.032	-9.990	-9.990	-9.990	-9.99	-9.99
322	0	17.094	0.046	0.862	0.068	-9.990	-9.990	-9.990	-9.990	-9.990	-9.990	-9.990	-9.99	-9.99

Continued on the next page...

NGC 6134 photometry, continued from the previous page

ID_B	ID_V	V	σ_V	$b-y$	σ_{by}	m_1	σ_{m_1}	β	σ_β	c_0	$E(b-y)$	σ_E	Fe/H	σ_{FeH}
323	0	15.764	0.010	0.618	0.033	0.119	0.048	2.633	0.014	0.331	0.277	0.042	-9.90	-9.90
325	0	15.884	0.053	0.918	0.094	-9.990	-9.990	-9.990	-9.990	-9.990	-9.990	-9.990	-9.99	-9.99
326	0	17.555	0.067	1.038	0.224	-9.990	-9.990	-9.990	-9.990	-9.990	-9.990	-9.990	-9.99	-9.99
327	0	16.193	0.021	0.706	0.056	0.096	0.070	2.668	0.025	-9.990	0.409	0.066	-9.90	-9.90
328	0	16.113	0.022	0.753	0.058	-9.990	-9.990	2.864	0.025	-9.990	0.658	0.067	-9.99	-9.99
330	0	15.519	0.016	0.612	0.026	0.099	0.030	2.660	0.029	-9.990	0.312	0.043	0.33	0.37
332	0	15.194	0.013	0.631	0.020	0.114	0.023	2.678	0.030	-9.990	0.350	0.041	0.74	0.31
333	0	13.401	0.004	0.442	0.009	0.114	0.012	2.784	0.006	0.823	0.274	0.014	-9.99	-9.99
335	0	15.603	0.018	0.768	0.031	0.019	0.032	2.917	0.046	-9.990	-9.990	-9.990	-9.99	-9.99
340	0	16.010	0.029	0.656	0.038	0.132	0.058	2.621	0.039	-9.990	0.291	0.067	-9.90	-9.90
342	0	15.617	0.026	1.618	0.036	0.563	0.083	2.665	0.067	-9.990	-9.990	-9.990	-9.90	-9.90
344	0	16.033	0.019	0.930	0.068	0.039	0.083	2.674	0.019	-9.990	0.639	0.075	-9.90	-9.90
345	0	16.090	0.020	0.844	0.056	0.021	0.074	2.941	0.131	-9.990	-9.990	-9.990	-9.99	-9.99
346	0	15.687	0.015	0.644	0.027	0.267	0.062	2.596	0.033	-9.990	0.190	0.062	-9.90	-9.90
347	0	15.973	0.026	0.860	0.119	-9.990	-9.990	-9.990	-9.990	-9.990	-9.990	-9.990	-9.99	-9.99
352	0	15.213	0.011	0.581	0.022	0.117	0.028	2.645	0.030	0.381	0.259	0.043	0.27	0.32
355	0	16.954	0.036	1.231	0.125	-9.990	-9.990	-9.990	-9.990	-9.990	-9.990	-9.990	-9.99	-9.99
356	0	13.423	0.009	0.482	0.021	0.114	0.034	-9.990	-9.990	-9.990	-9.990	-9.990	-9.99	-9.99
359	0	13.422	0.001	0.541	0.004	-9.990	-9.990	-9.990	-9.990	-9.990	-9.990	-9.990	-9.99	-9.99
360	0	16.816	0.052	1.123	0.109	-9.990	-9.990	-9.990	-9.990	-9.990	-9.990	-9.990	-9.99	-9.99
361	0	14.697	0.008	0.595	0.015	0.128	0.021	2.665	0.011	0.448	0.294	0.021	0.66	0.26
369	330	14.918	0.010	0.522	0.018	0.217	0.022	2.620	0.022	-9.990	-9.990	-9.990	0.75	0.23
373	0	16.439	0.017	0.780	0.055	0.207	0.094	2.597	0.029	-9.990	0.336	0.085	-9.90	-9.90
375	0	15.804	0.018	0.679	0.029	0.043	0.040	2.926	0.047	-9.990	-9.990	-9.990	-9.99	-9.99
376	325	14.140	0.007	0.465	0.012	0.169	0.015	2.619	0.011	-9.990	0.106	0.019	0.16	0.15
378	0	17.345	0.060	0.827	0.228	0.177	0.265	-9.990	-9.990	-9.990	-9.990	-9.990	-9.99	-9.99
381	0	14.080	0.009	0.500	0.016	0.104	0.022	2.739	0.007	0.673	0.285	0.021	-9.99	-9.99
384	0	14.778	0.005	0.566	0.011	0.118	0.016	2.714	0.019	-9.990	0.336	0.024	0.76	0.25
386	0	17.143	0.072	0.954	0.126	-9.990	-9.990	-9.990	-9.990	-9.990	-9.990	-9.990	-9.99	-9.99
387	0	16.936	0.043	0.974	0.052	-9.990	-9.990	-9.990	-9.990	-9.990	-9.990	-9.990	-9.99	-9.99
388	0	16.093	0.012	0.978	0.037	-9.990	-9.990	2.980	0.103	-9.990	-9.990	-9.990	-9.99	-9.99
390	0	15.067	0.010	0.907	0.016	0.054	0.030	2.818	0.023	-9.990	0.746	0.031	-9.99	-9.99
392	0	16.786	0.028	0.865	0.114	-9.990	-9.990	-9.990	-9.990	-9.990	-9.990	-9.990	-9.99	-9.99
393	279	13.930	0.007	0.458	0.010	0.123	0.011	2.755	0.018	0.718	0.258	0.023	-9.99	-9.99
395	0	15.840	0.018	0.927	0.043	-9.990	-9.990	2.677	0.061	-9.990	0.649	0.083	-9.90	-9.90
396	0	15.314	0.016	0.570	0.022	0.248	0.027	2.596	0.078	-9.990	0.134	0.106	0.74	0.36
397	0	16.906	0.049	0.694	0.071	0.265	0.075	-9.990	-9.990	-9.990	-9.990	-9.990	-9.99	-9.99
400	0	17.824	0.092	0.696	0.312	-9.990	-9.990	-9.990	-9.990	-9.990	-9.990	-9.990	-9.99	-9.99
403	0	15.629	0.020	0.647	0.040	0.130	0.053	2.849	0.192	-9.990	0.520	0.197	-9.99	-9.99
404	0	12.083	0.004	0.866	0.007	0.328	0.008	2.592	0.014	-9.990	0.345	0.023	-9.90	-9.90
406	0	17.345	0.036	1.191	0.340	-9.990	-9.990	-9.990	-9.990	-9.990	-9.990	-9.990	-9.99	-9.99
409	0	16.512	0.022	1.018	0.056	0.082	0.100	-9.990	-9.990	-9.990	-9.990	-9.990	-9.99	-9.99
410	0	13.596	0.008	0.453	0.012	0.166	0.016	2.772	0.024	0.780	0.261	0.029	-9.99	-9.99
412	0	16.696	0.049	1.337	0.130	-9.990	-9.990	-9.990	-9.990	-9.990	-9.990	-9.990	-9.99	-9.99
414	0	16.901	0.029	0.822	0.083	0.142	0.100	-9.990	-9.990	-9.990	-9.990	-9.990	-9.99	-9.99
415	0	14.979	0.008	0.617	0.018	0.122	0.024	2.658	0.014	0.416	0.308	0.026	0.59	0.29
418	0	16.632	0.026	1.156	0.090	0.326	0.170	-9.990	-9.990	-9.990	-9.990	-9.990	-9.99	-9.99
421	0	12.256	0.005	0.865	0.011	0.304	0.013	2.604	0.010	-9.990	0.375	0.020	-9.90	-9.90
422	0	16.959	0.055	1.036	0.170	-9.990	-9.990	-9.990	-9.990	-9.990	-9.990	-9.990	-9.99	-9.99
423	0	14.380	0.005	0.507	0.010	0.177	0.016	2.625	0.016	-9.990	0.147	0.023	0.41	0.17
425	0	14.418	0.012	0.553	0.016	-9.990	-9.990	-9.990	-9.990	-9.990	-9.990	-9.990	-9.99	-9.99
426	0	15.649	0.018	1.350	0.051	0.241	0.101	2.627	0.038	-9.990	0.871	0.091	-9.90	-9.90
427	0	15.548	0.016	0.641	0.040	0.116	0.047	2.693	0.020	-9.990	0.381	0.047	-9.90	-9.90
428	0	12.398	0.005	0.846	0.009	0.300	0.016	2.596	0.007	-9.990	0.348	0.016	-9.90	-9.90
429	0	16.582	0.021	0.844	0.055	0.046	0.075	2.860	0.047	-9.990	0.728	0.075	-9.99	-9.99
432	0	15.661	0.017	0.657	0.039	0.177	0.048	2.603	0.053	-9.990	0.251	0.082	0.51	0.47
434	276	16.174	0.029	1.055	0.056	0.038	0.066	2.754	0.072	-9.990	0.822	0.093	-9.99	-9.99
440	0	15.654	0.019	1.348	0.048	0.241	0.073	2.698	0.076	-9.990	-9.990	-9.990	-9.99	-9.99
442	0	17.275	0.052	0.854	0.171	0.251	0.230	-9.990	-9.990	-9.990	-9.990	-9.990	-9.99	-9.99
443	0	17.494	0.105	0.814	0.195	0.327	0.280	-9.990	-9.990	-9.990	-9.990	-9.990	-9.99	-9.99
444	0	11.887	0.114	0.880	0.131	0.289	0.111	2.628	0.104	-9.990	0.439	0.206	-9.90	-9.90
445	0	14.250	0.004	0.684	0.009	-9.990	-9.990	2.797	0.015	-9.990	-9.990	-9.990	-9.99	-9.99
447	0	13.472	0.099	1.719	0.138	-9.990	-9.990	-9.990	-9.990	-9.990	-9.990	-9.990	-9.99	-9.99
449	216	13.952	0.007	0.480	0.013	0.106	0.022	2.770	0.059	-9.990	0.297	0.061	-9.99	-9.99
450	329	14.588	0.008	0.538	0.015	0.105	0.019	2.682	0.009	0.484	0.271	0.018	0.32	0.25
451	0	15.713	0.012	0.813	0.035	0.066	0.043	2.839	0.036	-9.990	0.677	0.052	-9.99	-9.99
453	0	17.438	0.058	1.084	0.202	-9.990	-9.990	-9.990	-9.990	-9.990	-9.990	-9.990	-9.99	-9.99
460	378	16.976	0.033	0.973	0.100	0.173	0.142	-9.990	-9.990	-9.990	-9.990	-9.990	-9.99	-9.99
461	0	16.686	0.025	0.709	0.048	0.208	0.064	2.689	0.065	-9.990	0.421	0.097	-9.90	-9.90
463	0	15.093	0.006	0.571	0.014	0.110	0.017	2.659	0.020	0.407	0.270	0.028	0.31	0.21
465	0	13.462	0.013	0.449	0.018	0.119	0.026	-9.990	-9.990	-9.990	-9.990	-9.990	-9.99	-9.99
468	191	16.349	0.027	0.947	0.078	0.088	0.110	2.893	0.092	-9.990	-9.990	-9.990	-9.99	-9.99
469	415	16.899	0.036	0.804	0.124	0.176	0.161	-9.990	-9.990	-9.990	-9.990	-9.990	-9.99	-9.99
472	0	17.831	0.057	0.984	0.159	-9.990	-9.990	-9.990	-9.990	-9.990	-9.990	-9.990	-9.99	-9.99
473	0	16.982	0.029	0.957	0.107	-9.990	-9.990	-9.990	-9.990	-9.990	-9.990	-9.990	-9.99	-9.99
475	0	16.989	0.051	0.727	0.113	0.255	0.146	-9.990	-9.990	-9.990	-9.990	-9.990	-9.99	-9.99
477	0	17.643	0.089	0.782	0.198	-9.990	-9.990	-9.990	-9.990	-9.990	-9.990	-9.990	-9.99	-9.99
478	0	15.406	0.016	0.643	0.026	0.177	0.030	2.645	0.023	-9.990	0.295	0.041	1.08	0.36
481	0	17.064	0.058	0.767	0.187	0.188	0.216	-9.990	-9.990	-9.990	-9.990	-9.990	-9.99	-9.99
483	0	17.468	0.052	0.966	0.143	-9.990	-9.990	-9.990	-9.990	-9.990	-9.990	-9.990	-9.99	-9.99

Continued on the next page...

NGC 6134 photometry, continued from the previous page

ID_B	ID_V	V	σ_V	$b-y$	σ_{by}	m_1	σ_{m_1}	β	σ_β	c_0	$E(b-y)$	σ_E	Fe/H	σ_{FeH}
484	0	15.337	0.017	1.756	0.047	0.358	0.168	2.639	0.056	-9.990	1.220	0.151	-9.90	-9.90
486	0	17.540	0.058	0.865	0.100	-9.990	-9.990	-9.990	-9.990	-9.990	-9.990	-9.990	-9.99	-9.99
489	195	16.903	0.024	0.956	0.115	-9.990	-9.990	-9.990	-9.990	-9.990	-9.990	-9.990	-9.99	-9.99
490	0	16.499	0.046	0.792	0.064	-9.990	-9.990	-9.990	-9.990	-9.990	-9.990	-9.990	-9.99	-9.99
491	0	17.132	0.043	0.724	0.109	-9.990	-9.990	-9.990	-9.990	-9.990	-9.990	-9.990	-9.99	-9.99
493	0	12.023	0.002	0.455	0.004	0.135	0.010	2.741	0.013	0.909	0.239	0.017	-9.99	-9.99
494	0	14.719	0.007	0.531	0.016	0.122	0.018	2.677	0.027	-9.990	0.252	0.035	0.47	0.23
501	0	15.257	0.010	0.806	0.032	0.064	0.044	2.867	0.032	-9.990	0.695	0.047	-9.99	-9.99
504	0	13.183	0.009	0.488	0.024	0.139	0.030	2.702	0.113	-9.990	0.243	0.130	0.68	0.48
507	0	15.400	0.025	0.793	0.051	-9.990	-9.990	-9.990	-9.990	-9.990	-9.990	-9.990	-9.99	-9.99
508	**397**	13.566	0.008	0.440	0.011	0.149	0.015	2.777	0.005	0.794	0.258	0.016	-9.99	-9.99
510	0	13.932	0.007	0.563	0.019	0.108	0.024	2.693	0.031	-9.990	0.307	0.040	0.51	0.34
511	0	17.479	0.038	1.009	0.198	-9.990	-9.990	-9.990	-9.990	-9.990	-9.990	-9.990	-9.99	-9.99
515	0	16.871	0.019	1.076	0.116	-9.990	-9.990	-9.990	-9.990	-9.990	-9.990	-9.990	-9.99	-9.99
516	419	17.419	0.037	0.798	0.077	-9.990	-9.990	-9.990	-9.990	-9.990	-9.990	-9.990	-9.99	-9.99
521	0	17.211	0.049	0.727	0.070	-9.990	-9.990	-9.990	-9.990	-9.990	-9.990	-9.990	-9.99	-9.99
523	0	17.351	0.052	1.129	0.177	-9.990	-9.990	-9.990	-9.990	-9.990	-9.990	-9.990	-9.99	-9.99
524	227	13.802	0.111	0.482	0.157	0.100	0.148	-9.990	-9.990	-9.990	-9.990	-9.990	-9.99	-9.99
525	0	14.338	0.006	0.510	0.012	0.110	0.022	-9.990	-9.990	-9.990	-9.990	-9.990	-9.99	-9.99
527	249	12.374	0.002	0.832	0.005	0.307	0.007	2.519	0.126	-9.990	-9.990	-9.990	-9.99	-9.99
529	0	17.360	0.053	0.993	0.394	-9.990	-9.990	-9.990	-9.990	-9.990	-9.990	-9.990	-9.99	-9.99
531	0	17.489	0.075	1.015	0.112	-9.990	-9.990	-9.990	-9.990	-9.990	-9.990	-9.990	-9.99	-9.99
533	0	16.986	0.040	0.851	0.180	-9.990	-9.990	-9.990	-9.990	-9.990	-9.990	-9.990	-9.99	-9.99
536	299	14.666	0.006	0.551	0.012	0.127	0.017	-9.990	-9.990	-9.990	-9.990	-9.990	-9.99	-9.99
537	0	16.372	0.028	0.691	0.122	-9.990	-9.990	-9.990	-9.990	-9.990	-9.990	-9.990	-9.99	-9.99
538	0	17.405	0.088	0.919	0.223	-9.990	-9.990	-9.990	-9.990	-9.990	-9.990	-9.990	-9.99	-9.99
539	0	16.421	0.027	1.455	0.169	-9.990	-9.990	-9.990	-9.990	-9.990	-9.990	-9.990	-9.99	-9.99
542	0	16.714	0.034	0.840	0.121	-9.990	-9.990	-9.990	-9.990	-9.990	-9.990	-9.990	-9.99	-9.99
545	255	16.308	0.016	0.825	0.053	0.021	0.068	-9.990	-9.990	-9.990	-9.990	-9.990	-9.99	-9.99
546	0	14.618	0.010	1.603	0.031	0.509	0.051	2.600	0.031	-9.990	0.910	0.084	-9.90	-9.90
550	0	17.339	0.049	1.000	0.177	-9.990	-9.990	-9.990	-9.990	-9.990	-9.990	-9.990	-9.99	-9.99
552	0	15.683	0.018	1.439	0.073	0.413	0.122	2.603	0.043	-9.990	0.822	0.131	-9.90	-9.90
554	0	12.795	0.035	0.411	0.046	0.149	0.051	2.770	0.035	-9.990	0.224	0.060	-9.99	-9.99
555	0	16.015	0.022	0.673	0.141	-9.990	-9.990	-9.990	-9.990	-9.990	-9.990	-9.990	-9.99	-9.99
556	165	13.942	0.007	0.485	0.013	0.117	0.015	2.756	0.022	0.719	0.286	0.028	-9.99	-9.99
557	145	11.906	0.002	0.862	0.007	0.332	0.008	2.598	0.010	-9.990	-9.990	-9.990	-9.90	-9.90
558	0	15.103	0.011	1.318	0.038	0.329	0.052	2.638	0.055	-9.990	-9.990	-9.990	-9.90	-9.90
559	0	14.408	0.010	0.482	0.017	0.131	0.018	2.876	0.019	-9.990	0.392	0.028	-9.99	-9.99
561	0	16.655	0.045	0.917	0.067	0.088	0.084	2.702	0.097	-9.990	0.659	0.135	-9.90	-9.90
562	0	16.563	0.001	0.809	0.048	-9.990	-9.990	-9.990	-9.990	-9.990	-9.990	-9.990	-9.99	-9.99
563	0	13.623	0.006	0.493	0.011	0.128	0.015	2.670	0.043	-9.990	0.208	0.051	0.35	0.19
565	0	17.168	0.041	1.056	0.127	-9.990	-9.990	-9.990	-9.990	-9.990	-9.990	-9.990	-9.99	-9.99
568	0	16.627	0.037	0.841	0.182	-9.990	-9.990	-9.990	-9.990	-9.990	-9.990	-9.990	-9.99	-9.99
570	0	16.489	0.052	0.799	0.157	0.045	0.181	-9.990	-9.990	-9.990	-9.990	-9.990	-9.99	-9.99
571	0	16.905	0.040	1.166	0.105	-9.990	-9.990	-9.990	-9.990	-9.990	-9.990	-9.990	-9.99	-9.99
572	352	11.846	0.012	0.825	0.014	0.329	0.015	2.595	0.010	-9.990	-9.990	-9.990	-9.90	-9.90
574	**0**	12.463	0.006	0.479	0.012	0.112	0.014	2.738	0.016	0.851	0.264	0.023	-9.99	-9.99
576	290	12.230	0.005	0.844	0.007	0.260	0.008	2.585	0.009	-9.990	-9.990	-9.990	-9.99	-9.99
577	0	16.528	0.038	0.752	0.073	0.127	0.077	-9.990	-9.990	-9.990	-9.990	-9.990	-9.99	-9.99
579	0	16.663	0.018	0.726	0.056	0.163	0.087	2.515	0.114	-9.990	-9.990	-9.990	-9.99	-9.99
580	0	16.344	0.037	0.768	0.059	0.139	0.064	-9.990	-9.990	-9.990	-9.990	-9.990	-9.99	-9.99
585	240	12.278	0.006	0.655	0.007	0.125	0.009	2.622	0.005	-9.990	0.294	0.011	0.31	0.10
586	189	15.027	0.014	0.638	0.023	0.120	0.027	2.655	0.069	-9.990	0.323	0.085	0.59	0.35
587	0	15.599	0.012	0.631	0.030	0.110	0.033	2.644	0.090	-9.990	0.306	0.112	0.35	0.39
588	0	15.426	0.010	1.101	0.025	0.312	0.036	2.583	0.032	-9.990	-9.990	-9.990	-9.99	-9.99
589	157	17.378	0.046	0.789	0.132	-9.990	-9.990	-9.990	-9.990	-9.990	-9.990	-9.990	-9.99	-9.99
594	0	15.035	0.013	0.599	0.038	0.067	0.046	2.903	0.195	-9.990	-9.990	-9.990	-9.99	-9.99
595	0	17.523	0.052	1.144	0.264	-9.990	-9.990	-9.990	-9.990	-9.990	-9.990	-9.990	-9.99	-9.99
598	129	12.934	0.005	0.444	0.006	0.178	0.010	2.768	0.009	0.849	0.246	0.015	-9.99	-9.99
599	321	12.960	0.006	0.433	0.008	0.124	0.008	2.767	0.005	0.844	0.248	0.014	-9.99	-9.99
600	293	16.020	0.021	0.627	0.038	0.182	0.054	2.631	0.035	-9.990	0.259	0.062	-9.90	-9.90
601	185	14.232	0.008	0.523	0.015	0.115	0.018	2.702	0.010	0.568	0.280	0.019	0.51	0.25
603	0	17.039	0.057	0.919	0.129	0.041	0.160	2.685	0.139	-9.990	0.645	0.208	-9.90	-9.90
606	163	14.150	0.004	0.556	0.012	0.101	0.015	2.607	0.151	-9.990	0.201	0.194	-0.32	0.38
608	267	15.998	0.018	0.785	0.036	-9.990	-9.990	2.911	0.056	-9.990	-9.990	-9.990	-9.99	-9.99
612	0	15.934	0.023	0.613	0.046	-9.990	-9.990	-9.990	-9.990	-9.990	-9.990	-9.990	-9.99	-9.99
615	0	15.646	0.012	0.692	0.023	0.110	0.039	2.614	0.061	-9.990	0.323	0.082	0.17	0.38
616	**159**	13.193	0.010	0.433	0.022	0.125	0.026	2.771	0.026	0.823	0.251	0.036	-9.99	-9.99
617	0	14.952	0.014	0.568	0.025	0.117	0.029	2.659	0.015	0.419	0.266	0.032	0.40	0.36
619	197	13.251	0.004	0.440	0.008	0.157	0.011	2.764	0.009	0.807	0.243	0.016	-9.99	-9.99
621	0	15.411	0.018	0.605	0.025	-9.990	-9.990	-9.990	-9.990	-9.990	-9.990	-9.990	-9.99	-9.99
624	0	16.952	0.035	0.823	0.104	-9.990	-9.990	-9.990	-9.990	-9.990	-9.990	-9.990	-9.99	-9.99
628	37	16.595	0.034	0.687	0.053	0.196	0.090	2.648	0.066	-9.990	-9.990	-9.990	-9.99	-9.99
629	0	11.989	0.002	0.820	0.007	0.305	0.008	2.597	0.011	-9.990	0.325	0.018	-9.90	-9.90
630	175	14.958	0.009	0.549	0.018	0.111	0.025	2.688	0.019	0.462	0.288	0.029	0.46	0.34
631	0	17.208	0.079	0.760	0.130	-9.990	-9.990	-9.990	-9.990	-9.990	-9.990	-9.990	-9.99	-9.99
635	0	15.837	0.017	1.491	0.084	0.260	0.136	2.564	0.052	-9.990	-9.990	-9.990	-9.99	-9.99
641	134	17.577	0.078	0.894	0.154	-9.990	-9.990	-9.990	-9.990	-9.990	-9.990	-9.990	-9.99	-9.99
642	0	17.043	0.032	0.823	0.075	0.206	0.112	-9.990	-9.990	-9.990	-9.990	-9.990	-9.99	-9.99
644	0	13.725	0.007	0.440	0.010	0.129	0.011	2.736	0.019	0.703	0.221	0.023	-9.99	-9.99

Continued on the next page...

NGC 6134 photometry, continued from the previous page

ID_B	ID_V	V	σ_V	$b-y$	σ_{by}	m_1	σ_{m_1}	β	σ_β	c_0	$E(b-y)$	σ_E	Fe/H	σ_{FeH}
646	417	14.503	0.009	0.561	0.012	0.123	0.015	2.669	0.018	0.470	0.270	0.025	0.53	0.19
647	**53**	11.673	0.011	0.277	0.012	0.209	0.196	2.898	0.012	-9.990	-9.990	-9.990	-9.99	-9.99
648	199	13.142	0.004	0.466	0.007	0.144	0.011	2.743	0.012	0.787	0.249	0.017	-9.99	-9.99
649	0	13.208	0.048	0.478	0.078	0.193	0.135	1.938	0.221	-9.990	-9.990	-9.990	-9.99	-9.99
650	0	15.615	0.036	0.539	0.046	0.161	0.053	2.242	0.243	-9.990	-9.990	-9.990	-9.99	-9.99
651	115	15.384	0.016	0.695	0.026	0.089	0.031	2.868	0.030	-9.990	0.590	0.042	-9.99	-9.99
652	188	12.716	0.049	0.424	0.059	0.112	0.061	3.136	0.074	-9.990	-9.990	-9.990	-9.99	-9.99
653	0	13.311	0.011	0.473	0.014	0.111	0.014	2.771	0.199	-9.990	0.291	0.199	-9.99	-9.99
656	265	14.708	0.008	0.574	0.013	0.306	0.018	2.601	0.018	-9.990	0.118	0.030	1.31	0.20
657	213	16.575	0.026	0.652	0.052	0.242	0.085	2.615	0.051	-9.990	0.234	0.094	-9.90	-9.90
658	0	14.477	0.008	0.525	0.014	0.108	0.017	2.704	0.015	0.548	0.285	0.022	0.40	0.25
659	0	15.114	0.011	0.522	0.021	0.107	0.026	2.768	0.060	-9.990	0.333	0.064	-9.99	-9.99
661	138	14.154	0.006	0.451	0.010	0.141	0.013	2.610	0.010	-9.990	0.095	0.017	-0.22	0.13
663	67	14.366	0.006	0.472	0.010	0.178	0.012	2.597	0.013	-9.990	0.084	0.021	-0.01	0.10
664	345	16.583	0.033	0.694	0.073	0.164	0.091	2.556	0.042	-9.990	-9.990	-9.990	-9.99	-9.99
668	4	17.091	0.029	1.050	0.116	0.069	0.179	-9.990	-9.990	-9.990	-9.990	-9.990	-9.99	-9.99
669	0	12.934	0.006	0.443	0.008	0.160	0.010	2.788	0.007	0.883	0.270	0.015	-9.99	-9.99
670	263	13.731	0.003	0.451	0.012	0.123	0.015	2.748	0.011	0.732	0.245	0.020	-9.99	-9.99
672	0	14.996	0.010	0.554	0.015	0.106	0.024	-9.990	-9.990	-9.990	-9.990	-9.990	-9.99	-9.99
675	374	15.638	0.011	0.573	0.021	0.269	0.027	2.599	0.021	-9.990	0.131	0.038	0.96	0.26
677	0	15.362	0.012	0.633	0.028	0.108	0.039	2.716	0.021	-9.990	0.405	0.037	-9.90	-9.90
678	0	14.008	0.006	0.474	0.016	0.112	0.023	2.717	0.021	-9.990	0.251	0.028	0.28	0.34
679	**87**	13.564	0.006	0.441	0.009	0.138	0.010	2.759	0.033	0.765	0.255	0.036	-9.99	-9.99
681	0	15.656	0.013	0.587	0.026	0.187	0.034	2.609	0.025	-9.990	0.193	0.044	0.50	0.33
682	0	16.268	0.022	1.527	0.124	-9.990	-9.990	-9.990	-9.990	-9.990	-9.990	-9.990	-9.99	-9.99
683	0	13.950	0.005	0.462	0.007	0.112	0.008	2.656	0.108	-9.990	0.167	0.126	-0.04	0.12
685	210	16.804	0.023	0.791	0.065	0.099	0.084	-9.990	-9.990	-9.990	-9.990	-9.990	-9.99	-9.99
689	162	13.033	0.005	0.436	0.009	0.170	0.010	2.796	0.013	0.884	0.268	0.019	-9.99	-9.99
692	131	13.761	0.005	0.453	0.010	0.121	0.012	2.768	0.019	0.757	0.268	0.024	-9.99	-9.99
693	187	12.636	0.004	0.463	0.007	0.118	0.008	2.754	0.015	0.861	0.263	0.019	-9.99	-9.99
694	69	14.194	0.008	0.479	0.011	0.113	0.015	2.724	0.019	0.615	0.250	0.024	-9.99	-9.99
695	0	12.920	0.008	0.394	0.014	0.121	0.019	2.824	0.007	0.942	0.267	0.018	-9.99	-9.99
697	177	14.259	0.005	0.502	0.014	0.109	0.020	2.708	0.003	0.579	0.268	0.014	0.34	0.28
700	0	14.279	0.009	0.569	0.023	0.212	0.034	-9.990	-9.990	-9.990	-9.990	-9.990	-9.99	-9.99
701	0	15.399	0.014	1.476	0.048	0.328	0.105	2.668	0.038	-9.990	1.057	0.095	-9.90	-9.90
703	0	13.347	0.005	0.467	0.007	0.171	0.011	2.768	0.009	0.802	0.282	0.016	-9.99	-9.99
704	0	14.729	0.008	0.540	0.012	0.112	0.015	2.682	0.026	0.471	0.271	0.032	0.44	0.20
706	0	15.875	0.016	0.876	0.035	-9.990	-9.990	2.800	0.024	-9.990	0.712	0.045	-9.99	-9.99
707	136	11.157	0.005	0.263	0.016	-9.990	-9.990	-9.990	-9.990	-9.990	-9.990	-9.990	-9.99	-9.99
711	254	13.465	0.010	0.450	0.011	0.121	0.010	2.763	0.010	0.781	0.259	0.018	-9.99	-9.99
712	0	16.294	0.026	0.920	0.063	-9.990	-9.990	2.728	0.053	-9.990	-9.990	-9.990	-9.99	-9.99
715	0	14.543	0.007	0.517	0.011	0.111	0.013	2.703	0.020	0.539	0.275	0.025	0.42	0.19
716	335	13.936	0.006	0.447	0.010	0.110	0.012	2.746	0.015	-9.990	0.242	0.021	-9.99	-9.99
718	0	17.099	0.064	0.815	0.152	-9.990	-9.990	-9.990	-9.990	-9.990	-9.990	-9.990	-9.99	-9.99
719	311	16.269	0.021	1.487	0.060	-9.990	-9.990	2.578	0.124	-9.990	-9.990	-9.990	-9.99	-9.99
720	0	16.007	0.015	0.693	0.030	0.113	0.049	2.399	0.152	-9.990	-9.990	-9.990	-9.99	-9.99
722	142	11.818	0.004	0.914	0.006	0.377	0.007	2.588	0.008	-9.990	-9.990	-9.990	-9.99	-9.99
723	0	15.507	0.016	0.617	0.026	0.104	0.034	2.609	0.057	-9.990	-9.990	-9.990	-0.12	0.34
725	350	15.924	0.014	0.818	0.021	-9.990	-9.990	2.806	0.044	-9.990	-9.990	-9.990	-9.99	-9.99
727	0	15.765	0.028	0.613	0.039	0.138	0.037	2.615	0.144	-9.990	0.244	0.185	0.23	0.38
729	0	14.215	0.006	0.478	0.014	0.114	0.020	2.711	0.030	0.590	0.248	0.036	0.32	0.30
730	0	14.395	0.006	0.505	0.012	0.103	0.014	2.702	0.021	0.552	0.265	0.026	0.25	0.20
733	0	15.650	0.026	0.631	0.038	-9.990	-9.990	-9.990	-9.990	-9.990	-9.990	-9.990	-9.99	-9.99
735	229	14.382	0.005	0.505	0.011	0.107	0.017	2.706	0.018	0.563	0.269	0.023	0.32	0.25
736	119	14.665	0.008	0.528	0.012	0.164	0.017	2.603	0.011	-9.990	0.145	0.020	0.09	0.16
737	158	14.047	0.021	0.517	0.024	0.100	0.024	2.743	0.021	0.687	0.305	0.034	-9.99	-9.99
739	0	14.919	0.007	0.571	0.016	0.259	0.019	2.609	0.013	-9.990	0.148	0.025	1.07	0.20
740	0	16.311	0.013	1.577	0.072	0.170	0.123	-9.990	-9.990	-9.990	-9.990	-9.990	-9.99	-9.99
742	190	13.298	0.019	0.430	0.023	0.162	0.021	2.793	0.014	0.850	0.261	0.029	-9.99	-9.99
745	262	15.051	0.010	0.718	0.018	-9.990	-9.990	2.912	0.017	-9.990	-9.990	-9.990	-9.99	-9.99
746	153	13.938	0.005	0.480	0.010	0.110	0.011	2.747	0.028	0.707	0.274	0.032	-9.99	-9.99
748	0	16.222	0.032	1.715	0.091	-9.990	-9.990	-9.990	-9.990	-9.990	-9.990	-9.990	-9.99	-9.99
750	0	15.261	0.094	0.596	0.108	0.138	0.100	2.570	0.085	-9.990	-9.990	-9.990	-9.99	-9.99
754	0	13.833	0.004	0.480	0.008	0.108	0.010	2.737	0.010	0.697	0.265	0.016	-9.99	-9.99
757	173	17.038	0.028	0.732	0.128	0.292	0.157	2.638	0.047	-9.990	0.324	0.157	-9.90	-9.90
759	215	15.030	0.007	0.561	0.018	0.119	0.025	2.671	0.044	-9.990	0.274	0.054	0.50	0.32
760	56	13.473	0.004	0.458	0.007	0.121	0.011	2.750	0.013	0.763	-9.990	-9.990	-9.99	-9.99
761	90	16.569	0.029	0.973	0.074	0.097	0.092	2.732	0.082	-9.990	-9.990	-9.990	-9.99	-9.99
762	357	14.997	0.011	0.558	0.021	0.123	0.023	2.678	0.027	0.439	0.279	0.038	0.59	0.30
763	217	15.067	0.017	0.577	0.025	0.109	0.028	2.574	0.060	-9.990	-9.990	-9.990	-9.99	-9.99
766	193	12.369	0.002	0.454	0.008	0.125	0.013	2.764	0.011	0.905	0.263	0.017	-9.99	-9.99
768	0	16.286	0.028	0.780	0.056	0.186	0.082	2.560	0.039	-9.990	-9.990	-9.990	-9.99	-9.99
770	0	16.183	0.056	1.545	0.165	-9.990	-9.990	-9.990	-9.990	-9.990	-9.990	-9.990	-9.99	-9.99
774	0	14.881	0.008	0.548	0.012	0.112	0.021	2.686	0.018	0.464	0.283	0.023	0.46	0.28
775	0	14.951	0.015	0.542	0.020	0.130	0.024	2.499	0.152	-9.990	-9.990	-9.990	-9.99	-9.99
779	288	16.129	0.013	0.804	0.060	0.022	0.074	2.687	0.054	-9.990	0.544	0.087	-9.90	-9.90
784	0	12.236	0.003	0.372	0.006	0.135	0.008	2.672	0.015	-9.990	0.097	0.019	0.03	0.11
785	0	17.142	0.051	1.035	0.115	0.110	0.148	-9.990	-9.990	-9.990	-9.990	-9.990	-9.99	-9.99
786	0	15.509	0.019	0.695	0.027	0.528	0.043	2.619	0.071	-9.990	-9.990	-9.990	-9.90	-9.90
788	0	14.187	0.024	0.981	0.028	-9.990	-9.990	-9.990	-9.990	-9.990	-9.990	-9.990	-9.99	-9.99

Continued on the next page...

NGC 6134 photometry, continued from the previous page

ID_B	ID_V	V	σ_V	$b-y$	σ_{by}	m_1	σ_{m_1}	β	σ_β	c_0	$E(b-y)$	σ_E	Fe/H	σ_{FeH}
791	0	17.138	0.025	1.181	0.146	-9.990	-9.990	-9.990	-9.990	-9.990	-9.990	-9.990	-9.99	-9.99
793	0	12.346	0.006	0.816	0.010	0.301	0.013	2.586	0.013	-9.990	-9.990	-9.990	-9.99	-9.99
794	127	17.139	0.037	0.945	0.162	0.166	0.215	-9.990	-9.990	-9.990	-9.990	-9.990	-9.99	-9.99
797	273	14.674	0.006	0.546	0.015	0.102	0.018	-9.990	-9.990	-9.990	-9.990	-9.990	-9.99	-9.99
802	0	17.446	0.077	0.754	0.096	-9.990	-9.990	-9.990	-9.990	-9.990	-9.990	-9.990	-9.99	-9.99
807	25	14.097	0.006	0.544	0.007	0.109	0.009	-9.990	-9.990	-9.990	-9.990	-9.990	-9.99	-9.99
808	0	16.762	0.032	0.979	0.068	0.088	0.169	-9.990	-9.990	-9.990	-9.990	-9.990	-9.99	-9.99
810	181	16.673	0.014	0.798	0.121	0.180	0.164	-9.990	-9.990	-9.990	-9.990	-9.990	-9.99	-9.99
811	0	14.265	0.041	0.518	0.052	-9.990	-9.990	-9.990	-9.990	-9.990	-9.990	-9.990	-9.99	-9.99
812	0	17.269	0.073	0.772	0.086	-9.990	-9.990	-9.990	-9.990	-9.990	-9.990	-9.990	-9.99	-9.99
813	139	16.107	0.020	0.685	0.034	0.106	0.043	-9.990	-9.990	-9.990	-9.990	-9.990	-9.99	-9.99
815	0	11.874	0.016	0.968	0.020	0.395	0.019	-9.990	-9.990	-9.990	-9.990	-9.990	-9.99	-9.99
817	0	17.709	0.087	0.963	0.100	-9.990	-9.990	-9.990	-9.990	-9.990	-9.990	-9.990	-9.99	-9.99
820	0	11.815	0.015	0.956	0.023	0.445	0.132	2.579	0.016	-9.990	-9.990	-9.990	-9.99	-9.99
822	160	13.441	0.004	0.466	0.007	0.122	0.008	2.743	0.028	0.754	-9.990	-9.990	-9.99	-9.99
824	0	17.374	0.047	0.600	0.158	-9.990	-9.990	-9.990	-9.990	-9.990	-9.990	-9.990	-9.99	-9.99
826	0	16.898	0.037	0.713	0.056	0.271	0.121	-9.990	-9.990	-9.990	-9.990	-9.990	-9.99	-9.99
827	0	17.591	0.099	1.155	0.310	-9.990	-9.990	-9.990	-9.990	-9.990	-9.990	-9.990	-9.99	-9.99
829	0	16.609	0.050	0.765	0.081	0.401	0.155	2.430	0.137	-9.990	-9.990	-9.990	-9.99	-9.99
830	0	13.836	0.004	0.543	0.009	0.115	0.011	2.701	0.030	0.604	0.297	0.035	0.59	0.17
832	0	12.365	0.004	0.472	0.007	0.176	0.008	2.735	0.009	0.853	0.240	0.015	-9.99	-9.99
833	0	14.430	0.013	0.598	0.027	0.096	0.033	2.619	0.128	-9.990	0.252	0.162	-0.14	0.38
834	154	14.408	0.009	0.534	0.017	0.116	0.021	2.706	0.013	0.560	0.295	0.023	0.57	0.30
836	38	17.074	0.045	0.815	0.073	0.240	0.128	2.609	0.087	-9.990	0.368	0.153	-9.90	-9.90
838	0	17.896	0.119	1.079	0.189	-9.990	-9.990	-9.990	-9.990	-9.990	-9.990	-9.990	-9.99	-9.99
839	0	12.380	0.020	0.887	0.026	0.280	0.027	2.708	0.172	-9.990	0.613	0.265	-9.90	-9.90
841	0	14.274	0.033	0.622	0.036	-9.990	-9.990	-9.990	-9.990	-9.990	-9.990	-9.990	-9.99	-9.99
843	0	16.591	0.091	0.756	0.181	-9.990	-9.990	-9.990	-9.990	-9.990	-9.990	-9.990	-9.99	-9.99
844	0	16.253	0.037	0.906	0.059	-9.990	-9.990	-9.990	-9.990	-9.990	-9.990	-9.990	-9.99	-9.99
845	0	17.050	0.063	0.717	0.095	0.299	0.099	2.516	0.142	-9.990	-9.990	-9.990	-9.99	-9.99
846	0	14.083	0.009	0.484	0.011	0.123	0.013	2.738	0.012	0.671	0.266	0.020	-9.99	-9.99
847	0	16.141	0.036	0.775	0.055	0.175	0.066	2.599	0.075	-9.990	0.349	0.117	-9.90	-9.90
848	0	16.050	0.025	0.692	0.030	0.084	0.048	-9.990	-9.990	-9.990	-9.990	-9.990	-9.99	-9.99
849	0	14.363	0.005	0.486	0.007	0.111	0.009	2.729	0.014	0.610	0.261	0.019	-9.99	-9.99
852	280	15.013	0.006	0.629	0.014	0.375	0.022	2.570	0.017	-9.990	-9.990	-9.990	-9.99	-9.99
853	**161**	11.988	0.004	0.498	0.007	0.120	0.009	2.736	0.017	0.898	0.277	0.021	-9.99	-9.99
856	0	14.745	0.009	0.557	0.021	0.116	0.023	2.670	0.020	0.451	0.269	0.032	0.44	0.29
857	0	13.920	0.006	0.488	0.010	0.112	0.013	2.742	0.018	0.700	0.276	0.023	-9.99	-9.99
859	0	11.915	0.016	0.439	0.021	0.162	0.021	2.636	0.075	-9.990	0.105	0.093	0.20	0.23
860	183	17.405	0.052	1.125	0.122	-9.990	-9.990	-9.990	-9.990	-9.990	-9.990	-9.990	-9.99	-9.99
861	22	14.835	0.010	0.658	0.022	0.140	0.029	2.646	0.022	-9.990	0.322	0.036	0.76	0.34
863	0	17.507	0.049	0.993	0.150	-9.990	-9.990	-9.990	-9.990	-9.990	-9.990	-9.990	-9.99	-9.99
865	0	13.582	0.005	0.436	0.008	0.137	0.012	2.781	0.032	0.798	0.261	0.034	-9.99	-9.99
868	0	14.642	0.008	0.547	0.013	0.115	0.014	2.673	0.020	0.464	0.265	0.027	0.42	0.19
871	97	17.041	0.029	0.774	0.080	0.182	0.129	2.603	0.071	-9.990	0.350	0.139	-9.90	-9.90
872	0	12.391	0.026	0.841	0.047	0.308	0.052	2.541	0.097	-9.990	-9.990	-9.990	-9.99	-9.99
873	0	14.970	0.066	0.600	0.074	0.171	0.063	2.669	0.022	-9.990	0.294	0.080	-9.90	-9.90
875	0	12.262	0.009	0.848	0.013	0.302	0.015	2.586	0.016	-9.990	-9.990	-9.990	-9.99	-9.99
876	128	14.800	0.007	0.549	0.015	0.106	0.021	2.680	0.016	0.461	0.278	0.024	0.37	0.27
877	0	13.737	0.007	0.447	0.009	0.121	0.010	2.782	0.012	0.783	0.276	0.018	-9.99	-9.99
879	0	16.186	0.026	0.801	0.060	0.074	0.073	2.859	0.068	-9.990	0.683	0.093	-9.99	-9.99
880	0	17.296	0.064	1.079	0.126	-9.990	-9.990	-9.990	-9.990	-9.990	-9.990	-9.990	-9.99	-9.99
881	0	14.380	0.007	0.508	0.013	0.111	0.015	2.704	0.012	0.558	0.269	0.019	0.38	0.22
883	0	17.336	0.077	0.905	0.117	-9.990	-9.990	-9.990	-9.990	-9.990	-9.990	-9.990	-9.99	-9.99
885	0	14.782	0.009	0.534	0.012	0.116	0.017	2.698	0.026	0.504	0.285	0.031	0.53	0.24
886	0	15.948	0.008	0.698	0.060	-9.990	-9.990	-9.990	-9.990	-9.990	-9.990	-9.990	-9.99	-9.99
890	0	17.088	0.067	1.119	0.179	0.014	0.212	-9.990	-9.990	-9.990	-9.990	-9.990	-9.99	-9.99
891	0	13.574	0.006	0.478	0.011	0.108	0.016	2.726	0.016	0.690	-9.990	-9.990	-9.99	-9.99
896	218	14.871	0.008	0.568	0.014	0.116	0.015	2.674	0.013	0.446	0.285	0.020	0.51	0.20
899	141	12.284	0.004	0.848	0.007	0.299	0.012	2.594	0.012	-9.990	-9.990	-9.990	-9.99	-9.99
900	0	17.268	0.067	1.066	0.428	-9.990	-9.990	-9.990	-9.990	-9.990	-9.990	-9.990	-9.99	-9.99
903	0	16.230	0.025	1.598	0.049	0.018	0.108	2.707	0.068	-9.990	1.329	0.109	-9.90	-9.90
905	0	17.409	0.072	1.127	0.143	-9.990	-9.990	-9.990	-9.990	-9.990	-9.990	-9.990	-9.99	-9.99
906	**9**	12.280	0.011	0.504	0.020	0.167	0.027	2.693	0.034	0.731	0.241	0.044	1.05	0.40
912	0	13.421	0.002	0.415	0.005	0.143	0.007	2.792	0.006	0.835	0.251	0.013	-9.99	-9.99
915	0	16.323	0.024	0.906	0.051	-9.990	-9.990	2.961	0.060	-9.990	-9.990	-9.990	-9.99	-9.99
916	0	17.845	0.121	1.009	0.297	-9.990	-9.990	-9.990	-9.990	-9.990	-9.990	-9.990	-9.99	-9.99
917	0	17.453	0.088	0.775	0.183	-9.990	-9.990	-9.990	-9.990	-9.990	-9.990	-9.990	-9.99	-9.99
919	182	12.577	0.005	0.479	0.008	0.161	0.009	2.742	0.012	0.848	0.256	0.018	-9.99	-9.99
922	0	17.158	0.061	1.359	0.190	-9.990	-9.990	-9.990	-9.990	-9.990	-9.990	-9.990	-9.99	-9.99
925	174	12.348	0.004	0.312	0.008	0.123	0.008	2.895	0.007	-9.990	-9.990	-9.990	-9.99	-9.99
926	0	16.488	0.015	0.746	0.065	0.175	0.102	2.513	0.082	-9.990	-9.990	-9.990	-9.99	-9.99
929	0	12.218	0.005	0.836	0.009	0.320	0.011	2.602	0.010	-9.990	0.341	0.018	-9.90	-9.90
930	0	12.269	0.004	0.423	0.006	0.130	0.008	2.778	0.009	0.939	0.248	0.015	-9.99	-9.99
933	126	12.529	0.004	0.379	0.007	0.156	0.014	2.850	0.010	1.016	0.270	0.016	-9.99	-9.99
934	0	16.988	0.047	0.977	0.109	0.032	0.118	2.606	0.098	-9.990	0.596	0.176	-9.90	-9.90
936	0	13.575	0.005	0.468	0.010	0.103	0.012	2.740	0.021	0.734	0.257	0.025	-9.99	-9.99
938	0	15.432	0.011	0.744	0.023	-9.990	-9.990	2.921	0.017	-9.990	-9.990	-9.990	-9.99	-9.99
939	89	17.097	0.038	1.064	0.052	-9.990	-9.990	-9.990	-9.990	-9.990	-9.990	-9.990	-9.99	-9.99
941	0	14.931	0.010	0.544	0.013	0.125	0.015	2.652	0.018	0.410	0.232	0.026	0.32	0.18

Continued on the next page...

NGC 6134 photometry, continued from the previous page

ID_B	ID_V	V	σ_V	$b-y$	σ_{by}	m_1	σ_{m_1}	β	σ_β	c_0	$E(b-y)$	σ_E	Fe/H	σ_{FeH}
942	0	17.308	0.059	1.037	0.064	-9.990	-9.990	-9.990	-9.990	-9.990	-9.990	-9.990	-9.99	-9.99
943	0	15.188	0.008	0.550	0.015	0.222	0.021	2.623	0.019	-9.990	0.163	0.030	0.92	0.23
944	0	16.628	0.032	0.965	0.066	-9.990	-9.990	-9.990	-9.990	-9.990	-9.990	-9.990	-9.99	-9.99
945	0	15.795	0.016	0.696	0.031	0.213	0.069	2.664	0.040	-9.990	0.362	0.063	-9.90	-9.90
948	0	13.556	0.006	0.450	0.007	0.173	0.008	2.797	0.017	0.827	0.282	0.021	-9.99	-9.99
951	0	16.796	0.037	1.389	0.180	-9.990	-9.990	-9.990	-9.990	-9.990	-9.990	-9.990	-9.99	-9.99
952	0	17.266	0.043	1.045	0.089	-9.990	-9.990	-9.990	-9.990	-9.990	-9.990	-9.990	-9.99	-9.99
953	0	15.795	0.013	0.626	0.026	0.285	0.050	2.406	0.106	-9.990	-9.990	-9.990	-9.99	-9.99
957	0	12.933	0.005	0.457	0.009	0.149	0.009	2.602	0.009	-9.990	0.090	0.015	-0.22	0.09
963	104	17.411	0.094	0.920	0.110	0.058	0.136	-9.990	-9.990	-9.990	-9.990	-9.990	-9.99	-9.99
966	0	14.662	0.008	0.543	0.013	0.118	0.013	2.698	0.014	0.515	0.293	0.020	0.60	0.19
967	133	15.369	0.010	0.552	0.017	0.130	0.019	2.627	0.033	0.355	0.207	0.045	0.13	0.20
969	46	13.338	0.006	0.485	0.008	0.106	0.009	2.734	0.011	0.740	0.266	0.017	-9.99	-9.99
970	0	16.232	0.020	1.511	0.103	-9.990	-9.990	2.631	0.069	-9.990	-9.990	-9.990	-9.99	-9.99
979	0	15.923	0.018	0.635	0.036	0.131	0.042	2.631	0.041	-9.990	0.285	0.064	0.41	0.45
983	0	14.123	0.007	0.546	0.013	0.113	0.017	2.683	0.012	0.529	0.278	0.019	0.45	0.23
985	0	13.971	0.004	0.474	0.006	0.113	0.009	2.756	0.013	0.715	0.283	0.018	-9.99	-9.99
988	88	16.870	0.059	0.864	0.092	0.012	0.134	2.847	0.118	-9.990	0.743	0.154	-9.99	-9.99
991	0	14.700	0.002	0.605	0.011	0.111	0.015	2.651	0.012	0.427	0.291	0.018	0.35	0.17
994	0	13.725	0.006	0.509	0.010	0.127	0.012	2.642	0.005	-9.990	0.188	0.013	0.13	0.14
995	59	14.426	0.006	0.565	0.014	0.116	0.019	2.670	0.008	0.479	0.278	0.018	0.46	0.24
997	0	15.033	0.027	0.592	0.059	0.129	0.070	2.523	0.083	-9.990	-9.990	-9.990	-9.99	-9.99
1001	0	13.679	0.007	0.425	0.010	0.130	0.013	2.671	0.018	-9.990	0.145	0.023	0.15	0.16
1003	0	16.411	0.029	0.701	0.047	0.157	0.066	2.656	0.031	-9.990	0.371	0.064	-9.90	-9.90
1004	122	15.199	0.005	0.584	0.011	0.094	0.025	2.668	0.020	0.409	0.298	0.027	0.26	0.32
1010	0	17.037	0.035	0.805	0.053	0.298	0.114	-9.990	-9.990	-9.990	-9.990	-9.990	-9.99	-9.99
1013	0	15.422	0.006	0.592	0.020	0.104	0.031	2.639	0.019	0.361	0.266	0.033	0.11	0.35
1018	0	14.278	0.014	0.490	0.025	0.184	0.028	2.571	0.134	-9.990	-9.990	-9.990	-9.99	-9.99
1019	0	13.975	0.014	0.483	0.021	0.166	0.021	2.523	0.085	-9.990	-9.990	-9.990	-9.99	-9.99
1022	0	15.849	0.020	0.821	0.050	0.156	0.061	2.625	0.038	-9.990	0.432	0.075	-9.90	-9.90
1023	24	12.699	0.004	0.458	0.008	0.152	0.010	2.779	0.010	0.893	0.276	0.016	-9.99	-9.99
1025	0	11.643	0.008	0.753	0.009	0.229	0.011	2.631	0.014	-9.990	0.354	0.021	-9.90	-9.90
1027	0	14.918	0.017	0.702	0.079	-9.990	-9.990	2.747	0.228	-9.990	-9.990	-9.990	-9.99	-9.99
1028	0	17.218	0.119	0.704	0.164	-9.990	-9.990	-9.990	-9.990	-9.990	-9.990	-9.990	-9.99	-9.99
1029	0	15.414	0.015	0.619	0.029	0.102	0.035	2.642	0.020	0.364	0.295	0.040	0.21	0.40
1034	0	15.456	0.018	0.655	0.025	0.164	0.029	2.658	0.062	-9.990	0.330	0.079	1.18	0.44
1037	0	15.634	0.014	0.593	0.025	0.106	0.030	2.613	0.026	0.323	0.237	0.044	-0.13	0.29
1040	0	13.260	0.007	0.435	0.011	0.125	0.015	2.782	0.017	0.836	0.264	0.023	-9.99	-9.99
1042	0	14.899	0.013	1.415	0.044	0.300	0.082	2.648	0.257	-9.990	0.957	0.482	-9.90	-9.90
1045	11	11.643	0.009	0.899	0.012	0.364	0.012	2.600	0.011	-9.990	0.370	0.022	-9.90	-9.90
1046	0	14.919	0.008	0.614	0.016	0.132	0.019	2.632	0.030	0.393	0.268	0.041	0.37	0.20
1047	86	17.380	0.085	0.877	0.180	-9.990	-9.990	-9.990	-9.990	-9.990	-9.990	-9.990	-9.99	-9.99
1049	0	11.149	0.013	1.579	0.024	0.095	0.091	2.658	0.076	-9.990	1.193	0.121	-9.90	-9.90
1050	0	14.430	0.007	0.503	0.012	0.123	0.019	2.725	0.023	0.591	0.271	0.029	-9.99	-9.99
1051	0	17.326	0.053	0.898	0.094	0.022	0.163	-9.990	-9.990	-9.990	-9.990	-9.990	-9.99	-9.99
1052	0	17.513	0.042	0.801	0.162	-9.990	-9.990	-9.990	-9.990	-9.990	-9.990	-9.990	-9.99	-9.99
1054	0	16.921	0.048	0.979	0.103	-9.990	-9.990	-9.990	-9.990	-9.990	-9.990	-9.990	-9.99	-9.99
1057	0	13.949	0.008	0.478	0.010	0.125	0.012	2.890	0.011	-9.990	-9.990	-9.990	-9.99	-9.99
1059	0	15.977	0.024	0.767	0.047	0.053	0.059	2.881	0.073	-9.990	-9.990	-9.990	-9.99	-9.99
1061	0	16.184	0.127	0.912	0.150	-9.990	-9.990	-9.990	-9.990	-9.990	-9.990	-9.990	-9.99	-9.99
1063	0	16.639	0.029	1.585	0.137	-9.990	-9.990	-9.990	-9.990	-9.990	-9.990	-9.990	-9.99	-9.99
1066	13	14.362	0.006	0.588	0.017	0.118	0.021	2.747	0.038	-9.990	0.370	0.043	-9.99	-9.99
1068	0	15.675	0.014	1.360	0.050	0.157	0.105	2.638	0.031	-9.990	0.935	0.080	-9.90	-9.90
1069	0	13.166	0.007	0.438	0.011	0.122	0.018	2.751	0.016	0.799	0.237	0.022	-9.99	-9.99
1071	0	15.413	0.015	1.447	0.038	0.202	0.093	2.641	0.046	-9.990	1.003	0.092	-9.90	-9.90
1073	0	15.138	0.029	0.681	0.041	0.172	0.043	2.387	0.131	-9.990	-9.990	-9.990	-9.99	-9.99
1074	0	16.037	0.020	0.679	0.033	0.119	0.046	2.608	0.051	-9.990	0.301	0.076	0.14	0.44
1076	0	15.935	0.038	0.663	0.047	-9.990	-9.990	-9.990	-9.990	-9.990	-9.990	-9.990	-9.99	-9.99
1078	0	15.261	0.016	1.371	0.037	0.164	0.061	2.586	0.082	-9.990	-9.990	-9.990	-9.99	-9.99
1080	0	14.731	0.028	0.960	0.050	-9.990	-9.990	-9.990	-9.990	-9.990	-9.990	-9.990	-9.99	-9.99
1082	0	16.880	0.081	1.242	0.212	-9.990	-9.990	-9.990	-9.990	-9.990	-9.990	-9.990	-9.99	-9.99
1083	0	14.004	0.016	0.467	0.034	0.109	0.043	2.725	0.030	-9.990	0.241	0.048	-9.99	-9.99
1092	0	14.773	0.004	0.886	0.014	0.413	0.030	2.585	0.016	-9.990	-9.990	-9.990	-9.99	-9.99
1095	0	16.316	0.027	0.689	0.049	0.177	0.062	2.629	0.066	-9.990	0.314	0.100	-9.90	-9.90
1098	0	15.809	0.019	0.996	0.057	-9.990	-9.990	2.826	0.109	-9.990	-9.990	-9.990	-9.99	-9.99
1101	0	14.710	0.006	0.517	0.013	0.138	0.014	2.588	0.035	-9.990	-9.990	-9.990	-9.99	-9.99
1107	0	12.292	0.005	0.858	0.009	0.306	0.011	2.593	0.010	-9.990	-9.990	-9.990	-9.90	-9.90
1108	0	17.498	0.131	1.273	0.336	-9.990	-9.990	-9.990	-9.990	-9.990	-9.990	-9.990	-9.99	-9.99
1109	0	13.327	0.006	0.470	0.010	0.121	0.014	2.747	0.022	0.774	0.262	0.026	-9.99	-9.99
1110	0	14.589	0.006	0.543	0.014	0.108	0.018	2.697	0.012	0.519	0.294	0.020	0.45	0.25
1112	0	16.511	0.047	0.843	0.080	-9.990	-9.990	-9.990	-9.990	-9.990	-9.990	-9.990	-9.99	-9.99
1115	0	14.060	0.005	0.556	0.011	0.100	0.017	2.693	0.012	0.559	0.302	0.018	0.38	0.23
1116	0	15.908	0.017	0.919	0.037	0.207	0.066	2.621	0.035	-9.990	0.493	0.067	-9.90	-9.90
1117	0	17.589	0.050	0.858	0.114	-9.990	-9.990	-9.990	-9.990	-9.990	-9.990	-9.990	-9.99	-9.99
1118	0	17.057	0.040	1.157	0.158	-9.990	-9.990	-9.990	-9.990	-9.990	-9.990	-9.990	-9.99	-9.99
1125	0	14.522	0.020	0.701	0.034	0.011	0.054	2.848	0.189	-9.990	-9.990	-9.990	-9.99	-9.99
1128	0	17.000	0.031	1.094	0.111	-9.990	-9.990	-9.990	-9.990	-9.990	-9.990	-9.990	-9.99	-9.99
1135	0	15.734	0.010	0.651	0.024	0.124	0.038	2.591	0.387	-9.990	0.258	0.509	-9.90	-9.90
1136	0	15.946	0.025	0.667	0.040	0.113	0.048	2.536	0.440	-9.990	-9.990	-9.990	-9.99	-9.99
1144	0	16.690	0.052	0.864	0.110	0.180	0.158	-9.990	-9.990	-9.990	-9.990	-9.990	-9.99	-9.99

Continued on the next page...

NGC 6134 photometry, continued from the previous page

ID_B	ID_V	V	σ_V	$b-y$	σ_{by}	m_1	σ_{m_1}	β	σ_β	c_0	$E(b-y)$	σ_E	Fe/H	σ_{FeH}
1149	0	16.376	0.042	0.977	0.130	0.081	0.183	-9.990	-9.990	-9.990	-9.990	-9.990	-9.99	-9.99
1153	0	16.173	0.172	0.744	0.187	-9.990	-9.990	-9.990	-9.990	-9.990	-9.990	-9.990	-9.99	-9.99
1154	0	13.419	0.003	0.463	0.006	0.167	0.007	2.790	0.007	0.832	0.288	0.014	-9.99	-9.99
1156	0	14.585	0.020	0.522	0.030	0.132	0.042	2.769	0.094	-9.990	0.328	0.099	-9.99	-9.99
1158	0	15.443	0.013	0.630	0.024	0.102	0.030	2.663	0.013	-9.990	0.331	0.029	0.46	0.37
1162	0	16.264	0.022	0.690	0.048	0.128	0.075	2.662	0.057	-9.990	0.377	0.085	-9.90	-9.90
1163	0	16.524	0.116	0.588	0.168	0.253	0.170	-9.990	-9.990	-9.990	-9.990	-9.990	-9.99	-9.99
1165	0	17.622	0.044	1.010	0.149	-9.990	-9.990	-9.990	-9.990	-9.990	-9.990	-9.990	-9.99	-9.99
1167	0	16.366	0.031	0.717	0.051	0.207	0.078	2.642	0.467	-9.990	0.347	0.600	-9.90	-9.90
1171	0	15.219	0.009	0.597	0.026	0.112	0.032	2.656	0.014	0.392	0.289	0.032	0.38	0.38
1174	0	15.492	0.053	0.738	0.074	0.164	0.096	2.887	0.197	-9.990	-9.990	-9.990	-9.99	-9.99
1176	0	17.229	0.050	0.839	0.079	-9.990	-9.990	2.520	0.126	-9.990	-9.990	-9.990	-9.99	-9.99
1178	0	16.729	0.047	1.556	0.115	-9.990	-9.990	-9.990	-9.990	-9.990	-9.990	-9.990	-9.99	-9.99
1179	0	14.858	0.010	0.561	0.017	0.104	0.023	2.679	0.014	0.453	0.288	0.024	0.37	0.31
1180	0	15.421	0.012	0.605	0.028	0.103	0.037	2.645	0.024	0.365	0.285	0.042	0.21	0.43
1184	0	13.993	0.011	0.494	0.017	0.115	0.018	2.655	0.051	-9.990	0.194	0.062	0.08	0.21
1187	0	13.927	0.006	0.467	0.009	0.135	0.013	2.758	0.018	0.723	0.267	0.023	-9.99	-9.99
1188	0	16.081	0.020	0.841	0.031	0.106	0.068	2.707	0.091	-9.990	0.593	0.112	-9.90	-9.90
1191	0	16.792	0.035	0.758	0.066	0.296	0.127	2.568	0.094	-9.990	-9.990	-9.990	-9.99	-9.99
1194	0	11.638	0.028	0.940	0.035	-9.990	-9.990	2.496	0.057	-9.990	-9.990	-9.990	-9.99	-9.99
1196	0	13.426	0.011	0.384	0.014	0.153	0.013	2.627	0.071	-9.990	-9.990	-9.990	-0.12	0.16
1202	0	14.303	0.008	0.521	0.012	0.103	0.019	2.718	0.008	0.590	0.300	0.016	0.38	0.28
1204	0	16.534	0.042	0.718	0.077	0.167	0.115	2.641	0.475	-9.990	0.360	0.595	-9.90	-9.90
1205	0	14.483	0.009	0.566	0.017	0.154	0.026	2.634	0.021	0.428	0.220	0.032	0.48	0.28
1209	0	13.762	0.011	0.676	0.016	0.108	0.019	2.689	0.164	-9.990	0.409	0.188	-9.90	-9.90
1216	0	12.403	0.009	0.480	0.015	0.125	0.016	2.733	0.135	-9.990	0.257	0.136	-9.99	-9.99
1219	0	17.228	0.050	0.950	0.104	-9.990	-9.990	-9.990	-9.990	-9.990	-9.990	-9.990	-9.99	-9.99
1220	0	17.481	0.117	0.970	0.234	-9.990	-9.990	-9.990	-9.990	-9.990	-9.990	-9.990	-9.99	-9.99
1224	0	17.262	0.035	0.989	0.126	-9.990	-9.990	-9.990	-9.990	-9.990	-9.990	-9.990	-9.99	-9.99
1227	0	14.639	0.009	0.536	0.015	0.118	0.019	2.720	0.014	-9.990	0.315	0.022	0.64	0.29
1228	0	15.126	0.023	0.777	0.036	0.565	0.048	2.496	0.060	-9.990	-9.990	-9.990	-9.99	-9.99
1230	0	16.690	0.036	0.825	0.086	0.637	0.163	2.422	0.258	-9.990	-9.990	-9.990	-9.99	-9.99
1231	0	16.649	0.030	0.685	0.045	0.229	0.064	2.681	0.084	-9.990	-9.990	-9.990	-9.90	-9.90
1234	0	16.528	0.019	0.701	0.034	0.342	0.064	2.629	0.044	-9.990	0.262	0.078	-9.90	-9.90
1239	0	14.113	0.009	0.581	0.017	0.220	0.022	2.534	0.105	-9.990	-9.990	-9.990	-9.99	-9.99
1245	0	13.989	0.004	0.445	0.011	0.167	0.015	2.631	0.009	-9.990	0.103	0.017	0.22	0.16
1246	0	13.682	0.006	0.493	0.011	0.142	0.015	2.751	0.212	-9.990	0.283	0.212	-9.99	-9.99
1249	0	15.401	0.020	0.533	0.037	-9.990	-9.990	-9.990	-9.990	-9.990	-9.990	-9.990	-9.99	-9.99
1253	0	12.101	0.012	0.863	0.017	0.314	0.021	2.575	0.032	-9.990	-9.990	-9.990	-9.99	-9.99
1258	0	15.723	0.014	0.629	0.027	0.141	0.044	2.581	0.076	-9.990	-9.990	-9.990	-9.99	-9.99
1261	0	17.202	0.046	1.222	0.280	-9.990	-9.990	-9.990	-9.990	-9.990	-9.990	-9.990	-9.99	-9.99
1262	0	14.615	0.008	0.589	0.012	0.325	0.014	2.566	0.016	-9.990	-9.990	-9.990	-9.99	-9.99
1264	0	15.878	0.035	0.812	0.091	-9.990	-9.990	-9.990	-9.990	-9.990	-9.990	-9.990	-9.99	-9.99
1269	0	16.491	0.100	0.768	0.153	-9.990	-9.990	-9.990	-9.990	-9.990	-9.990	-9.990	-9.99	-9.99
1270	0	12.927	0.008	0.455	0.015	0.183	0.020	2.837	0.376	-9.990	0.321	0.376	-9.99	-9.99
1272	0	16.092	0.026	0.673	0.060	0.145	0.079	2.607	0.175	-9.990	0.284	0.233	-9.90	-9.90
1273	0	16.484	0.044	0.695	0.125	0.227	0.168	2.658	0.253	-9.990	0.347	0.354	-9.90	-9.90
1276	0	12.596	0.013	0.507	0.018	0.118	0.021	2.725	0.025	0.794	0.275	0.033	-9.99	-9.99
1277	0	15.115	0.012	0.539	0.014	-9.990	-9.990	-9.990	-9.990	-9.990	-9.990	-9.990	-9.99	-9.99
1278	0	15.510	0.015	0.700	0.032	0.150	0.051	2.709	0.414	-9.990	0.454	0.492	-9.90	-9.90
1281	0	13.630	0.049	0.614	0.057	-9.990	-9.990	2.647	0.264	-9.990	-9.990	-9.990	-9.99	-9.99
1283	0	17.479	0.061	1.045	0.166	-9.990	-9.990	-9.990	-9.990	-9.990	-9.990	-9.990	-9.99	-9.99
1291	0	17.490	0.068	1.109	0.085	-9.990	-9.990	-9.990	-9.990	-9.990	-9.990	-9.990	-9.99	-9.99
1294	0	16.903	0.140	1.108	0.234	-9.990	-9.990	-9.990	-9.990	-9.990	-9.990	-9.990	-9.99	-9.99
1295	0	11.872	0.007	0.361	0.011	0.128	0.022	2.476	0.454	-9.990	-9.990	-9.990	-9.99	-9.99
1298	0	15.911	0.021	1.013	0.050	-9.990	-9.990	2.902	0.087	-9.990	-9.990	-9.990	-9.99	-9.99
1299	0	17.541	0.073	1.490	0.124	-9.990	-9.990	-9.990	-9.990	-9.990	-9.990	-9.990	-9.99	-9.99
1303	0	13.358	0.003	0.516	0.011	0.107	0.016	2.730	0.124	-9.990	0.291	0.125	-9.99	-9.99
1304	0	14.812	0.007	0.561	0.019	0.109	0.024	2.736	0.367	-9.990	0.337	0.368	-9.99	-9.99
1306	0	14.005	0.014	0.517	0.025	0.114	0.031	3.067	0.298	-9.990	-9.990	-9.990	-9.99	-9.99
1308	0	15.030	0.024	2.037	0.072	-9.990	-9.990	2.865	0.358	-9.990	-9.990	-9.990	-9.99	-9.99
1310	0	16.342	0.029	0.700	0.066	0.184	0.084	2.500	0.135	-9.990	-9.990	-9.990	-9.99	-9.99
1311	0	15.188	0.010	0.696	0.022	0.094	0.034	-9.990	-9.990	-9.990	0.426	0.572	-9.90	-9.90
1312	0	16.019	0.213	0.838	0.232	-9.990	-9.990	-9.990	-9.990	-9.990	-9.990	-9.990	-9.99	-9.99
1314	0	14.422	0.007	0.553	0.020	0.277	0.028	2.591	0.098	-9.990	-9.990	-9.990	-9.99	-9.99
1316	0	16.210	0.111	0.817	0.158	-9.990	-9.990	-9.990	-9.990	-9.990	-9.990	-9.990	-9.99	-9.99
1319	0	16.256	0.036	0.652	0.075	-9.990	-9.990	-9.990	-9.990	-9.990	-9.990	-9.990	-9.99	-9.99
1320	0	17.696	0.073	0.860	0.353	-9.990	-9.990	-9.990	-9.990	-9.990	-9.990	-9.990	-9.99	-9.99
1322	0	15.314	0.010	0.598	0.033	0.105	0.037	2.608	0.110	-9.990	0.237	0.145	-0.17	0.39
1325	0	15.260	0.015	0.678	0.026	0.076	0.037	-9.990	-9.990	-9.990	0.396	0.627	-9.90	-9.90
1330	0	16.750	0.034	0.819	0.084	-9.990	-9.990	-9.990	-9.990	-9.990	-9.990	-9.990	-9.99	-9.99
1331	0	14.173	0.028	1.993	0.035	0.604	0.058	2.642	0.119	-9.990	1.359	0.383	-9.90	-9.90
1334	0	16.265	0.016	0.695	0.035	0.143	0.063	2.915	0.202	-9.990	-9.990	-9.990	-9.99	-9.99
1340	0	15.030	0.061	0.662	0.068	0.016	0.060	-9.990	-9.990	-9.990	-9.990	-9.990	-9.99	-9.99
1351	0	16.595	0.044	0.691	0.079	0.185	0.093	2.717	0.471	-9.990	0.454	0.584	-9.90	-9.90
1354	0	12.298	0.011	0.884	0.015	0.297	0.020	2.573	0.265	-9.990	-9.990	-9.990	-9.99	-9.99
1355	0	15.528	0.025	0.722	0.043	0.124	0.063	2.676	0.380	-9.990	0.429	0.449	-9.99	-9.99
1359	0	17.335	0.060	0.766	0.142	-9.990	-9.990	-9.990	-9.990	-9.990	-9.990	-9.990	-9.99	-9.99
1361	0	13.805	0.055	0.495	0.061	0.134	0.053	2.840	0.183	-9.990	0.372	0.194	-9.99	-9.99
1367	0	12.898	0.005	0.478	0.018	0.154	0.030	2.568	0.224	-9.990	-9.990	-9.990	-9.99	-9.99

Continued on the next page...

NGC 6134 photometry, continued from the previous page

ID_B	ID_V	V	σ_V	$b-y$	σ_{by}	m_1	σ_{m_1}	β	σ_β	c_0	$E(b-y)$	σ_E	Fe/H	σ_{FeH}
1368	0	15.248	0.023	0.839	0.040	0.109	0.063	2.540	0.277	-9.990	-9.990	-9.990	-9.99	-9.99
1371	0	14.826	0.082	0.537	0.147	0.185	0.151	-9.990	-9.990	-9.990	-9.990	-9.990	-9.99	-9.99
1375	0	17.244	0.080	1.402	0.138	-9.990	-9.990	-9.990	-9.990	-9.990	-9.990	-9.990	-9.99	-9.99
1377	0	14.964	0.014	0.558	0.019	0.122	0.029	-9.990	-9.990	-9.990	-9.990	-9.990	-9.99	-9.99
1380	0	15.664	0.112	0.712	0.163	-9.990	-9.990	-9.990	-9.990	-9.990	-9.990	-9.990	-9.99	-9.99
1388	0	16.421	0.108	1.545	0.181	-9.990	-9.990	-9.990	-9.990	-9.990	-9.990	-9.990	-9.99	-9.99
1390	0	15.516	0.193	0.714	0.321	-9.990	-9.990	-9.990	-9.990	-9.990	-9.990	-9.990	-9.99	-9.99
1394	0	12.747	0.173	0.600	0.267	-9.990	-9.990	-9.990	-9.990	-9.990	-9.990	-9.990	-9.99	-9.99
1399	0	13.995	0.014	0.479	0.031	0.144	0.044	-9.990	-9.990	-9.990	-9.990	-9.990	-9.99	-9.99
1401	0	17.213	0.121	1.149	0.230	-9.990	-9.990	-9.990	-9.990	-9.990	-9.990	-9.990	-9.99	-9.99
1410	0	14.118	0.011	0.438	0.012	0.164	0.033	-9.990	-9.990	-9.990	-9.990	-9.990	-9.99	-9.99
1411	0	17.242	0.126	1.564	0.142	-9.990	-9.990	-9.990	-9.990	-9.990	-9.990	-9.990	-9.99	-9.99
1412	0	14.375	0.007	0.527	0.009	0.150	0.068	-9.990	-9.990	-9.990	-9.990	-9.990	-9.99	-9.99
1415	0	12.694	0.010	0.487	0.013	0.200	0.049	-9.990	-9.990	-9.990	-9.990	-9.990	-9.99	-9.99
1420	0	17.394	0.080	1.007	0.211	-9.990	-9.990	-9.990	-9.990	-9.990	-9.990	-9.990	-9.99	-9.99
1426	0	14.327	0.013	0.527	0.028	0.134	0.044	-9.990	-9.990	-9.990	-9.990	-9.990	-9.99	-9.99
1432	0	15.808	0.015	0.753	0.056	0.017	0.074	-9.990	-9.990	-9.990	-9.990	-9.990	-9.99	-9.99
1435	0	15.175	0.112	1.236	0.181	-9.990	-9.990	-9.990	-9.990	-9.990	-9.990	-9.990	-9.99	-9.99
1438	0	16.414	0.031	0.815	0.047	0.052	0.056	-9.990	-9.990	-9.990	-9.990	-9.990	-9.99	-9.99
1439	0	12.566	0.118	0.528	0.173	-9.990	-9.990	-9.990	-9.990	-9.990	-9.990	-9.990	-9.99	-9.99
1440	0	13.657	0.171	0.661	0.254	-9.990	-9.990	-9.990	-9.990	-9.990	-9.990	-9.990	-9.99	-9.99
1446	0	17.388	0.067	0.743	0.090	-9.990	-9.990	-9.990	-9.990	-9.990	-9.990	-9.990	-9.99	-9.99
1450	0	16.307	0.171	0.861	0.261	-9.990	-9.990	-9.990	-9.990	-9.990	-9.990	-9.990	-9.99	-9.99
1451	0	17.793	0.077	1.231	0.272	-9.990	-9.990	-9.990	-9.990	-9.990	-9.990	-9.990	-9.99	-9.99
1454	0	16.506	0.106	0.881	0.119	-9.990	-9.990	-9.990	-9.990	-9.990	-9.990	-9.990	-9.99	-9.99
1455	0	15.853	0.029	0.618	0.049	0.145	0.054	-9.990	-9.990	-9.990	-9.990	-9.990	-9.99	-9.99
1459	0	15.709	0.151	0.715	0.200	0.069	0.201	-9.990	-9.990	-9.990	-9.990	-9.990	-9.99	-9.99
1461	0	16.187	0.025	0.674	0.053	0.185	0.058	-9.990	-9.990	-9.990	-9.990	-9.990	-9.99	-9.99
1463	0	12.417	0.009	0.863	0.011	0.280	0.017	-9.990	-9.990	-9.990	-9.990	-9.990	-9.99	-9.99
1466	0	15.865	0.092	0.852	0.136	-9.990	-9.990	-9.990	-9.990	-9.990	-9.990	-9.990	-9.99	-9.99
1469	0	14.579	0.030	0.569	0.050	0.124	0.052	-9.990	-9.990	-9.990	-9.990	-9.990	-9.99	-9.99
1471	0	12.641	0.183	0.937	0.283	0.279	0.308	-9.990	-9.990	-9.990	-9.990	-9.990	-9.99	-9.99
1472	0	17.323	0.090	0.818	0.125	-9.990	-9.990	-9.990	-9.990	-9.990	-9.990	-9.990	-9.99	-9.99
1478	0	17.344	0.124	1.118	0.199	-9.990	-9.990	-9.990	-9.990	-9.990	-9.990	-9.990	-9.99	-9.99
1479	0	15.534	0.013	0.627	0.029	0.125	0.035	-9.990	-9.990	-9.990	-9.990	-9.990	-9.99	-9.99
1482	0	13.838	0.134	0.433	0.210	0.037	0.229	-9.990	-9.990	-9.990	-9.990	-9.990	-9.99	-9.99
1484	0	12.859	0.006	0.464	0.008	0.129	0.011	-9.990	-9.990	-9.990	-9.990	-9.990	-9.99	-9.99
1485	0	16.516	0.030	0.652	0.138	0.459	0.155	-9.990	-9.990	-9.990	-9.990	-9.990	-9.99	-9.99
1487	0	16.628	0.020	0.729	0.058	-9.990	-9.990	-9.990	-9.990	-9.990	-9.990	-9.990	-9.99	-9.99
1494	0	15.013	0.200	0.902	0.214	-9.990	-9.990	-9.990	-9.990	-9.990	-9.990	-9.990	-9.99	-9.99
1500	0	13.312	0.015	0.406	0.021	0.153	0.030	-9.990	-9.990	-9.990	-9.990	-9.990	-9.99	-9.99
1501	0	17.187	0.024	1.040	0.330	-9.990	-9.990	-9.990	-9.990	-9.990	-9.990	-9.990	-9.99	-9.99
1503	0	15.276	0.012	0.619	0.037	0.118	0.041	-9.990	-9.990	-9.990	-9.990	-9.990	-9.99	-9.99
1504	0	15.713	0.164	0.698	0.229	-9.990	-9.990	-9.990	-9.990	-9.990	-9.990	-9.990	-9.99	-9.99
1505	0	13.230	0.005	0.365	0.010	0.149	0.015	-9.990	-9.990	-9.990	-9.990	-9.990	-9.99	-9.99
1508	0	15.276	0.033	1.217	0.064	-9.990	-9.990	-9.990	-9.990	-9.990	-9.990	-9.990	-9.99	-9.99
1514	0	15.739	0.178	1.676	0.222	-9.990	-9.990	-9.990	-9.990	-9.990	-9.990	-9.990	-9.99	-9.99
1518	0	16.289	0.101	1.546	0.123	-9.990	-9.990	-9.990	-9.990	-9.990	-9.990	-9.990	-9.99	-9.99
1523	0	15.592	0.020	0.541	0.026	0.175	0.026	-9.990	-9.990	-9.990	-9.990	-9.990	-9.99	-9.99
1526	0	13.662	0.163	0.478	0.240	-9.990	-9.990	-9.990	-9.990	-9.990	-9.990	-9.990	-9.99	-9.99
1530	0	11.739	0.220	0.142	0.331	-9.990	-9.990	-9.990	-9.990	-9.990	-9.990	-9.990	-9.99	-9.99
1532	0	12.773	0.010	0.283	0.022	0.153	0.027	-9.990	-9.990	-9.990	-9.990	-9.990	-9.99	-9.99
1534	0	16.240	0.010	1.083	0.120	-9.990	-9.990	-9.990	-9.990	-9.990	-9.990	-9.990	-9.99	-9.99
1536	0	17.462	0.118	1.222	0.159	-9.990	-9.990	-9.990	-9.990	-9.990	-9.990	-9.990	-9.99	-9.99
1540	0	14.172	0.010	0.495	0.022	0.133	0.027	-9.990	-9.990	-9.990	-9.990	-9.990	-9.99	-9.99
1542	0	16.256	0.052	0.702	0.079	0.134	0.093	-9.990	-9.990	-9.990	-9.990	-9.990	-9.99	-9.99
1550	0	16.385	0.012	0.673	0.026	0.207	0.035	-9.990	-9.990	-9.990	-9.990	-9.990	-9.99	-9.99
1552	0	16.301	0.021	0.844	0.128	0.113	0.149	-9.990	-9.990	-9.990	-9.990	-9.990	-9.99	-9.99
1553	0	14.292	0.005	0.557	0.013	0.290	0.020	-9.990	-9.990	-9.990	-9.990	-9.990	-9.99	-9.99
1557	0	16.627	0.027	0.686	0.138	-9.990	-9.990	-9.990	-9.990	-9.990	-9.990	-9.990	-9.99	-9.99
1560	0	16.145	0.020	0.689	0.089	0.136	0.101	-9.990	-9.990	-9.990	-9.990	-9.990	-9.99	-9.99
1564	0	16.120	0.032	0.625	0.048	0.240	0.064	-9.990	-9.990	-9.990	-9.990	-9.990	-9.99	-9.99
1565	0	11.899	0.010	0.268	0.014	0.223	0.015	-9.990	-9.990	-9.990	-9.990	-9.990	-9.99	-9.99
1568	0	16.725	0.148	0.877	0.184	-9.990	-9.990	-9.990	-9.990	-9.990	-9.990	-9.990	-9.99	-9.99
1572	0	15.612	0.016	0.651	0.027	0.132	0.045	-9.990	-9.990	-9.990	-9.990	-9.990	-9.99	-9.99
1578	0	16.485	0.024	0.648	0.047	-9.990	-9.990	-9.990	-9.990	-9.990	-9.990	-9.990	-9.99	-9.99
1585	0	17.048	0.069	0.855	0.188	-9.990	-9.990	-9.990	-9.990	-9.990	-9.990	-9.990	-9.99	-9.99
1589	0	11.811	0.013	0.289	0.014	0.077	0.020	-9.990	-9.990	-9.990	-9.990	-9.990	-9.99	-9.99
1594	0	16.562	0.120	0.906	0.169	-9.990	-9.990	-9.990	-9.990	-9.990	-9.990	-9.990	-9.99	-9.99
1596	0	15.659	0.039	1.388	0.152	-9.990	-9.990	-9.990	-9.990	-9.990	-9.990	-9.990	-9.99	-9.99
1598	0	15.065	0.007	0.966	0.045	-9.990	-9.990	-9.990	-9.990	-9.990	-9.990	-9.990	-9.99	-9.99
1599	0	14.233	0.012	0.389	0.030	-9.990	-9.990	-9.990	-9.990	-9.990	-9.990	-9.990	-9.99	-9.99
1600	0	14.467	0.009	0.516	0.015	0.142	0.018	-9.990	-9.990	-9.990	-9.990	-9.990	-9.99	-9.99

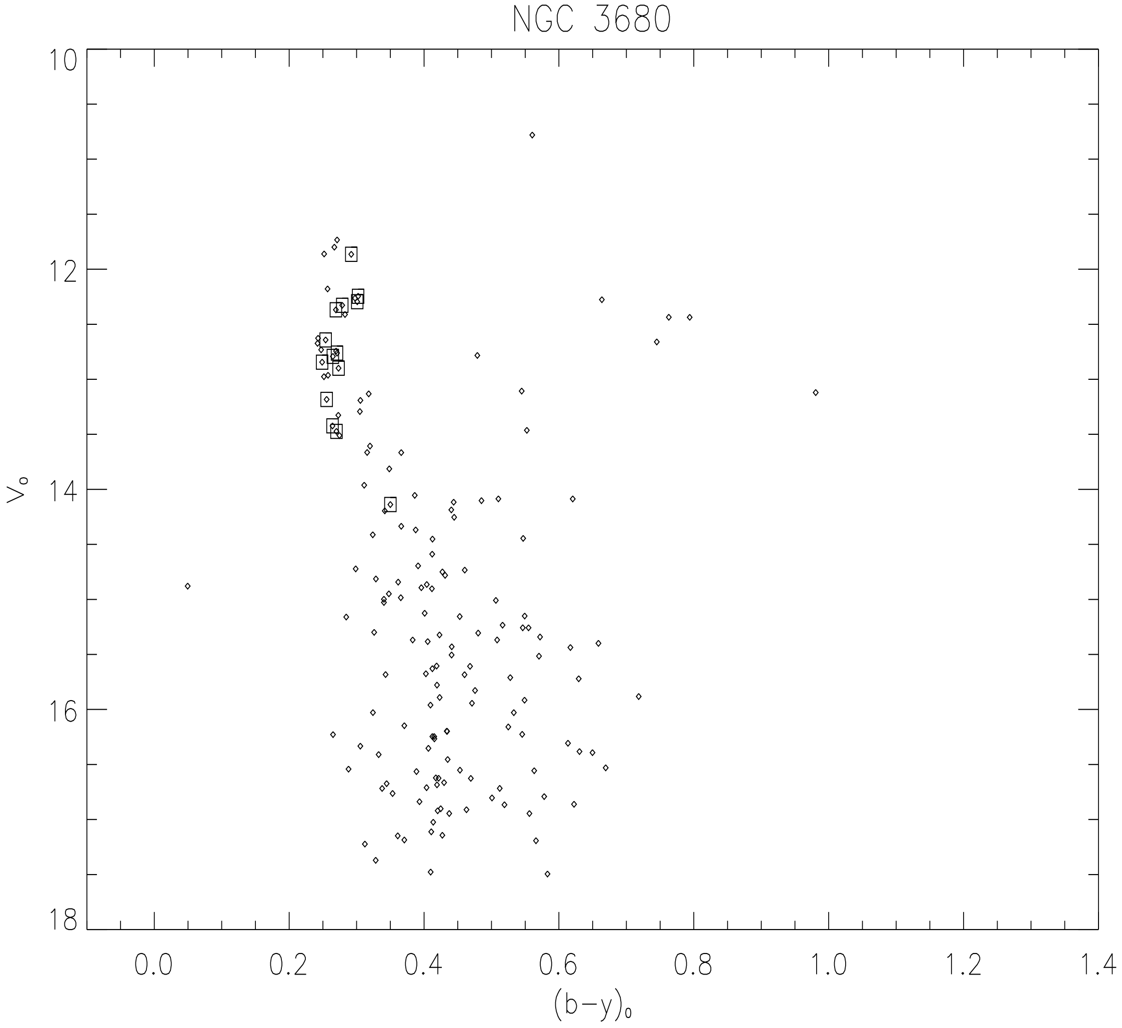

Figure E.2: Colour-magnitude diagram of NGC 3680. The stars that are single cluster members according to Nordström *et al.* [53] are indicated.

Table E.2: Photometric results for NGC 3680. ID_B is the star number I have used. ID_N is the star number in Nordström *et al.* [53]. Note that the stars 21A, 25A, and 46A in Nordström *et al.* are given the numbers 121, 125, and 146. $ID_N = 0$ means that this star was not observed by Nordström *et al.* [53]. Stars that are single cluster members according to the spectroscopy by Nordström *et al.* are printed in **bold**. I present Strömgren indices for 162 stars. I note that in Nordström *et al.* [53] V, $b-y$, and $B-V$ photometry for an additional 70 stars not included in my sample can be found. The results presented here as well as previously published data are available through anonymous `ftp`, *cf.* appendix F.

ID_B	ID_N	V	σ_V	$b-y$	σ_{by}	m_1	σ_{m_1}	β	σ_β	$E(b-y)$	σ_E	Fe/H	σ_{FeH}
2	0	15.553	0.091	0.551	0.115	-9.990	-9.990	2.449	0.236	-9.990	-9.990	-9.90	-9.90
3	0	15.087	0.047	0.455	0.084	0.252	0.091	2.562	0.042	-9.990	-9.990	-9.90	-9.90
5	0	14.935	0.012	0.470	0.020	0.166	0.041	2.772	0.475	0.276	0.475	-9.90	-9.90
7	1045	15.895	0.058	0.571	0.066	0.458	0.137	2.551	0.125	-9.990	-9.990	-9.90	-9.90
10	**42**	12.977	0.003	0.308	0.008	0.157	0.012	2.729	0.062	0.088	0.063	-9.90	-9.90
11	**43**	12.553	0.004	0.312	0.006	0.164	0.009	2.665	0.011	0.025	0.015	0.11	0.11
12	0	15.484	0.015	0.369	0.023	0.112	0.037	2.712	0.451	0.145	0.509	-9.90	-9.90
13	**60**	14.323	0.015	0.393	0.022	0.222	0.025	2.623	0.129	0.025	0.162	-9.90	-9.90
14	0	16.067	0.030	0.761	0.060	0.332	0.119	3.084	0.197	-9.990	-9.990	-9.90	-9.90
16	61	14.438	0.017	0.488	0.034	0.276	0.057	2.509	0.164	-9.990	-9.990	-9.90	-9.90
17	58	12.917	0.007	0.290	0.010	0.164	0.010	2.688	0.049	-9.990	-9.990	0.16	0.14
18	1044	16.431	0.005	0.455	0.043	0.165	0.047	2.642	0.123	0.127	0.154	-9.90	-9.90
19	1043	14.287	0.013	0.528	0.017	0.267	0.022	2.601	0.014	0.095	0.028	0.88	0.21
20	1023	14.880	0.000	0.434	0.013	0.159	0.020	2.636	0.041	0.102	0.051	0.16	0.22
21	1042	14.630	0.007	0.590	0.012	0.230	0.016	2.597	0.025	0.162	0.036	0.68	0.16
22	1022	15.064	0.011	0.093	0.017	0.179	0.018	2.872	0.049	0.019	0.053	-9.90	-9.90
24	1039	15.442	0.018	0.589	0.024	0.269	0.029	2.603	0.027	0.151	0.046	-9.90	-9.90
26	0	15.622	0.020	0.660	0.028	0.380	0.030	2.553	0.017	-9.990	-9.990	-9.90	-9.90
27	1037	14.598	0.008	0.367	0.012	0.120	0.013	2.628	0.023	0.048	0.031	-0.48	0.15
28	4059	15.814	0.026	0.455	0.037	0.191	0.041	2.688	0.387	0.183	0.449	-9.90	-9.90
29	59	12.621	0.015	0.806	0.027	0.558	0.034	2.620	0.026	0.249	0.061	-9.90	-9.90
31	0	15.078	0.036	0.439	0.041	0.288	0.056	2.307	0.147	-9.990	-9.990	-9.90	-9.90
32	9005	15.345	0.019	0.328	0.025	0.155	0.024	2.724	0.027	0.102	0.038	-9.90	-9.90
33	4069	15.526	0.029	0.615	0.059	0.499	0.071	2.606	0.470	0.076	0.804	-9.90	-9.90
35	51	14.907	0.232	0.342	0.320	0.227	0.342	2.954	0.370	-9.990	-9.990	-9.90	-9.90
38	4055	16.332	0.035	0.414	0.058	0.120	0.067	2.616	0.118	0.078	0.162	-9.90	-9.90
40	40	12.461	0.006	0.707	0.014	0.406	0.018	2.581	0.011	-9.990	-9.990	-9.90	-9.90
41	12	16.859	0.082	0.388	0.104	0.237	0.100	2.911	0.242	-9.990	-9.990	-9.90	-9.90
43	4054	16.806	0.055	0.461	0.066	0.237	0.110	2.649	0.089	0.117	0.133	-9.90	-9.90
45	**45**	12.049	0.002	0.335	0.005	0.149	0.013	2.667	0.018	0.053	0.022	0.03	0.17
46	2006	15.867	0.017	0.386	0.025	0.148	0.038	2.640	0.060	0.067	0.077	-9.90	-9.90
47	1034	16.413	0.057	0.308	0.065	0.193	0.061	-9.990	-9.990	-9.990	-9.990	-9.90	-9.90
48	1030	17.209	0.060	0.457	0.112	0.116	0.145	2.627	0.166	0.128	0.240	-9.90	-9.90
49	1035	16.567	0.040	0.673	0.063	0.314	0.066	2.664	0.061	0.314	0.110	-9.90	-9.90
50	1006	15.184	0.015	0.384	0.018	0.140	0.017	2.642	0.025	0.071	0.036	-0.12	0.19
51	**39**	12.430	0.002	0.345	0.006	0.150	0.009	2.656	0.008	0.049	0.012	0.00	0.11
52	2005	16.128	0.009	0.514	0.045	0.291	0.066	2.680	0.081	0.203	0.117	-9.90	-9.90
53	2015	15.963	0.038	0.462	0.054	0.222	0.065	2.546	0.111	-9.990	-9.990	-9.90	-9.90
55	38	12.448	0.002	0.341	0.005	0.153	0.009	2.648	0.012	-9.990	-9.990	-0.06	0.11
57	0	15.194	0.006	0.549	0.019	0.118	0.065	2.243	0.170	-9.990	-9.990	-9.90	-9.90
58	**37**	13.029	0.011	0.292	0.014	0.147	0.019	2.676	0.016	0.024	0.023	-0.09	0.25
59	4052	17.370	0.018	0.414	0.082	0.216	0.115	2.778	0.128	0.219	0.155	-9.90	-9.90
60	4048	16.901	0.029	0.555	0.076	0.383	0.123	2.562	0.107	-9.990	-9.990	-9.90	-9.90
61	221	16.595	0.047	0.376	0.141	0.179	0.171	2.459	0.138	-9.990	-9.990	-9.90	-9.90
62	121	14.774	0.003	0.455	0.021	0.240	0.035	2.571	0.056	-9.990	-9.990	-9.90	-9.90
63	1005	17.296	0.070	0.454	0.103	0.209	0.145	-9.990	-9.990	-9.990	-9.990	-9.90	-9.90
65	4047	16.100	0.028	0.592	0.038	0.417	0.088	2.559	0.064	-9.990	-9.990	-9.90	-9.90
66	4045	16.214	0.048	0.576	0.064	0.340	0.093	2.557	0.090	-9.990	-9.990	-9.90	-9.90
67	1003	17.023	0.083	0.436	0.103	0.068	0.115	-9.990	-9.990	-9.990	-9.990	-9.90	-9.90
69	1004	15.906	0.027	0.672	0.039	0.447	0.060	2.550	0.059	-9.990	-9.990	-9.90	-9.90
70	21	14.520	0.011	0.409	0.016	0.179	0.017	2.620	0.023	0.054	0.033	0.11	0.18
71	16	13.317	0.014	0.361	0.027	0.171	0.031	2.710	0.303	0.127	0.338	-9.90	-9.90
72	4050	16.431	0.045	0.458	0.055	0.197	0.063	2.590	0.091	0.057	0.137	-9.90	-9.90
73	**46**	13.368	0.005	0.299	0.008	0.155	0.011	2.684	0.013	-9.990	-9.990	0.07	0.15
77	36	13.478	0.004	0.348	0.007	0.152	0.008	2.646	0.015	-9.990	-9.990	-0.06	0.09
78	1002	17.377	0.075	0.609	0.117	0.733	0.147	2.493	0.226	-9.990	-9.990	-9.90	-9.90
79	0	15.553	0.015	0.426	0.021	0.197	0.036	2.597	0.034	-9.990	-9.990	-9.90	-9.90
80	9014	17.328	0.051	0.470	0.077	0.177	0.079	2.542	0.134	-9.990	-9.990	-9.90	-9.90
82	2033	15.568	0.018	0.448	0.029	0.162	0.031	2.645	0.037	0.125	0.054	-9.90	-9.90
83	0	16.518	0.039	0.349	0.083	0.250	0.134	2.839	0.059	0.211	0.107	-9.90	-9.90
84	2046	16.213	0.102	0.367	0.114	0.098	0.132	2.284	0.112	-9.990	-9.990	-9.90	-9.90
85	6027	12.046	0.004	0.295	0.010	0.155	0.012	2.704	0.006	0.059	0.013	0.12	0.17
86	4042	16.895	0.044	0.447	0.083	0.147	0.098	2.652	0.172	0.137	0.220	-9.90	-9.90
87	32	12.928	0.005	0.313	0.010	0.156	0.011	2.666	0.013	-9.990	-9.990	0.02	0.14
88	6028	12.596	0.009	0.326	0.021	0.167	0.035	2.700	0.031	0.082	0.041	-9.90	-9.90

Continued on the next page...

NGC 3680 photometry, continued from the previous page

ID_B	ID_N	V	σ_V	$b-y$	σ_{by}	m_1	σ_{m_1}	β	σ_β	$E(b-y)$	σ_E	Fe/H	σ_{FeH}
89	22	13.376	0.004	0.349	0.004	0.152	0.010	2.641	0.010	-9.990	-9.990	-0.11	0.12
90	2032	13.648	0.004	0.595	0.007	0.473	0.011	2.582	0.013	-9.990	-9.990	-9.90	-9.90
92	2002	15.169	0.009	0.409	0.012	0.166	0.016	2.632	0.027	0.072	0.036	0.11	0.18
93	4044	15.418	0.009	0.559	0.016	0.327	0.037	2.557	0.062	-9.990	-9.990	-9.90	-9.90
94	146	13.512	0.005	0.316	0.008	0.162	0.010	2.689	0.007	0.060	0.012	0.24	0.13
95	**35**	13.084	0.004	0.316	0.006	0.158	0.007	2.664	0.016	-9.990	-9.990	0.04	0.08
96	2031	15.213	0.024	0.384	0.026	0.165	0.025	2.642	0.028	0.062	0.043	-9.90	-9.90
98	0	16.382	0.013	0.477	0.046	0.385	0.073	2.596	0.122	-0.009	0.183	-9.90	-9.90
99	0	12.968	0.020	0.522	0.023	0.277	0.026	2.355	0.129	-9.990	-9.990	-9.90	-9.90
100	4002	13.161	0.003	0.295	0.005	0.156	0.005	2.675	0.014	0.023	0.016	0.03	0.07
101	0	16.869	0.029	0.462	0.060	0.277	0.091	2.611	0.110	0.048	0.161	-9.90	-9.90
106	2030	14.637	0.007	0.456	0.009	0.201	0.020	2.625	0.014	0.092	0.022	0.50	0.22
107	4009	16.451	0.038	0.458	0.067	0.150	0.085	2.596	0.050	0.085	0.104	-9.90	-9.90
108	2001	15.584	0.029	0.702	0.035	0.232	0.053	2.525	0.045	-9.990	-9.990	-9.90	-9.90
109	**15**	12.512	0.006	0.322	0.017	0.168	0.022	2.741	0.036	0.109	0.041	-9.90	-9.90
110	2049	16.736	0.056	0.496	0.074	0.220	0.093	2.604	0.094	0.094	0.149	-9.90	-9.90
111	2023	17.130	0.118	0.480	0.134	0.162	0.141	2.595	0.060	0.097	0.174	-9.90	-9.90
112	**30**	13.608	0.011	0.307	0.012	0.160	0.010	2.676	0.010	-9.990	-9.990	0.13	0.13
113	2024	14.998	0.012	0.372	0.016	0.135	0.021	2.658	0.020	0.080	0.029	-9.90	-9.90
114	33	11.918	0.002	0.314	0.003	0.164	0.003	2.650	0.018	0.009	0.021	-0.01	0.04
115	2025	16.639	0.034	0.478	0.041	0.257	0.065	2.632	0.080	0.100	0.112	-9.90	-9.90
116	3001	12.812	0.002	0.286	0.005	0.157	0.006	-9.990	-9.990	-9.990	-9.990	-9.90	-9.90
118	2029	16.577	0.030	0.693	0.044	0.494	0.083	2.580	0.112	-9.990	-9.990	-9.90	-9.90
120	2051	17.408	0.079	0.355	0.118	0.186	0.125	2.579	0.047	-9.990	-9.990	-9.90	-9.90
123	29	11.984	0.003	0.310	0.005	0.165	0.005	2.650	0.018	0.005	0.021	-0.01	0.06
124	25	13.695	0.007	0.318	0.008	0.153	0.008	2.665	0.006	-9.990	-9.990	0.00	0.09
125	**125**	13.658	0.008	0.313	0.010	0.159	0.013	2.650	0.028	0.010	0.034	-0.06	0.16
127	0	15.340	0.013	0.496	0.020	0.235	0.028	2.588	0.022	-9.990	-9.990	-9.90	-9.90
128	24	13.791	0.008	0.363	0.009	0.163	0.011	2.648	0.019	0.051	0.024	0.12	0.13
129	4011	14.553	0.007	0.431	0.013	0.209	0.021	2.611	0.017	0.050	0.027	0.32	0.20
130	23	13.998	0.007	0.391	0.008	0.170	0.016	2.620	0.013	0.042	0.020	-0.01	0.16
131	2063	15.869	0.019	0.503	0.036	0.206	0.063	2.642	0.129	0.155	0.163	-9.90	-9.90
132	3016	15.507	0.025	0.466	0.028	0.227	0.043	2.585	0.038	-9.990	-9.990	-9.90	-9.90
133	2052	16.948	0.024	0.396	0.044	0.121	0.086	2.617	0.070	0.063	0.107	-9.90	-9.90
134	2060	15.700	0.019	0.613	0.031	0.265	0.036	2.607	0.026	0.178	0.049	-9.90	-9.90
135	14	12.363	0.004	0.300	0.007	0.155	0.008	2.691	0.025	0.047	0.029	0.10	0.10
136	2054	16.727	0.077	0.331	0.090	0.126	0.080	2.545	0.155	-9.990	-9.990	-9.90	-9.90
138	28	15.134	0.019	0.391	0.026	0.151	0.026	2.603	0.019	-9.990	-9.990	-0.35	0.24
139	4015	13.292	0.010	0.588	0.015	0.452	0.020	2.554	0.146	-9.990	-9.990	-9.90	-9.90
140	4014	15.790	0.040	0.462	0.061	0.174	0.061	2.571	0.109	-9.990	-9.990	-9.90	-9.90
141	0	15.049	0.018	0.447	0.028	0.207	0.031	2.614	0.025	0.068	0.044	-9.90	-9.90
142	7021	16.012	0.019	0.519	0.027	0.223	0.036	2.659	0.087	0.189	0.110	-9.90	-9.90
143	7020	14.301	0.011	0.487	0.016	0.261	0.016	2.595	0.023	0.057	0.035	0.64	0.16
144	3020	16.976	0.048	0.621	0.095	0.301	0.105	2.532	0.081	-9.990	-9.990	-9.90	-9.90
145	4013	16.145	0.013	0.453	0.033	0.174	0.042	2.599	0.135	0.071	0.178	-9.90	-9.90
148	2058	15.793	0.015	0.511	0.024	0.227	0.032	2.615	0.074	0.117	0.098	-9.90	-9.90
151	2057	16.492	0.097	0.656	0.105	0.346	0.095	2.652	0.107	0.265	0.193	-9.90	-9.90
154	2055	16.810	0.058	0.465	0.070	0.170	0.079	2.483	0.079	-9.990	-9.990	-9.90	-9.90
157	3022	14.271	0.004	0.663	0.008	0.346	0.011	2.568	0.019	-9.990	-9.990	-9.90	-9.90
158	4016	16.076	0.023	0.466	0.029	0.254	0.033	2.675	0.092	0.158	0.117	-9.90	-9.90
160	2091	14.966	0.008	0.474	0.021	0.167	0.025	2.603	0.062	0.097	0.083	-0.02	0.23
162	3054	15.860	0.037	0.446	0.043	0.147	0.045	2.640	0.101	0.122	0.129	-9.90	-9.90
165	**10**	12.827	0.005	0.297	0.006	0.148	0.009	2.686	0.015	0.041	0.018	-0.03	0.12
167	3023	17.096	0.005	0.506	0.063	0.240	0.090	2.638	0.121	0.140	0.168	-9.90	-9.90
168	3053	16.902	0.041	0.381	0.081	0.206	0.096	2.663	0.045	0.075	0.101	-9.90	-9.90
169	3055	15.690	0.054	0.484	0.059	0.225	0.071	2.627	0.054	0.110	0.094	-9.90	-9.90
170	8	16.748	0.014	0.432	0.039	0.160	0.047	2.611	0.047	0.072	0.074	-9.90	-9.90
171	2098	12.845	0.007	0.788	0.008	0.494	0.013	2.608	0.015	0.231	0.030	-9.90	-9.90
172	9	14.147	0.008	0.354	0.010	0.161	0.010	2.659	0.023	0.057	0.028	0.17	0.13
174	2100	15.310	0.018	0.444	0.025	0.160	0.026	2.626	0.023	0.099	0.039	-9.90	-9.90
176	2093	13.850	0.004	0.359	0.015	0.144	0.021	2.614	0.223	0.017	0.281	-9.90	-9.90
178	3024	16.811	0.028	0.512	0.044	0.262	0.083	2.686	0.124	0.219	0.165	-9.90	-9.90
180	0	12.621	0.003	0.837	0.012	0.555	0.015	2.594	0.016	0.216	0.034	-9.90	-9.90
182	5	12.858	0.006	0.285	0.011	0.161	0.012	2.703	0.031	0.047	0.036	0.16	0.17
186	7	13.305	0.009	1.024	0.015	0.635	0.020	2.583	0.016	-9.990	-9.990	-9.90	-9.90
187	2097	16.849	0.076	0.473	0.089	0.170	0.105	2.693	0.121	0.211	0.166	-9.90	-9.90
188	3049	16.715	0.036	0.712	0.068	0.504	0.106	2.664	0.137	0.296	0.273	-9.90	-9.90
189	2096	14.371	0.013	0.483	0.015	0.247	0.014	2.582	0.061	-9.990	-9.990	-9.90	-9.90
190	73	15.028	0.014	0.405	0.019	0.155	0.020	2.642	0.029	0.084	0.040	0.09	0.22
191	**4**	12.947	0.007	0.314	0.011	0.164	0.014	2.626	0.086	-0.018	0.106	-0.22	0.21
192	2095	14.380	0.008	0.385	0.010	0.127	0.013	2.574	0.248	-9.990	-9.990	-9.90	-9.90
193	**6**	12.480	0.004	0.344	0.006	0.153	0.008	2.668	0.024	0.061	0.028	0.11	0.10
194	2094	14.239	0.006	0.429	0.012	0.189	0.018	2.532	0.390	-9.990	-9.990	-9.90	-9.90
195	3050	14.918	0.007	0.503	0.016	0.248	0.023	2.642	0.027	0.141	0.039	-9.90	-9.90
196	3026	15.491	0.002	0.523	0.022	0.350	0.061	2.471	0.087	-9.990	-9.990	-9.90	-9.90
198	3051	16.383	0.032	0.477	0.062	0.212	0.071	2.625	0.066	0.107	0.107	-9.90	-9.90
200	3027	15.336	0.038	0.592	0.046	0.273	0.063	2.523	0.085	-9.990	-9.990	-9.90	-9.90
202	0	13.851	0.019	0.409	0.039	0.224	0.045	2.549	0.119	-9.990	-9.990	-9.90	-9.90
203	0	14.271	0.011	0.553	0.021	0.190	0.086	2.322	0.113	-9.990	-9.990	-9.90	-9.90
206	0	15.443	0.024	0.598	0.044	0.287	0.058	2.617	0.058	0.171	0.093	-9.90	-9.90

Continued on the next page...

NGC 3680 photometry, continued from the previous page

ID_B	ID_N	V	σ_V	$b-y$	σ_{by}	m_1	σ_{m_1}	β	σ_β	$E(b-y)$	σ_E	Fe/H	σ_{FeH}
207	0	13.148	0.007	0.301	0.008	0.155	0.008	2.679	0.013	-9.990	-9.990	0.06	0.11
208	0	10.965	0.018	0.603	0.022	0.392	0.020	-9.990	-9.990	-9.990	-9.990	-9.90	-9.90
213	0	17.105	0.033	0.463	0.054	0.328	0.121	-9.990	-9.990	-9.990	-9.990	-9.90	-9.90
215	0	16.343	0.059	0.568	0.069	0.207	0.111	-9.990	-9.990	-9.990	-9.990	-9.90	-9.90
216	0	17.130	0.041	0.599	0.160	0.136	0.174	-9.990	-9.990	-9.990	-9.990	-9.90	-9.90
217	0	17.680	0.171	0.626	0.224	0.535	0.337	-9.990	-9.990	-9.990	-9.990	-9.90	-9.90
219	0	17.662	0.097	0.453	0.209	0.248	0.218	-9.990	-9.990	-9.990	-9.990	-9.90	-9.90
226	0	16.538	0.037	0.449	0.055	0.137	0.055	2.783	0.096	0.276	0.112	-9.90	-9.90
227	0	17.050	0.124	0.562	0.132	-9.990	-9.990	-9.990	-9.990	-9.990	-9.990	-9.90	-9.90
232	0	16.988	0.078	0.544	0.106	0.129	0.103	-9.990	-9.990	-9.990	-9.990	-9.90	-9.90
233	0	15.615	0.050	0.484	0.056	0.289	0.047	-9.990	-9.990	-9.990	-9.990	-9.90	-9.90
236	0	16.741	0.061	0.606	0.072	0.379	0.153	-9.990	-9.990	-9.990	-9.990	-9.90	-9.90
238	0	17.087	0.053	0.468	0.073	0.110	0.136	-9.990	-9.990	-9.990	-9.990	-9.90	-9.90
239	0	17.555	0.038	0.371	0.079	0.408	0.099	-9.990	-9.990	-9.990	-9.990	-9.90	-9.90
241	0	17.333	0.070	0.404	0.087	0.129	0.092	-9.990	-9.990	-9.990	-9.990	-9.90	-9.90
260	0	17.046	0.146	0.665	0.163	-9.990	-9.990	-9.990	-9.990	-9.990	-9.990	-9.90	-9.90
269	0	16.411	0.029	0.589	0.060	-9.990	-9.990	-9.990	-9.990	-9.990	-9.990	-9.90	-9.90

Appendix F

Anonymous `ftp`

The results of this thesis are available through anonymous `ftp`. I have also made data from previously published data available, *i.e.* $B-V$ photometry of NGC 6134 by Viskum [71] and Strömgren photometry of NGC 3680 by Nissen [49], Nordström *et al.* [53], and Twarog *et al.* [68]. Get the files by accessing the computer system at Aarhus University by using the following procedure:

- `ftp obs.aau.dk`
- Type user name: `anonymous` and type your e-mail address as password.
- Change directory to `pub/bruntt`. The `README` file found here describes the contents of the directory.
- Download all the tables containing the data by typing `mget *` and disconnect by typing `quit`.

Important notice: The Strömgren data may be used freely - although a reference to this thesis must be given!

Appendix G

Dansk Resumé

I Maj 1996 rejste jeg til Det europæiske Sydobservatorium (ESO) i Chile. Jeg var på observatoriet i tre uger, hvor jeg anvendte de to danske teleskoper. Med det danske 1.54m teleskop tog jeg i løbet af fem nætter billeder med Strömgren filtre af to åbne hobe: NGC 6134 og NGC 3680. Med den danske 50cm "Strömgren Automatic Telescope" (SAT) undersøgte jeg over en periode på 22 døgn variation i lysstyrke i Strömgren filtre af to variable stjerner: FG Virginis og α Circini.

Jeg har udnyttet Strömgren fotometrien til at bestemme vigtige astrofysiske parametre for de to åbne hobe NGC 6134 og NGC 3680. Det drejer sig om den interstellare rødfarvning, afstanden til hobene og deres aldre - samt temperaturen, lysstyrken og indholdet af tunge grundstoffer i stjernerne. I kapitel 5 har jeg præsenteret de observationelle resultater.

Af de to hobe er NGC 3680 tidligere blevet grundigt studeret (Nordström *et al.* [53]), mens vores viden om NGC 6134 - før resultaterne fra dette speciale - er begrænset (Frandsen *et al.* [29]). Således har jeg anvendt mine resultater for NGC 3680 som referance: Mine resultater stemmer godt overens med tidligere opnåede resultater!

I den lidt yngre hob NGC 6134 er der tidligere fundet syv variable stjerner (Frandsen *et al.* [29]). Man kan udlede interessante informationer om disse variable stjerner ud fra deres svingningsperioder ved at sammenligne teoretiske stjernemodeller med observationerne. For at kunne gøre dette er det dog nødvendigt at kende de fundamentale parametre for disse stjerner: Rødfarvningen, afstanden, alderen for stjernerne i hoben, - men også temperaturen og lysstyrken af de enkelte stjerner. Med resultaterne fra dette speciale er vi nået et godt stykke videre med dette. Dog mangler vi stadig information om stjernernes rotationshastigheder samt bestemmelse af hvilke af stjernerne i feltet, der faktisk tilhører hoben. Disse informationer kan findes ud fra spektroskopiske målinger, som vil blive foretaget allerede i foråret 1999.

Jeg har konstrueret lyskurverne for de to variable stjerner FG Vir og α Cir (figur 7.2 og 7.3) ud fra 22 nættes målinger med SAT teleskopet. Disse stjerner er begge tidligere blevet undersøgt meget grundigt ud fra et meget større data-materiale end mit.

Mine resultater for δ Scuti stjernen FG Vir er blevet udnyttet af Michael Viskum [72], [73], der fra ESO på samme tidspunkt undersøgte variationen af stjernen ud fra spektroskopiske målinger. Ved at sammenligne amplituderne af variationen i Strömgren filtre målt med SAT og variationen i bredden af spektrallinjer har han bestemt detaljerede astrofysiske egenskaber (*e.g.* middeltæthed, radius, masse, afstand) for FG Vir, som jeg har beskrevet i kapitel 8. Mine målinger er også blevet inkluderet i et meget stort dataset for FG Vir, - disse resultater vil blive publiseret af Breger *et al.* [10] i 1999.

Den variable stjerne α Cir er tidligere blevet undersøgt af Medupe *et al.* [48] og Baldry *et al.* [6] med forskellige metoder. Variationen i stjernens lysstyke skyldes en stående bølge, der udbreder sig gennem stjernen. Mine resultater stemmer overens med Medupe *et al.* [48] og Baldry *et al.* [6], - og kan fortolkes således, at der er et knudepunkt i den stående bølge, som ligger tæt ved overfladen, *cf.* kapitel 8.2. Dette forklarer det kraftige fald i amplitude når man sammenligner variationen af lyset ved kortere og længere bølgelænder (se figur 8.2).

Lad mig fremhæve at jeg har lagt hovedvægten af mit arbejde i reduktionen og fortolkningen af fotometrien for de to åbne hobe NGC 3680 og NGC 6134. Mine resultater viser at Strömgren fotometri er et værdifuldt redskab til at uddrive viden om stjernehobes egenskaber og de enkelte stjerners fysiske parametre. Et krav er dog, at man laver omfattende optagelser af standard stjerner! Specielt vil resultaterne for NGC 6134 i nær fremtid føre til værdifuld information om de variable stjerner i denne hob, når de spektroskopiske målinger af stjernerne er blevet udført.